RECYCLING OF TUNGSTEN CARBIDE-BASED SCRAP METAL: SELECTIVE DISSOLUTION OF THE COBALT BINDER PHASE AND RECOVERY OF VALUABLE CONSTITUENTS USING A COMPLEXING AGENT-AIDED ACID LEACH PROCESS

Alan Shemi

A thesis submitted to the Faculty of Engineering and the Built Environment, University of Witwatersrand, Johannesburg in fulfillment of the requirements for the degree of Doctor of Philosophy

January, 2022

DECLARATION

I, Alan Shemi, declare that this thesis is my own unaided work. It is being submitted to the degree of Doctor of Philosophy to the University of the Witwatersrand, Johannesburg. It has not been submitted before for any other degree or examination in any other University.

28th January 2022

Abstract

Cemented tungsten carbides provide a pre-mined and easily accessible secondary source of tungsten and cobalt critical metals. The ability of acidic media to leach and collect metallic species from the cemented carbide composite material is based on one mechanism: metallic binder dissolution. However, members of the iron group, namely, Fe, Ni and Co, when used as binders in cemented carbide, wet the grains of tungsten carbide (WC) making it very difficult to remove them from between the grains during reclamation.

This research project explored the possibility of designing a technique wherein the Co binder phase is selectively extracted whilst leaving the WC hard phase intact. It is this possibility wherein the properties of cemented carbide were investigated so as to understand the possibilities and limitations of the approach. The properties of cemented tungsten carbide were evaluated using a Field Emission Scanning Electron Microscope (FESEM), a Rockwell Hardness Tester and a GX50 inverted metallurgical microscope.

Preliminary tests in 1M sulphuric acid showed that an acidic oxidative environment enabled Co binder dissolution to extraction levels where selective dissolution of the cobalt binder metal is guaranteed. Initial tests gave a Co extraction of 8.7% in 6 h. Further tests gave a Co extraction of up to 99.6% in 10.5 days. The dissolution process and recovery of constituents was studied using various techniques including a statistical Design of Experiments (DOE) for modeling optimum leaching conditions, factor range finding tests for analysis of influence of process parameters, reagent selection tests for finding a suitable lixiviant and a conceptual kinetic model for describing Co dissolution from the binder matrix. Leaching, precipitation, solvent extraction and electrorecovery techniques were used for leach liquor purification and resource recovery of WC and Co constituents. Co dissolution followed kinetic models, $x = kt$ and $1-(1-x)^{1/3} = kt$ and activation energies: 56.70kJmol^{-1} and 21.07kJmol^{-1} suggesting chemical reaction and thin film diffusion control. Co dissolution exhibited a strong dependence on temperature, leaching time and acid concentration. The DOE regression model predicted a maximum Co extraction rate of 25.0% at optimal leaching conditions of 82°C, 2M H_2SO_4 and 10 h leaching time. The Co extraction rate found experimentally was 24.1%. Using optimal conditions and increased leaching time gave 97.6% Co extraction in 4.2 days. An increase in temperature from 82 to 92°C yielded 98.2% Co extraction in 1.5 days. Factor perturbation plot revealed temperature as the key

driver of the Co dissolution process. A dosage of 5% (v/v) lactic acid strongly impacted Co extraction in the first 1 h but waned with increasing leaching time due to poor mass transfer in the inner core of the button. The recovered WC powder exhibited well faceted fine particles; the electro-recovered Co metal showed morphological integrity and the economic factors indicated economic process viability, thus presenting a possible practical application of the cemented tungsten carbide recycling process.

PUBLICATIONS AND PRESENTATIONS

Refereed Journal Article

Shemi, A., Magumise, A., Ndlovu, S., Sacks, N., 2018. Recycling of tungsten carbide scrap metal: A review of recycling methods and future prospects. Minerals Engineering, Vol. 122, pp. 195-205.

Refereed Conference Proceeding

Shemi, A., Ndlovu, S., Sacks, N., 2018. Scrap Recycling of Tungsten-based Secondary Material for the Recovery of Tungsten Monocarbide (WC) and Other Valuable Constituents Using an Acid Leach Process: A Preliminary Study. Extraction Conference, Ottawa, Ontario, Canada, 26th – 29th August 2018.

Journal Article in Progress

Shemi, A., Ndlovu, S., Sacks, N., 2021. Extraction of Cobalt from Binary-Phase Cemented Tungsten Carbide (WC-Co) Using H_2SO_4: Identification and Optimization of Influential Factors Using Statistical Design of Experiments. Minerals Engineering.

Conference Paper in Progress

Shemi, A., Ndlovu, S., Sacks, N., 2021. Comparison of Organic and Inorganic Acid Leaching of Metals from Cemented Carbide. European Metallurgical Conference 2021. June 27-30, Salzburg, Austria.

DEDICATION

To my wife Alice and three children, Ettric, Lerato and Elvin,
for the understanding, support, patience and love

ACKNOWLEDGEMENTS

It's a great pleasure and privilege to express my deep sense of gratitude to my research supervisor, Prof. S. Ndlovu for the many inspirational discussions, insight, constant encouragement and technical guidance throughout the course of my doctoral studies. My sincere gratitude goes to my co-supervisor, Prof. N. Sacks for her many helpful suggestions, scholarly criticism and technical support throughout this work.

My thanks are also due to:

- Prof. G. Simate
- Prof. V. Sibanda
- Bruce Mothibedi
- Caleb Phali
- Members of the Metal Extraction and Recovery Group for their invaluable support, co-operation and team work

The National Research Foundation (NRF) and the Department of Science and Innovation (DSI) of South Africa are gratefully acknowledged for their financial contribution to this research work.

The DSI-NRF Centre of Excellence in Strong Materials (CoE-SM) is gratefully acknowledged for its financial support towards this research work.

I would like to thank my colleagues, friends and relatives for their unrelenting support and encouragement.

I would like to express my special thanks to my wife Alice, children Ettric, Lerato and Elvin, brother Kebby, sisters Alice and Joyce who have supported me with affection, inspiration and encouragement throughout my studies.

And finally, I am grateful to God Almighty from whom all blessings flow. I am eternally grateful for His sustaining grace and for granting me strength and ability to complete my studies.

"In Christ alone, my hope is found; He is my light, my strength and my salvation"

Table of Contents

LIST OF FIGURES

LIST OF TABLES

List of symbols

Δ	Change of a quantity
E	Energy (J)
G	Gibbs free energy (J)
H	Enthalpy (J)
S	Entropy (J/K)
T	Temperature (K)
p	Pressure (Pa)

A	surface area (m^2)
E_a	Activation energy (J/mol)
M	Molarity, concentration of solution, moles per litre (Mol/L)
E	Potential (V)
Eh	Electrode potential (V)
E^o	Standard potential (V)
F	Faraday constant (96 489 A/mol)
pH	Potential of hydrogen
Eh	Electrode potential
I_P	Peak current
I_A	Average current
K_r	Rate constant
R	Ideal gas constant (8.314 J/K.mol)
t	Time (s)
T	Absolute temperature (K), temperature (°C)
T_{off}	pulse off time (s)
T_{on}	pulse length (s)
wt.%	weight percentage
xi	i^{th} value in a data set
ρ	Density (g/cm^3)
kWh	kilo Watt hour ($3.6x10^6$ J)
pK_a	negative log of a dissociation constant
ΔG°	Standard conditions Gibbs free energy
ΔH°	Standard conditions enthalpy (J)
ΔS°	Standard conditions entropy (J/K)

List of Abbreviations

ASTM	American Society for Testing and Materials
DC	direct current (A)
OCP	open circuit potential (V)
PED	pulse (d) electrodeposition

SD	standard deviation
SHE	standard hydrogen electrode

CHAPTER ONE

INTRODUCTION

1.1 Background

Cemented tungsten carbides, also known as hardmetals, are a range of composite materials, which consist of hard tungsten carbide (WC) particles bonded together by a metallic binder. Cemented carbides are made using sintered compositions of one or more metallic carbides; usually the carbides of tungsten (W), Ti, Ta and Nb, with an auxiliary binding metal of the iron group, usually Co and to a lesser extent Ni (Trent, 1946; Exner, 1979).

The tungsten metal used in the cemented carbide manufacturing process is sourced from both primary as well as secondary resources (**Fig.1.1**). Primary resources contribute about 66% from virgin tungsten (Bhosale et al., 1990). Secondary resources contribute about 34% of which 10% is from scrap generated as rejects during processing and about 24% from used or worn-out tools and wear parts from industry. It has been estimated that reject material generated from the production process, worn-out or used tools and wear parts from industry, typically contains 40-95% tungsten (Bhosale et al., 1990; Trent, 1946). This indicates that tungsten-based scrap recycling is vital to the supply and demand of tungsten raw materials. Surveys and forecasts show that tungsten carbide scrap will become an increasingly important source of raw material for the worldwide tungsten industry (Kimball, 2014).

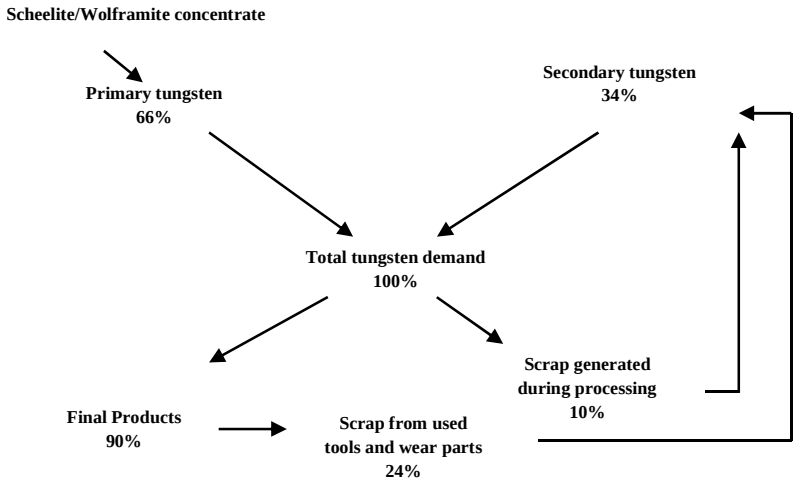

Fig.1.1: Tungsten Flow Sheet (Bhosale et al, 1990)

Although South Africa has no exploitable tungsten reserves, it has tungsten processing industries that manufacture tungsten-based products. The tungsten raw materials used in these industries are sourced from countries abroad. The potential of developing efficient alternative methods of recycling tungsten-based scrap would optimize the utilization of local secondary tungsten resources and generate revenue. For countries without tungsten reserves, the recycling of tungsten-based scrap metal has the potential to cut down on import costs by about 20-30% and lower raw material costs by about 15-50% (Lassner and Schubert, 1999; Bhosale, et al., 1990). Thus, tungsten resources have the potential to reduce, to a considerable extent, South Africa's dependence on foreign supply of tungsten raw materials.

The high value and strategic importance and impact of tungsten on the global economy (**Table1.1**), coupled with the need for energy conservation, resource preservation, and stricter implementation and enforcement of environmental legislation, has caused the scientific community to focus on finding innovative and alternative methods of recycling tungsten-based secondary material.

Table 1.1: Tungsten Production and Price Estimates

Scheelite/Wolframite Concentrate Price Estimate: (USD11, 500-14, 500/tonne, >65% WO_3) (CTOMS, 2019)
Annual Concentrate Production Estimate: ~86,400 tonnes (Kimball, 2017) = USD1.13billion
Tungsten Finished Products Price Estimate Broad range: USD25 – 2,500/Kg Majority: USD100 – 350/Kg (Midwest Tungsten Service, 2019)

As the major constituents of hardmetal scrap, W and Co are amenable to metallurgical and chemical processes of recovery. They could be re-used if the cobalt bond between the carbide and the cobalt metal binder could be removed (Barnard, 1971). Currently, the zinc process is

widely used to recycle cemented carbide scrap, but this method is highly energy intensive and requires costly equipment (Gurmen, 2005). However, selective leaching of the cobalt binder phase could be a potential alternative to the zinc process in view of lower energy consumption and environmental impact (Gurmen, 2005). The challenge with conventional acid leaching methods, though, is slow dissolution kinetics (Barnard, 1971) which some authors (Lin et al, 1995; Guedes de Carvalho and Neves, 1992) have attributed to tungsten passivation. It is, therefore, postulated that if the use of an organic chelating agent can solubilize tungsten in a complexation reaction, then this could eliminate the passivation effect which in turn would allow cobalt dissolution, using an inorganic acid, to occur without obstruction.

Therefore, this study is focused on using sulphuric acid, an inorganic acid, in conjunction with lactic acid, an organic chelating agent, to selectively and optimally extract the cobalt binder phase as well as recover tungsten monocarbide (WC) solid particles from WC-6wt%Co manufacturing scrapped inserts.

1.2 Problem Statement

Although the recycling of cemented tungsten carbide scrap metal has been the subject of much study, published information on the complexation agent-aided acid leaching of the scrap metal appears to be non-existent. Therefore, the current study sought to address this scientific knowledge gap and to provide a novel approach to recycle hardmetal scrap. The dissimilar cemented carbide phases, WC and Co, when leached using sulphuric acid, an inorganic acid, in conjunction with lactic acid, an organic chelating agent, will yield WC and Co to achieve optimum recovery of both valuable constituents from cemented carbide secondary material.

1.3 Novelty

The conventional method of leaching cemented carbide (WC-Co) was based on cobalt dissolution using inorganic acids. This reaction, however, was adversely affected by the formation of insoluble tungsten precipitates. The presence of tungsten precipitates hindered the diffusion of reactants and products. The conventional leaching method, nevertheless, was modified to make it optimal by utilizing a combination of an inorganic acid such as sulphuric acid and an organic acid such as lactic acid. Lactic acid is an organic chelating agent with a high selectivity for tungsten complexation and solubilization. The two acids possessing significantly

different chemical properties, when combined, produced a composite lixiviant with characteristics different from the individual acids. The modification of replacing an inorganic acid with a composite lixiviant to enhance the leachability of the cobalt in the cemented tungsten carbide is the novel part of this study. In this work, process conditions were optimized and high cobalt extraction efficiencies were achieved within short leaching times. In addition, key valuable constituents, WC and Co, were successfully recovered from cemented tungsten carbide-cobalt secondary material. The recovered materials are highly valuable and are of strategic importance to South Africa as well as the global economy.

1.4 Research Objectives

The aim of this study was to develop a cemented tungsten carbide-cobalt (WC-Co) secondary material recycling method, which is energy and cost efficient, environmentally friendly and converts all the scrap metal constituents into valuable products. This aim was achieved by the following objectives:

- Investigation of parameters which promote cobalt dissolution in WC-Co using the acid leach process
- Investigation of the response characteristics of WC-Co during leaching so as to understand the limitations of the recovery process
- Derivation of a conceptual reaction kinetic model for WC-Co dissolution
- Identification and optimization of factors which influence WC-Co dissolution
- Purification and enrichment of WC-Co leach liquor using a solvent extraction process
- Recovery of Co from WC-Co leach liquor using an electro-recovery process
- Recovery of W from WC-Co leach liquor by precipitation
- Determination of the cost implications of the overall recovery process
- Determination of the conditions which were favourable for acid recycling in the acid leach process

1.5 Research Methodology

The following major tasks were involved in the research methodology for this study: literature review, experimental design, laboratory testing and laboratory test data analysis, drawing conclusions from results and recommendations.

1.6 Thesis Lay out

This section provides a snapshot of the chapters and sections that are covered in this thesis, which comprises eleven chapters. Each chapter begins with a short introduction that highlights the areas that are addressed in various sections of the chapter. A summary is provided at the end of each chapter to focus the reader on what has been addressed and also guides the reader to subsequent chapters. A schematic representation of the thesis layout is summarized in the flowchart in **Figure 1.2**.

Chapter 1 *Introduction:* This chapter provides the motivation for the research, the problem statement, and the overall objectives of the study.

Chapter 2 *Literature Review:* This chapter sets out to review related literature on the recycling of cemented tungsten carbide scrap metal. The chapter includes general knowledge on cemented tungsten carbide production and microstructure and the current thermal, physical, chemical, electrochemical and electrolytic means of recovery.

Chapter 3 *Experimental Design:* This chapter describes the materials and methods used in the study.

Chapters 4-8: These chapters describe the laboratory tests and findings as depicted in **Figure 1.2**.

Chapter 9 *Process Flowsheet Development:* This chapter focuses on the development of the general flow of unit processes, equipment used as well as techno-economic evaluation of the process.

Chapter 10 *Conclusions and Recommendations:* This chapter concludes the thesis with a summary of the findings and recommendations.

References to all articles used in the study are provided at the end of each chapter. The appendix section provides other important data.

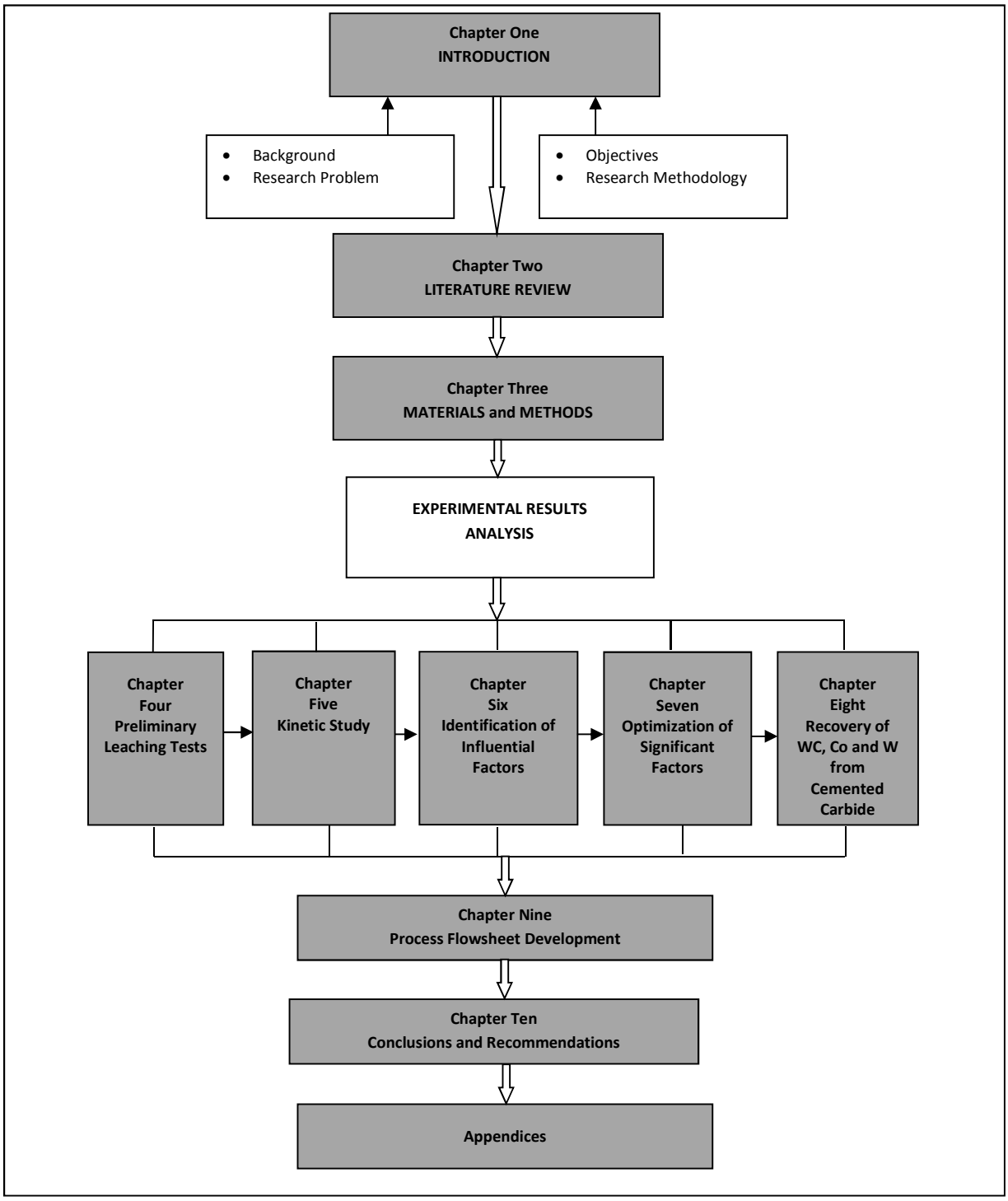

Fig.1.2: Thesis Layout

1.7 Summary

In this introductory chapter, the background, problem statement, novelty and objectives of the research study were discussed. This was followed by a short description of the research methodology and thesis layout. The next chapter reviews relevant literature.

1.8 References

Barnard, P.G., 1971. Reclamation of Refractory Carbides from Carbide Materials. USA, Patent No. 3, 595, 484.

Bhosale, S.N., Mookherjee, S., Pardeshi, R.M., 1990. Current Practices in Tungsten Extraction and Recovery. High Temperature Materials and Processes, Vol. 9, Issue 2-4.

CTOMS., 2019. Tungsten concentrate price. http://news.chinatungsten.com/en/tungsten-price/tungsten-concentrate-price.

Exner, H.E., 1979. Physical and Chemical Nature of Cemented Carbides. International Metals Reviews, Vol. 4, pp. 149-173.

Guedes de Carvalho, R.A., Neves, O.R., 1992. Leaching of Scheelite ($CaWO_4$) Under Quasi-Stagnant Solution Conditions. Hydrometallurgy, Vol. 28, pp. 45-64.

Gurmen, S., 2005. Recovery of Nano-Sized Cobalt Powder from Cemented Carbide Scrap. Turkish Journal of Engineering and Environmental Science. Vol.29, pp. 343-350.

Kimball, S.M., 2014. Mineral Commodity Summaries. United States Geological Survey, Reston, Virginia.

Kimball, S.M., 2017. Mineral Commodity Summaries. United States Geological Survey, Reston, Virginia.

Lassner, E., Schubert, W.D., 1999. Tungsten: Properties, Chemistry, Technology of the Element, Alloys and Chemical Compounds. Kluwer Academic/Plenum Publishers, New York.

Lin, J.C., Lin, J.Y., Lee, S.L., 1995. Process for Recovering Tungsten Carbide from Cemented Tungsten Carbide Scraps by Selective Electrolysis. US, Patent No. 5,384,016.

Midwest Tungsten Service., 2019. Tungsten and costs. https://www.tungsten.com/tips/tungsten-and-costs/. Retrieved, 5 December 2019.

Trent, E.M., 1946. Process of Separating Hard Constituents from Sintered Hard Metals. US Patent No. 2,407,752.

CHAPTER TWO

LITERATURE REVIEW

The aim of this literature review is to give a general overview of cemented tungsten carbide constituents, sources, production processes, microstructure and recycling methods. In this review, the importance of selecting a route for recycling cemented tungsten carbide secondary material, based on its chemical and physical characteristics, and subsequent preference towards an acid leach process is highlighted. The chapter ends with a review of important hydrometallurgical processes which will be used in the study.

2.1 Cemented Tungsten Carbides

Cemented tungsten carbides are widely employed in the manufacturing, petrochemical, aerospace, construction, gas drilling and mining sectors as tools and wear parts (Smith, 1942; ITIA, 2010). Owing to its unique physical and chemical properties, tungsten has become one of the most strategic and critical metals vital to modern technology and industry. Cemented carbide makes up approximately 60% of all industrial products from tungsten (Law-West and Perron, 2009; ITIA, 2010).

Due to their unique properties, cemented carbides have long proven their superiority over super hard materials in certain high-tech tooling and engineering applications. The super hard materials namely diamond, the hardest of all, followed by Cubic Boron Nitride (CBN), polycrystalline Diamond (PCD) and ceramics (Al_2O_3, SiC, SIALON etc.) all have very low toughness and are thus, prone to brittle fracture (Sandvik Hyperion, 2016). Cemented carbides, on the other hand, have a unique combination of high hardness and good toughness and thus, constitute the most versatile hard materials group for engineering and tooling applications (Exner, 1979; Sandvik Hyperion, 2016).

2.1.1 Production Processes

The chief economic minerals of tungsten are wolframite [(Fe, Mn) WO_4] and scheelite ($CaWO_4$) (Ilhan et al., 2013). Generally, tungsten minerals are digested with HCl, NaOH or $NaCO_3$ solutions in order to leach out tungsten (Paulino et al., 2012; Amer, 2000; Srinivas et al., 2000;

Kahruman and Yusufoglu, 2006; Gurmen et al, 1999). The leach solutions undergo several purification steps to produce ammonium paratungstate (APT), the most important precursor for tungsten intermediate products being tungsten trioxide (WO_3), tungsten blue oxide ($W_{18}O_{49}$), tungstic acid (H_2WO_4) and ammonium metatungstate ($(NH_4)_6H_2W_{12}O_{40}$). The digestion and purification steps are illustrated in **Fig.2.1**.

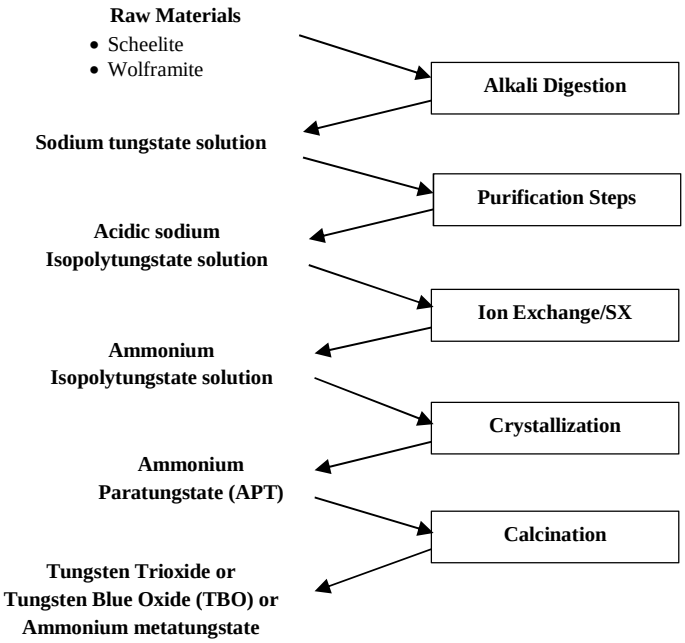

Fig.2.1. Tungsten Hydrometallurgy-Modern Process (Lassner and Schubert, 1999)

Tungsten trioxide (WO_3) from the purification step (**Fig.2.1**) undergoes hydrogen reduction to produce metallic tungsten (W) powder according to the reaction:

$$2WO_3 + 6H_2 \rightarrow 2W + 6H_2O \qquad (2.1)$$

At temperatures between 1,300 and 1,700°C, in a carburization furnace and under a hydrogen atmosphere, metallic tungsten (W) powder is contacted with high-purity carbon black (C) powder. Under these conditions tungsten reacts with carbon to produce granular tungsten monocarbide (WC) according to the reaction (Lassner and Schubert, 1999):

$$W + C \rightarrow WC \qquad (2.2)$$

The granular tungsten monocarbide (WC) produced from the carburization furnace is used as feed material for the production of cemented tungsten carbide (WC-Co) hardmetal using a

manufacturing process shown in **Fig.2.2**. The figure displays the whole manufacturing process from carburization to the finished hardmetal product.

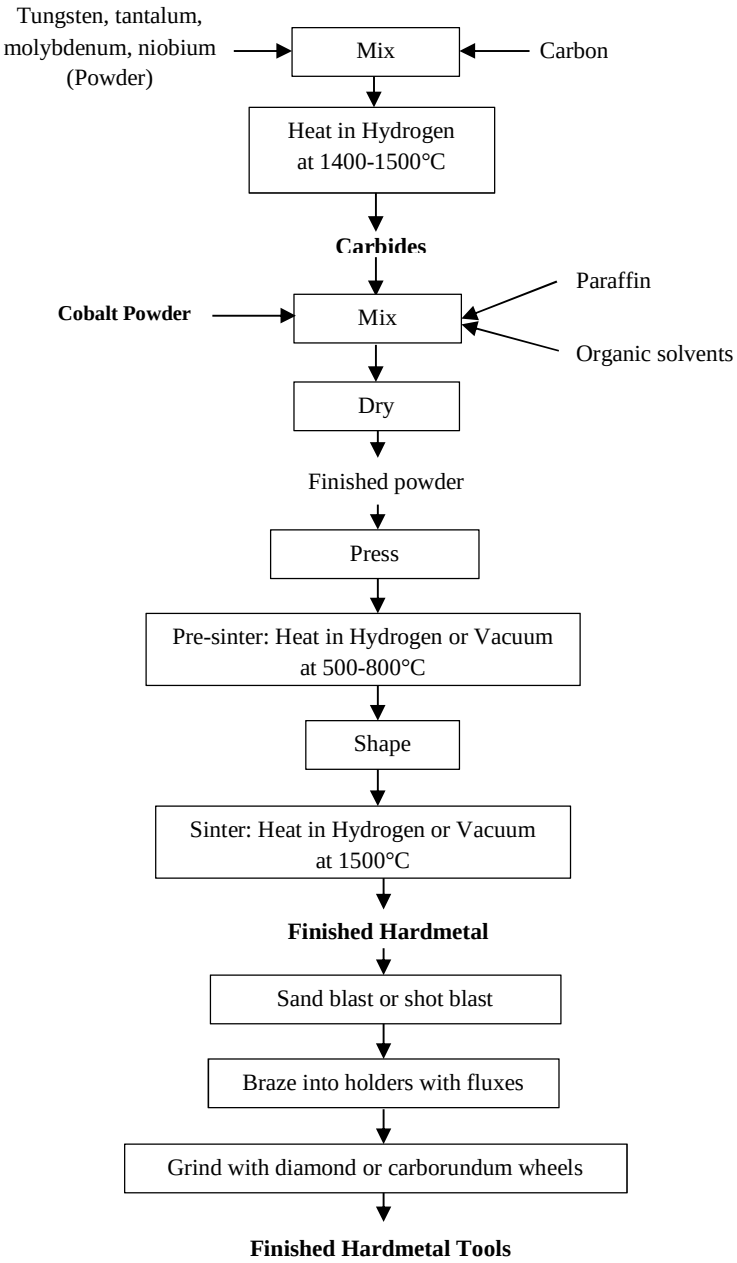

Fig.2.2. Steps in the manufacture of hardmetal tools (Kusaka et al, 1986)

Other than WC, other refractory carbide phases of the transition metals used in the cemented carbide manufacturing process include TiC, TaC, Cr_3C_2 or Mo_2C. These refractory carbides are combined with a tough binder metal, most often Co, in some cases Ni or other metals from the Fe group (Exner, 1979) to produce cemented carbide. For cemented tungsten carbide, the term

"cemented" refers to the tungsten carbide (WC) particles being captured in the metallic binder metal (Co) and "cemented" together, forming a covalent bond between the WC grains and the cobalt metal (e.g. WC-Co) during the sintering process (General Carbide, 2016).

A notable feature of the sintering process is tungsten carbide solubility in the cobalt binder metal. At the liquid-phase sintering temperature of 1,500°C, tungsten carbide undergoes dissolution according to the reaction (Exner, 1979; Rudiger et al, 1971):

$$WC \rightarrow W + C \qquad (2.3)$$

As a consequence of this reaction (**Eqn. 2.3)**, the cobalt binder is, therefore, more appropriately called a 'cobalt-based alloy' binder (W-C-Co) because it contains some amount of dissolved tungsten (Ghandehari and Schussler, 1980; Suzuki and Kubota, 1966; Kellner et al, 2009; Viswanadham et al, 1983; Exner, 1979). The extent to which the tungsten dissolution occurs is, however, not very well defined.

Carbides and binders are graded into three categories. In metallurgical terms, WC is referred to as the alpha (α) phase; the binder metal(s) (Co, Ni etc.) is the beta (β) phase; and any single or combination of other carbide phases for example, TiC, TaC, NbC, Cr_3C_2 or, Mo_2C, etc., is the gamma (γ) phase. The gamma phases are carbides of a cubic lattice. The three phases, α, β and γ, can be combined using different permutations depending on the desired characteristics of the end-use product. **Table 2.1** shows various cemented carbide types obtained from a combination of α, β and γ phases using different permutations. Carbides based on WC-Co, (α+β), compositions are referred to as 'straight or machine grade carbides' (Sandvik Hyperion, 2016). The current research work is based on the straight or machine grade (α+β) type of cemented carbide.

Table 2.1: Cemented Carbide Types

Cemented Carbide Types					
α-Phase	β-Phase (Binder)	γ-Phase	Composition	Grade	Properties
WC	**Co**	-	**WC-Co**	**Binary phase alloy (Straight/Machine grade)**	• *Hardness,* • *Fracture toughness* • *Wear resistance* • *Impact resistance*
	Co	TiC	WC-Co-TiC	Ternary phase (α+β+γ) alloy	
	Co	TaC	WC-Co-TaC	Ternary phase (α+β+γ) alloy	
	Co	Cr_3C_2	WC-Co-Cr_3C_2	Ternary phase (α+β+γ) alloy	
	Co	Mo_2C	WC-Co-Mo_2C	Ternary phase (α+β+γ) alloy	

2.1.2 Alloy Constituents

Tungsten and cobalt, two major components in cemented carbide (WC-6wt.%Co), are valuable and strategic metals known for their many industrial applications.

One of tungsten's most important uses is in the production of cemented tungsten carbide, also referred to as cemented carbide or hardmetal (Sandvik Hyperion, 2016; Exner, 1979). As a valuable metal, tungsten's strategic importance in the world is reflected by its steady increase in global demand (**Figure 2.3**) (Smith, 1942; Shield, 2011; European Commission, 2014; EASAC Report, 2016; Godlewska and Grohol, 2017; USGS, 2017). This trend has mainly been driven by the metal's unique properties utilized in the production of numerous end-use tools and wear parts like rocket engine nozzles, drill bits and inserts, punches and dies, saw blades, valves and cutters etc. The physical and chemical properties of tungsten and its alloys, for instance, their excellent cutting and wear resistance, serve to provide important end-use products for industrial consumption.

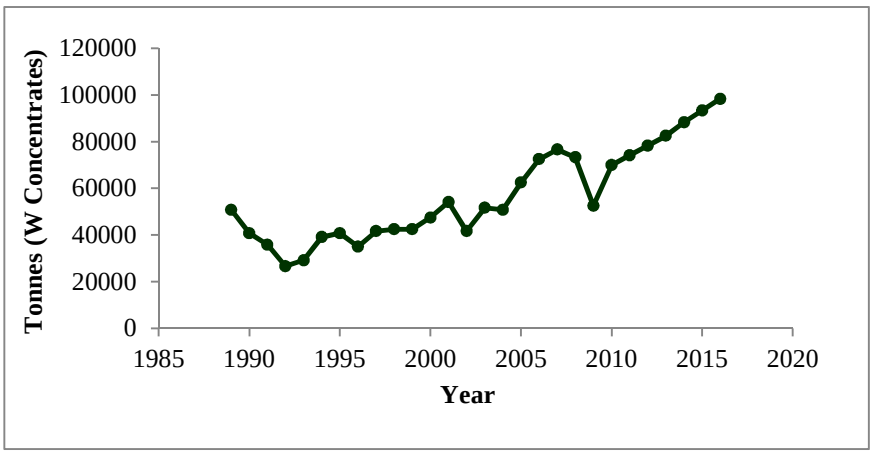

Fig.2.3. Tungsten demand by year (Source: ITIA, 2017)

Tungsten is relatively low in abundance, constituting only about 0.00013% of the earth's crust and is ranked 18th in quantity amongst the metallic elements (Smith, 1942; Shield, 2011; Barnard et al, 1971; Sandvik Hyperion, 2016). As a finite resource, tungsten's sustainability over the long term is of prime interest to all stakeholders. Surveys and forecasts show that cemented tungsten carbide scrap will continue to be an increasingly important source of raw materials for the worldwide tungsten industry (Kimball, 2014). Therefore, in line with the concept of sustainable development, it is essential that more efficient, environmentally-friendly and economic recovery and re-use of the world's finite tungsten resources be achieved (Smith, 1942; Lassner and Schubert, 1999).

Cobalt is an essential element for many important applications in today's society due to its many unique properties. The importance of cobalt to rechargeable batteries, electronics, catalysts, alloys and healthcare has resulted in the metal being referred to as a technology enabling element (Cobalt Institute, 2019). The metal's unique physical-chemical properties translate into several key characteristics that have made cobalt one of the most strategic and critical metals essential to modern technologies. Cobalt produces many vibrant colours, is wear resistant, oxidation resistant, conducts electricity and is ferromagnetic. These properties have led to cobalt's use in several industrial applications integral for a greater quality of life and a sustainable future (Cobalt Institute, 2019).

2.1.2.1 Tungsten

Tungsten is a greyish white lustrous metal with a body-centred cubic crystalline structure (Autler et al, 1965); electronic configuration, [Xe] $4f^{14}5d^{4}6s^{2}$; atomic number, 74; valence, +2, +3, +4, +5, +6 and +7; the +6 state is most common; in the +4, +5 and +6 state, tungsten forms a variety of complexes; tungsten is a metal of the transition series; atomic mass, 183.84g; specific gravity, 19.2 at 20°C; melting point, 3,422°C and boiling point, 5,930°C. Elemental tungsten resists attack by oxygen, acids, and alkalis (Emsley, 1991). Tungsten typically combines with oxygen to form tungstic oxide, WO_3, which is insoluble in aqueous acidic media but dissolves in aqueous alkaline solutions to form tungstate ions, WO_4^{2-} and WO_5^{2-} (Chen, 2013).

Of all metals in pure form, tungsten has the highest melting point, the lowest vapour pressure (at >1, 650 °C), the highest tensile strength (Hammond, 2004) and the lowest coefficient of thermal expansion. These properties originate from the strong covalent bonds formed between tungsten atoms by the 5d electrons (Lassner and Schubert, 1999). The main markets for tungsten are the cemented carbides; steel alloys; lamp industry; electronic and electrical industries, and chemical applications.

2.1.2.1.1 Refractory carbide phase

There are two predominant phases in binary cemented carbide (WC-Co) alloys namely, the cobalt binder phase and the tungsten carbide (WC), hard phase. The tungsten carbide (WC) phase is the basic and most widely used hard component of cemented carbide. Tungsten, in combination with carbon, forms tungsten carbide (WC) which counts as a refractory carbide defined by a melting point of >1800°C, very high hardness and good chemical resistance. Tungsten carbide can exist in two phases, WC and W_2C, and have hardness of 2000-2700HV (Upadhyaya, 1998; Totalmateria, 2020). Tungsten carbide powders are typically monocrystalline WC with carbon content ≈ 6.1% or eutectic WC/W_2C with carbon content ≈ 4% (Totalmateria, 2020). Typical properties of tungsten and tungsten carbide are presented in **Table 2.2**. A schematic view of tungsten carbide grains located in cemented carbide hardmetal is shown in **Figure 2.4**. The refractory carbide phase in the cemented carbide hardmetal used in the current study is monocrystalline WC.

Table 2.2: Tungsten and tungsten carbide properties (Totalmateria, 2020)

Type	Melting Point	Density
W	3410°C	19.3gcm^{-3}
WC	2870°C	17.2gcm^{-3}
W_2C	2730°C	15.8gcm^{-3}

2.1.2.2 Cobalt

Cobalt is a hard, lustrous, silver-gray metal with a hexagonal close-packed (hcp) crystallographic structure; electronic configuration, [Ar] $3d^7$ $4s^2$; atomic number, 27; valence, +2, +3; cobalt is a metal of the transition series; atomic mass, 58.93g; specific gravity, 8.90 gcm^{-3} at 20°C; melting point, 1,495°C and boiling point, 2,927°C. At ordinary temperatures, cobalt reacts slowly with mineral acids, and very slowly with moist, but not with dry, air. Cobalt metal is weakly reducing and passivates under oxidation by forming an oxide film (Housecroft and Sharpe, 2008). Cobalt forms insoluble hydroxides in alkaline solutions (Garcia et al, 2008). Cobalt has ferromagnetic properties and exists in two allotropic modifications; the hexagonal close-packed (hcp) α phase and the face centred cubic (fcc) β phase (Cobalt News, 1998; Dille et al, 1997). The β phase is only stable at temperatures above 417°C (Akre, 2008).

Common oxidation states of cobalt include the +2 and +3. As an amphoteric oxide (Earnshaw and Greenwood, 1997), cobalt compounds with oxidation states ranging from −3 to +5 are also known. A common oxidation state for simple compounds is +2 (cobalt (II)). The cobalt (II) salts form the pink-coloured metal aquo complex $[Co(H_2O)_6]^{2+}$ in water.

Cobalt has a diverse market. The main market is high-performance alloys for gas turbines and aircraft jet engines (Shedd, 2006; Donachie, 2002); cobalt-based alloys like Vitallium (Co-Cr-Mo) for making orthopedic and prosthetics parts (Disegi, 1999; Michel et al, 1991); alloys of Cr, Co and WC for making cutting tools and wear parts (Campbell, 2008); special alloys of Al, Ni, Co and Fe, known as Alnico, and of samarium-cobalt for making permanent magnets (Luborsky et al, 1957).

Rechargeable Lithium batteries (LiBs) have received a lot of attention and have a market value almost 10 times that of the non-rechargeable types (Saxman, 2017). The most widely employed cathode material is $LiCoO_2$, typically comprising ~28 mass% of a LiB (Xu et al, 2008). The $LiCoO_2$-based rechargeable batteries are used in mobile devices, electric cars, laptops, portable medical equipment, and other devices (Shilling, E, 2017; Hawkins, 2001; Hart and Sarkissian, 2016). The global lithium-ion battery market has been estimated at $30 billion in 2015 and an increase is predicted to over US$75 billion by 2024 (The Guardian, 2019). Several cobalt compounds are oxidation catalysts. Cobalt is used as a catalyst in the Fischer-Tropsch process for the hydrogenation of carbon monoxide into liquid fuels (Khodakov et al, 2007). A catalyst derived from Co-Mo is used in the hydrodesulphurization and impurity removal from petroleum (Hawkins, 2001). Other cobalt uses include pigmentation of glass, glazes, and ceramics (Witteveen and Farnau, 1921; Venetskii, 1970); cobalt-60 (Co-60 or ^{60}Co), a gamma-ray source radioisotope (Audi et al, 2003; Mandeville and Fullbright, 1943); cobalt (II) sulphate, used in storage batteries and electroplating baths and an additive to soils and animal feeds ; cobalt acetate, a precursor to oil drying agents and catalysts that allow paints and varnishes to harden (Donaldson and Beyersmann, 2005).

2.1.2.2.1 Binder phase

The binder phase is the second predominant metallic phase in cemented carbides. Often Co, in some cases Ni or other metals from the Fe group, is used most extensively as the bonding metal in WC-based hardmetals (Exner, 1979). The binder is present in the microstructure as a continuous thin film separating the carbide particles (Rettenmayer et al, 1988; Roebuck and Almond, 1988). Some researchers have advanced the view that at the liquid-phase sintering temperature of 1,500°C, tungsten carbide undergoes dissolution. As a consequence of this reaction, the cobalt binder is, therefore, more appropriately called a ‘cobalt-based alloy’ binder (W-C-Co) because it contains some amount of dissolved tungsten (Ghandehari and Schussler, 1980; Suzuki and Kubota, 1966; Kellner et al, 2009; Viswanadham et al, 1983; Exner, 1979). Upadhyaya (1998) found that in WC-Co alloys, the binder phase is actually a dilute cobalt alloy (Co-W-C) containing tungsten and carbon as solutes and can exist in either of two hcp or fcc allotropic forms or a mixture of both. Nevertheless, for the hardmetals sufficiently rich in Co, a Co skeleton forms in the sintered product in addition to the carbide skeleton (Upadhyaya, 1998).

The tungsten carbide particles are captured in the metallic binder material and "cemented" together, forming a metallurgical bond between the WC particles and the binder (e.g. WC-Co) during the sintering process (General Carbide, 2016). A schematic view of the binder phase in cemented carbide hardmetal is shown in **Figure 2.4** and a three dimensional view in **Figure 2.5.** The binder phase in the cemented carbide hardmetal used in the current study is Co metal.

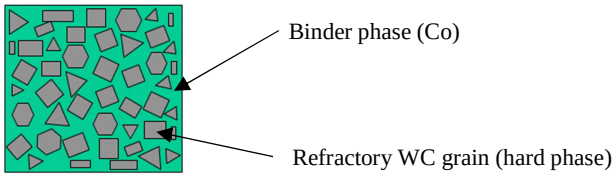

Fig.2.4: A schematic view of tungsten carbide grains and the binder phase located in cemented carbide

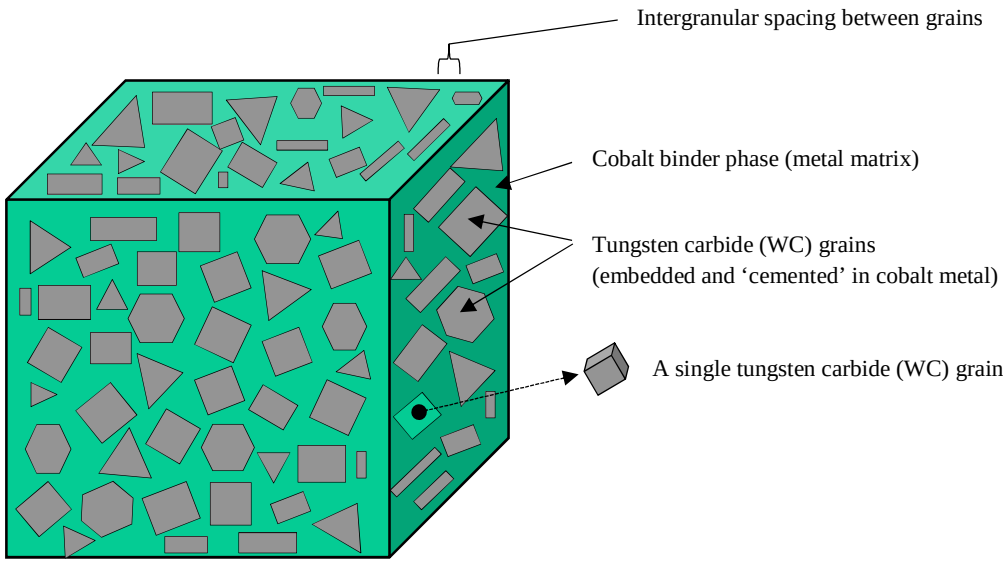

Fig.2.5: A three-dimension schematic view of tungsten carbide grains embedded in the Co binder metal

2.1.2.3 Eta phase

Eta (η) phase is a ternary compound of tungsten, cobalt and carbon (W-Co-C) which forms as a result of carbon deficiency in WC-Co alloys and therefore exists as a third phase other than the carbide and binder phase (Upadhyaya, 1998). The 'η' phase is known to exist in two forms as

M_6C carbide ranging from $W_{3.2}Co_{2.8}C$ to W_2Co_4C (Hellsing et al, 1983) or $M_{12}C$ carbide of fixed composition W_6Co_6C (Johansson, 1978).

Both types of phases, M_6C and $M_{12}C$, are indistinguishable physically. Johansson (1978) showed that M_6C represents a metastable form which can undergo in-situ decomposition from $M_6C \rightarrow \beta + M_{12}C + WC$ by a fairly sluggish reaction. However, Bolton and Keely (1982) suggested that, with a relatively fast cooling rate, in commercial tungsten carbide alloys, the presence of M_6C is more probable than that of $M_{12}C$.

Freytag and Exner (1977) explain that the extent to which the 'η' phase forms in WC-Co alloys depends on the carbon deficiency level. At minor carbon deficiency levels, the 'η' phase is not produced at the sintering temperature but forms on subsequent cooling: WC + liq. → WC + η + liq. In doing so, it occurs as isolated areas in which considerable amounts of WC and the binder phase are consumed during its growth. Partially dissolved and rounded WC grains are associated with such 'η' phase areas. Further cooling can lead to a peritectic decomposition of the 'η' phase, η + liq. → WC + β. The cooling rate and carbon content determine how much of the 'η' phase is retained at room temperature. For instance, minor deficiency levels could lead to a complete disappearance of the 'η' phase on cooling, whereas the 'η' phase is retained at high carbon deficiency levels regardless of the cooling rate.

Upadhyaya (1998) was a proponent of the view that, with fairly high levels of carbon deficiency, the 'η' phase is present at the sintering temperature and is retained after cooling. It is therefore, generally agreed that, the final 'η' phase distributions and morphologies are controlled by the carbon content developed during sintering and cooling. Angelo and Subramanian (2009) explained further, that if the ratio of W:C is <1, carbon in the form of graphite which leads to porosity and product deterioration precipitates. When the ratio W:C is >1, the η (eta)-phase precipitates and leads to embrittlement of the alloy (Ellis, 1970; Gabriel et al, 1986; Angelo and Subramanian, 2009). The brittle η (eta}-phase reduces the transverse rapture strength of the WC-Co alloys. The morphologies of the eta phase, which range from finely dispersed particles at low carbon deficiency to large areas of 'η' phase in highly carbon deficient alloys, are depicted in **Figures 2.6** and **2.7**.

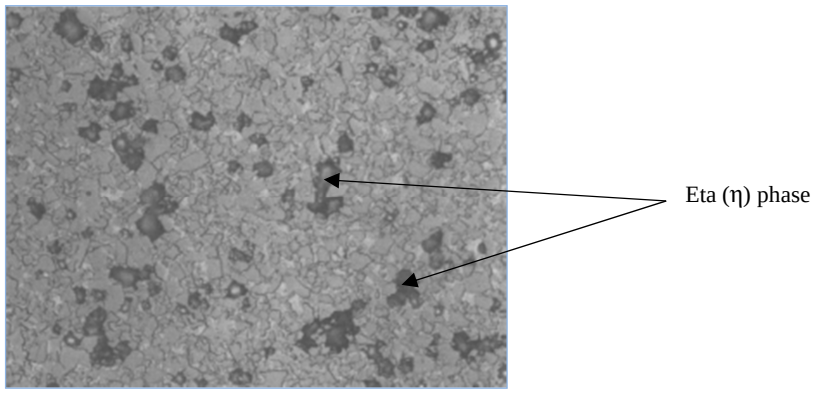

Figure 2.6: Microstructure of cemented carbide (85.5WC-12Co-3.5Cr) showing well dispersed eta phase, (WC, grain size 3μm). Murakami etching (x1500) (courtesy, Dr. H. Pastor, CERMep, Grenoble)

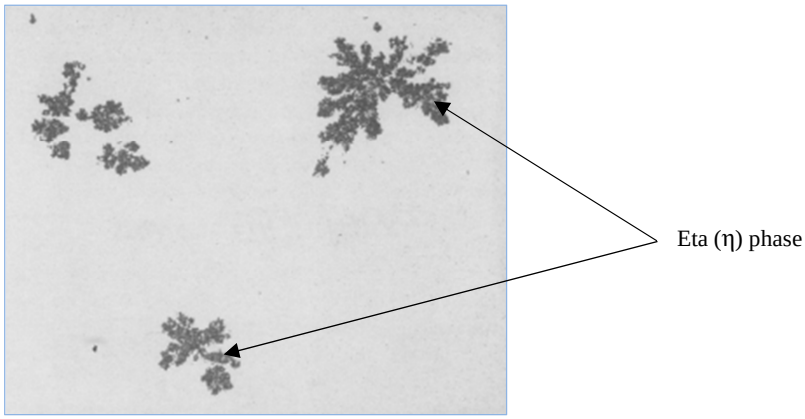

Figure 2.7: Microstructure of cemented carbide showing eta phase, light Murakami etching (10s), x1500 (courtesy, Dr. H. Pastor, CERMep, Grenoble)

In leaching processes, the presence of the 'eta' phase could lead to intensified formation of insoluble reaction products within cemented carbide channels. The insoluble products exacerbate passivation. Alar et al (2017), in their study, observed that the 'eta' phase enhanced the formation of a passive layer on the surface of cemented carbide samples thereby reducing the tendency for the sample to dissolve while increasing the stability of the oxides being formed.

2.1.2.4 Precipitates

Precipitates, generally observed in the binder phase of cemented carbides, are non-metallic impurities, graphite, carbides, and intermetallic compounds precipitated during cooling or heat treatment in the solid state (Upadhyaya, 1998). If the ratio of W:C is <1, carbon precipitates in

the form of graphite which leads to porosity and product deterioration. According to Freytag and Exner (1977), in technical WC-Co hardmetals, a three phase region (η + WC + liquid) exists, even if the carbon content corresponds to stoichiometric WC. In quenched alloys, this phase retains and lowers the magnetic saturation. But if the alloy is cooled slowly, the 'η' phase reacts with the carbon supersaturated in the binder to form WC and Co_3W. Hoffmann and Mohs (1974) suggest that the eta-carbide W_6Co_6C precipitates from the supersaturated solution, after cooling from the sintering temperature initially as Co_2W_4C, change composition to the more cobalt rich variations, Co_3W_3C and Co_4W_2C, then finally decays into an intermetallic compound, Co_3W. From the phase diagram of W-C-Co system, this intermetallic should not be present at any temperature. However, a local concentration gradient can arise due to slow diffusion of tungsten in cobalt. It is more likely, according to Johnsson (1972) and Lai and Jinhui (1985), that the transformation of the cubic into the hexagonal phase is the reason for the formation of the intermetallic due to the sudden decrease of tungsten solubility in the binder phase. If present in the binder phase, the effect of precipitates during cemented carbide leaching could be akin to that of the 'eta' phase.

2.1.3 Microstructural Parameters

2.1.3.1 Grain size

In the production of cemented carbides, the grain size of carbide phases is the most carefully controlled variable besides carbon control (Upadhyaya, 1998). Generally, two methods are used for the measurement of grain size on the planar surface (Roebuck, 1986). In the Jeffries method, a fixed area 'A' is superimposed on the image and the average area of each grain is calculated from:

$$\bar{A} = \frac{Total\ number\ of\ grains\ within\ fixed\ area + \frac{1}{2} grain\ intersected\ by\ boundary}{A} \qquad (2.4)$$

The Jeffries grain size is defined as $\sqrt{A}$

In the Heyn method, grain size is obtained by lineal analysis. A line is placed across the sample at random and the arithmetic mean linear intercept, or Heyn grains size $\bar{I}$, is derived from:

$$\bar{I} = \frac{L}{N} \qquad (2.5)$$

Where L is the total length of the line across WC and N is the number of WC grains traversed. The measurement of grain size using the Heyn technique can be performed using Image-J software (Schneider et al, 2018).

Cemented carbide grain sizes are typically categorized into 4 classes as illustrated in **Table 2.3**.

Table 2.3: Tungsten carbide grain size standard specification (Sandvik, 2005)

Standard Specification Grain Size (µm)	**>0.2**	**0.2-0.5**	**0.5-0.9**	**1.0-1.3**	**1.4-2.0**	**2.1-3.4**	**3.5-5.0**	**>5.0**
Classification	Nano	Ultra-Fine	Sub-micron	**Fine**	Medium	Medium Course	Course	Extra Course

According to Warren and Waldron (1972), and Lee and Gurland (1978), carbide grain size is directly related to the intergranular mean free path. In their treatises, the authors demonstrated that the smaller the grain size, the narrower the intergranular mean free path. It can be surmised, therefore, that, due to the narrow mean free path, it is more difficult for solvents to penetrate carbides of the smaller grain size class compared to the ones with a larger grain size. In his work, Trapp (1949) found that dissolution of the binder metal proved to involve real difficulty owing to the limited penetration achieved by solvents. In the current work, the WC grain size in the cemented carbide hardmetal used in the experiments is 1.0-1.3µm (‘fine’ size).

2.1.3.2 Contiguity

Contiguity is a quantitative measure of tungsten carbide particle skeleton formation in sintered WC-Co alloys. However, whether tungsten carbide particles form a continuous skeleton or not is still debatable (Exner, 1983). Cited by Upadhyaya (1998), Warren and Waldron (1972) suggested that in the majority of hardmetals, based on Gurland’s theory of particle contact, the carbide phase exists as a continuous skeleton both during and after sintering. The presence of a skeleton structure in WC-Co hard alloys is a generally supported view (Exner, 1979; Johnsson, 1973). Although there are still advocates of the view that all carbide grains are separated from each other by thin cobalt layers (Hanjered et al, 1986), a modified skeleton theory of contiguity is now more generally accepted (Exner and Gurland, 1970). Contiguity is defined as the ratio of grain boundary surface (WC/WC interface) to total surface (WC/WC interface + WC/Co

interface) (Gurland, 1959). Contiguity is therefore, a measure of the degree of contact between carbide grains. The contiguity equation is expressed as (Upadhyaya, 1998):

$$C_\alpha = \frac{2(N_L)_{\alpha\alpha}}{2(N_L)_{\alpha\alpha} + (N_L)_{\alpha\beta}} \quad (2.6)$$

Where, $(N_L)_{\alpha\alpha}$ and $(N_L)_{\alpha\beta}$ are the average number of intercepts per unit length of test lines with the traces of carbide-carbide grain boundaries and carbide-binder interface respectively. Alternatively, contiguity can be evaluated using mean values of carbide size and binder width (Gurland and Bradzil, 1955). The equation is presented as:

$$C_\alpha = 1 - \frac{\bar{I}_{carbide} V_{binder}}{\bar{I}_{carbide} V_{carbide}} \quad (2.7)$$

Where, $\bar{I}_{carbide}$ = mean intercept carbide size, $\bar{I}_{carbide}$ = mean free path of binder

$V_{carbide}$, V_{binder} = volume fractions of the different phases, $V_{carbide}$ = 1- V_{binder}

Contiguity varies with cobalt content, sintering time and temperature (Exner and Fischmeister, 1966; Warren and Waldron, 1972; Gurland, 1959; Lee et al, 1980). Contiguity decreases with increase in binder content (Warren and Waldron, 1972). This is ascribed to the fact that the probability of the spatial coincidence of carbides decreases with the increase of binder content (Upadhyaya, 1998). At the start of sintering, contiguity is high, but decreases and attains equilibrium at the end of sintering. Contiguity decreases with increasing temperature, but the impact of temperature on contiguity has been found to be relatively small (Warren and Waldron, 1972; Deshmukh and Gurland, 1986).

Contiguity studies in cemented carbides are imperative because this parameter has an effect on the mechanical properties of hardmetal. Contiguity is an important aspect to consider in cemented carbide leaching processes since it gives an indication of the ease with which a solvent can navigate narrow channels. The contiguity parameter also gives an indication of the ease with which a WC residue skeleton can be disintegrated. For instance, a low contiguity could result in a loose residue skeleton which can disintegrate easily and vice versa.

2.1.3.3 Mean binder free path

The mean binder free path, which depends on both the cobalt content and the particle size, is a measure of the thickness of the cobalt layer. The distribution of the cobalt phase exists as a

continuous cobalt network with fluctuating width of the branches (Exner, 1979). The mean binder free path, measured in the binder phase, is defined by the arithmetic mean of the distance from one carbide/binder interface to the other. Using an experimentally determined value of mean carbide grain size (d_{wc}), contiguity of carbide phase (C) and volume fraction of the binder phase (V_{Co}), the mean binder free path is usually calculated using the following equation (Warren and Waldron, 1972; Lee and Gurland, 1978):

$$d_{Co} = \frac{1}{(1+C)} d_{WC} \frac{V_{Co}}{V_{WC}} \qquad (2.8)$$

Where d_{Co} and V_{WC} are mean binder free path and volume fraction of carbide phase respectively.

Roebuck and Bennet (1986) reported that a reasonably accurate estimate of the mean binder free path in binary phase WC/Co hard metals can be obtained by this equation. In leaching processes, the mean binder free path is what determines the size of the channels for mass transfer and diffusion during leaching. It can, therefore, be inferred, based on the direct relationship between the binder free path (d_{Co}) and the carbide grain size (d_{wc}), that the bigger the grain size, the wider the mean binder free path, and the easier it is for a solvent to access the inner core of the solid pieces of cemented carbide hardmetal and vice versa.

2.2 Scrap Generation

The hardmetals manufacturing processes and applications industries generate appreciable amounts of cemented tungsten carbide reject material and worn out or used parts from their operations, respectively. The manufacturing process rejects are typically due to cracks and chips in the tool cutting edges or the tools not meeting desired dimensions or specifications. The reject material tends to accumulate over time and due to its high tungsten content can be reclaimed for re-use in the fabrication of new tools and wear parts (Barnard et al, 1971).

A global mass flow of tungsten in 2010, as reported by Leal-Ayala et al (2015), is illustrated in **Figure 2.8.** The figure is a Sankey diagram visualization tool that presents the mass flow of tungsten. The diagram shows quantitative information about tungsten flows, their relationships and their transformations. The diagram also highlights inefficiencies and potential savings in connection with material use. From the diagram, it is observed that 24,000 tonnes of end-of-life

scrap containing 10-99% tungsten was consumed in 2010. This represented about 23.8% of total tungsten demand in that year.

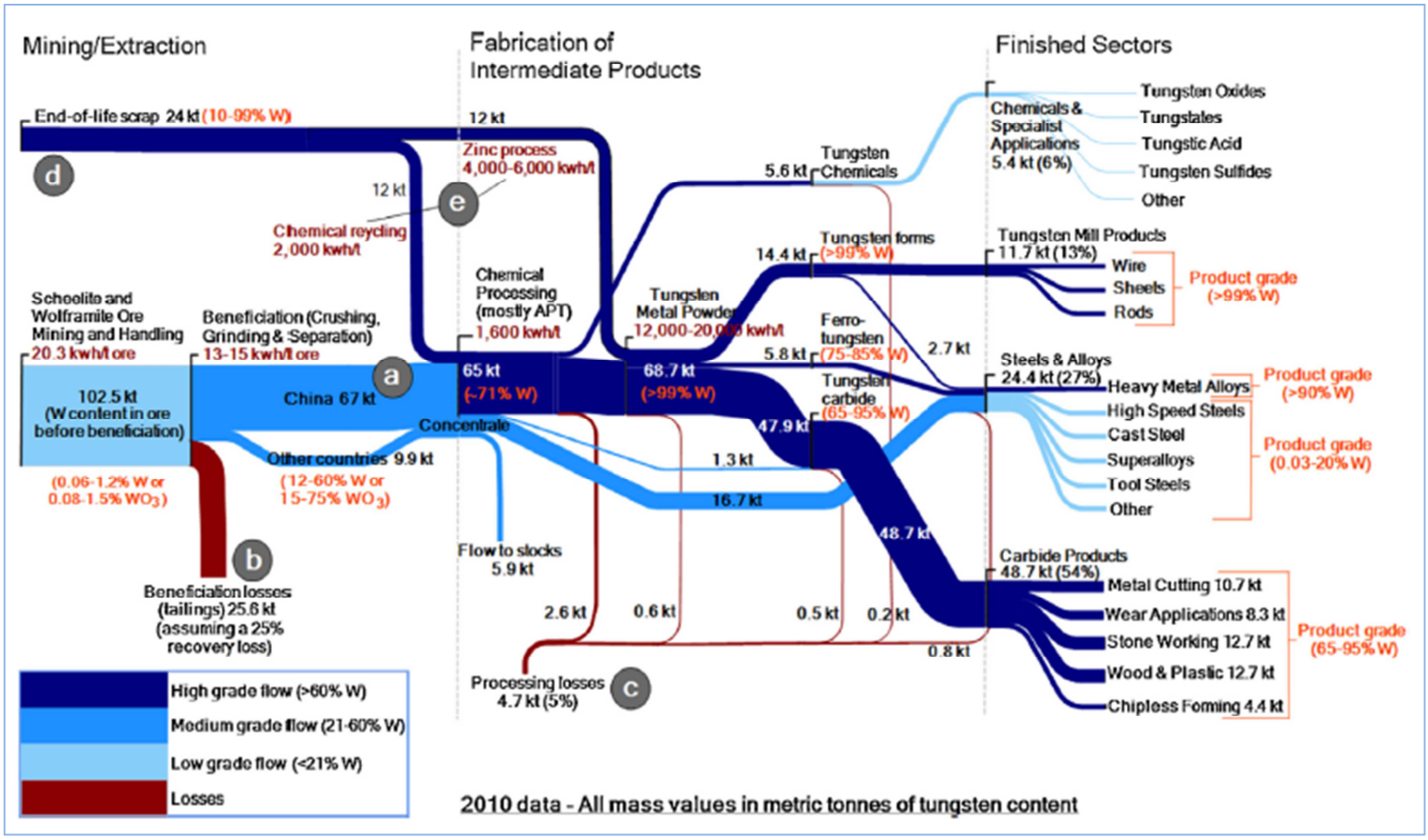

Fig.2.8: Global mass flows of tungsten in 2010 (adapted from Leal-Ayala et al, 2015)

2.2.1 Scrap from Industrial Applications

Tungsten, in its pure metallic form, can be used to manufacture products or it may be combined with other elements to form composite materials such as cemented tungsten carbides, mill products, steels and alloys (ITIA, 2010). Cemented tungsten carbide tools are the workhorses for the shaping of metals, alloys, wood, composites, plastics and ceramics, as well as for the mining and construction industries. Tungsten mill products are either tungsten metal products, such as lighting filaments, electrodes, electrical and electronic contacts, wires, sheets, rods or tungsten alloys (Lassner and Schubert, 1999). Tungsten remains an important constituent for tool steels, high speed steels, stellites and creep-resistant steels and alloys. Various cemented tungsten

carbide grades and their applications in industry are shown in **Table 2.4**. These materials constitute scrap from industrial applications when rejected.

Table 2.4: Different WC-Co grades and their application (CDI, 2006)

WC	Co	TaC	TiC	NbC	Industrial Application
97	3	-	-	-	Precision boring
94	6	-	-	-	General machining
93	7	-	-	-	Cast iron machining
91	9	-	-	-	Cast iron machining
87	13	-	-	-	Wear applications
82	18	-	-	-	Heavy impact uses
80	20	-	-	-	Heavy shock- bar drawing
92.1	5.8	1.8	-	0.3	General machining
74.4	6	7.2	10	2.4	Precision Finishing
79.1	6.7	7	4.9	2.3	Form tooling
75.6	10.7	5.4	6.7	1.6	Interrupted cutting
83.8	13	-	3.2	-	Dies, heavy stock
82	15	3	-	-	Extrusion dies/ can tooling

The availability of various types of tungsten-bearing scrap can be seen from the tungsten consumption pattern shown in **Table 2.5.**

Table 2.5: Tungsten Consumption by end-use (%) (Bhosale et al, 1990)

Tungsten Consumption	U.S	Japan	Free World
Cemented Carbide:			
Metal cutting	28	32	30
Mining and drilling	15	4	11
Wear parts	19	21	8
Other	-	1	6
Total	62	58	55
Tungsten metal	23	17	15
Steels	5	23	20
Other	10	2	10

Tungsten-bearing scrap materials from industrial applications are in different forms and have varying purity. The different types of scrap containing tungsten and their corresponding tungsten contents are shown in **Table 2.6.** The variation in scrap characteristics has invariably called for equally varied and unique processing techniques corresponding to the nature of the scrap.

Table 2.6: Typical tungsten content in tungsten scrap materials (Lassner and Schubert, 1999)

No.	Scrap Type	%Wt.	Group
1	High-purity	≥ 99	**Hard Scrap** (solid pieces)
2	Oxide dispersed W alloys (ThO_2, ZrO_2,CeO_2, La_2O_3)	96-98	
3	Hardmetal pieces (also containing Co, Ta)	60-97	
4	Heavy metal W alloys	92-94	
5	W - Cu	60-90	
6	Pure W powder	98 ≥ 99	
7	W grinding sludge	30-60	
8	W cutting sludge	70-80	**Soft Scrap** (fine particles, powder, dust, timings, sludges)
9	Hard metal powder	60-95	
10	Hard metal grinding sludge	15-60	
11	Heavy metal powder	92-97	
12	Heavy metal turnings	92-97	
13	W-Cu powder and green compacts	50-90	
14	Floor sweepings (different sources)	40-60	

Several processes for recycling cemented tungsten carbide scrap have been proposed (Lassner and Schubert, 1999; Bhosale et al., 1990; Katiyar et al, 2014). These processes, classified into three categories namely, direct, indirect and semi-direct recycling (Shemi et al, 2018) are discussed in the sections that follow.

2.3 Current Tungsten Recycling Methods

2.3.1 Direct Recycling

As direct recycling is understood, the as-supplied material is transformed to a powder of the same composition by either physical treatment (Trent, 1946; Barnard et al, 1971; Lassner and Schubert, 1999) or chemical treatment (Hartline III et al, 1976).

In the zinc process (Trent, 1946; Barnard et al, 1971) cemented carbide secondary material is contacted with molten Zn at 900-1050°C, and forms a zinc-cobalt alloy thus, breaking the WC-Co bond. In the second stage, vacuum distillation of the Zn leaves behind friable material that can be used as virgin material. The zinc process has the advantage of high recovery with yields as high as 95%. However, the process consumes high amounts of electricity and requires specialized equipment to ensure an efficient and successful operation (Gurmen, 2005). A report by Leal-Ayala et al (2015) (**Figure 2.8)** indicates that the zinc process has a higher energy consumption of around 4,000–6,000 kWh per tonne of tungsten processed compared to 2000 kWh per tonne for chemical processing.

In the cold-stream process, material is impacted against a hard carbide surface (Lassner & Schubert, 1999). This process has advantages of a low operating temperature which prevents oxidation, the ability to retain a high purity, particle size control and good compressibility of the powders obtained. The process, however, suffers from incomplete separation of metal carbides from the binding material and requires specialized expensive equipment (Hartline III et al., 1976).

In carbide carburization sintering, cemented carbide scrap containing 15wt% Co is oxidized at 850°C, into a mixture of WO_3 and $CoWO_4$ (Joost, et al., 2012; Pirso et al, 2006). Results have shown that the microstructure of reactive- sintered WC-Co composites is fine grained and identical to that of the original WC-Co microstructure and has similar mechanical properties. However, the large amount of energy required and the considerable number of steps needed to attain re-usable metal carbide powder offset the advantages of the process.

Within the direct recycling category, the zinc process is displayed as the main representative. For instance, Shedd (2000), cited by Kutcher et al (2017), reported that about 25% of the cemented carbide scrap passed through such facilities in the USA. Karhumaa and Kurkelaat (2013) added that at least 10% of the raw material demand in Europe is supplied by the zinc process. The pre-process requirements for this recycling category is that the composition of scrap must be the same as the final product and it must be of high purity. This processing route is suitable for treating straight grade WC-Co scrap which does not contain other carbides. It is the preferred route for hardmetal type of scrap and heavy metal turnings (Shemi et al, 2018).

2.3.2 Indirect Recycling

Indirect recycling involves chemical modification of the component metals into intermediate products which are then processed to obtain pure metals (Lin et al, 1995; Lin et al, 1996). Electrochemical reactions are known to bring about nickel binder dissolution and WC conversion into WO_3. Results have shown that an electrochemical conversion of tungsten into oxide and near 100% nickel dissolution thus yielding Ammonium Paratungstate (APT) and $NiSO_4$ as pure commercial products is possible (Kuntyi et al, 2007). The major drawback to this process is the several number of conversion steps involved from the intermediate product to the final product.

Nitrate salts such as $NaNO_3$ or mixtures of $NaNO_3$ and Na_2CO_3, when roasted with tungsten carbide scrap, in a process known as nitrate fusion, convert tungsten to water soluble Na_2WO_4. The nitrate fusion process has the advantage of a high throughput and very high recoveries. It has, however, limitations of high exothermic reactions and the generation of large quantities of toxic nitrous oxide fumes. The exothermic reactions are considered hazardous and the toxic nitrous fumes, an enormous pollution problem (Bhosale, et al., 1990). Notably, if made less hazardous by some advanced technology, the energy from the exothermic reactions could be harvested and utilized as part of process improvement.

Typically, indirect processing implies dissolution; leach purification, crystallization, calcination, reduction and finally carburation in order to obtain tungsten carbide (WC) (Kutcher et al, 2017). Indirect methods have the advantage of producing ‘virgin Ammonium para tungstate (APT)’, the most important precursor for tungsten intermediate products such as tungsten trioxide, tungsten blue oxide, tungstic acid and ammonium metatungstate. However, long reaction times and the use of several conversion steps are the main disadvantages. According to Kutcher et al (2017), two commercial practices exist inside this category, an oxidation process with chemical digestion or an alkaline salt fusion method. Shedd (2000), cited by Kutcher (2017), showed that a share of about 35% of the hard metal scrap in the USA is handled by indirect processing methods, with an even higher amount of 85% in Germany (Gille and Meier, 2012). This recycling category is suitable for treating lower grade scrap and straight grade WC-Co scrap which contain other carbides. The typical scrap materials treated are grinding sludges, floor sweepings, contaminated powder qualities, tungsten-copper and solid pieces etc (Shemi et al, 2018).

2.3.3 Semi-Direct Recycling

With the larger amount of hard metal scrap being handled by the foregoing two recycling categories, the third and last class, the semi-direct method, only plays a minor role in today's recycling market (Kutcher et al, 2017). According to this category, semi-direct recycling is a selective dissolution process. In this method, one component is dissolved chemically, leaving the other phase(s) intact (Lassner and Schubert, 1999). The dissolution, under controlled conditions, is targeted at the binder metal(s) without significant dissolution or alteration of the metal carbide grains. The dissolution mechanism weakens the integrity of the carbide alloy structure thereby allowing attrition to occur easily. The non-acid soluble phase of the cemented carbide such as tungsten monocarbide (WC) is retained as residue and the resultant leach liquor is separated for purification and recovery of the dissolved metal (s). Therefore, no extensive procedure should be theoretically necessary for obtaining re-usable WC powder and the recovery of dissolved metals may require subsequent processing using conventional techniques (Gille and Meier, 2012; Schiesser, 2003; Meyer, 1979). In this recycling category, straight grade WC-Co scrap and tungsten carbide grades mixed with other carbides can be treated. Binary (α-β) and ternary (α-β-γ) phase cemented carbides can be processed. However, scrap such as grinding sludges, floor sweepings and contaminated powders are deemed not suitable for this route due to the indiscriminate nature of these materials (Lassner & Schubert, 1999).

Investigated by several researchers, semi-direct processing has shown potential for solubilization of leachable cemented carbide phases (Trapp, 1949; Ghandehari and Schussler, 1980; Vanderpool, 1983; Lin et al, 1996; Gurmen et al, 2005; Kojima, 2005; Edtmaier et al, 2005; Freemantle and Sacks, 2015; Seo and Kim, 2016; Venkateswaran et al, 1996). The processing routes in the semi-direct category typically include inorganic acidic, organic acid, hydrothermal, electrochemical, leach milling, melt-leach or a combination of any of the aforementioned techniques. However, several issues in this recycling category are reported in literature. A number of previous research efforts are reviewed below.

In inorganic acid leaching, hardmetal scrap is directly reacted with a metallic acid. A study by Gurmen and co-researchers (2005) showed that 91.5% Co could be extracted from cemented carbide scrap powder (<90 μm) within 2hrs of leaching using 0.5M HNO_3 solution at 25°C, solid liquid ratio of 1:10 and a stirring speed of 900 rpm. The dissolved Co was precipitated to

$Co(OH)_2$ using NaOH and then calcined to cobalt powder (99.7%) at >300°C in an argon atmosphere for 0.5hrs. The powder was further processed under a hydrogen reduction atmosphere for 1.5 hrs to obtain cobalt powder with a sub-micron structure. However, despite the short recycle time and high extraction efficiencies of the process, the energy cost associated with 'hardmetal' comminution prior to leaching could outweigh these advantages. Notably, the mechanical pulverization of cemented carbide solid pieces causes troubles, since this category of materials serves for machining others (Kutcher et al, 2017).

In organic acid leaching, an organic lixiviant is used as a solvent. Using 3.6M acetic acid, Edtmaier and co-workers (2005) reported a cobalt extraction of up to 85% from a ternary phase cemented carbide scrap metal within a recycle time of 2.6 – 6.5 days. The scrap comprising several hard phases other than WC was reacted within a temperature range of 40-80°C, under a simultaneous introduction of pure oxygen at a pressure of 1-5 bars. The best results were obtained by using pure oxygen at 5 bars. Under these conditions, W, Cr, V and Fe were co-extracted with cobalt but WC and other carbide phases of Nb, Ta and Ti remained unaffected. The authors reported that the subsequent processing of the dissolved metals, if required, could be recovered through known chemical means. The high extraction efficiency achieved in this work showed that hardmetal is amenable to organic acids. However, high pressure conditions and consumption of pure oxygen have high cost implications which could negatively impact the economics of this process.

Using a similar approach to the foregoing study, Freemantle and Sacks (2015) reacted 'oversize material' rejects from the zinc recycling process with acetic acid at pH < 4, a temperature of 80°C for 21 days, under atmospheric conditions. The residue was washed, dried, crushed in ethanol, then milled to the same grain size range (1.6-2.0μm) as 'virgin' or 'zinc processed' powders. Although deemed unsuitable for manufacturing the same grade of mining tools as those from 'virgin' or 'zinc processed powders, the authors reported that the 'acetic powders' obtained from their process could be used for different commercial applications. For instance, the 'acetic powders' could be used for commercial applications that require tools that possess a high fracture toughness, such as milling media, shims and possibly coal and hard-rock mining (Morrison, 2015). The main drawback with this process, however, is the long recycle time of 21 days. The long recycle time is indicative of the slow kinetics of the process.

In hydrothermal acid leaching, hardmetal scrap is reacted with a solvent under high temperature conditions. A study by Kojima et al (2005) demonstrated that the Co binder phase could be efficiently extracted in 0.5M HCl at a temperature of 110°C in an autoclave within 24hrs. Other acids, H_2SO_4 and HNO_3, were also tried, but they did not perform better than HCl. After the hydrothermal treatment, the WC skeleton became very brittle and pulverized easily with ball milling. The authors reported that the mechanical property of the re-sintered products of the 'hydrothermal' WC powders was a little degraded by the formation of 'eta' (η) phase due to WC particle oxidation. This was, however, overcome by improving the powder drying process. Notably, the recycle time and ease of disintegration are an advantage for the process. However, the degradation of 'hydrothermal' WC powders due to oxidation and energy costs associated with operating under high temperature conditions could be drawbacks for the process.

Electrochemical recycling is an electrolytic-based process. With this technique, the binder metal in the hardmetal scrap is selectively extracted by anodic dissolution using an electric current. A study by Ghandehari and Schussler (1980) showed that cemented carbide (WC-6%wt.Co) cutting tool inserts could be recycled by electrochemical dissolution at a constantly applied potential using 1.2M H_3PO_4 in an inert nitrogen saturated atmosphere. The process produced WC skeleton that could easily be disintegrated with ball milling. The recovered metal carbide powder was treated for oxygen removal and carbon content adjustment, then graded and blended for reuse. The report showed Co extraction efficiencies in the range 71.7 - 96.7%. The high extraction efficiencies and the ease of WC skeleton disintegration are an advantage for the process. However, the requirement of an inert atmosphere saturated with nitrogen, use of costly H_3PO_4 and an electrolytic set up in conjunction with ball milling could make this process costly and raises environmental concerns regarding chemical waste disposal.

In a similar electrochemical experiment, Lin and co-researchers (1996) reported that scrap pieces of cemented carbide could be electrolytically processed by applying a constant-potential of 0.2 - 0.6V to an electrolytic cell containing scrap in 1M HCl and 0.1M citric acid electrolyte. The process produced smaller scrap pieces with an outer layer of loosely bound particles of WC surrounding a core of WC particles still cemented together by the binder. The relatively loosely bound WC particles were readily removed from the core by grinding. To achieve complete disintegration, the process was repeated. This involved a periodic transfer of the basket to the

grinder and then to the screen for separation of WC particles from the core scrap and then back to the cell. The cobalt in the electrolyte was bled out for electro-winning at concentrations greater than 20gpl to avoid electroplating Co in the cell. This process was reported to have minimal anode passivity due to the addition of citric acid. The authors neither reported the recoveries nor the recycle time achieved by the process. Notably, technical applicability and operational simplicity could be the major concerns with this technique.

In another electrochemical experiment, Vanderpool (1983) showed that 68g of cemented carbide could be treated using an electrolytic process using a hydroxide electrolyte to retard the formation of metal oxides during electrolysis thereby permitting the recovery of carbides without the necessity for intermediate reduction and carburization steps. NaOH and LiOH were used as alternative electrolytes using 75-10 Amps and 10 volts for a period of 2 hrs under atmospheric conditions. In this process, the carbide particles settled to the bottom of the vessel from which they were recovered by decantation or filtration, then washed and dried. Any binder metal dissolved in the electrolyte was subsequently recovered as a salt by evaporation or addition of a precipitating agent. The salt was separated and thermally reduced to obtain metal powder. This process has the advantage of complete disintegration of the scrap material. However, consumption of costly reagents like NaOH, KOH, and LiOH, could outweigh the benefits of the process. Notably, neither the recovery rate nor recycle time were reported.

In leach milling, hardmetal scrap is reacted with a solvent simultaneously with milling. In their work, Seo and Kim (2016) describe a pretreatment approach prior to acid leaching of WC-Co hard metal cutting tool scrap. The scrap pieces were heated from room temperature to 900°C at 5°C min^{-1} for 3hrs in an oxygen atmosphere to produce WO_3 and $CoWO_4$. The oxidized scrap was ground to powder using a planetary ball mill to increase the surface area for improved reaction. A volume of 200ml malic acid solutions at 0.1 to 3M concentrations were used to selectively dissolve Co from 10g of the oxidized WC-Co powder. The malic acid solution was maintained at 20, 30, 40, 50, 60 and 70°C while agitating at 200 rpm during dissolution experiments. Hydrogen peroxide (H_2O_2) at 2 vol% was added in order to decompose a thin layer of insoluble tungstic acid ($WO_3 \cdot H_2O$) covering the $CoWO_4$ surface by forming a soluble peroxotungstic acid complex ($WO_3 \cdot H_2O_2 \cdot H_2O$). The role of H_2O_2 in the reaction was to dissolve the tungstic acid after its formation. The authors report that Co dissolution from $CoWO_4$ in

concentrated malic acid was improved by both H_2O_2 addition and wet milling although the effect of wet milling was more significant. Ultimately, 98% of Co was extracted after 144 hrs (6 days) in 3M malic acid solution with 2% H_2O_2 during wet milling. However, in spite of the high Co extractions, the authors observed that the use of malic acid and H_2O_2 is rather costly and H_2O_2 discharge in waste water can be harmful to the environment. In addition, the pretreatment at 900°C in an oxygen atmosphere is also costly.

In melt leaching, the hardmetal scrap is first heated to the melting point of the binder medium then cooled and acid leached to selectively dissolve the binder metal. The technique was first proposed by Trapp (1949) and later promoted by Venkateswaran et al (1996) who named it the 'menstruum process.' In this process, the hardmetal mass is heated to a temperature of at least 1,800°C, whereby some of the cobalt bond is exuded and the mass is made porous. Even large pieces of scrap are readily and rapidly dissolved in the carbon-saturated Fe or Co melt bath at 1,550-1,600°C and are converted into WC solid particles, which settle rapidly to the bottom of the melt bath due to their high density. After the remaining molten metal above the settled mass is poured off, the WC-Fe residue is further processed by leaching with HCl at 90-100°C to gain a pure, coarse grained and well faceted WC powder. The 'menstruum process' has the advantage of handling large pieces of hardmetal scrap which are difficult to treat using other recycling techniques. This process is, however, energy intensive.

The foregoing review of semi-direct recycling methods gives a general overview of advantages and disadvantages of current methods as well as potential areas for further research. Although common hydrometallurgical techniques have been shown to retrieve the binder metal, several issues reported in literature include: partial oxidation, high energy requirements, slow dissolution of the binder, non-removable films, reagent consumption, technical applicability concerns, treatment costs and environmental concerns.

2.3.3.1 Lixiviants Used in Semi-direct Recycling

In hydrometallurgy, a lixiviant is a liquid medium used to selectively extract a desired metal from an ore or mineral (AIME, 1917). A lixiviant assists in rapid and complete leaching and the metal can be recovered from the ore in a concentrated form after leaching. Lixiviants may work by altering the redox state of an ore, or by altering the Eh and/or pH of the leaching environment.

In hydrometallurgical processes, the lixiviants which play a key role could either be acidic or alkaline. The acidic solvents may be inorganic or organic. A few commonly used lixiviants are briefly reviewed here as knowledge of their properties is essential for the selection of suitable conditions for a leaching process.

Sulphuric Acid

Sulphuric acid is a mineral acid composed of sulphur, oxygen and hydrogen, with the molecular formula H_2SO_4. Also known as vitriol, sulphuric acid is a highly corrosive, diprotic and strong inorganic acid; density, 1.84gcm^{-3}, molecular weight, 98.07gmol^{-1} and boiling point, 337°C. It is a colourless, odourless, and slightly yellow viscous liquid that is soluble in water at all concentrations (Lide, 2007). The 98% grade is more stable in storage, and is the usual form of what is described as concentrated sulphuric acid. The acid has strong dehydrating and oxidizing properties at high concentrations (Housecroft, 2008), possesses different chemical properties and therefore has a wide range of applications some of which include metal extraction and chemical synthesis (Earnshaw and Greenwood, 1997). Sulphuric acid is stable, easier to handle, relatively cheap compared to other acids and allows good solubilization of metals. The average cost of sulphuric acid (98%w/w) is USD24.4.00/Litre (Chem Supply, 2020).

Hydrochloric acid

Hydrochloric acid is a mineral acid composed of hydrogen and chlorine with the molecular formula HCl. Also known as muriatic acid or spirit of salt, hydrochloric acid is a clear, colourless aqueous solution of hydrogen chloride gas. It is a highly corrosive, strong monoprotic inorganic acid with many industrial uses (Lide, 2007); HCl (37%) density, 1.16gcm^{-3} and molecular weight, 36.46gmol^{-1}. The boiling point of hydrochloric acid decreases with increasing acid concentration; at 20.2% concentration, hydrochloric acid as a binary mixture of hydrochloric acid and H_2O has a constant-boiling azeotrope at 108.6°C (Lide, 2007; Perry et al., 1984). At higher concentrations, hydrochloric acid forms corrosive acid mists, dissolves many metals, forms oxidized metal chlorides and hydrogen gas, and reacts with basic compounds such as $CaCO_3$ or $CaSO_4$ to form soluble chlorides. HCl is used in many processes such as ore treatment, metal extraction, separation, purification, and water treatment (Earnshaw and

Greenwood, 1997). The average cost of hydrochloric acid (37%w/w) is USD 32/Litre (Chem Supply, 2020).

Nitric acid

Nitric acid, also known as aqua fortis or spirit of niter, is an inorganic acid composed of nitrogen, hydrogen and oxygen with a chemical formula HNO_3. Nitric acid is a highly corrosive, monoprotic, toxic and strong mineral acid with strong oxidizing characteristics (Housecroft and Sharpe, 2008); HNO_3 (68%) density, 1.41 gcm^{-3} ; molecular weight, 63.20 $gmol^{-1}$; normally colourless, but tends to acquire a yellow cast due to the accumulation of oxides of nitrogen if stored for a long time. Nitric acid (68% w/w) as a binary mixture of nitric acid and H_2O has a constant-boiling azeotrope at 121°C (Dean, 1992). Ordinary nitric acid has a concentration of 68% (w/w) and when the concentration is more than 86%, the acid forms nitric acid fumes. Nitric acid is subject to thermal or light decomposition to form nitrous gas (Housecroft and Sharpe, 2008). The main important uses of nitric acid include production of explosives, etching and dissolution of metals. As a component of aqua regia, nitric acid is used for purification and extraction of gold, and in chemical synthesis (Thiemann, 2005). The average cost of nitric acid (68-70%w/w) is USD 56/Litre (Chem Supply, 2020).

Phosphoric Acid

Phosphoric acid, also known as orthophosphoric acid, is a weak acid with the chemical formula H_3PO_4. It is a non-toxic compound which, when pure, is solid at room temperature and pressure. H_3PO_4 density, 1.88gcm^{-3}; molecular weight, 97.99 $gmol^{-1}$; melting point, 42.4°C and boiling point, 407°C. All three hydrogens are acidic to varying degrees and can be lost from the molecule as H^+ ions (protons). When all three H^+ ions are removed, the result is an orthophosphate ion PO_4^{3-}, commonly called "phosphate". Removal of one or two protons gives dihydrogen phosphate ion, $H_2PO_4^-$ and the hydrogen phosphate ion, HPO_4^{2-} respectively. Phosphoric acid is commonly stocked as an aqueous solution at 85% (w/w) concentration. It is a colourless, odourless, and non-volatile syrupy liquid. The dominant use of phosphoric acid is for fertilizers, consuming approximately 90% of production (Schrödter et al, 2008). Phosphate acid is used in soaps and detergents, food industry, water treatment and toothpastes. Other specific applications include: anti-rust treatment, acid fuel cells, production of activated carbon and

compound semi-conductor processing. The average cost of phosphoric acid is USD 56.4/Litre (Chem Supply, 2020).

Acetic Acid

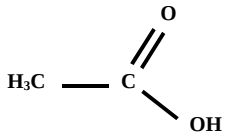

Fig.2.9: Acetic acid ($C_2H_4O_2$) molecular structure

Acetic acid is colourless liquid organic compound with the chemical formula CH_3COOH also written as CH_3CO_2H or $C_2H_4O_2$; density, 1.05gcm^{-3}; molecular weight, 60.05gmol^{-1}; melting point, 16.6°C and boiling point, 118.1°C. When undiluted, it is sometimes called glacial acetic acid. Acetic acid is the main component of vinegar apart from water making up not less than 4% by volume. The hydrogen centre in the carboxyl group (−COOH) in carboxylic acids such as acetic acid can separate from the molecule by ionization (Haynes, 2016). The reaction is presented as:

$$CH_3COOH \rightleftharpoons CH_3COO^- + H^+ \qquad (2.9)$$

Because of this release of the proton (H^+), acetic acid has acidic character. Acetic acid is a weak monoprotic acid. The acetic acid molecular structure is shown in **Figure 2.9**. In aqueous solution, acetic acid has a pK_a value of 4.76 (Goldberg et al, 2002). Its conjugate base is acetate (CH_3COO^-). A 1.0 M solution (about the concentration of domestic vinegar) has a pH of 2.4, indicating that merely 0.4% of the acetic acid molecules are dissociated. However, in very dilute ($< 10^{-6}$ M) solution acetic acid is >90% dissociated. The largest market for acetic acid is its use as a chemical reagent for the production of chemical compounds (Cheung et al, 2004; Malveda and Funada, 2003). The average cost of acetic acid is USD 24/Litre (Chem Supply, 2020).

Citric Acid

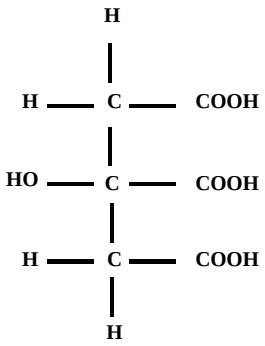

Fig.2.10: Citric acid ($C_6H_8O_7$) molecular structure

Citric acid is a weak organic acid that has the chemical formula $C_6H_8O_7$ and structural formula, $CH_2COOH\text{-}C(OH)COOH\text{-}CH_2COOH$; density, $1.66gcm^{-3}$; molecular weight, $192.12gmol^{-1}$; melting point, 153°C and boiling point, 310°C. It occurs naturally in citrus fruits. The conjugate base of citric acid is citrate ($C_6H_5O_7^{-3}$). The citric acid molecular structure is illustrated in **Figure 2.10**. Citric acid is normally considered to be a tribasic acid, with pKa values of 3.13, 4.76 and 6.39. Citric acid is used as a chelating agent (Alexander, 2014). The citrate ion forms complexes with metallic cations. The stability constants for the formation of these complexes are quite large because of the chelate effect. Consequently, it forms complexes even with alkali metal cations.

However, when a chelate complex is formed using all three carboxylate groups, the chelate rings have 7 and 8 members, which are generally less stable thermodynamically than smaller chelate rings. In consequence, the hydroxyl group can be deprotonated, forming part of a more stable 5-membered ring, as in ammonium ferric citrate, $(NH_4)_5Fe(C_6H_4O_7)_2 \cdot 2H_2O$ (Matzapetakis et al 1998). The dominant market for citric acid include food and drink, cleaning and chelating agent (Verhoff, 2016), cosmetics, pharmaceuticals and dietary supplements. The average cost of citric acid is USD 72/Kg (Chem Supply, 2020).

Lactic acid

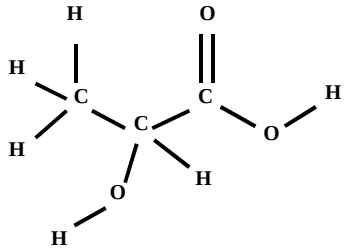

Fig.2.11: Lactic acid ($C_3H_6O_3$) molecular structure

Lactic acid is an organic acid with the molecular formula $C_3H_6O_3$ and structural formula $CH_3CH(OH)COOH$; density, $1.29gcm^{-3}$; molecular weight $90.08gmol^{-1}$; melting point 16.8°C and boiling point 122°C; hygroscopic and monoprotic. Lactic acid has been observed to be corrosive to metal and tissue. While in liquid state lactic acid is a colourless solution, white in solid state and extremely soluble in water and ethanol (Westhoff and Starr, 2012).

Lactic acid can be produced naturally as well as synthetically. The acid is carboxylic with the general formula, R–COOH. R refers to the hydroxyl (CH_3CH (OH)) molecule and COOH the carboxylate group. The lactic acid molecular structure is exhibited in **Figure 2.11**. In solution, lactic acid can ionize a proton from the carboxyl group, producing the lactate anion CH_3CH (OH) COO^-. Lactic acid has a dissociation constant of 3.86 pKa. Compared to acetic acid (4.76 pKa), lactic acid's pKa is 1 unit less, meaning lactic acid deprotonates ten times more easily than acetic acid does (Benninga, 1990; Groot et al, 2010). In other words, that means lactic acid is a stronger acid than acetic acid. In its conjugate form, lactic acid plays a role in several biochemical and electrochemical processes (Martinez et al, 2013). The average cost of lactic acid (88%w/w) is USD 68.8/Litre (Chem Supply, 2020).

Tartaric acid

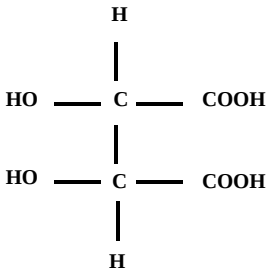

Fig.2.12: Tartaric acid ($C_4H_6O_6$) molecular structure

Tartaric acid is a white, water-soluble, crystalline and *diprotic* organic acid with the molecular formula $C_4H_6O_6$ and structural formula HOOCCH (OH) CH (OH) COOH; density 1.79gcm^{-3}; molecular weight 150.09gmol^{-1}; melting point 169-172°C and boiling point, 275°C. Tartaric acid occurs naturally, most notably in grapes. Its salt, potassium bitartrate, commonly known as cream of tartar, develops naturally in the process of winemaking. As a diprotic acid, it is a *dicarboxylic acid*, a molecule with two carboxyl groups with a general molecular formula HOOC-R-COOH (Kassaian, 2002; softschools.com, 2019). The tartaric acid molecular structure is presented in **Figure 2.12**. Tartaric acid has a dissociation constant of 2.98 pKa. Compared to acetic acid (4.76 pKa), tartaric acid's pKa is 2 units less, meaning tartaric acid deprotonates twenty times more easily than acetic acid does. Tartaric acid has several industrial applications. It has been observed to chelate metal ions such as calcium and magnesium and has served in the farming and metal industries as a chelating agent for complexing micronutrients in soil fertilizer and for cleaning metal surfaces consisting of aluminium, copper, iron, and alloys of these metals, respectively (Kassaian, 2002). Other applications of tartaric acid are in the pharmaceutical and food industry (Blair and DeFraties, 2000). The average cost of tartaric acid is USD 100/Kg (Chem Supply, 2020).

Maleic acid

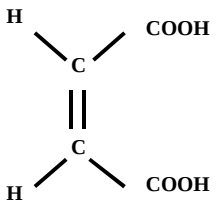

Fig.2.13: Maleic acid ($C_4H_4O_4$) molecular structure

Maleic acid is a *diprotic* white water-soluble organic compound with the molecular formula $C_4H_4O_4$ and structural formula HOOCCH=CHCOOH; density, 1.64gcm^{-3}; molecular weight; 116.07gmol^{-1}; melting point 135°C (decomposes) and boiling point 202°C. It is a *dicarboxylic acid*, a molecule with two carboxyl groups. The maleic acid molecular structure is shown in **Figure 2.13**. It is electrophilic - a molecule that has a tendency to attract or acquire electrons. Maleic acid has a dissociation constant of 3.02 pKa. Compared to acetic acid (4.76 pKa), maleic acid's pKa is 1.7 units less, meaning it deprotonates 17 times more easily than acetic acid does.

Maleic acid has few applications. The maleate ion is the ionized form of maleic acid. The maleate ion is useful in biochemistry and the pharmaceutical industry. Maleic acid is also used as an adhesion promoter for different substrates, for example, galvanized steel. Although not practiced commercially, maleic acid can be converted into maleic anhydride by dehydration, to malic acid by hydration, and to succinic acid by hydrogenation (Amoa, 2007). The average cost of maleic acid is USD 154/Kg (Chem Supply, 2020).

2.4.3.1.1 Metal Complexation

A complex has been defined as a species formed by the association of two or more simpler species each capable of independent existence (Rossotti and Rossotti, 1961). When one of the simpler species is a metal ion, the resulting entity is known as a metal complex. A characteristic feature of such a complex is that a metal atom occupies a central position in it. This is exemplified by cobalt in hexamminecobalt (III) ion, platinum in tetratchloroplatinate (II) ion, and copper in bis(glycinato) copper (II) shown in **Figures 2.14, 2.15** and **2.16** respectively. The metal-centred structure may carry a negative, positive or zero charge. Almost every kind of metal atom can serve as a central atom, but some kinds of atoms do so more readily than others. Atoms of the transition series, for example Co, W, Fe, Ni, Cu, Pt, Cr, V, Mo, etc., are excellent in this function, whereas, alkali metals are rarely found in this role (Dwyer and Mellor, 1964).

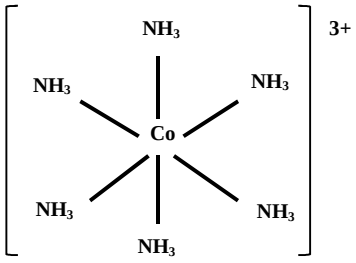

Fig.2.14: Cobalt in hexamminecobalt (III) ion

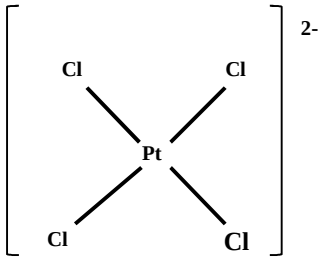

Fig.2.15: Platinum in tetratchloroplatinate (II) ion

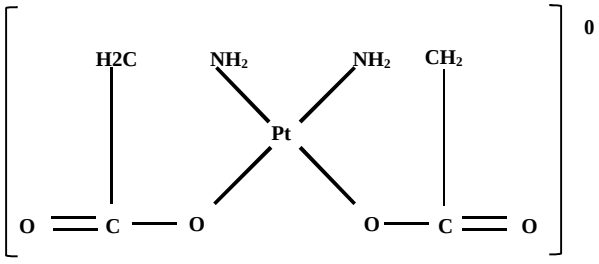

Fig.2.16: Copper in bis (glycinato) copper (II)

When the central metal atom of a complex is bound to its immediate neighbours by covalent bonds formed as a result of the metal atom accepting an electron pair from each non-metal atom, the non-metal atom is referred to as the donor and the metal atom, the acceptor atom. Alternatively, the non-metal atom is called the coordinating atom and the bond between it and the metal atom, a coordinate bond. However, metal atoms themselves sometimes contribute electrons to the bond as they do in $'\pi'$ bonding. Nevertheless, a more generally used convention, which is preferable, is to call any negative ion or polar molecule bound to a metal atom, a ligand and the bond between them, a metal-ligand bond (Dwyer and Mellor (1964). The term ligand comes from the Latin word *ligare,* which means to bind. Ligands have at least one donor atom with an electron pair used to form covalent bonds with the central atom. Ligands can further be categorized as monodentate, bidentate, tridentate, etc. where the concept of teeth (**dent**) is introduced, hence the idea of 'bite' angle. A monodentate ligand has only one donor atom used to bond to the central metal atom (Petrucci et al, 2017; Porterfield, 2013).

Monodentate Ligands

The term "monodentate" can be translated as "one tooth", referring to the ligand binding to the central atom through only one atom at one point. Some examples of monodentate ligands are: chloride ions (referred to as chloro when it is a ligand), water (referred to as aqua when it is a ligand), hydroxide ions (referred to as hydroxo when it is a ligand) and ammonia (referred to as amine when it is a ligand) (Petrucci et al, 2017).

Bidentate Ligands

Bidentate ligands have two donor atoms, which allow them to bind to a central metal atom at two points. Common examples of bidentate ligands are: ethylenediamine (en), the oxalate ion (ox) and actelyacetonate ($acac^-$). **Figure 2.17** shows ethylenediamine: the nitrogen atoms on the edges each have two free electrons that can be used to bond to a central metal atom. Ethylenediamine (en) is a bidentate ligand that forms a five-membered ring in coordinating to a metal ion M (Porterfield, 2013; Morgan and Drew, 1920).

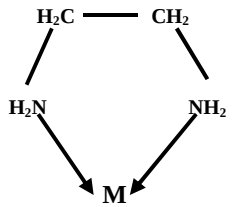

Fig.2.17: Ethylenediamine (en), a bidentate ligand

Acetylacetonate ($acac^-$) is a bidentate ligand that coordinates metal ions through oxygen atoms. $Acac^-$ is a hard base, so it prefers hard acid cations. With divalent metal ions, $acac^-$ forms neutral, volatile complexes such as Cu $(acac)_2$ and Mo $(acac)_2$ that are useful for chemical vapour deposition (CVD) of metal thin films.

Polydentate Ligands

Polydentate ligands have more than one atom available for coordination to the metal atom and they form stronger complexes than monodentate ligands (Cox, 2004). However, in forming a metal chelate, a polydentate or multidentate chelating agent may not use all its donor atoms (Morgan and Drew, 1920). Polydentate ligands include bidentate, tridentate, quadridentate, quinquedentate, hexadentate, and octadentate chelating molecules. EDTA, a hexadentate ligand, is an example of a polydentate ligand that has six donor atoms with electron pairs that can be used to bond to a central metal atom or ion. An alternative system of classification of chelating agents suggested by Diehl (1937) is based on the nature of the functional groups which are described as: (1) basic or coordinating for example, NH_2, (2) acidic, for example, -COOH.

Ambidentate Ligands

Unlike polydentate ligands, ambidentate ligands can attach to the central atom using either of its two donor atoms. A good example of this is thiocyanate, SCN^-, which can attach to a central metal atom either at the sulphur atom or the nitrogen atom (Petrucci et al, 2007; Porterfield, 2013).

Chelation

Chelation is a process in which a polydentate ligand bonds to a metal ion, forming a ring. It has been found that some ligands get attached to the metal atom by more than one donor atom in such a manner as to form a heterocyclic ring (**Figure 2.17**). This type of ring is called a chelate ring, the ion or molecule (ligand) from which it is formed, a chelating agent and the process of forming the chelate ring, chelation. First discovered by Morgan (Morgan and Drew, 1920), the first molecules identified were those with two donor atoms with a 'claw' like mode of attachment to the metal atom, hence the name chelate. According to Dwyer and Mellor (1964), any metal complex in which one or more chelate rings are present is defined as a metal chelate. However, many compounds function as chelating agents by the loss of one or more protons as is the case with oxalic acid and carboxylic acids. Although it is the anion that combines with the metal atom, it is, nevertheless, customary to call the parent molecule a chelating agent (Dwyer and Mellor, 1964). As the name implies, chelating ligands have high affinity for metal ions compared to ligands with only one binding group which are called monodentate, single 'tooth' ligands (Cox, 2004).

Atoms known to function as donors in metal complexes are shown in **Table 2.7**. Those shown in boldface have been observed as donor atoms in chelating molecules.

Table 2.7: Donor atoms in metal complexes

-	-	-	**H**
C	**N**	**O**	**F**
-	**P**	**S**	**Cl**
-	**As**	**Se**	**Br**
-	Sb	Te	**I**

Conditions necessary for chelation

If a molecule is to function as a chelating agent, it must fulfil at least two conditions. First, it must possess at least two appropriate functional groups, the donor atoms of which are capable of combining with a metal atom by donating a pair of electrons. These electrons may be contributed by basic coordinating groups such as NH_2 or acidic groups that have lost a proton such as –

COOH. Some acidic groups that combine with metal atoms by the replacement of hydrogen, known as, acidic groups are (Dwyer and Mellor, 1964):

-COOH (e.g., carboxylic acids)
-SO_2H
-OH (e.g., enolic and phenolic acid)
-SH

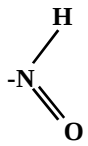

Basic coordinating groups include:

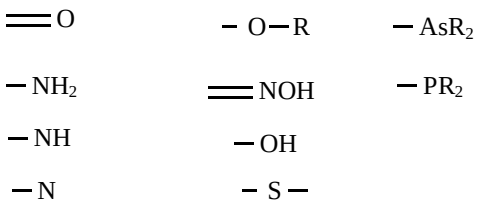

The second condition is that these functional groups must be so situated in the molecule that they permit the formation of a ring with a metal atom as the closing number. It's important to note that these two conditions are necessary, but they are not always sufficient for the formation of a chelate ring. Under some conditions, for example, in conditions of sufficiently low pH, a 'potential chelating molecule' may attach itself to a metal atom through only one ligand atom (Grinberg, 1962) as shown in **Figure 2.18**.

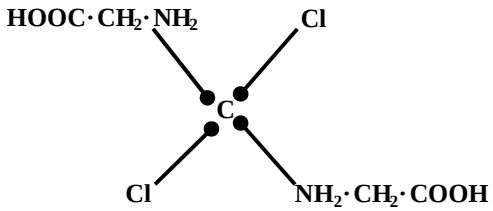

Fig.2.18: Central atom with 4 monodentated ligands attached

Chelation is sometimes influenced by steric factors. One chelating molecule may attach itself to a metal atom readily enough, but the addition of a second and third is hindered or even prevented

by the fact that there is a clash between the first and parts of the second and third when the latter move into the positions required for attachment. Whether such a clash will occur may sometimes depend on the size (atomic radius) of the central metal atom. The steric factor may sometimes manifest its influence by a lowering of the stability of the resulting metal complex (Dwyer and Mellor, 1964).

The metal-ligand bond

The strength and stability of the metal-ligand bond depends on the metal and the ligand size and electronegativity; specifically, their electronic structure. The ligand molecule 'L' may have other atoms attached to it, the number and nature of which will also influence the stability of the 'M – L' bond (Dwyer and Mellor, 1964).

Lewis (1916) and Langmuir (1919) were the first to identify a covalent bond with a pair of electrons—one from each atom, and both held in common. Some years later, Sidgwick (1927) developed an electronic interpretation of the structure of metal complexes in which one of the key ideas was the coordinate bond. The distinctive feature of this bond between 'M' and 'L' is that both electrons of the bond are contributed by one atom, L, known as the donor atom.

The stability of metal chelates

The solution stability of a metal complex is concerned with equilibrium of the type (Dwyer and Mellor, 1964: Petrucci et al, 2007):

$$M + nL = ML_n \qquad (2.10)$$

By applying the law of mass action to equation 2.xi, the equilibrium constant may be expressed as:

$$\beta_n^o = \frac{\{ML_n\}}{\{M\}\{L\}^n} \qquad (2.11)$$

Where, {M} is the activity of the species M, {L}, the activity of the species L, and β_n^o is the over-all thermodynamic stability constant for the reaction.

The constant that is determined experimentally is usually the concentration or stoichiometric stability constant β_n^o in which concentrations of the species (indicated by square brackets) replace activities. Thus,

$$\beta_n^o = \frac{[ML_n]}{[M][L]^n} \qquad (2.12)$$

Knowledge of the stability constants of metal complexes is useful for understanding their behaviour in solution. As a matter of fact, conditions required for the optimal or complete formation of a metal complex may be predicated on the basis of its stability constant.

Metal–chelate complex formation mechanism

The metal-chelate complex formation mechanism refers to the step-by-step analysis of reactions involved in the conversion of reactants to products. The general reaction profile for a metal (M) – ligand (L) interaction is presented as (Chauhan et al, 2015):

$$M + L \leftrightarrows [ML]^* \leftrightarrows [ML] \leftrightarrows [ML]^{**} \leftrightarrows ML \qquad (2.13)$$

Energetic collision	Transition state	Intermediate state	Transition state	Final product

It can be seen in **Eqn (2.13)** that there are two transition states where the ligand substitution may take place. A schematic representation of **Eqn (2.13)** is given in **Figure 2.19**, which suggests that the metal and ligand interact due to the energetic collision of the two molecules. Nevertheless, there are different transition states and intermediate stages between the reactant conversion and the product formation. An intermediate occurs at the local energy minimum, whereas the transition state always occurs at an energy maximum point and cannot be isolated (Chauhan et al, 2015).

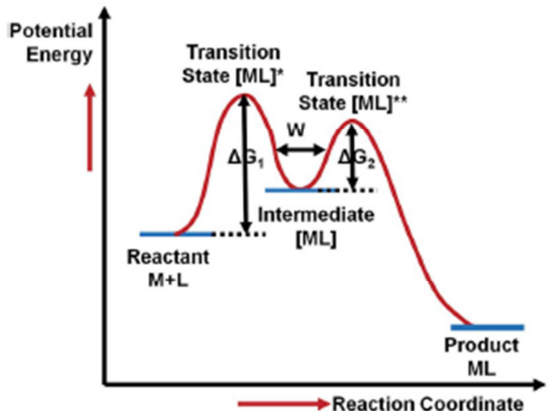

Fig.2.19: Metal-Ligand interaction-general mechanism (adapted from Chauhan et al, 2015)

The mechanism of metal-ligand complex (ML) formation can also be demonstrated in terms of a rapid pre-equilibrium. The reaction is carried out in an aqueous phase and the water molecules are replaced by another ligand in the coordination sphere of the metal. The reaction mechanism can be divided into two steps (Chauhan et al, 2015):

(1) Metal-water complexation (formation of an outer sphere complex $[M(H_2O)]^{a+}$
(2) Metal-chelate complexation (replacement of the water molecules by the ligand).

The reaction of metal-chelate complexation in an aqueous system is shown in **Figure 2.20**, which depicts that initially, the metal-complex contains water molecules as ligands and then the other ligand is substituting the first one in the rate determining step. Thus, the metal-ligand complex formation reaction can be considered a ligand substitution reaction. The ligand substitution reaction is presented as (Chauhan et al, 2015):

$$[ML_nX]^{z+}\ Y^- \leftrightarrows [ML_nY]^{z+} + X^- \qquad (2.14)$$

Different mechanisms (associative, dissociative, interchange) for the ligand substitution reaction are shown in **Figure 2.21**.

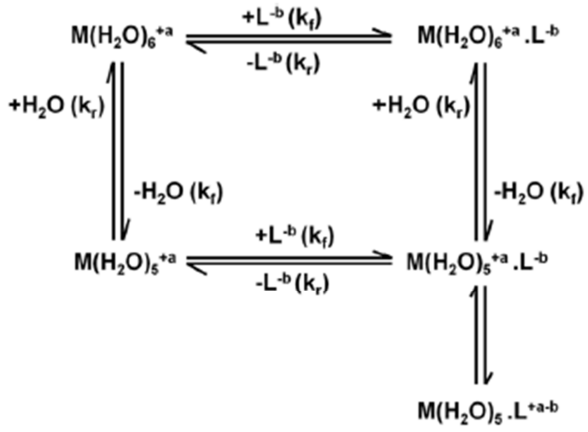

Fig.2.20: Schematic representation of the reaction mechanism for metal-complex formation in an aqueous system (adapted from Chauhan et al, 2015)

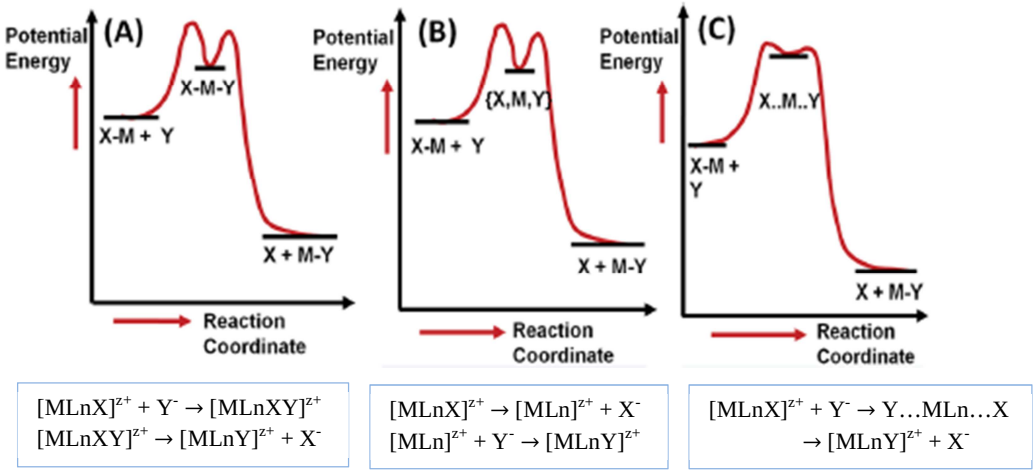

Fig.2.21: Ligand substitution mechanisms – (a) associative, (b) dissociative, (c) interchange (Adapted from Chauhan et al, 2015)

The chelate effect

Metal chelates are inherently more stable than closely related non-chelate complexes. This is known as the chelate effect (Dwyer and Mellor, 1964). A detailed study of several cadmium complexes by Spike and Parry (1953) showed that the stability of the metal chelate in each case was greater than that of the corresponding non-chelate complex. A summary of some of their results is shown in **Table 2.8.**

Table 2.8: Cadmium complexes and the chelate effect

Complex		Log Stability constant
$[Cd(NH_3)_2]^{2+}$	Non-chelate	4.950
$[Cd(NH_2CH_3)_2]^{2+}$	Non-chelate	4.808
$[Cd(en)]^{2+}$	**chelate**	**5.836**
$[Cd(NH_3)_4]^{2+}$	Non-chelate	7.44
$[Cd(NH_2CH_3)_4]^{2+}$	Non-chelate	6.55
$[Cd(en)_2]^{2+}$	**chelate**	**10.62**

en = ethylenediamine chelate complex

A thermodynamic perspective of the chelate effect has been offered by some authors. According to Chauhan et al (2015), for a given metal-ligand reaction, the formation constant for the chelation process can be calculated using the thermodynamic relationship given as:

$$\Delta G^\circ = -RT \ln(K) = \Delta H^\circ - T(\Delta S^\circ) \qquad (2.15)$$

In this relationship, enthalpy (ΔH) contributes to the thermodynamics of the complexation process in the form of ligand repulsion, distortion and crystal field stabilization energy (Hyv¨onen, 2008) whereas, the entropy (ΔS) includes all probability factors that control the stability of the complex. Schwarzenbach (1952) delineated the combined effect of these two terms (enthalpy and entropy) as the 'chelate effect', which refers to the enhanced stability of a metal-ligand complex due to the chelation process. Therefore, the strong stability of chelate complexes can be considered to be a combined effect of the enthalpy and various forms of entropy of the reaction (Chauhan et al, 2015).

Specificity and selectivity in the formation of metal chelates

The results of stability constant measurements have shown that the ability of metal ions to form chelates is not chelate-specific. Equally, the ability of ligands to form chelates is not metal-specific. It seems highly unlikely that a particular chelating agent can combine with only one kind of metal and no other. Absolute specificity in this sense is not attainable. However, products formed from metal complexation with ligands may be specific in terms of their unique characteristics. In this sense, specificity resides not in the reagent but the product of the test (Dwyer and Mellor, 1964).

While chelating agents do not exhibit absolute specificity in their reactions with metal ions, they may exhibit varying degrees of selectivity according to circumstances. For example, chelating agents are used as selective precipitants in analytical chemistry. 8-Hydroxyquinoline forms water-insoluble precipitates with upwards of thirty different metals. This number may be reduced by controlling the pH of the solution from which precipitation takes place (Dwyer and Mellor, 1964).

Metal complexation by carboxylate ligands

As stated earlier, many compounds function as chelating agents by the loss of one or more protons. Although it is the anion that combines with the metal atom, it is, nevertheless, customary to call the parent molecule a chelating agent (Dwyer and Mellor, 1964). An alternative system of classification of chelating agents suggested by Diehl (1937) is based on the nature of the functional groups which are described as basic or coordinating for example, NH_2 or acidic, for example, -COOH, -SO_2H, -SH, -OH, etc. The acidic functional group of the type -

COOH is associated with carboxylic, hydroxycarboxylic and benzenocarboxylic acids. The carboxylic acids with one functional group (-COOH) are called monocarboxylic, those with two functional groups (HOOC-R-COOH), dicarboxylic. Hydroxycarboxylic and Benzenocarboxylic acids have a varying number of functional groups.

Monocarboxylic acids

Monocarboxylic acids have one functional group (–COOH) with one proton and are therefore monodentate chelates. The loss of the proton allows them to bind to a central metal atom at one point. Some examples of monocarboxylic acid ligands are: acetic acid (CH_3COOH) with its acetate anion, CH_3COO^- (Haynes, 2016) and formic acid (HCOOH) with its formate anion, $HCOO^-$ (Reutemann and Kieczka, 2000).

Dicarboxylic acids

Dicarboxylic ligands have two functional groups and are therefore bidentate chelates. The loss of two protons allows them to bind to a central metal atom at two points. Common examples of dicarboxylic ligands are: oxalic acid ($C_2H_2O_4$) with its oxalate anion $C_2O_4^{2-}$(Ullmann's Encyclopedia, 2005), malonic acid ($C_3H_4H_4$) with its anion, $C_3H_2H_4^{2-}$(Hildbrand and Pollak, 2001), maleic acid ($C_4H_4O_4$), with its maleate anion $C_4H_2O_4^{2-}$(Lohbeck, et al, 2000), tartaric acid ($C_4H_6O_6$) with its tartrate anion, $C_4H_4O_6^{2-}$ (Lide, 2005) and fumaric acid ($C_4H_4O_4$), with its fumarate anion, $C_4H_2O_4^{2-}$ (Lohbeck, et al, 2000). The resemblance between maleic and fumaric acid is because maleic acid is the cis-isomer of butenedioic acid, whereas fumaric acid is the trans-isomer.

Hydroxycarboxylic acids

Hydroxycarboxylic acids are hydroxyl-based carboxylic ligands which have a varying number of functional groups, which allow them to bind to a central metal atom. Common examples of h*ydroxy*carboxylic ligands are: citric acid ($C_6H_8O_7$) with its citrate anion, $C_6H_5O_7^{-3}$(Alexander, 2014) lactic acid ($C_3H_6O_3$) with its lactate anion, $C_3H_5O_3^{-1}$. The lactic acid ligand can also be bidentate when the chelating behaviour of the lactate anion ($C_3H_4O_3^{-2}$) is coordinated through one oxygen atom of the carboxylate group and the oxygen of the hydroxo group (Cariati et al, 1977).

Benzenocarboxylic acids

Benzenocarboxylic acids are benzene-based carboxylic ligands which have a varying number of functional groups, which allow them to bind to a central metal atom. An example of Benzenocarboxylic ligand is salicylic acid ($C_7H_6O_3$) with its salicylic anion, $C_7H_5O_3^-$ (Fiege et al, 2002).

Metal complexation by carboxylic acid ligands is exemplified by the complexation reaction of Co with an acetic acid ligand as shown in **Eqn. 2.2**. Cobalt acetate may be formed by the reaction between cobalt oxide or hydroxide and acetic acid. In this reaction, the acetic acid ligand forms a metal complex with the Co^{2+} cation through proton removal from the acetate chelate and shifting the equilibrium in favour of the metal complex, cobalt acetate. The cobalt acetate tetrahydrate has been shown by X-ray crystallography to adopt an octahedral structure, the central cobalt centre being coordinated by four water molecules and two acetate ligands as shown in **Eqn. 2.3** (Van Niekerk and Schoening, 1953).

$$2CH_3COOH + 3H_2O + CoO \rightleftharpoons (CH_3COO)_2Co\cdot 4H_2O \qquad (2.16)$$

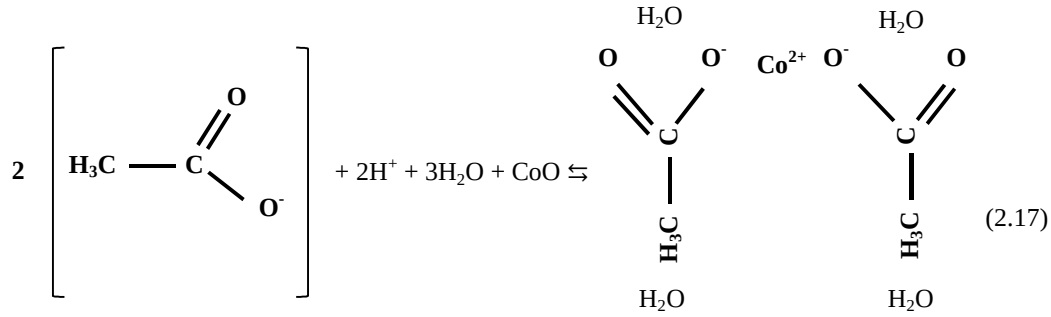

(2.17)

In the foregoing discourse, information on inorganic and organic acids, their chemical and physical properties including their commercial applications in industry has been presented. Metal complexation, its relevance and the mechanisms involved were highlighted. This information will be used as a basis for lixiviant selection discussed in the next section.

2.4.3.1.2 Lixiviant selection

A combination of inorganic and organic acids has been suggested as the route for overcoming the challenges previously highlighted in section 2.4.3. The basis for suggesting the two types of lixiviants is discussed in this section.

Inorganic acids

Inorganic acids also called mineral acids have strong oxidizing properties. They extract metals by proton attack. The hydronium ion reacts with a metal causing it to become oxidized thus inducing metal dissolution (Bronsted, 1931). Therefore, inorganic acids are strongly recommended for metal solubilization. However, not all inorganic acids are suitable candidates in terms of cost, ease of use, toxicity, corrosiveness and eco-friendliness. A careful selection to find the best candidate is certainly required. A number of potential acids are briefly discussed below:

As a strong oxidant, HNO_3 has strong metal dissolving properties. Nitric acid mixed with HCl in a ratio of 3:1 makes aqua regia, a reagent that can dissolve the noble metals gold, platinum, and palladium. As a lone acid, nitric acid, with its strong oxidizing properties, can be used to effectively extract Co from cemented carbide. However, HNO_3 is an expensive lixiviant and the large evaporative losses associated with its low boiling point at 121°C makes its use costly. In addition, the toxicity and corrosive nature of concentrated nitrate solutions constitutes an environmental hazard (Matjie et al, 2005; Nayak and Chitta, 2009).

HCl is a strong acid that can be used to form metal chloride salts. It has the advantage of complete dissociation in water and is capable of extracting Co from cemented carbide successfully. Despite these advantages, HCl is an expensive lixiviant in terms of acid cost and the evaporative losses associated with its low boiling point at 108.6°C makes its use just as costly as nitric acid. Moreover, at higher concentrations, corrosive mists of concentrated chloride solutions constitute an environmental hazard (Matjie et al, 2005; Nayak and Chitta, 2009). The corrosive mists react with construction materials, forming harmful chlorinated organic compounds (Peek et al, 2009).

Sulphuric acid has strong oxidizing properties (Housecroft, 2008). Although corrosive at high concentrations, the acid possesses different chemical properties and therefore has a wide range of applications some of which include metal extraction and chemical synthesis (Earnshaw and Greenwood, 1997). Sulphuric acid is stable, easier to handle, relatively cheap compared to other acids and allows good solubilization of metals (Lide, 2007; Perry et al., 1984).

Based on these observations, sulphuric acid is preferred for Co dissolution in cemented carbide hardmetal.

Organic acids

Organic acids also known as organic ligands have weak oxidizing properties, compared to inorganic acids, due to their poor dissociation in aqueous solutions. However, organic acids have strong 'metal-ligand bond' complexation properties. Almost all transition metals form complexes in the presence of organic ligands. These complexes show high water solubility and chemical stability (Dwyer and Mellor, 1964).

Organic acids extract metals through proton removal from the organic chelate thereby allowing the ligand anion to attach to the metal ion and shifting the equilibrium in favour of the metal complex. The metal chelate complexes formed are quite stable due to the chelate effect (Dwyer and Mellor, 1964; Spike and Parry, 1953). Utilization of organic chelate properties to either form useful metal complexes like cobalt acetate, a precursor to oil drying agents and catalysts that allow paints and varnishes to harden (Donaldson and Beyersmann, 2005) or the formation of tungsten lactate in order to suppress and stop tungsten from forming unwanted products are reported in literature (Cruywagen et al, 1993). These properties make organic chelates the preferred choice for metal complexation.

In the current work, an organic acid chelate could be used to suppress tungsten by forming a soluble tungsten complex salt thus, preventing it from forming undesirable insoluble tungsten products which obstruct mass transfer and cause poor diffusion in cemented carbide hardmetal leaching systems.

A number of organic acids, which can be used for metal complexation, have been previously discussed in section 2.4.3.1.1. These are acetic, formic, oxalic, malonic, maleic, tartaric, fumaric,

citric, lactic and salicylic acid. Previous research efforts have shown that organic acids from the dicarboxylic and hydroxycarboxylic class could make good candidates for complexation of metals from the transition series (Guedes de Carvalho and Neves, 1992; Van Niekerk and Schoening, 1953).

Based on these observations, lactic, maleic and tartaric acid are the preferred chelating agents for tungsten complexation. The three acids will, therefore, be subjected to reagent selection trials in order to select the best, which will then be used as a companion to sulphuric acid and the two will be used together in the cemented carbide leaching system. Sulphuric acid will be aimed at promoting Co dissolution, whereas the organic chelating agent will be aimed at promoting tungsten complexation in order to suppress the formation of slow equilibria polyanion precipitates.

2.4 Selective Dissolution in Semi-direct Leaching Reactions

Selective dissolution studies of WC-Co hardmetals are of great importance for understanding their properties and performance in leaching systems. In selective dissolution, one component is dissolved chemically, leaving the other phase(s) unaffected. In this technique, conditions are created which enhance the dissolution of a particular metal of interest while suppressing the dissolution of the other metal(s). This can be achieved by exploring the differences in the thermodynamic stability of the respective aqueous species of the metals in a given leaching system. Therefore, Eh-pH diagrams guide the thermodynamic stability differences and have been found to be a fundamental useful tool when designing selective dissolution processes. Another useful tool in designing leaching systems is leaching kinetics which provides information on reaction rates.

Depending on the prevailing reaction mechanism(s), the reaction products expected from selective dissolution reactions could be fluid, solid or both. When the reaction(s) taking place do not involve a product layer mechanism, the outcome of the reactions is a fluid product and the unreacted skeleton residue is retained. However, if the reaction(s) taking place involve(s) a product layer controlled mechanism, solid products are to be expected and will form part of the retained skeleton residue. Based on this observation, selective dissolution processes could take

one of two routes: 1) product layer-free route shown in **Figures 2.22** or 2) product layer-inclusive route shown in **Figure 2.23**.

In the examples shown in the figures, it is assumed that the material undergoing selective dissolution has low contiguity, hence the loose final skeleton structure which can easily be disintegrated.

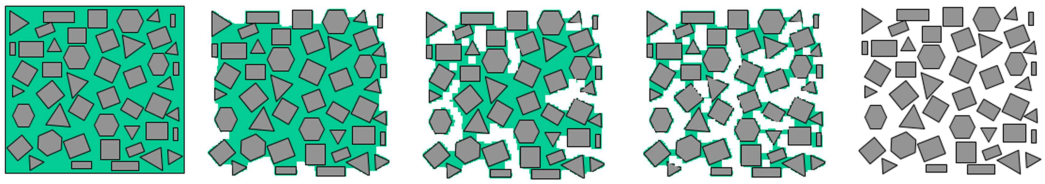

Fig.2.22: Product layer-free route 1: (a) unleached, (b) <50% leached (c) ~50% leached with some open channels, (d) >50% leached with >50% open channels, (e) ~100% leached with all channels open.

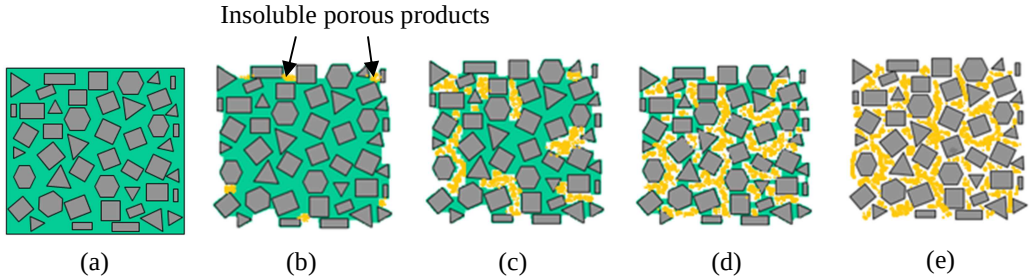

Fig.2.23: Product layer-inclusive route 2: (a) unleached , (b) <50% leached with a bit of solid formation on the surface, (c) ~50% leached with the insoluble product in channels, (d) >50% leached with the insoluble product in channels, (e) ~100% leached with the solid product in channels

2.5 Kinetics of Leaching Reactions

Metal extraction efficiencies and recovery from metal bearing materials is determined by both the chemical kinetics of reactions involved and the mineralogy of the material being leached (Tzeferis and Agatzini-Leonardou, 1994; Valix et al., 2001). Therefore, the ease or difficulty of extracting metals such as cobalt from the cemented carbide binder phase will be reflected in the extraction efficiencies. Whereas the main objective with thermodynamic data is the possibility of a chemical reaction taking place and in which direction a process occurs but, in itself tells nothing about its rate, reaction kinetics is concerned with understanding the rates of chemical reactions and the type of mechanism controlling the reaction.

2.5.1 Reaction Mechanisms

For leaching processes, chemical kinetics can be described in the framework of heterogeneous non-catalytic solid-fluid reactions in conjunction with the shrinking core model. This is the most widely accepted model for describing solid-liquid reaction kinetics of non-porous particles. The extraction of cobalt from cemented carbide using acidic media like sulphuric acid solution is an example of a solid-fluid reaction.

2.5.1.1 Shrinking Core Model

Although there is not much information on the use of the shrinking core model for modeling the cemented carbide-sulphuric acid leaching process, the use of the shrinking core model has been studied extensively in hydrometallurgy (Crundwell, 1995; Veglio et al., 2001). The shrinking core model for the solid-liquid systems is generally applied to describe the shrinkage of ore particles during mineral leaching reactions which are a key unit operation in hydrometallurgical processing. The key principle in all processes where the shrinking core model is applied is the establishment of a link between the leaching kinetics and the changes in the size of the particles undergoing a reaction. The shrinking core model is based on the assumptions that the reaction is irreversible, the particle is spherical, the reaction interface shrinks uniformly and that the reaction is non-catalytic. The limitations of the shrinking core model are that it is idealized and assumes an even distribution of the target metal throughout the particles, ignoring the presence of other constituents which may affect the overall process. The shrinking core model, therefore, works well for very porous solids.

Based on the shrinking core model, the mechanism of heterogeneous non-catalytic reactions may be considered to consist of six steps (Wen, 1968). These include: (1) diffusion of the fluid reactants across the fluid film surrounding the solid, (2) diffusion of the fluid reactants through porous solid layer, (3) adsorption of the fluid reactants at the solid reactant surface, (4) chemical reaction with the solid surface, (5) desorption of the products from the solid reaction surface, and (6) diffusion of the product away from the reaction surface through the porous solid media and through the fluid film surrounding the solid.

For spherical particles involving the quasi-steady state diffusion, the reactant passes through the reacted portion of the particle to the unreacted core followed by the chemical reaction with the

solid surface. Since these steps take place consecutively, if any of the above steps is much slower than all the others, that step becomes the rate-determining or reaction controlling step. Identification of this step is, therefore, very important. From the six steps that comprise a reaction, three rate determining steps are suggested. 1) Diffusion through the mass boundary layer: film diffusion, 2) Chemical reaction at the reactant-product interface and 3) Diffusion through the porous product layer.

2.7.1.1.1 Film diffusion limiting step

At any given time t, the amount of B reactant present in a particle is presented as (Levenspiel, 1972):

$$N_B(t) = \rho_B \, {}^4/_3 \pi r r_c^3 \qquad (2.18)$$

Where N is the number of moles, B is the solid reactant, t is instantaneous time, ρ is the density of the solid particle, r_c is the radius of the unreacted core of the solid particle, R is the original radius of the solid particle.

The decrease in volume or radius of the unreacted core accompanying the disappearance of N_B moles of the solid reactant is presented as:

$$-dN_B = -4\rho_B \pi r r_c^2 dr_c \qquad (2.19)$$

The rate of reaction in terms of the shrinking radius of the unreacted core is presented as:

$$-\frac{1}{S}\frac{dN_B}{dt} = -\frac{\rho_B}{R^2}\frac{r_c^2 dr_c}{dt} = bk_m C_{AB} \qquad (2.20)$$

Where, C_{AB} is the concentration of reactant A in the bulk solution; k_m is the mass transfer coefficient, b is the moles of reactant A. From stoichiometry, the rate of reaction of B is taken as:

$$-\frac{1}{S}\frac{dN_B}{dt} = -\frac{1}{4\pi R^2}\frac{1}{b}\frac{dN_B}{dt} = -\frac{1}{S}\frac{dN_A}{dt} \qquad (2.21)$$

The rate of consumption of A = the rate of reaction of B.

Therefore,

$$-\frac{1}{S}\frac{dN_A}{dt} = k_m (C_{AB} - C_{AS}) \qquad (2.22)$$

$$-\frac{1}{S}\frac{dN_B}{dt} = bk_m (C_{AB} - C_{AS}) \qquad (2.23)$$

Where, C_{AS} is the concentration of A on the particle surface.

For $C_{AS} = 0$,

$$-\frac{1}{S}\frac{dN_B}{dt} = bk_m(C_{AB}) = \text{constant } \boldsymbol{t}$$

Integrating **Equation 2.20**,

$$-\frac{\rho_B}{R^2}\int_R^{r_c} r_c^2 \frac{dr_c}{dt} = bk_m C_{AB}\int_0^1 dt \qquad (2.24)$$

$$\boldsymbol{t} = \frac{\rho_B R}{3bk_m C_{AB}}\left[1-\left(\frac{r_c}{R}\right)^3\right] \qquad (2.25)$$

When $r_c = 0$ and $\boldsymbol{t} = \boldsymbol{t}_{comp}$

$$\boldsymbol{t_{comp}} = \frac{\rho_B R}{3bk_m C_{AB}} \qquad (2.26)$$

$$\boldsymbol{t_{comp}} = \frac{\boldsymbol{\rho_B R}}{\boldsymbol{3bk_m C_{AB}}} \cong \frac{\boldsymbol{R}}{\boldsymbol{k_m}} \qquad \textbf{(2.27) Film diffusion}$$

In the above model, showing the film diffusion reaction control mechanism, the reaction time, is inversely related to the mass transfer coefficient (k_m) and directly related to the solid particle size (R). Both particle size and mass transfer have an influence on the film diffusion reaction control mechanism. However, mass transfer has a greater influence. Therefore, agitation, which aids mass transfer, has a significant influence on a leaching process that is film diffusion controlled. The leaching rate increases with increased agitation as the diffusion layer becomes thinner.
Diving **Equation 2.25** by **Equation 2.26**,

$$\frac{\boldsymbol{t}}{\boldsymbol{t_{comp}}} = 1-\left(\frac{r_c}{R}\right)^3 = X_B \qquad (2.28)$$

Where X_B is the fractional conversion of reactant B; $\boldsymbol{t}_{comp}$ is the reaction completion time.

2.7.1.1.2 Chemical reaction limiting step

For a chemical reaction limiting step, the chemical reaction at the surface is much slower than diffusion of reactants through the diffusion and product layer. Therefore, the concentration of A at the unreacted core surface is the same as that of the bulk solution C_{AB}.

Since the progress of the reaction is unaffected by the presence of a product layer, the quantity of the material reacting is proportional to the available surface of the unreacted core (Levenspiel, 1972).

At steady state,

$$-\frac{1}{4\pi r_c^2}\frac{dN_B}{dt} = -\frac{b}{4\pi r_c^2}\frac{dN_A}{dt} = bk_r(C_{AB}) \quad (2.29)$$

Where, k_r is the first order rate constant for the surface reaction
Writing N_B in terms of the shrinking radius and integrating,

$$-\rho_B\int_R^{r_c} dr_c = bk_r C_{AB}\int_0^t dt \quad (2.30)$$

$$\boldsymbol{t} = \frac{\rho_B}{bk_r C_{AB}}[R - r_c] \quad (2.31)$$

$$\boldsymbol{t_{comp}} = \frac{\rho_B R}{bk_r C_{AB}} \quad (2.32)$$

$$\boldsymbol{t_{comp}} = \frac{\rho_B R}{bk_r C_{AB}} \cong \frac{R}{k_r} \quad \textbf{(2.33) Chemical reaction}$$

In the above model, showing the chemical reaction control mechanism, the reaction time, is inversely related to the reaction rate constant (k_r) and directly related to the solid particle size (R). This shows that both particle size and reaction rate have an influence on the chemical reaction control mechanism. However, reaction rate has a greater influence. Therefore, temperature and reactant concentration, which aid reaction rate, have a significant influence on a leaching process that is chemical reaction controlled. Higher temperature and concentration give higher reaction rates.

Diving **Equation 2.31** by **Equation 2.32**,

$$\frac{t}{t_{comp}} = 1 - \frac{r_c}{R} = 1 - (1-X_B)^{1/3} \quad (2.34)$$

Where, X_B is the fractional conversion of reactant B.

2.7.1.1.3 Product layer diffusion limiting step

The concentration of reactant A is uniform and approaches zero at the unreacted core surface (Levenspiel, 1972).

$$D_e = D\left(\frac{\theta}{T}\right) \qquad 2.35$$

Where, D_e is the effective diffusivity, θ is the porosity of the product layer; T is the tortuosity (property of a path or curve being twisted or having many turns) usually greater than 1.

Applying Fick's law of diffusion at steady state,

$$-\frac{dN_A}{dt} = 4\pi r^2 D_e \frac{dC_A}{dr} \qquad (2.36)$$

Integrating,

$$-\frac{dN_A}{dt}\int_R^{r_c}\frac{dr}{r^2} = 4\pi D_e \int_{C_{AB}}^{0} dC_A \qquad (2.37)$$

$$-\frac{dN_A}{dt}\left(\frac{1}{r_c} - \frac{1}{R}\right) = -4\pi D_e C_{AB} \qquad (2.38)$$

The conditions of a reacting particle at any time are presented as:

$$\frac{4\pi\rho_B r_c^2}{b}\frac{dr_c}{dt}\left(\frac{1}{r_c} - \frac{1}{R}\right) = -4\pi D_e C_{AB} \qquad (2.39)$$

Assuming that the size of the unreacted core changes with time and as the core shrinks, the ash layer becomes thicker lowering the rate of diffusion of reactant A.

Integrating **Equation 2.39**,

$$-\rho_B \int_R^{r_c}\left(\frac{1}{r_c} - \frac{1}{R}\right) r_c^2\, dr_c = bD_e C_{AB}\int_0^1 dt \qquad (2.40)$$

$$t = \frac{\rho_B R^2}{6bD_e C_{AB}}\left[1 - 3\left(\frac{r_c}{R}\right)^2 + 2\left(\frac{r_c}{R}\right)^3\right] \qquad (2.41)$$

$$\boldsymbol{t_{comp} = \frac{\rho_B R^2}{6bD_e C_{AB}}} \qquad (2.42)$$

$$\boldsymbol{t_{comp} = \frac{\rho_B R^2}{6bD_e C_{AB}} \cong \frac{R^2}{D_e}} \qquad \textbf{(2.43) Product layer}$$

In the above model, showing the product layer reaction control mechanism, the reaction time, is inversely related to effective diffusivity (D_e) and directly related to the square of the solid particle size (R). This shows that both particle size and diffusion have an influence on the product layer reaction control mechanism. Therefore, agitation, which aids diffusion, has a significant influence on a leaching process that is product layer diffusion controlled. The leaching rate increases with increased agitation as the transfer and diffusion of products and reactants become enhanced.

Dividing **Equation 2.41** by **Equation 2.42**,

$$\frac{t}{t_{comp}} = 1 - 3(\frac{r_c}{R})^2 + 2(\frac{r_c}{R})^3 \qquad (2.44)$$

$$\frac{t}{t_{comp}} = 1 - 3(1 - X_B)^{2/3} + 2(1 - X_B) \qquad (2.45)$$

It is, therefore, useful to express the reaction rates in terms of particle conversion or fractions reacted. Equations governing the three rate controlling regimes (Levenspiel, 1972) are illustrated in **Table 2.9**.

a) Film diffusion control
b) Chemical reaction control
c) Ash layer diffusion control

Table 2.9: Shrinking Core Models **(**Levenspiel, 1972**)**

Regime	Equation
Film diffusion control	$X = kt$
Chemical reaction control	$1 - (1 - x)^{1/3} = kt$
Product (ash) layer diffusion control	$1 - 3(1 - x)^{2/3} + 2(1 - x) = kt$

x = fractional conversion; t = time (hours); k = rate constant (hr^{-1})

2.5.1.2 Activation Energy Model

For leaching processes, reaction kinetics and rate controlling mechanisms may also be described in the framework of heterogeneous non-catalytic solid-liquid reactions based on activation energies. The Arrhenius equation-based reaction constant k is one common approach used in calculating activation energies. The Arrhenius **Equation 2.46** gives a quantitative relation between the rate constant (***k)*** and temperature (**T**):

$$k = Ae^{\frac{-E_a}{RT}} \qquad \textbf{(2.46)}$$

Where, ***A*** is the frequency factor or pre-exponential constant, E_a is the activation energy, ***T*** is the absolute temperature in Kelvin and ***R*** is the gas constant.

Taking natural logarithms on both sides and dividing throughout by 2.303, **Equation 2.46** becomes:

$$logk = -\frac{E_a}{2.303RT} + logA \qquad (2.47)$$

By setting k_1 and k_2 as ***rate constants*** for the reaction at two different temperatures T_1 and T_2 **Equation 2.47** becomes,

$$logk_1 = logA - \frac{E_a}{2.303RT_1} \qquad (2.48)$$

And

$$logk_2 = logA - \frac{E_a}{2.303RT_2} \qquad (2.49)$$

Subtracting **Equation (2.48)** from Equation **(2.49)** yields,

$$logk_2 - logk_1 = \frac{E_a}{2.303R}\left[\frac{1}{T_1} - \frac{1}{T_2}\right] \qquad (2.50)$$

From **Equation 2.47**, the activation energy (E_a) can be computed from the slope of the Arrhenius plot of **logK** versus $\mathbf{T^{-1}}$**.** Alternatively, the activation energy (E_a) can be calculated using **Equation 2.50**.

It is clear, from **Equation 2.47**, that as the value of activation energy E_a increases, the value of ***k*** decreases and, therefore the reaction rate decreases. Conversely, as the value of activation energy E_a decreases, the value of ***k*** increases and, therefore the reaction rate increases. The magnitude of

the activation energy can provide positive evidence for the rate controlling regimes (Habashi, 1968; Potgieter et al., 2006). Activation energies governing these rate controlling regimes are illustrated in **Table 2.10.**

Table 2.10: Activation Energies for Rate Controlling Mechanisms (Habashi, 1969)

Regime	Activation Energy
Product (Ash) layer diffusion control	< 20 $kJmol^{-1}$
Film diffusion control	20 - 50 $kJmol^{-1}$
Chemical reaction control	> 50 $kJmol^{-1}$

2.5.2 Kinetics of Cemented Carbide acid Leaching

The semi-direct selective leaching of cemented carbide entails removal of the binder medium from the matrix, leaving behind a finely divided tungsten carbide (WC) which can be recycled in the fabrication of new tools. The binder medium is most often Co, in some cases Ni or other metals from the Fe group (Exner, 1979). The extraction efficiency and recovery of the binder medium is mainly determined by the chemical kinetics of reactions involved and the material phases present. However, there is not much information in literature about the leaching kinetics of the binder medium dissolution out of the cemented tungsten carbide.

Using nitric acid, Gurmen and Friedrich (2005) investigated the leaching kinetics of cobalt from powderized cemented carbide scrap material, particle size, $<90\mu m$, and chemical composition: W (75.86%wt.), Co (8.14%wt.), C (6.07%wt.), Ti (4.18%wt.), Nb (1.35%wt.), Ni (1.00%wt.) and Fe (3.4%wt.). They found that the leaching process followed the kinetic model $1\text{-}3(1\text{-}x)^{2/3} + 2(1\text{-}x) = kt$ and the activation energy was determined to be 13.77kJ mol^{-1} at 25-70°C. Under the leaching conditions of 25°C, 0.5M HNO_3 concentration, 1/10 solid to liquid ratio and an agitation rate of 900rpm, a leaching efficiency of 91.5% was achieved in 2hrs. The authors concluded that the leaching of cobalt from powdered cemented carbide in nitric acid solution was controlled by product (ash) layer diffusion.

Kutcher and co-researchers (2017) studied the chemical kinetics of leaching cemented carbide cutting inserts in aqueous media consisting of HCl and H_2O_2 oxidant. Hydrogen peroxide was

employed in order to provide an oxidative environment for the leaching reaction. The experiments were performed within a temperature range of 30 – 80°C, acid concentration range of 0.1 to 2.0M and hydrogen peroxide concentration range of 1 to 4M. Their findings showed that the process was generally controlled by diffusion. However, their report did not specify whether the diffusion reaction mechanism was film or product layer controlled. Notably, the extent of Co extraction was not specified either. In their second study (Kutcher et al, 2018), the authors used formic acid and hydrogen peroxide oxidant to study interactions between possible leaching mechanisms of hardmetals. Their results still displayed a diffusion restricted mechanism. Neither the type of diffusion control mechanism nor the extent of binder metal extraction was stated in their results.

2.6 Precipitation

Precipitation is a chemical reaction that occurs in aqueous solution when two ions bond together to form an insoluble salt which is known as a precipitate. Nielsen (1970) suggested that precipitation is the formation of one or more new phases with a composition different from that of the original multicomponent single-phase system. Precipitation occurs through the formation of compounds with low solubility. The solid is formed as a result of exceeding its saturation solubility. The solubility behaviour of sparingly soluble salts in aqueous solutions is of great importance in many hydrometallurgical processes. Some applications include: selective precipitation to remove impurities thus refining a metal bearing-solution; precipitation of a metal compound from a large volume and re-dissolving it in a smaller volume hence increasing the metal ion concentration in solution; precipitation of metal powders from solution using hydrogen reduction (Jackson, 1986; Garrels and Christ, 2007; Gurney, 2012).

Precipitation processes are reliable, well proven and relatively simple. Conditions that can trigger a precipitation reaction include but are not limited to: Redox reactions, pH change and ion addition (Monhemius, 1977; Jackson, 1986). Four known important types of insoluble metal salt precipitates are hydroxides, sulphides, phosphates and arsenates (Monhemius, 1977). The selective precipitation of metal hydroxides by controlled changes of pH is perhaps the best known and most widely used method for the removal of certain metals from impure leach liquors. Equally important for solution purification is the selective precipitation of metal sulphides by the use of gaseous hydrogen sulphide (Monhemius, 1977).

Nielsen (1970) explains that there are four stages of a precipitation process. Precipitation starts with nucleation on impurity particles (or seeds), or with the formation of embryos. The nuclei grow into crystallites. Strickland-Constab1e and Mason (1963) observed that sometimes the growth process is accompanied by the formation of new secondary nuclei so that crystallites of two or more sized groups are present. The crystallites may form a stable suspension or they may coagulate. When the crystallites or the coagulated clusters in a liquid become larger, they tend to sediment. This is usually the last step of the process, and the growth of the individual particles seems to have ceased. However, if the system is observed for a very long time, it is evident that the smaller crystallites re-dissolve and the larger ones grow further. Thermodynamically, the system is not stable until all the solute in excess of the amount corresponding to the solubility is united into a single crystal and this is the theoretical termination (Nielsen, 1970). The stages of the precipitation process are illustrated in **Figure 2.24**.

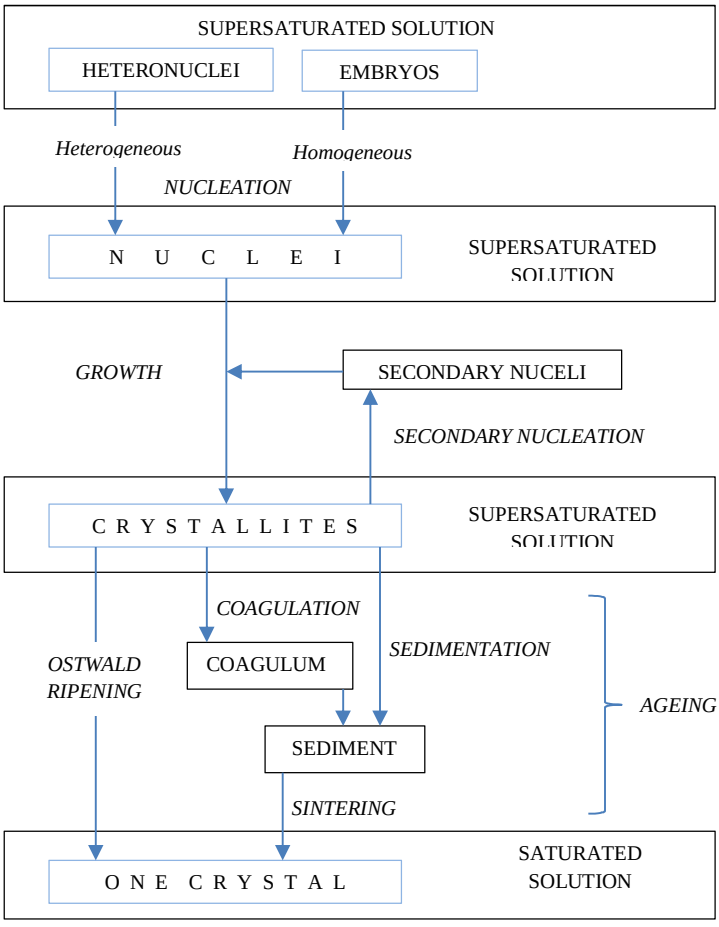

Figure 2.24: Ways and stages of precipitation processes (Nielsen, 1970)

Supersaturation

Supersaturation occurs when the concentration of a species in solution is greater than its saturation solubility. The degree of supersaturation is the driving force in precipitation. If the concentration is significantly greater than saturation, then there is higher tendency to form a precipitate (Jackson, 1986; Garrels and Christ, 2007; Gurney, 2012). Precipitation is not possible unless the solution is supersaturated. A saturated solution can be made supersaturated by temperature change or fractionation through evaporation or crystallization of the solvent. Another way of making a supersaturated solution is to mix two solutions which react chemically, for instance, electrolyte precipitation from aqueous solution or salting out; addition of a poor solvent to a solution in a good solvent (Nielsen, 1970). Supersaturation is represented as:

$$S = \frac{(C - C_e)}{C_e} \qquad (2.51)$$

Where, C is the solute concentration and Ce is the equilibrium or saturated solubility.

Solubility and Solubility product

Ionic compounds dissolve to the point where the solution is saturated and no more solid can dissolve; that is to say when supersaturation occurs. Saturated solubility is represented as:

$$M_m P_n = mM^{z+} + nP^{y-} \qquad (2.52)$$

The concentration of the saturated solution is termed the solubility. In such a saturated solution, equilibrium is established. The solubility product is the *equilibrium constant* for the reaction in a saturated solution. The solubility product constant may be expressed in terms of activity or concentrations and for a solid compound with unity activity (Jackson, 1986; Garrels and Christ, 2007; Gurney, 2012).

$$K_{sp} = \left[M^{z+} \right]^m \left[P^{y-} \right]^n \qquad (2.53)$$

The solubility product is called as such because it is literally the product of the solubilities of the ions in moles per Litre ($molL^{-1}$).

Precipitation of a compound from an aqueous solution is determined by its solubility product, K_{sp}. If an ion is present in solution in some definite concentration, it can be precipitated by a second ion only if that second ion is present in sufficient concentration for the solubility product constant of the compound in question to be exceeded i.e. supersaturation is attained (Jackson, 1986; Garrels and Christ, 2007; Gurney, 2012).

Given a reaction shown in **Equation 2.51** as:

$$M_m P_n = mM^{z+} + nP^{y-} \qquad (2.54)$$

And for a given metal ion solubility, if

$$Q = \left[M^{z+}\right]^m \left[P^{y-}\right]^n \qquad (2.55)$$

Then,

$Q < K_{sp}$ Solution unsaturated; No precipitation

$Q > K_{sp}$ Solution supersaturated; Precipitation occurs

The K_{sp} governs the extent to which the solid can be taken into or precipitated from a solution.

Precipitation can play a significant role in cemented carbide leaching. It can either be employed to remove impurities from leach liquor or to recover metals of interest. In the current study, precipitation will be employed as purification step to remove impurities from the cemented carbide leach liquor prior to the solvent extraction process. Precipitation of tungsten as scheelite from the raffinate solution after the solvent extraction process will be attempted.

Commercial applications

As a separation technique, precipitation is a well-established process that is widely accepted and commercially applied in the cobalt processing industry. Cobalt is produced mostly as a by-product of other major metal extraction processes, mainly copper and nickel (Fisher, 2011; Hawkins, 1998). Thus, after leaching a copper-cobalt ore, acid-soluble minerals of both Cu and Co undergo dissolution and report to the pregnant leach solution (PLS) (Mwema et al, 2002; Ferron, 2008). After solvent extraction of Cu, the solution stream contains very little Cu but almost all the Co together with base metals are treated for Co recovery. The chemical

composition of the stream is typically, Cu, 0.2-0.5gpl, Co, 2-3gpl, Fe, 1-2gpl, Mn, 1gpl, and Al, 1gpl.

The most widely employed flowsheets use sequential metal hydroxide precipitation to remove impurities from the Co stream. In the first step, iron, aluminium, and manganese are removed by a combination of oxidation and precipitation using a mixture of air and SO_2. After oxidation of Iron to the 3+ state and manganese to the 4+ state, Fe (III), Al, and most Mn (FAM) are removed from the Co stream using lime at pH 3-4.5 in a series of stirred tanks. In the second step, residual Cu is precipitated at pH 5.5-6 using lime. The underflow (U/F) FAM precipitates, report to the tailings and the Cu precipitates are recycled back to the leaching process. The overflow (O/F) Co stream can be treated in a variety of ways, depending on the product preference, the product purity required, and the prevailing economic conditions and constraints (Sole et al, 2019). The usual product choices include cobalt hydroxide, cobalt carbonate, cobalt sulphate or cobalt metal.

Cobalt hydroxide (II) precipitates at pH 7.5, but to achieve quantitative cobalt precipitation, pH 8–8.5 is required. Typical precipitants include $Ca(OH)_2$, MgO, CaO and NaOH. Several operators employ a two stage precipitation. The first stage is controlled at pH7.5 with MgO to maximize the cobalt product grade by minimizing the presence of unreacted magnesia in the product. The second stage is controlled at pH 8.5 with lime to ensure that cobalt recoveries exceed 99%. Cobalt hydroxide is produced using magnesia at Tenke Fungurume Mining, Mutanda Mining, Kamoto Copper, Sicomines, China Dongfang Mining, and MKM (La Minière de Kalumbwe Myunga). The theoretical cobalt content of a dry pure cobalt hydroxide is 63.4% (the balance being hydroxide of no value). Typical moisture content for these types of filter cakes is around 50% or higher. Hydroxides do not filter as well as carbonates. Slow oxidation of the hydroxide to the oxide occurs in air. However, adding an antioxidant to the hydroxide prevents the product from oxidizing without affecting its chemical performance characteristics (Sole et al, 2019).

The precipitation of cobalt carbonate is achieved with a suitable carbonate base, such as soda ash (Na_2CO_3), ideally at a temperature of 60°C (Boynton, 1980). Limestone ($CaCO_3$) can also be used, but its low solubility leads to poor utilization; in addition, $CaSO_4$ is co-precipitated and this contaminates the final product. Quantitative precipitation of cobalt carbonate requires pH 8–8.5.

To achieve high-purity cobalt carbonate, significant removal of Fe, Cu, Zn, and Mn is required. Boss Mining is the only operation currently employing soda ash for cobalt carbonate precipitation. Copper and cobalt are co-precipitated from a process bleed stream after iron removal: the product contains only ~11% Co, but has a moisture content exceeding 70%. Significant losses of both Cu and Co also report to the iron cake (Sole et al, 2019).

2.7 Solvent Extraction

Solvent extraction is the removal of one or more components of a leach or other solution by transfer of a metallic species from the aqueous phase into an immiscible non-aqueous or organic phase for the purpose of extraction, purification or concentration (Ritcey and Ashbrook, 1979; Jackson, 1986). The transfer is driven by a chemical potential until equilibrium is reached. The solvent that is enriched in solute is called the extract or loaded organic and the aqueous feed solution that is depleted in solute is called the raffinate. The solvent extraction method is one of the favoured separation techniques because of its simplicity, speed, and wide scope (Kislik, 2012). This extraction technique is used in numerous chemical industries to produce pure chemical compounds ranging from pharmaceuticals and bio-medicals to heavy organics and metals, in analytical chemistry and in environmental waste purification (Rydberg et al, 2004).

Extraction

The solvent extraction procedure involves a contact of two immiscible liquids such as organic and aqueous liquid phases in a vessel, usually a separating funnel (Gani et al, 2006). The aqueous solution is mixed intimately with an immiscible organic phase containing the active extractant at which time the active extractant transfers the desired metal from the aqueous phase into the organic phase. The technique entails liquid-liquid interaction that involves the distribution of a solute between two immiscible liquid phases in contact with each other (Rydberg et al, 2004). In solvent extraction, extractable metal species can be divided into four categories:

- Metal cations, e.g. Cu^{2+}, Ni^{2+}, and Co^{2+}
- Complex metal anions, $[Ag(CN)_2]^-$, $[CuCl_4]^{2-}$
- Complex metal cations, e.g. $[Cu(NH_3)_4]^{2+}$

- Neutral metal species.

The solvent extraction principle is illustrated in **Figure 2.25**.

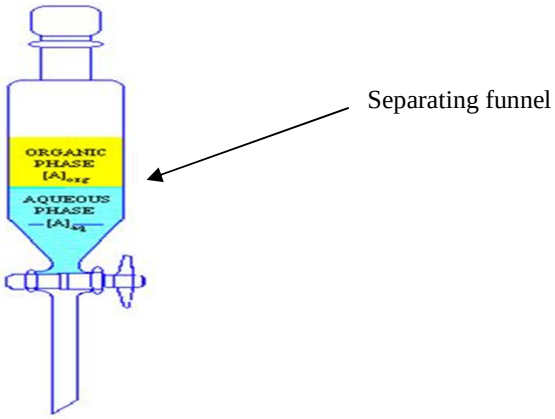

Fig.2.25: A schematic representation of solvent extraction. A solute A is distributed between the upper layer, for example an organic solvent, and the lower layer, an aqueous phase (Rydberg et al, 2004).

The vessel (a separatory funnel) contains two layers of liquids; one is usually an aqueous solution while the other, an organic solvent. The organic phase often settles as the upper layer when it has a lower density than the aqueous solution, but the opposite situation also occurs. A solute *A*, which initially is dissolved in one of the two liquids, eventually distributes between the two phases. When this distribution reaches equilibrium, the solute has one concentration $[A]_{aq}$ in the aqueous phase and another concentration $[A]_{org}$ in the organic phase (Rydberg et al, 2004; Habashi, 1983).

A typical extraction reaction where an organic extractant removes Cu^{2+} from a pregnant leach solution is exemplified by the following reaction (Davenport et al, 2002):

$$2RH + Cu^{2+} + SO4^{2-} = R_2Cu + 2H^{+} + SO4^{2-} \quad (2.56)$$

Organic extractant	Aqueous pregnant leach solution	Loaded organic	Raffinate

Where, RH is the aldoxime or ketoxime extractant

Distribution ratio

Distribution ratio (D) is a measure of how well-extracted a species is. The distribution ratio of the solute A is expressed as (Rydberg et al, 2004):

$$D = \frac{[A]_{org}}{[A]_{aq}} \quad (2.57)$$

Where D is the ratio of the total analytical concentration of the substance in the organic phase to its total analytical concentration in the aqueous phase, irrespective of whether the organic phase is the lighter or heavier one. D, usually measured at equilibrium, is also called the distribution coefficient or the extraction coefficient. If a second solute, B, is present, the distribution ratios for the various solutes are indicated by D_A, D_B, and so on. If D_B is different from D_A, then species A and B can be separated from each other. Depending on the system, solvent extraction is a function of temperature, pH, and concentration of a species in the system (Rydberg et al, 2004).

Separation Factor

Separation factor (SF) is one distribution ratio divided by another. It is a measure of the ability of the system to separate two solutes (Rydberg et al, 2004). For example, if the distribution ratio for nickel (D_{Ni}) is 10 and the distribution ratio for solver (D_{Ag}) is 200, then the silver/nickel separation factor ($SF_{Ag/Ni}$) is equal to $\frac{D_{Ag}}{D_{Ni}} = SF_{Ag/Ni} = 20$.

Stripping

After extraction, the "loaded organic" phase is mixed intimately with an aqueous stripping solution, most often an acid that provides the driving force required to strip the loaded metal from the organic phase into the aqueous stripping phase. The proton (H^+) in the acid displaces the metal ion from its link with the extractant and takes its place while the displaced metal ion goes into solution and bonds with the acid conjugate to form a salt. The protonation reaction is the driving force behind stripping the loaded metal from the organic phase. A typical stripping reaction where an acid solution removes Cu^{2+} from a loaded organic extractant is exemplified by the following reaction (Davenport et al, 2002):

$$R_2Cu + 2H^+ + SO4^{2-} = 2RH + Cu^{2+} + SO4^{2-} \quad (2.58)$$

Loaded organic extractant	Acid solution	Stripped organic extractant	Strip loaded solution

Where, RH is the aldoxime or ketoxime extractant

The "stripped organic" is recycled back to extraction while the strip loaded solution (aqueous phase), now containing the desired metal, goes to final metal recovery as a pregnant leach solution (Ritcey and Ashbrook, 1979; Jackson, 1986; Habashi, 1983; Gupta and Mukherjee, 1990).

Extraction and Stripping Isotherms

The distribution of a dissolved component between two phases can be illustrated by equilibrium isotherms or distribution curves. The procedure for creating an extraction isotherm entails agitating different quantities of organic and aqueous phases in a separating funnel. After phase separation, the aqueous phase is analyzed with respect to an element and the element content in the organic phase is calculated. The isotherm is obtained by plotting the concentration of the element in organic phase against the concentration of the element in the aqueous phase (Rydberg et al, 2004; Jackson, 1986). Similarly, a stripping isotherm involves agitating different quantities of loaded organic and an aqueous acidic solution in a separating funnel. After phase separation, the aqueous phase is analyzed with respect to an element and the element content in the organic phase is calculated through mass balance. The equilibrium isotherm for stripping is obtained by plotting the concentration of the element in aqueous phase against the concentration of the element in the organic phase (Rydberg et al, 2004; Jackson, 1986).

Generic reactions for the extraction and stripping of a metal ion M^{2+} is presented as:

$$\text{Extraction: } 2RH_{(org)} + M^{2+}{}_{(aq)} = R_2M_{(org)} + 2H^+{}_{(aq)} \quad (2.59)$$

$$\text{Stripping: } R_2M(org) + 2H^+{}_{(aq)} = 2RH_{(org)} + M^{2+}{}_{(aq)} \quad (2.60)$$

These reactions show that extraction and stripping could be dependent on pH. However, it is important to note that not all extraction and stripping reactions in solvent extraction are pH dependent. For those that are pH dependent, Le Chatelier's principle applies. The high pH (low H^+ ion concentration) favours extraction, while low pH (high H^+ ion concentration) favours

stripping. Based on their pH dependency, for those that are, pH isotherms can be used to determine optimum extraction and stripping pH levels for individual metal ions. The important value to consider in extraction and stripping is the transfer capacity of the system in gpl metal ion, i.e. the difference in gpl metal ion between loaded and stripped organic per volume of reagent used (Ritcey and Ashbrook, 1979; Jackson, 1986; Habashi, 1983; Gupta and Mukherjee, 1990).

The McCabe-Thiele diagram

The McCabe-Thiele diagram is constructed by determining the equilibrium isotherm for extraction or stripping via experiments. After the equilibrium isotherm has been plotted into the diagram, an operating line can be constructed by starting at the point where the metal content of stripped organic (S.O.) intersects the equilibrium isotherm and drawing the line up and to the right with a slope equal to the ratio of the aqueous/organic flow rates (or loaded organic/aqueous feed) until it intersects the vertical line representing the metal content of the aqueous phase feed. From the upper intersection point, a horizontal line to the isotherm curve leftwards and then a vertical line to the operating line are drawn creating a step (**Figure 2.26**).

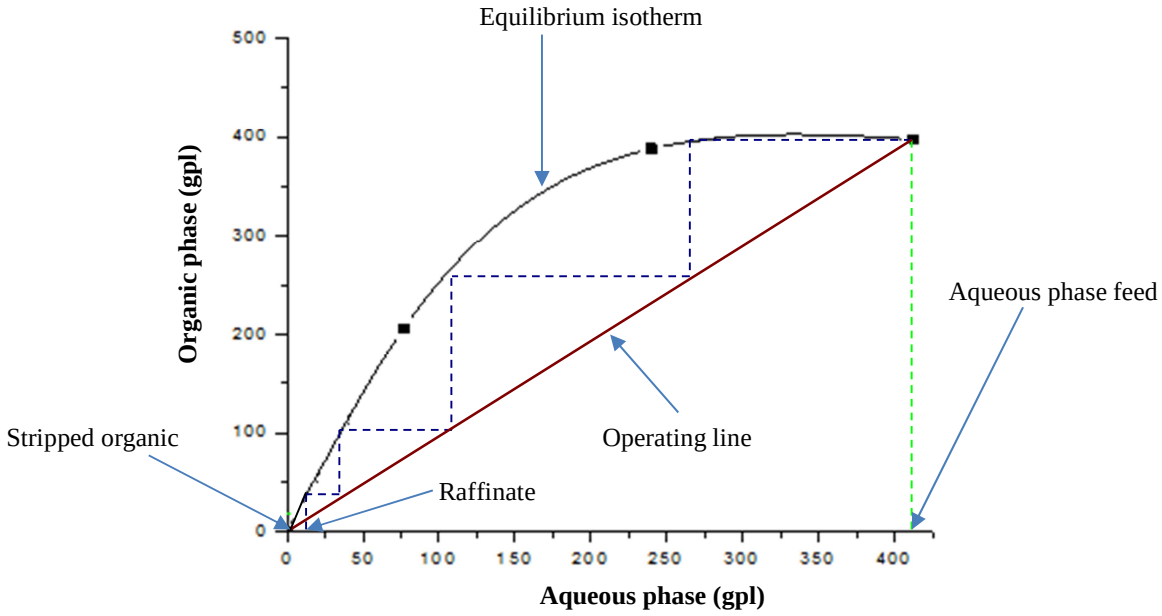

Fig.2.26: McCabe-Thiele diagram for extraction

This procedure is repeated until a satisfactory degree of extraction from the aqueous phase has been obtained. Each horizontal line in the McCabe-Thiele diagram corresponds to one step in the mixer-settler or one extraction stage. A McCabe-Thiele diagram for stripping is constructed in a similar way. However, for stripping, the aqueous phase (acid solution) will be on the y-axis and the organic phase (loaded organic), on the x-axis (Ritcey and Ashbrook, 1979; Jackson, 1986; Habashi, 1983; Gupta and Mukherjee, 1990).

Extractants

There are five classes of metal extractants as characterized by structure, extraction mechanism and the metal species extracted: chelation, ion pairing, neutral or solvating, organic acids and ligand substitution. Chelation, for instance, refers to "claw", which is a graphic description of the way in which the organic extractant binds a metal ion. i.e., the extractant chemically bonds to the metal ion at two sites in a manner similar to holding an object between the ends of the thumb and the index finger. In many cases, upon bonding with the metal ion, the extractant releases a hydrogen ion into the aqueous solution from which the metal was extracted (Jackson, 1986; Habashi, 1983). The organic extractant used in the current study is Cyanex 272 (bis (2,4,4-trimethylpentyl)/ phosphinic acid). It is a dialkyl phosphinic acid extractant widely used for the separation of Co from Ni to produce high purity cobalt salts and cobalt metal. Since the active component of Cyanex 272 extractant is a phosphinic acid, it is an acid based chelating agent and metals are extracted through a metal complexation cation exchange mechanism. The Cyanex 272 extractant will be dissolved in Shellsol D70/Shellsol 2375/Kerosene diluent.

Extraction selectivity

The selectivity of a solvent extraction circuit for a given metal is important because it determines product purity. In addition, impurities can affect downstream processing. The key factors that influence the selectivity of a solvent extraction circuit as opposed to the selectivity of an extractant are (Ritcey and Ashbrook, 1979; Habashi, 1983):

- The structure of the extractant molecule and the chemistry involved in the extraction process.
- The pH in extraction and stripping
- The influence of the diluent

- The aqueous chemistry of the pregnant leach solution, in particular the relative concentrations of the competing metals present, the speciation of the metal complexes and the types of anion present.
- Differences in the extraction kinetics of competing metals.

Influence of the diluent

The selection of the diluent is usually made on the basis of flash point, viscosity and environmental parameters. However, the main areas of influence a diluent can have on the selectivity of the organic extractant are (Gupta and Mukherjee, 1990; Rydberg et al, 2004) to:

- Increase the solubility in the organic phase of the metal - extractant complex.
- Act as an equilibrium modifier.
- Influence the selectivity of the extractant.

In cemented tungsten carbide leaching systems, the solvent extraction technique is mainly focused on the purification and concentration of the leach liquor containing the metal ions extracted from the hardmetal.

Commercial applications

Solvent extraction is a well-established liquid-liquid separation technique and commercially applied in the cobalt processing industry. Production of higher purity cobalt products requires technologies like solvent extraction for purification of cobalt streams (Roux et al. 2007). The treatment of high grades of copper-cobalt ores produces pregnant leach solution tenors rich in Cu (e.g. 15–20 gpl), but low in Co (e.g. 3 gpl). Therefore, after solvent extraction of Cu, the solution stream containing Co is treated for Co recovery.

Cobalt streams can be purified by extracting cobalt from Ca, Mg and Ni impurities through the use of Cyanex 272 extractant or Ionquest 290 at pH 5.0-5.8. Typically, pH control is required because of the higher pH range in which these reagents operate (**Figure 2.27**). Sodium or ammonium hydroxide can be used for pH control, usually in a pre-neutralization mode that makes pH control easier and may not require interstage neutralization (Sole et al, 2019). The typical chemical composition of cobalt advance electrolyte produced from solvent extraction is: Co, 60,000 ppm; Mn, 2000 ppm; Al, 1500 ppm; Mg, <10,000 ppm; Ni, 60 ppm; Fe, <3 ppm; Cu,

<2 ppm; Zn, <3 ppm (Cole and Feather, 2008). A summary of Co solvent extraction and Co stripping data from commercial operations is shown in **Tables 2.11** and **2.12**.

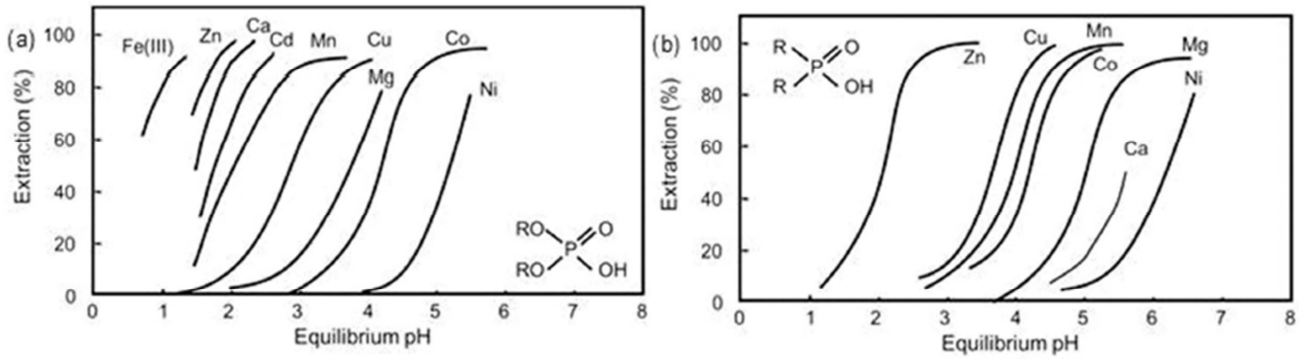

Fig. 2.27 Order of selectivity of base metal extraction for (a) organophosphoric (D2EHPA) and (b) organophosphinic (Cyanex 272 extractant or Ionquest 290) acid extractants (adapted from Sole & Cole, 2002).

Table 2.11: Summary of the commercial application of Co solvent extraction

Solvent Extraction									
Co Feed (gpl)	Extractant Type	Extractant conc (v/v)	Diluent Type	Extraction Stages	pH	O/A	Temp °C	Co in Raffinate (gpl)	Plant
3.0	Cyanex 272	7	-	3	5.4-5.6	1:1.5	40	<0.01	Kasase Cobalt Company Limited[1] (Blanchard, 1995; Morin et al., 1996; Fisher and Pavlides,1998; Sole et al, 2005)
4.8	Cyanex 272	**15**	Shellsol K	5	5.0-5.3	1	-	-	Knightsbridge Cobalt, SA[2] (Cole, P.M., 2002; Alexander, 2001)
0.2	Cyanex 272	5	Shellsol D70	3	-	-	-	<3.5	Tati Nickel[3] (Sole et al, 2005)
1.9	Cyanex 272	7	Paraffin	5	5.5-5.65			<0.01	Nkomati, SA[4] (Sole et al, 2005)
15-18	D2EHPA	15	SSX 210	7	5.4	2.7-7.5	40-45	<0.5	Anglo Platinum Rustenburg Base metals, Refinery[5] (Ritcey et al., 1975; Clemente et al., 1980)
0.5	Cyanex 272	3	Kerosol 200	5	-	-	-	-	Hartley Platinum[6] (Sole et al, 2005)

Table 2.12: Summary of the commercial application of Co stripping

Stripping							
Strip Liquor Type	Strip Liquor (gpl)	Stripping Stages	pH	O/A	Temp °C	Loaded Strip Liquor (gpl)	Plant
H_2SO_4 (Co)	5-10 (47)	3	-	1:1	65	50	KCCL[1] (Blanchard, 1995; Morin et al., 1996; Fisher and Pavlides,1998; Sole et al, 2005)
H_2SO_4	180	**2**	4	10	-	80	Knightsbridge Cobalt, SA[2] (Cole, P.M., 2002; Alexander, 2001)
-	-	2	-	-	-	-	Tati Nickel[3] (Sole et al, 2005)
-	-	3	-	-	-	25	Nkomati, SA[4] (Sole et al, 2005)
H_2SO_4	10%	3	-	1:8-1:12	-	-	Anglo Platinum Rustenburg Base metals, Refinery[5] (Ritcey et al., 1975; Clemente et al., 1980)
H_2SO_4	150	3	-	-	-	-	Hartley Platinum[6] (Sole et al, 2005)

2.8 Electrorecovery

Electrorecovery is an electrochemical process of using electrical energy to recover metals that have been put into solution from their ores through leaching or purification of copper anodes. The process involves applying an external voltage to an electrochemical cell to drive the electrochemical reaction (Davenport et al, 2002; Jackson, 1986). There are two types of electrorecovery processes, electro-refining and electro-winning. Electro-refining is the electro-dissolution of an impure metal and re-deposition of the same metal in a purer form. Electro-winning, also called electro-extraction is the electrodeposition of a metal from solution containing ions of this metal. Both electro-refining and electro-winning processes are electrodeposition techniques that have found wide commercial application in the electrorecovery of precious and non-ferrous metals some of which include Au, Ag, Cu, Co, Ni, Ti, Zn, Cd etc. (Moore, 1990; Jackson, 1986).

Metal electro-deposition is carried out in a cell filled with an electrolyte containing a suitable salt solution of the metal being deposited (Palanna, 2009). The electrolyte cell contains electrically equivalent amounts of cations and anions in an aqueous solvent. A direct current is passed

through the electrolyte solution between the anode and the cathode electrodes to perform the electrodeposition process (Jaganraj et al, 2016; Jackson, 1986). The cathode is the electrode on which metal deposition is taking place. The anode is the electrode that may be either inert or soluble depending on the electrodeposition technique being carried out (Davenport et al, 2002). When an electric current is passed through the electrolyte and a soluble anode is being used, the anode metal M dissolves as M^{n+} ions and the cathodic reduction of M^{n+} ions from the electrolyte and deposition of metal on the cathode surface takes place. In a situation where the anode is insoluble, the main anodic reaction is the evolution of oxygen and the cathodic reduction of M^{n+} ions from the electrolyte salt solution and deposition of metal on the cathode surface occurs. This results in M^{n+} ion depletion. Therefore, the electrolyte has to be replenished from time to time in order to maintain M^{n+} ion concentration (Palanna, 2009; Davenport et al, 2002; Moore, 1990). The reactions are presented as:

Electro-refining reaction

$M_{anode} \rightarrow M^{n+}_{solution} + ne^-$ (anodic dissolution of metal oxidation) (2.61)

$M^{n+}_{solution} + ne^- \rightarrow M$ (cathodic reduction of Mn+) (2.62)

Electro-winning reaction

$2H_2O \rightarrow O_2 + 4H^+ + 4e^-$ (anodic evolution of oxygen) (2.63)

$2M^{2+}_{solution} + 4e^- \rightarrow 2M$ (cathodic reduction of M^{2+}) (2.64)

The mechanism of electrodeposition can be presented in three steps (Palanna, 2009):

The first step is the diffusion of metal ion from bulk electrolyte to the cathodic surface

$M_{anode} \rightarrow M^{n+}_{solution}$ (Bulk diffusion)

The second step is the reduction of the metal ions on the metal surface to form an adsorbed atom layer.

$M^{n+}_{solution} + ne^- \rightarrow M_{ad\ substrate}$ (Formation of atomic layer) (2.65)

The third stage is the growth of deposition resulting in thickening of layer into macroscopic deposit.

$M_{ad\ atom} + M_{atom} \rightarrow M_{substrate} \rightarrow$ Thickening (2.66)

Electrodeposition is schematically illustrated in **Figures 2.28** and **2.29**.

Me = metal electrode

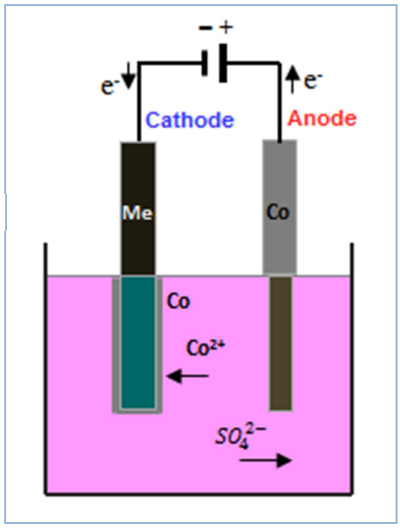

Fig.2.28: A schematic representation of electro-refining type of electrodeposition of cobalt (Ausetute, 2020).

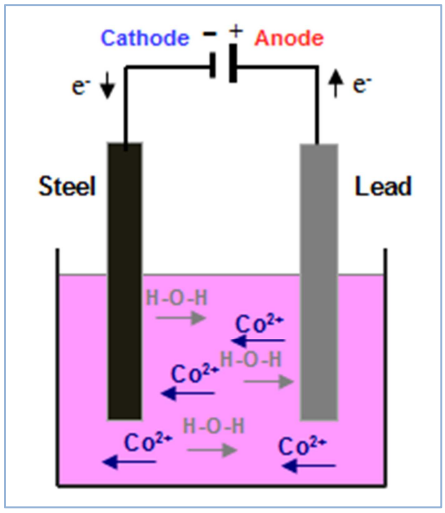

Fig.2.29: A schematic representation of electro-winning type of electrodeposition of cobalt (Sharma et al, 2005).

In metal electrodeposition processes, the quality of deposition formed is determined by several factors. Some of the factors include: the distance between the electrodes, the applied voltage and current and the geometry of the part being plated. Other factors include: current density, pH, temperature, flowrate, metal ion concentration and cell dimensions (Palanna, 2009). Electrodeposition can be achieved through two techniques, the continuous mode or pulse

electroplating (PED) mode. PED entails a series of pulses of equal amplitude, polarity and duration, separated by zero current (Sierra et al, 2017). A pulsed current electrodeposition scheme is illustrated in **Figure 2.30**.

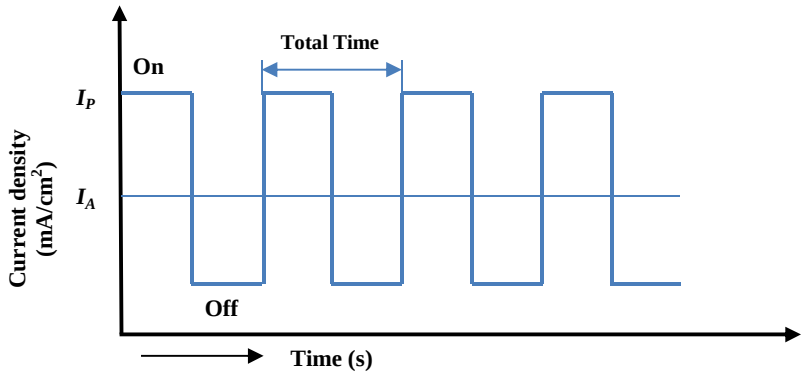

Figure 2.30: Pulse current scheme

Where, I_A is the average current density and I_P is the peak current density.

In the pulse current technique, each pulse consists of an on-time (t_{on}) and off time (t_{off}) sequence. During t_{on}, the potential and current is applied and during t_{off}, there is zero current applied (Chandrasekar and Pushpavanam, 2008). During the t_{on} period, ions in the cell become depleted around the high density areas. During the t_{off} period, the ions are evenly distributed and become available for deposition during the next cycle. The on and off process allows for better leveling of deposit, grain size control, minimizes porosity and nodular growths (Chandrasekar and Pushpavanam, 2008). Sierra and co-workers (2017), in agreement with other PED researchers, noted that Pulse Current Electrodeposition is a technique of special interest due to the advantages it has like easy operation, high control in the amount deposited, homogeneity and purity of the deposited material and low cost.

In the current study, electrorecovery will be employed to recover Co metal which will be leached into solution from cemented carbide (WC-6%wt.Co) hardmetal.

Commercial applications

Electrorecovery has been commercially practiced in the electroplating industry for many years. In cobalt processing, Co metal can be electro-recovered from purified advance cobalt electrolyte by electro-winning (EW) using undivided cells or membrane-divided cells (Louis 2009; Sole

2013). Metal impurities such as copper, iron, and zinc which have high upgrading ratios in EW are removed first (Louis 2009). The EW process is fairly forgiving with regard to the levels of other elements such as magnesium and manganese and complete removal of these species is not necessary, although an electrolyte bleed is required to avoid their uncontrolled buildup (Louis, 2009). A high concentration of sodium (up to ~20 gpl) improves the conductivity of the electrolyte (Louis 2009). Many flowsheet options exist for cobalt metal production. In modern flowsheets, a cobalt hydroxide cake, quantitatively free of Fe, is re-dissolved in anolyte from EW. Residual Cu and Zn are removed to levels below 1 ppm using TP 260 IX resin; alternatively, because the aminophosphonic-acid resins have relatively low loading capacity, Cu may be removed first using an iminodiacetic-acid resin and then the pH adjusted and Zn removed with TP 260 (Jurrius et al. 2014). As necessary, Ni is removed to levels below 20 ppm using Dow's HPPA resin. The electrolyte is then sufficiently pure to ensure the production of premium-grade metal (Sole et al, 2019).

Cobalt may be electro-won using chloride or sulphate electrolyte. In sulphate media, Co(II) in the purified electrolyte is reduced to metal at the cathode, but hydrogen evolution is thermodynamically favoured because cobalt is less noble than the hydrogen ion as can be seen from the standard reduction potential of cobalt (**Equation 2.75**). The hydrogen evolution is in competition with the cobalt deposition (**Equation 2.76**). This is not desirable because it represents a loss of current usage, and, therefore, it must be kept to a minimum. The over potential for hydrogen evolution is, however, such that use of a high Co concentration in the electrolyte (~60gpl), high temperature (~60°C), and high current density can reduce the tendency for this reaction to occur. Other process conditions, including pH control and the addition of organic and/or inorganic additives, allow efficient current utilization. The main cathodic reactions are represented as (Sole et al, 2019; Moskalyk and Alfantazi, 2000):

$$Co^{2+} + 2e^- = Co \qquad E° = -0.28V \qquad (2.67)$$

$$2H^+ + 2e^- = H_2 \qquad E° = 0.00V \qquad (2.68)$$

At the anode, water is oxidized to produce oxygen. The main anodic reactions are dependent on the type of electrolyte and are as follows (Sole et al, 2019; Moskalyk and Alfantazi, 2000; Akre, 2008):

Sulphate electrolyte

$$2H_2O = O_2 + 4e^- + 4H^+ \quad E° = -1.23V \quad (2.69)$$

Chloride electrolyte

$$2Cl^- = Cl_2 + 2e^- \quad E° = -1.36V \quad (2.70)$$

The overall cell reactions are represented as:

$$2CoSO_4 + 2H_2O = 2Co + O_2 + 2H_2SO_4 \quad E° = -1.51V \quad (2.71)$$

$$CoCl_2 + HClO + HCl = Co + Cl_2 + H_2O \quad E° = -1.64V \quad (2.72)$$

These reactions are thermodynamically unfavourable. For this reason, cobalt electro-winning requires precise control of operating parameters, such as temperature, Co concentration, pH and current density, in order to produce high-quality cathode (Louis 2009; Akre, 2008). To date, the most popular electro-winning recovery process for cobalt metal involves a sulphate medium (Honey et al, 1997). The disadvantage with chloride solutions is that more advanced cell designs are needed for safe handling of toxic chlorine gas liberated at the anodes and chlorine solutions are more corrosive than sulfate solutions. Chlorine may react with organics in solution or construction materials, forming harmful chlorinated organic compounds (Peek et al, 2009). In Co EW, power consumption is estimated at 3.5 kWh/kg Co, based on a current density of 300 A/m^2, cell voltage of 3.5 V, cathodic current efficiency of 70%, and rectifier efficiency of 90%. In a plant at Colborne Refinery, Canada, Plating parameters are a current density of 200 A/m^2 and a cell temperature of 50°C (Agnew et al, 1988; Agnew et al, 1990; Agnew and Krause, 1991). Cobalt cathode produced to the required specification is the most marketable and saleable cobalt product. The cobalt metal is traded, at the London Metal Exchange (LME), according to two specifications: premium (99.83%) and standard grade (99.73%).

2.9 Process Optimization

Process optimization is the discipline of adjusting a process so as to make the best or most effective use of some specified set of parameters without violating some constraint. The most common goals are minimizing cost and maximizing throughput and efficiency. Optimization is one of the major quantitative tools in industrial decision making. When optimizing a process, the goal is to maximize one or more of the process specifications, while keeping all others within their constraints (Biegler, 2010). This can be done by using a ‘process mining tool’, discovering the critical activities and bottlenecks and acting only on them.

2.9.1 Types of Optimization

Fundamentally, there are three parameters that can be adjusted to affect optimal performance. These are:

- Topological or Equipment optimization
  Topological optimization is concerned with using equipment to its fullest advantage
- Operating procedures
  Operating-procedure-optimization is concerned with instructions detailing relevant steps to accomplishing tasks or activities of a process in the best way possible.
- Parametric or Control optimization
  Parametric optimization is concerned with operating variables such as temperature, pressure, pH, solid to liquid ratio, flowrate and agitation rate etc. for a given process.

2.9.2 Components of Optimization

For any given scope of optimization problems for a system or process, the task is to find the best solution for the process within constraints. The task requires the following components (Biegler, 2010):

- An objective function or response that provides a scalar quantitative performance measure that needs to be minimized or maximized. This can be a systems cost, profit, yield or efficiency.
- A predictive model that describes the behaviour of the system. For the optimization problem this translates into a set of equations and inequalities termed constraints. These constraints comprise a feasible region that defines limits of performance for the system.
- Variables that appear in the predictive model. These variables must be adjusted to satisfy the constraints. This can usually be accomplished with multiple instances of variable values leading to a feasible region that is determined by a subspace of these variables.

Parametric optimization was found to be suitable and was therefore used in the current study.

2.9.3 Optimization Strategy

Optimization of a process normally requires two stages. The first stage entails screening of factors in order to identify the ones that have a significant effect on the process. The factors

identified as being significant become the focus of the optimization stage while the non-significant ones are kept constant. A schematic presentation of an optimization strategy which will be used in this study is illustrated in **Figure 2.31**.

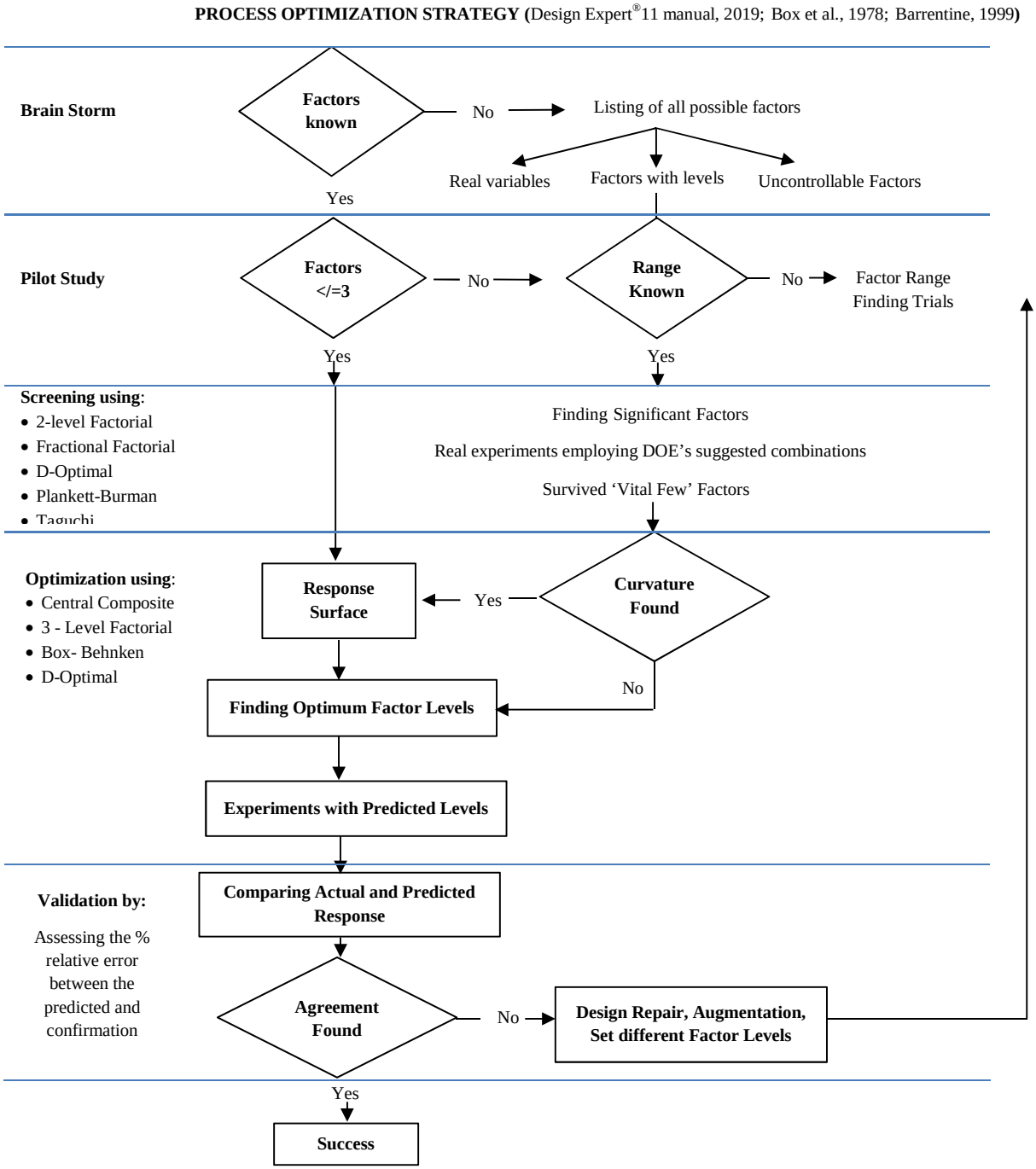

Fig.2.31: Schematic presentation of a process optimization strategy

Therefore, a statistical design of experiments (DOE) will be used as a research tool to accomplish this strategy. The advantage of using DOE is that it provides for a simultaneous study of several process parameters which offer useful information (Czitrom, 1999; Barrentine, 1999). By using DOE, the estimates of the effects of each factor are more precise and the interaction between factors can be estimated systematically. Thus, by using DOE there is experimental information in a large factor space which improves prediction of the desired response.

2.9.3.1 Screening of Factors

Prior to the actual screening process, all factors of interest are listed and using range finding trials, their ranges are determined. Not all process variables have the same impact on a process. Some have more influence than others. It is therefore, necessary to identify and focus resources on the vital few that have more influence and are the key drivers of the process. Identification of the vital few factors entails screening all the factors of interest one by one. Experimental design factors are classified as controlled factors and held constant factors. The controlled factors are the factors selected for investigation. The held constant factors are factors that may have an influence on the response but are of no particular interest to the study.

Factors are studied with their codified values of -1 and +1. The levels of controlled variables in coded units (Box et al., 1978) are obtained using the following formula:

$$\boldsymbol{coded\ value} = \frac{\boldsymbol{X - X_0}}{\boldsymbol{0.5(X_2 - X_1)}} \qquad (2.73)$$

Where, X = physical value, X_0 = mean, X_1 = lowest, X_2 = highest

Screening to find significant factors involves real experiments based on the design of experiments (DOE)'s suggested combinations. Available DOE formulations include: 2-Level Factorial, Fractional Factorial, D-Optimal, Plankett-Burman and Taguchi. The 2-Level Factorial will be used in the current study.

The significance of each factor and associated interactive effects are evaluated using a two level factorial statistical design in conjunction with statistical software based on quadratic programming.

The two-level factorial is denoted by:

2^k

Where,

k is the number of factors and $k \geq 3$.

The number 2 signifies two levels which are the low (-1) and the high (+1) factors levels. For k = 3, the number of experimental runs = 8; k = 4, number of experiments = 16.

Experimental results obtained from a full factorial design are analyzed statistically by using normal probability plot of effects for identification of significant factors; Pareto chart for identification of significant factors known as the vital few; residuals analysis for identification of outliers and centre points for checking curvature or non-linearity (Daniel, 1959; Design Expert®11 manual, 2019). Factors identified as being statistically significant are separated for optimization and the non-significant factors are kept constant.

2.9.3.2 Optimization of Factors

Optimization of significant factors involves real experiments based on the design of experiments (DOE)'s suggested combinations. Available DOE optimization formulations include: central composite rotatable design (CCRD), 3-Level Factorial, Box-Behnken and D-Optimal. The central composite rotatable design (CCRD) will be used in the current study. The CCRD is normally used in conjunction with the response surface methodology (RSM). RSM is a famous technique used to find optimal conditions by using a quadratic polynomial regression model and is applied after diagnostic or screening experiments (Box et al., 1978).

The data for fitting the second order response is collected by using CCRD. A CCRD consists of 2^k factorial points, coded±1, augmented by 2k axial points, coded ±α (**Table 2.13**) and n_c replicate points at the centre {(0,0,0…..,0)}, where k is the number of factors studied, α is the distance of an axial point from the centre (Khuri and Cornell, 1987).

Table 2.13: Axial points (Khuri and Cornell, 1987)

1	2	…k
-α	0	0
+α	0	0
0	-α	0
0	+α	0
0	0	-α
0	0	+α

To ensure a constant variance of the predicted response at all points equidistant from the design centre, the number of centre point replications, n_c, for the factors studied is calculated using the following equation (Khuri and Cornell, 1987).

$$\mathbf{n_c} \sim 0.8385\ (2^{k/2} + 2)^2 - 2^k\text{-}2k \qquad (2.74)$$

Where, $\mathbf{n_c}$ is the number of centre point replications and **k** is the number of factors studied.

The experimental results are analyzed statistically by using the analysis of variance (ANOVA) using Fisher's ratio test; standard errors of model coefficient (*t*-test) and the coefficient of determination (R^2) (Design Expert®11 manual, 2019). For uniformity and better comparison, factors are studied with their codified values. The relationship between the coded values and actual values for the five levels of each factor is shown in **Table 2.14.**

Table 2.14: Relationship between coded and actual values of the variable (Napier-Munn, 2000)

Code	Actual value of a factor
- λ	ξmin
-1	(ξmax + ξmin)/2 - (ξmax – ξmin)/2λ
0	(ξmax + ξmin)/2
+1	(ξmax + ξmin)/2 + (ξmax – ξmin)/2λ
+ λ	ξmax

ξmin and ξmax are the minimum and maximum values of the natural variables respectively,

$\lambda = 2^{(k-q)1/4}$

Where, λ is the distance of an axial point from the centre, *k* is the number of factors studied, *q* is a fraction of the number of factors. For a full factorial design, $q = 0$

For derivation of the model for k variables, a second order polynomial regression model is proposed as follows (Montgomery, 2013; Tripathy and Murthy, 2012):

$$y = \beta_o + \sum_{i=1}^{k} \beta_i x_i + \sum_{i=1}^{k} \beta_{ii} x_i^2 + \sum_{i=1}^{k} \sum_{j=i+1}^{k} \beta_{ij} x_i x_j + \varepsilon \text{.....(2.75)}$$

Where,

Y is the predicted response, $\boldsymbol{\beta_o}$ is the coefficient for intercept, $\boldsymbol{\beta_i}$ is the coefficient of linear effect, $\boldsymbol{\beta_{ii}}$ is the coefficient of quadratic effect, $\boldsymbol{\beta_{ij}}$ is the coefficient of interaction effect, **ε** is a term that represents other sources of variability not accounted for by the response function, $\boldsymbol{x_i}$ and $\boldsymbol{x_j}$ are predictor variables for independent factors.

Within predictor variable limits:

$$-\lambda \leq x_i \leq +\lambda; i = 1, 2, 3$$

The adequacy of the polynomial regression model is checked using the analysis of variance (ANOVA). The final regression model is used as a predictive tool to predict response results based on chosen variable levels within the predictor variable limits shown above.

The statistical properties of the model are tested by using normal plot of residues for checking outliers, residues vs run for counter checking outliers, and predicted values vs observed values for checking correlation efficiency (Box et al., 1978; Design Expert®11 manual, 2019). The Perturbation plot is used for checking individual behaviour of factors and the three dimensional surface plot is used for checking the response surface. The determination of optimum conditions is either based on numerical analysis (Design Expert®11 manual, 2019) or partial derivatives for locating stationary points (Khuri and Cornell, 1987). The predicted optimum conditions are checked for reproducibility of results by using confirmatory tests.

2.10 Summary

The aim of this literature review was to give a general overview of cemented carbide source, microstructure, and material flow, including past and present recycling methods as well as the importance of selecting a cemented carbide processing route.

It was highlighted in the review that the chief source of tungsten is wolframite and scheelite minerals. The minerals are processed to produce cemented carbide which accounts for about 60% of tungsten industrial production. At the same time, the global demand for tungsten is showing a steady upward trend. The review further demonstrated that cemented carbides microstructure is composed of valuable phases of tungsten and Co binder metals, a resource that can be reclaimed.

The review showed the need to find an efficient and economic means for the sustainability of tungsten's finite resources through recycling of worn out and used tools and parts which currently account for about a third of tungsten's raw materials.

The review highlighted past and present tungsten recycling methods which showed that currently the zinc process has found wide industrial application although it's known to be energy intensive and requires expensive equipment. Therefore, there is need to find alternative low cost and environmentally friendly recycling methods. The challenges with the current recycling techniques were acknowledged and a new alternative technique based on a hydrometallurgical approach was proposed.

The review showed the importance of selecting a route for cemented carbide recycling based on the material's chemical and physical characteristics and a preference towards an acid leach process was highlighted. In this review, the potential of using a complexing agent-aided acid leach method was presented and postulated to be a possible process route for the recovery of valuable constituents from cemented carbide.

The review highlighted the important tools and techniques required to develop the proposed technique for the optimal recycling of cemented carbide secondary material.

The next chapter discusses materials and methods used in the study.

2.11 References

Agnew, R., Garritsen, P., MacVicar, D., 1988. Production of Electrolytic Cobalt Rounds at Inco's Cobalt Refinery in Port Colborne, Ontario, Canada. Extractive Metallurgy of Nickel and

Cobalt, The Metallurgical Society/AIME, G.P. Tyroler, and C.A Landolt, eds., Phoenix, AZ, U.S.A., January 25-28, pp. 555-561.

Agnew, R., Kowal, L.D., Young, D., 1990. Process Optimization at Inco's Cobalt Refinery. Proceedings of the International Symposium on Electrometallurgical Plant Practice, P. L. Claessens and G.B. Harris, eds., Montreal, Canada, Pergamon Press, New York, October 22, pp. 221-231.

Agnew, R., Krause, E., 1991. Electrolytic cobalt production at Inco," Minemetal '91 Memorias - " Simposio Internacional de Mineria Y Metalurgia (2nd International Symposium on Mining and Metallurgy), Palacio de las Convenciones (International Convention Center), Havana, Cuba, Vol. 1, Nov. 20-22, pp. 520-533.

Akre, T., 2008. Electro-winning of Cobalt from Chloride Solutions: Anodic Deposition of Cobalt Oxide on DSA. Doctoral Thesis at Norwegian University of Science and Technology (NTNU).

Alar, Z., Alar, V., Fabijanic, T, A., 2017. Electrochemical Corrosion Behavior of Near-Nano and Nanostructured WC-Co Cemented Carbides. Metals, Vol. 7, pp. 69. doi:10.3390/met7030069.

Alexander, A., 2014. Citric Acid. Springer. ISBN 978-3-319-11232-9.

Alexander, D.C., 2001. Kolwezi Tailings treatment project: development of a flowsheet for the production of copper and cobalt metal. Proceedings Anglo American Metallurgical Symposium. Anglo American, Johannesburg, pp. 36.

Amer, A. M., 2000. Investigation of the direct hydrometallurgical processing of mechanically activated low-grade wolframite concentrate. Hydrometallurgy, Vol. 58, pp. 251-259.

American Institute of Mining Engineers (AIME)., 1917. Transactions of the American Institute of Mining Engineers, Princeton University, Vol. 49, pp. 617.

Amoa, K., 2007. Catalytic Hydrogenation of Maleic Acid at Moderate Pressures: A Laboratory Demonstration. Journal of Chemical Education. Vol. 84, Issue12, pp. 1948. doi:10.1021/ed084p1948.

Angelo, P.C., Subramanian, R., 2009. Powder Metallurgy: Science, Technology and Applications. ISBN: 978-8-120-3328-12. PHI Learning. New Delhi, India

Audi, G., Bersillon, O., Blachot, J., Wapstra, A, H., 2003. The NUBASE evaluation of nuclear and decay properties, Nuclear Physics A, 729: 3–128, Bibcode: 2003NuPhA.729....3A

Ausetute, 2020. Electro-winning Copper. http://.www.Ausetute.com.au. Retrieved, 16 May 2020.

Autler, S.H., Hulm, J.K., Kemper, R.S., 1965. Superconducting Technetium-Tungsten Alloys. Physical Review Journals Archive. Vol.140, Issue 4A, pp. A1133.

Barnard P.G, Starliper A.G, Kenworthy, H., 1971. Reclamation of Refractory Carbides from Carbide Materials. U.S Patent 3, 595, 484.

Barrentine, L.B., 1999. An Introduction to Design of Experiments: A Simplified Approach. ASQ Quality Press, Wisconsin.

Beltran-Porter, A., Cervilla, A., Caturla, F., Vila, M.J., 1983. Transition Metals Chemistry, Vol. 8, pp. 324;

Benninga, H., 1990. A History of Lactic Acid Making: A Chapter in the History of Biotechnology. Chemists and Chemistry, Vol. 11, Springer. ISBN 0792306252.

Bhosale S.N, Mookherjee S, Pardeshi R.M., 1990. Current Practices in Tungsten Extraction and Recovery. High Temperature Materials and Processes, Vol. 9, Issue 2-4.

Biegler, L.T., 2010. Nonlinear programming. Concepts, Algorithms, and Applications to Chemical Processes. MOS-SIAM, Philadelphia.

Blair, G. T.; DeFraties, J. J., 2000. Hydroxy Dicarboxylic Acids. Kirk Othmer Encyclopaedia of Chemical Technology. pp. 1–19.

Blanchard, F., 1995. Kilembe Treating the Stockpiles. Mining Environmental Management, Vol.3, Issue 2, pp. 30-32.

Bolton, D., Keely, R. J., 1982. International Journal of Refractory Metals and Hard Materials, Vol. 1, pp. 103.

Bosung, S., Sunjung, K., 2016. Cobalt Extraction from Tungsten Carbide-Cobalt (WC-Co) Hard Metal Scraps Using Malic Acid. International Journal of Mineral Processing, Vol. 151, pp. 1-7.

Box, G.E.P., Hunter, W.G., Hunter, J.S., 1978. Statistics for Experimenters: An Introduction to Design, Data Analysis and Model Building. John Wiley and Sons, New York.

Boynton, R. S., 1980. Chemistry and Technology of Lime and Limestone, 2nd edn. New York: John Wiley & Sons.

Bronsted, J.N., 1931. On The Dissolution of Metals in Acids. Journal of American Chemistry Society. Vol.53, Issue 10, pp. 3624-3644. https://doi.org/10.1021/ja01361a006.

Caldeira, M.M., Gil, V.M.S., 1986. Polyhedron, Vol. 5, pp. 381;

Caldeira, M.M., Ramos, M.L., Gil, V.M.S., 1987. Canadian Journal of Chemistry, Vol. 65, pp. 827.

Campbell, F, C., 2008. "Cobalt and Cobalt Alloys". Elements of Metallurgy and Engineering Alloys. ISBN 978-0-87170-867-0.

Cariati, F., Morazzoni, F., G. M. Zanderighi, G.M., 1977. Chelating Properties of Lactate Anion. Perturbing Effect of Additional Ligands on Bis(DL-lacta to)-metal(II) Complexes. Inorganica Chimica Acta, Vol. 21, pp. 133-140.

CDI., 2006. Cobalt in Cemented Carbides. Retrieved, 15 February 2016.

Chandrasekar, M.S., Pushpavanam M., 2008. Pulse and pulse reverse plating-Conceptual, advantages and applications, Electrochimica Acta, Vol. 53, Issue 8, pp. 3313–3322

Chauhan, G., Pant, K. K., Nigam, K. D. P., 2015. Chelation technology: A promising Green Approach for Resource Management and Waste Minimization, The Royal Society of Chemistry, pp. 1-29. DOI: 10.1039/c4em00559g.

Chem Supply., 2020. https://www.chemsupply.com.au/. Retrieved, 10 February 2020.

Chen, Z.A., 2013. PEC Experiment Standard. Springer, Berlin/New York.

Cheung, H., Tanke, R.S., Torrence, G.P., 2004. Acetic Acid. Ullmann's Encyclopedia of Industrial Chemistry. Weinheim: Wiley-VCH.

Clemente, D.D.J., Dewar, B.I., Hill, J., 1980. MRR'S Cobalt Refining Operation - South Africa's First. Canadian Institute of Metallurgists 10th Annual Hydrometallurgical Meeting, Paper No. 7. Edmonton, Alberta, Canada.

Cobalt institute, 2019. Promoting the Sustainable and Responsible Production and Use of Cobalt in All Forms. https://www.cobaltinstitute.org/cobalt-uses.html. Retrieved, 7 December 2019.

Cobalt News., 1998. Cobalt Briefing, Bulletin, Cobalt Development Institute, Vol. 98, No.1, January, pp. 5-6.

Cole, P. M., Feather, A. M., 2008. Processing of African Copper Belt Copper-Cobalt Ores: Flowsheet Alternatives and Options, In Proceedings International Solvent Extraction Conference ISEC 2008, Vol. I, (B. A. Moyer, Ed.), Montreal: Canadian Institute of Mining, Metallurgy and Petroleum, pp. 131–138.

Cole, P.M., 2002. The introduction of solvent extraction steps during upgrading of a cobalt refinery. Hydrometallurgy, Vol. 64, 69–77.

Cox, P.A., 2004. Instant Notes in Inorganic Chemistry. BIOS Scientific Publishers, Taylor and Francis Group, London and New York

Crundwell, F. K., 1995. Progress in the Mathematical Modeling of Leaching Reactors. Hydrometallurgy 39, 321-335.

Cruywagen, J.J., Kruger, L., Rohwer, E.A., 1993. Molybdenum (VI) and Tungsten (VI) Complex Formation, Part 5. The Reaction with Lactate in 1.0 mol dm^{-3} Sodium Chloride Medium. Journal of Chemical Society, Dalton Transactions, pp. 105-109.

Cruywagen, J.J., Saayman, L.J., Noven, M.L., 1992. Journal of Crystallographic and Spectroscopic Research, Vol. 22, pp. 737

Czitrom, V., 1999. One-Factor-At-a-Time versus Designed Experiments. The American Statistician, Vol. 53, No. 2, pp. 126 – 131.

Daniel, C., 1959. Use of Half Normal Plots in Interpreting Factorial Two Level Experiments. Technometrics, 1 (4), 311-341.

Davenport, W.G., King, M., Schlesinger, M., Biswas, A.K., 2002. Extractive Metallurgy of Copper. Pergamon Press, Oxford.

Davies, L., Richardson, R., 1962. Journal of Less-Common Metals, Vol.4, pp. 104;

Dean, J.A., 1992. Lange's Handbook of Chemistry. McGraw Hill, New York.

Deshmukh, R., Gurland, J., 1986. Science of Hard Materials, (E. A. Almond, C. A. Brookes and R. Warren, eds.) Adam Hilger, Bristol, pp. 347.

Design Expert® 11 Manual., 2019. Internet Version: http://www.statease.com. Stat-Ease, Incorporation, Minneapolis. Retrieved, 5 August 2019.

Diehl, H., 1937. Chemical Revisions, Vol. 21, pp. 39.

Dille, J., Charlier, J., Winand, R., 1997. The Structure and Mechanical Properties of Thick Cobalt Electrodeposits. Journal of Materials Science, Vol. 32, pp. 2637-2646.

Disegi, J, A., 1999. Cobalt-base Alloys for Biomedical Applications. ASTM International. ISBN 0-8031-2608-5.

Donachie, M, J., 2002. Superalloys: A Technical Guide. ASM International. ISBN 978-0-87170-749-9.

Donaldson, J, D., Beyersmann, D., 2005. Cobalt and Cobalt Compounds in Ullmann's Encyclopedia of Industrial Chemistry, Wiley-VCH, Weinheim.

Dwyer, F.P., Mellor, D.P., 1964. Chelating Agents and Metal Chelates. Academic Press, New York and London

Earnshaw, A., Greenwood, N.N., 1997. Chemistry of the Elements (2nd Ed.). Butterworth-Heinemann, Oxford.

EASAC Report (2016) Priorities for Critical Materials for a Circular Economy. EASAC Policy Report 29. ISBN: 978-3-8047-3679-5.

Edtmaier, C., Schiesser, R., Meissl, C., Schubert, W.D., Rock, A., Schoen, A., Zeiler, B., 2005. Selective Removal of the Cobalt Binder in WC-Co Based Hard Metal Scraps By Acetic Acid Leaching. Hydrometallurgy, Vol. 76, pp. 63-71.

Ellis, J.L., 1970. British Patent No.:908412.

Emsley, John E., 1991. The Elements (2nd Ed.). New York: Oxford University Press. ISBN 978-0-19-855569-8.

European Commission., 2014. Report on Critical Raw Materials for the EU Report of the Ad hoc Working Group on Defining Critical Raw Materials. European Commission.

Exner, H. E., 1979. International Metals Reviews. Vol. 24, pp. 149.

Exner, H. E., 1983. Science of Hard Materials, (R. K. Viswanadham, D. J. Rowcliffe, and J. Gurland, eds.), Plenum Press, New York, pp. 233.

Exner, H. E., Fischmeister, H. F., 1966. Arch. Eisen., Vol. 37, pp. 417 and p. 499.

Exner, H. E., Gurland, J., 1970. Powder Metallurgy, Vol. 13, No. 25, pp. 13.

Exner, H.E., 1979. Physical and Chemical Nature of Cemented Carbides. International Metals Reviews, Vol. 4, pp. 149-173.

Ferron, C. J., 2008. Sulphur dioxide: A Versatile Reagent for the Processing of Cobaltic Oxide Minerals. Journal of Minerals, Metals and Materials Society, Vol. 60, Issue 10, pp. 50–54.

Fiege, H., Vogues, H-W., Hamamoto, T., Umemura, S., Iwata, T., Miki, H., Fujita, Y., Buysch, H-J., Garbe, D., Paulus, W., 2002. Phenol Derivatives. Ullmann's Encyclopedia of Industrial Chemistry. Weinheim: Wiley-VCH

Fisher, K.G., 2011. Cobalt processing Developments: The Southern African Institute of Mining and Metallurgy, 6th Southern African Base Metals Conference, pp. 237-257.

Fisher, K.G., Pavlides, A.G., 1998. The Kasese Cobalt Project. Proceedings Extraction Metallurgy Africa '98. South African Institute of Mining and Metallurgy, Johannesburg.

Freemantle, C., Sacks, N., 2015. Recycling of Cemented Tungsten Carbide Mining Tool Scrap. The Journal of the South African Institute of Mining and Metallurgy, Vol. 115, pp. 1207-1213.

Freytag, J., Exner, H. E., 1977. Modern Developments in Powder Metallurgy, Proceedings International Powder Metallurgy Conference (H. H. Hausner, and P. W. Taubenblat, eds.), MPIF, Princeton, Vol. 10, pp. 511.

Gabriel, A., Pastor, H., Deo, D. M., Basu, S., 1986. International Journal of Refractory Metals and Hard Materials, Vol. 5, No. 4, pp. 215.

Gani, R., Jimenez-Gonzalez, C., Kate, A., Crafts, P.A., Powell, M.J., Powell, L., Atherton, J.H., Cordiner, J.L., 2006. A Modern Approach to Solvent Selection. Chemical Engineering 113:30-43.

Garcia, E.M., Santos, J.S., Pereira, E.C., Freitas, M.B.J.G., 2008. Electrodeposition of Cobalt from Spent Li-ion Battery Cathodes by the Electrochemistry Quartz Crystal Microbalance Technique. Journal of Power Sources, Vol. 185, pp. 549-553.

Garrels, R.M., Christ, C.L., 2007. Solutions, Minerals, and Equilibria. Harper and Row, Michigan.

General Carbide., 2016. Designer's Guide to Tungsten Carbide. http://www.generalcarbide.com. Retrieved, 25 June 2016.

Ghandehari, M. H., Schussler, M., 1980. Process for Recovering Metal Carbide Powder from Cemented Carbides. US Patent No. 4, 234, 333.

Gille, G., Meier, A., 2012. Recycling von Refraktärmetallen, in Recycling und Rohstoffe (Ed.). By K.J. Thomé-Kozmiensky (TK-Verlag, Neuruppin). pp. 537–560.

Godlewska L, Grohol M., 2017. Study on the Review of the list of Critical Raw Materials - Final Report. SBN 978-92-79-47937-3. doi:10.2873/876644.

Goldberg, R., Kishore, N., Lennen, R., 2002. Thermodynamic Quantities for the Ionization Reactions of Buffers. Journal of Physical and Chemical Reference Data. Vol. 31, No.2, pp. 231-370.

Grinberg, A. A., 1962. The Chemistry of Complex Compounds. Pergamon Press, New York.

Groot, W., van Krieken, J., Slekersl, O., de Vos, S., 2010. Chemistry and Production of Lactic Acid, Lactide and Poly (Lactic Acid). In Auras, R., Lim, L., Selke, S.E., Tsuji, H (eds.). Poly (Lactic Acid). Hoboken: Wiley. ISBN 978-0-470-29366-9;

Guedes de Carvalho, R.A., Neves, O.R., 1992. Leaching of Scheelite ($CaWO_4$) Under Quasi-Stagnant Solution Conditions. Hydrometallurgy, Vol. 28, pp. 45-64.

Gupta, C.K., Mukherjee., 1990. Hydrometallurgy in Extraction Processes. CRC Press, Florida. ISBN: 978-084-936-8042

Gurland, J., 1959. Transactional Metal Society AIME, Vol. 215, pp. 601.

Gurland, J., Bradzil, P., 1955. Transactional Metal Society AIME, Vol. 203, pp. 31.

Gurmen, S., Friedrich, B., 2005. Recovery of Cobalt Powder and Tungsten Carbide from Cemented Carbide Scrap - Part I: Kinetics of Cobalt Acid Leaching. World of Metallurgy-Erzmetall. Vol. 57, pp. 143-147.

Gurmen, S., Timur, S., Arslan, C., Duman, I., 1999. Acidic Leaching of Scheelite Concentrate and Production of Hetero-Poly-Tungstate Salt. Hydrometallurgy, Vol.51, pp. 227-238.

Gurney, R.W., 2012. Ionic Processes in Solution. McGraw-Hill, New York.

Habashi, F., 1969. Principles of Extractive Metallurgy: General principles. Gordon and Breach, New York.

Habashi, F., 1983. A Text Book of Hydrometallurgy. Metallurgie Extractive, Quebec. ISBN: 978-298-0324-703

Hammond, C. R., 2004. The Elements, in Handbook of Chemistry and Physics (81st Ed.). CRC press. ISBN 978-0-8493-0485-9.

Hanjered, A., Hellsing, M., Andrian, H.O., Norden, A., 1986. Material Science Technology. Vol. 2, pp. 847.

Hart, D., Sarkissian, A., 2016. Deployment of Grid-Scale Batteries in the United States, Fairfax, Virginia: Schar School of Policy and Government, George Mason University, pp. 1–31.

Hartline III, A.G., Campbell, J.A., Magel, T.T., 1976. Process for Reclaiming Cemented Metal Carbide. USA, Patent No. 3, 953, 194.

Hawkins, M.J., 1998. Recovering Cobalt from Primary Sources and Secondary Sources, Journal of Metals, Vol. 50, No.10, pp. 46- 50.

Hawkins, M.J., 2001. Why we need cobalt. Applied Earth Science: Transactions of the Institution of Mining & Metallurgy, Section B. 110 (2): 66–71.

Haynes, W.M., 2016. CRC Handbook of Chemistry and Physics (97th Ed.). CRC Press, pp. 5-88. ISBN 9781498754293.

Hellsing, M., Henjered, A., Norden, H., Andren, H. O., 1983. Science of Hard Materials, (R. K. Viswanadham, D. J. Rowcliffe, and J. Gurland, eds.), Plenum Press, New York, p. 93 (1983)

Hildbrand, S., Pollak, P., 2001. Malonic Acid and Derivatives. Ullmann's Encyclopedia of Industrial Chemistry.

Hoffmann, A., and Mohs, R., 1974. Metallography. Vol. 28, pp. 661.

Honey, D.J., Muir, D.M., Hunt, P.R., 1997. Hydrometallurgical Processing Options for Nickel Sulphide Concentrates. Proceedings of the Nickel-Cobalt 97 International Symposium, Vol. 1 , The Metallurgical Society of CIM, W.C. Cooper and I. Mihaylov, eds., August 17-20, Sudbury, Canada, pp. 15-29. Inco Ltd., 1998, press release, 2nd quarter results to shareholders, Toronto, Canada, pp. 7-8.

Housecroft, C. E., Sharpe, A. G., 2008. Inorganic Chemistry (3rd Ed.). Prentice Hall. pp. 722. ISBN 978-0-13-175553-6).

Hyv¨onen, H., 2008. Ph.D. Thesis, University of Helsinki.

IIhan, S., Kalpakli, A.O., Kahruman, C., Yusufoglu, I., 2013. The Investigation of Dissolution Behaviour of Gangue Materials during the Dissolution of Scheelite Concentrate in Oxalic Acid Solution. Hydrometallurgy, Vol. 136, pp. 15-26.

International Tungsten Industry Association., 2010. Cemented Carbides – A Success Story. ITIA Newsletter, June 2010.

International Tungsten Industry Association., 2011. Primary Uses of Tungsten. International Tungsten Industry Association. http://www.itia.info/tungsten-primary-uses.html.

International Tungsten Industry Association., 2017. Information on tungsten: sources, properties and uses - Mining and Beneficiation. https://www.itia.info/mining-beneficiation.html. Retrieved, 24 March 2017.

Jackson, E., 1986. Hydrometallurgical Extraction and Reclamation. Halsted Press, New York. ISBN: 085-312-5686.

Jaganraj D., Karthick Y., Chakravarthi S., Balaji V., 2016. A review on study and analysis of nickel coating on solar collector applications, International Journal of Advanced Scientific and Technical Research, Vol. 5, Issue 6, pp. 228-233.

Johansson, T., Uhrenius, B., 1978. Metal Science, Vol. 12, pp. 83.

Johnsson, H., 1972. Powder Metallurgy, Vol. 15, No. 29, pp. 1.

Johnsson, H., 1973. Planseeber, Pulverment. Vol. 21, pp. 187.

Joost, R., Pirso, J., Viljus, M., 2012. Recycling of WC-Co Hard metals by Oxidation and Carbothermal Reduction in Combination with Reactive Sintering. Estonian Journal of Engineering, 18(2), pp. 127-139.

Jurrius, Y., Sole, K. C., Hardwick, E., 2014. Removal of Copper and Zinc from a Cobalt Electrolyte by Ion Exchange at Kamoto Copper Company's Luilu plant. Proceedings Hydrometallurgy 2014, Vol. 2, Montreal: Canadian Institute of Mining, Metallurgy & Petroleum, pp. 281−294.

Kahruman, C., Yusufoglu, I., 2006. Leaching Kinetics of Synthetic CaWO4 in HCl Solutions Containing H_3PO_4 as Chelating Agent. Hydrometallurgy, Vol.81, pp. 182-189.

Karhumaa, T., Kurkela, M., 2013. Review of the Hardmetal recycling market and the role of the zinc process as a recycling option. Paper presented at the 18th international Plansee seminar 2013, Reutte, 03–07 June 2013.

Kassaian, J.M., 2002. Tartaric acid in Ullmann's Encyclopaedia of Industrial Chemistry; VCH: Weinheim, Germany.

Katiyar, P.K., Randhawa, N.S., Hait, J., Jana, R.K., Singh, K, K., Mankhand, T.R., 2014. An Overview on Different Processes for Recovery of Valuable Metals from Tungsten Carbide Scrap. ICNFMM, Nagpur.

Kellner, F.J.J., Hildebrand, H., Virtanen, S., 2009. Effect of WC grain size on the corrosion behaviour of WC-Co based hard metals in alkaline solutions. International Journal of Refractory Metals and Hard Materials, Vol. 27, pp. 806-812.

Khodakov, A,Y., Chu, W., Fongarland, P., 2007. Advances in the Development of Novel Cobalt Fischer-Tropsch Catalysts for Synthesis of Long-Chain Hydrocarbons and Clean Fuels. Chemical Reviews. 107 (5): 1692–1744. doi:10.1021/cr050972v. PMID 17488058.

Khuri, A. I., Cornell, J. A., 1987. Response Surfaces: Designs and Analyses. Marcel Dekker, Inc., New York.

Kimball, S.M., 2014. Mineral Commodity Summaries. United States Geological Survey, Reston, Virginia.

Kislik, V.S., 2012. Solvent Extraction: Classical and Novel Approaches. Elsevier B.V. ISBN: 978-0-444-53778-2.

Knobler, C.B., Wilson, A.J., Hider, R.N., Jenson, I.W., Penfold, B.R., Robinson, W.T., Wilkins, C.J., 1983. Journal of Chemical Society, Dalton Transactions, 1299

Kojima, T., Shimizu, T., Sasai, R., Itoh, H., 2005. Recycling Process of WC-Co Cermets by Hydrothermal Treatment. Journal of Materials Science, Vol. 40, pp. 5167-5172.

Kuntyi, O.I., Ivashkin, V.R., Yavorskii, V.T., Zozulya, G.I., 2007. Electrochemical Processing of WC-Ni Pseudo alloys in Sulphuric Acid Solutions to Ammonium Paratungstate and Nickel (II) Sulphate. Russian Journal of Applied Chemistry, Vol. 80, No.11, pp. 1856-1859.

Kusaka, Y., Yokoyama, K., Sera, Y., Yamamoto, S., Sone, S., Kyono, H., Shirakawa, T., Goto, S., 1986. Respiratory Diseases in Hardmetal Workers: An Occupational Hygiene Study in a Factory. British Journal of Industrial Medicine, Vol. 43, pp. 474-485.

K*u*tcher, G., Luidold, S., Czettl, C., Storf, C., 2017. Disclosure of the Kinetic Relations of Semi-direct Cemented Carbide Leaching in Acid Media. In: Kim, H., Alam, S., Neelameggham, N., Oosterhof, H., Ouchi, T., Guan, X., (Eds). Rare Metal Technology. The Minerals, Metals and Materials Series. Springer, Cham.

Lai, Ho-Yi., Jinhui, Y., 1985. Proceedings, 11th International Plansee Seminar (H. Bildstein, and H. M. Ortner, eds.), Metallwerk Plansee, Reutte, Austria, Vol. 2, pp. 679.

Langmuir, I., 1919. Journal of American Chemical Society, Vol 41, pp. 868, 1543

Lassner E, Schubert W.D., 1999. Tungsten: Properties, Chemistry, Technology of the Element, Alloys and Chemical Compounds. Kluwer Academic/Plenum Publishers, New York.

Law-West, D., Perron, L., 2009. "Tungsten". The Canadian Encyclopaedia. Retrieved, 5 May 2020.

Leal-Ayala, D.R., Allwood, J.M., Petavratzi, E., Brown, T.J., Gunn, G., 2015. Resources, Conservation and Recycling, Vol. 103, pp. 19–28

Lee, H. C., Gurland, J., 1978. Material Science and Engineering, Vol. 33, pp. 12.

Lee, J. W., Jaffrey, D., Browne, J. D., 1980. Powder Metallurgy, Vol. 23, No. 2, pp. 57.

Levenspiel, O., 1972. Chemical Reaction Engineering. John Willey and Sons, New York.

Lewis, G. N., 1916. Journal of American Chemical Society, Vol. 38, pp. 762.

Lide, D, R, ed., 2007. CRC Handbook of Chemistry and Physics, Internet Version 2007, (87th Ed.), http:/www.hbcpnetbase.com, Taylor and Francis, Boca Raton, Florida. Retrieved, 18 August 2020.

Lin, J.C., Lin, J.Y., Jou, S.P., 1996. Selective Dissolution of the Cobalt Binder from Scraps of Cemented Tungsten Carbide in Acids Containing Additives. Hydrometallurgy, Volume 43, pp. 47-61.

Lin, J.C., Lin, J.Y., Lee, S.L., 1995. Process for Recovering Tungsten Carbide from Cemented Tungsten Carbide Scraps by Selective Electrolysis. US, Patent No. 5,384,016.

Lohbeck, K., Haferkorn, H., Fuhrmann, W., Fedtke, N., 2000. Maleic and Fumaric Acids in Ullmann's Encyclopedia of Industrial Chemistry, Wiley-VCH, Weinheim

Louis, P. E., 2009. Cobalt Electro-winning – Process and Technology, In Hydrometallurgy of Nickel and Cobalt, (J. J. Budac, R. Fraser, I. Mihaylov, V. G. Papangelakis, and D. J. Robinson, Eds.), Montreal: Canadian Institute of Mining, Metallurgy and Petroleum, pp. 554–569.

Luborsky, F. E., Mendelsohn, L. I., Paine, T. O., 1957. Reproducing the Properties of Alnico Permanent Magnet Alloys with Elongated Single-Domain Cobalt-Iron Particles. Journal of Applied Physics. 28 (344): 344.

Lundqvist, R., Lu, J.F., Svantesson, I., 1984. Acta Chemica Scandinavica Series A, Vol. 38, pp. 327

Malveda, M., Funada, C., 2003. Acetic Acid. Chemicals Economic Handbook. SRI International. pp. 602.5000.

Mandeville, C., Fulbright, H., 1943. The Energies of the γ-Rays from Sb122, Cd115, Ir192, Mn54, Zn65, and Co^{60}. Physical Review. 64 (9–10): 265–267. Bibcode: 1943. Physical Review 64-265M.

Martinez, F.A.C., Balciunas, E.M., Salgado, J.M., Gonzalez, D.J.M., Converti, A., Oileira, R.P.S., 2013. Lactic acid properties, applications and production: A review. Trends in Food Science and Technology, Vol. 30, pp. 70-83.

Matjie, R.H., Bunt, J.R., Van Heerden J.H.P., 2005. Extraction of Alumina from Coal Fly Ash generated from a selected low rank bituminous South African coal. Minerals Engineering, Vol. 18, pp. 299-310.

Matzapetakis, M., Raptopoulou, C.P., Tsohos, A., Papaefthymiou, V., Moon, S.N., Salifoglou, A., 1998. Synthesis, Spectroscopic and Structural Characterization of the First Mononuclear, Water Soluble Iron-Citrate Complex, $(NH_4)_5Fe(C_6H_4O_7)_2.2H_2O$. Journal of American Chemical Society. Vol. 120, No. 50, pp. 13266-13267.

Meyer, H., 1979. Verfahren zur Rückgewinnung von Ta(Nb)C-WC-TiC-Mischungen, pp. 10.

Michel, R., Nolte, M., Reich, M., Löer, F., 1991. "Systemic effects of implanted prostheses made of cobalt-chromium alloys". Archives of Orthopaedic and Trauma Surgery. 110 (2): 61–74. doi:10.1007/BF00393876. PMID 2015136.

Mikanova, E., Bartusek, M., 1981. Scr. Fac. Sci. Nut. Univ. Purkynianae, Brun, Vol. 11, pp. 439;

Monhemius, A.J., 1977. Precipitation Diagrams for Metal Hydroxides, Sulfides, Arsenates and Phosphates. Transactions of the Institute of Mining & Metallurgy. Vol. 86, pp. 202-206.

Montgomery, D.C., 2013. Design and Analysis of Experiments. John Wiley and Sons, New Jersey.

Moore, J.J., 1990. Chemical Metallurgy. Butterworth-Heinemann. ISBN 13: 978-0-408-05369-3.

Morgan, G. T., Drew, H. D. K., 1920. Journal of Chemical Society, Vol. 117, pp. 1456.

Morin, D., Battaglia, F., Hau, J.M., Ollivier, P., 1996. KCC project: 5% of the World's Cobalt Production by Means of Bioleaching. Chron. Rech. Min. (525).

Morrison, J., 2015. Director, Pilot Tools (Pty) Ltd, South Africa. Personal Communication.

Moskalyk, R.R., Alfantazi, A.M., 2000. Review of present cobalt recovery practice. Minerals and Metallurgical Processing, Vol. 17, No.4, pp. 205-216.

Mwema, M. D., Mpoyo, M., Kafumbila, K., 2002. Use of Sulphur Dioxide as Reducing Agent in Cobalt Leaching at Shituru Hydrometallurgical Plant. Journal of the South African Institute of Mining and Metallurgy, Vol.102, Issue 1, pp. 1–4.

Napier-Munn, T. J., 2000. The Central Composite Rotatable Design. JKMRC, The University of Queensland, Brisbane, Australia, pp. 1-9.

Nassimbeni, L.R., Niven, M.L., Cruywagen, J.J., Heyns, J.B.B., 1987. Journal of Crystallographic and Spectroscopic Research, Vol. 17, pp. 373;

Nayak, N., Chitta, R. P., 2009. Aluminium Extraction and Leaching Characteristics of Talcher Thermal Power Station Fly Ash with Sulphuric Acid. Fuel, pp. 53-58.

Nielsen, A.E., 1970. Precipitation. Croatica Chemica Acta. Vol. 42, pp. 319–333.

Osseo-Asare, K., 1982. Solution Chemistry of Tungsten Systems. American Society for Metals and the Metallurgical Society of AIME. Metallurgical Transactions B. Vol.13B, pp. 555-564.

Palanna O. G., 2009. Engineering Chemistry, Tata McGraw-Hill Education, pp.176-194.

Paulino, J.F., Afonso, J.C., Mantovano, J.L., Vianna, C.A., Cunha, J.W.S.D., 2012. Recovery of Tungsten by Liquid–Liquid Extraction from a Wolframite Concentrate after Fusion with Sodium Hydroxide. Hydrometallurgy, 127-128, pp. 121-124.

Peek, E., Åkre, T., Asselin, E., 2009. Technical and Business Considerations of Cobalt Hydrometallurgy. Journal of Mining, Vol. 61, No.10, pp. 43-53. JOM

Perry, R., Green D., Maloney, J., 1984. Perry's Chemical Engineers' Handbook (6th ed.). McGraw-Hill Book Company, New York.

Petrucci, R.H., Herring, F.G., Madura, J.D., Bissonnette, C., 20I7. General Chemistry: Principles and Modern Applications. Pearson Canada Inc.

Pirso, J., Viljus, M., Letunovits, S., Juhani, K., 2006. Reactive Carburizing: A Novel Production Method for High Quality Chromium Carbide-Nickel Cermets. International Journal of Refractory Metals and Hard Materials, Vol. 24, pp. 263-270.

Porterfield, W.W., 2013. Inorganic chemistry: A Unified Approach. Academic Press, New York.

Potgieter, J.H., Kabemba, M.A., Teodorovic, A., Potgieter-Vermaak, S.S., Augustyn, W.G., 2006. An investigation into the feasibility of recovering valuable metals from solid oxide compounds by gas phase extraction in a fluidized bed. Minerals Engineering, Vol. 19, pp. 140-146.

Rettenmayer, M., Exner, H. E., Moder, W., 1988. Material Science Technology, Vol. 4, pp. 984.

Reutemann, W., Kieczka, H., 2000. Formic Acid. Ullmann's Encyclopedia of Industrial Chemistry. ISBN 978-3-527-30673-2.

Ritcey, G.M., Ashbrook, A.W., 1979. Solvent Extraction: Principles and Applications to Process Metallurgy. Elsevier Scientific Publishing Company, Pennsylvania, USA. ISBN: 044-441-7702

Ritcey, G.M., Ashbrook, A.W., Lucas, B.H., 1975. Development of a Solvent Extraction Process for the Separation of Cobalt from Nickel. CIM Bull. Vol. 68, No. 1, pp. 111 – 123.

Robinson, W.T., Wilkins, C.J., 1986. Transition Metal Chemistry, Vol. 11, pp. 86

Roebuck, B., Almond, E. A., 1988. International Metal Reviews, Vol. 33, No. 2, pp. 90.

Roebuck, B., Bennett, E. G., 1986. Metallography, Vol. 19, pp. 27.

Rossotti, J. C., Rossotti, H., 1961. The Determination of Stability Constants. McGraw-Hill, New York.

Roux, L. M., Minnaar, E., Cilliers, P. J., Bellino, M., Dye, R., 2007. Comparison of Solvent Extraction and Selective Precipitation for the Purification of Cobalt Electrolytes at Luilu refinery, DRC. Proceedings, 4th Southern African Conference on Base Metals, Johannesburg: Southern African Institute of Mining and Metallurgy, pp. 343–364.

Rydberg, J., Cox, M., Musikas, C., Choppin, D.R., 2004. Solvent Extraction Principles and Practice. Marcel Dekker, New York. ISBN: 0-8247-5063-2.

Sandvik Hyperion, 2005. Cemented Carbide, Sandvik New Developments and Applications. https://www.hyperion.sandvik.com

Sandvik Hyperion., 2016. Carbide Recycling. https://www.hyperion.sandvik.com/. Retrieved, 15 September 2017.

Saxman, D., 2017. Advanced Materials for Advanced Batteries and Fuel Cells: Technologies and Global Markets. Wellesley, MA: BCC Research.

Schiesser, R., 2003. Wertstoffrecycling Wolframhältiger Sekundärrohstoffe. Ph.D. Thesis, TU Wien.

Schmidt, M., 2008. The Sankey Diagram in Energy and Material Flow. Management J. Ind. Ecol. 12 (2).

Schneider, C.A., Rasband, W.S., Eliceiri, K.W., 2018. NIH Image to ImageJ: 25 YEARS OF Image Analysis. Image J, U.S. National Institute of Health, Bethesda, Maryland, USA. Http://image.nih.gov/ij/.

Schrödter, K., Bettermann, G., Staffel, T., Wahl, F., Klein, T., Hofmann, T., 2008. "Phosphoric Acid and Phosphates". Ullmann's Encyclopedia of Industrial Chemistry. Weinheim: Wiley-VCH.

Schwarzenbach, G., 1952. Helv. Chim. Acta, Vol. 35, pp. 2344–2359.

Seo, B., Kim, S., 2016. Cobalt Extraction from Tungsten Carbide-Cobalt (WC-Co) Hard Metal Scraps Using Malic Acid. International Journal of Mineral Processing. Vol. 151, pp. 1-7.

Sharma, I.G., Alex, P., Bidaye, A.C., Suri, A.K., 2005. Electrowinning of cobalt from sulphate solutions. Hydrometallurgy, Vol, 80, pp. 132– 138.

Shedd, K, B., 2006. "Mineral Yearbook 2006: Cobalt"; "Commodity Report 2008: Cobalt". United States Geological Survey. Retrieved, 26 October 2020.

Shedd, K.B., 2000. Tungsten Recycling in the United States in 2000. http://pubs.usgs.gov/circ/circ1196-R/

Shemi, A., Magumise, A., Ndlovu, S., Sacks, N., 2018. Recycling of Tungsten Carbide Scrap Metal: A review of Recycling Methods and Future Prospects. Minerals Engineering, Vol.122, pp. 195-205.

Shield K.B., 2011. Tungsten Recycling in the United States in 2000. U.S. Geological Survey Circular, 1196-R.

Shilling, Erik., 2017. We May Not Have Enough Minerals To Even Meet Electric Car Demand. www.jalopnik.com. Retrieved, 25 August 2019.

Sidgwick, N. V., 1927. The Electronic Theory of Valency. Oxford Univ. Press, London and New York.

Sierra-Herrera, D.K., Sandoval-Amador, A., Montaez-Supelano, N.D., Pea-Ballesteros, D., 2017. The Effect of Pulsed Current Electrodeposition Parameters of Calcium Phosphates Coating on Ti6Al4V ELI. NASA Astrophysics Data Systems (ADS).

Smith G.R., 1942. Material Flow of Tungsten in the United States. Bureau of Mines Circular-1994.

Softschools.com., 2019. Tartaric Acid Formula. http://www.softschools.com/. Retrieved, 9 December 2019.

Sole, K. C., 2013. Electro-winning of Cobalt. Proceedings Electrometallurgy School, Johannesburg: Southern African Institute of Mining and Metallurgy.

Sole, K. C., Cole, P. M., 2002. Purification of Nickel by Solvent Extraction, In Ion Exchange and Solvent Extraction. A Series of Advances, Vol. 15, (Y. Marcus and A. K. Sen Gupta, Eds.), New York: Marcel Dekker, pp. 143–195.

Sole, K.C., Feather, A.M., Cole, P.M., 2005. Solvent extraction in southern Africa: An update of some recent hydrometallurgical developments. Hydrometallurgy, Vol. 78, pp. 52–78.

Sole, K.C., Parker, J., Cole, P.M., Mooiman, M.B., 2019. Flowsheet Options for Cobalt Recovery in African Copper–cobalt Hydrometallurgy Circuits. Mineral Processing and Extractive Metallurgy Review, Vol.40, Issue 3, pp.194-206.

Spike, C. G., Parry, R. W., 1953. American Chemical Society, Vol.75, pp. 2726-3770.

Srinivas, K., Sreenivas, T., Natarajan, R., Padmanabhan, N.P.H., 2000. Studies on the recovery of tungsten from a composite wolframite–scheelite concentrate. Hydrometallurgy, Vol.58, pp. 43-50.

Strickland-Constab1e, R.F., Mason, R. E. A., 1963. Nature, Vol. 197, pp. 897.

Suzuki, H., Kubota, H., 1966. The influence of binder phase composition on the properties of WC-Co cemented carbides. Plansee b.f. Pulver Metallurgy, 14:96.

The Guardian., 2019. Carmakers' electric dreams depend on supplies of rare minerals. Retrieved, 7 January 2018.

Thiemann, M., Scheibler, E., Wiegand, K.W., 2005. Nitric acid, Nitrous acid and Nitrogen Oxides – Ullmann Encyclopedia of Industrial Chemistry, Wiley-VCH, Weinheim.

Tomlinson, W., Ayerst, N., 1989. Anodic Polarization and Corrosion of WC-Co Hard Metals Containing Small Amounts of Cr3C2 and/ VC. Journal of Materials Science, Vol. 24, pp. 2348-2354.

Tomlinson, W.J., Linzell, C.R., 1988. Anodic Polarization and Corrosion of Cemented Carbides with Cobalt and Nickel Binders. Journal of Materials Science, Vol. 23, pp. 914-918.

Totalmateria., 2020. Tungsten Carbide Metals: Part One. http://www.totalmateria.com. Retrieved, 10 May 2020.

Trapp, G.J., 1949. Method of Recovering Hardmetal Carbides from Sintered Masses. USA Patent No. 2, 485, 175.

Trent, E.M., 1946. Process of Separating Hard Constituents from Sintered Hardmetals. US Patent No. 2,407,752.

Tripathy, S.K., Murthy, Y.R., 2012. Modeling and optimization of spiral concentrator for separation of ultrafine chromite. Powder Technology, Vol.221, pp. 387-394.

Tzeferis, P.G., Agatzini – Leonardou, S., 1994. Leaching of nickel and iron from Greek non-sulphide nickeliferous ores by organic acids. Hydrometallurgy 36, 345-360.

U.S. Geological Survey (2017) Mineral commodity summaries 2017: U.S. Geological Survey, 202 p., https://doi.org/10.3133/70180197. ISBN 978-1-4113-4104-3.

Ullmann's Encyclopedia of Industrial Chemistry, 2005. Wiley, pp. 17624/28029

Upadhyaya, G.S., 1998. Cemented Tungsten Carbides: Production, Properties and Testing. ISBN 13: 978-0-8155-1417-6, Noyes Publications. New Jersey, USA.

Valix, M., Tang, J. Y., Cheung, W. H., 2001b. The Effects of Mineralogy on the Biological Leaching of Nickel Laterite Ores. Minerals Engineering, Vol. 14, No. 12, pp. 1629-1635.

Van Niekerk, J.N., Schoening, F.R.L., 1953. The crystal structures of nickel acetate, $Ni(CH_3COO)_2 \cdot 4H_2O$, and cobalt acetate, $Co(CH_3COO)_2 \cdot 4H_2O$. Acta Crystallography, Vol.6, pp. 609-612.

Vanderpool, C.D., 1983. Electrolytic Disintegration of Sintered Metal Carbides. US Patent No. 4,385,972.

Veglio, F., Trifoni, M., Pagnanell, F., Toro, L., 2001. Shrinking core model with variable activation energy: a kinetic model of manganiferous ore leaching with sulphuric acid and lactose. Hydrometallurgy 60(2), 167-179.

Venetskii, S., 1970. The Charge of the Guns of Peace. Metallurgist, Vol. 14, No. 5, pp. 334–336.

Venkateswaran, S., Schubert, W-D., Lux, B., Osterman, M., Kieffer, B., 1996. W-Scrap Recycling By the Melt Bath Technique. International Journal of Refractory Metals and Hard Materials, Vol. 14, pp. 263-270.

Verhoff, F.H., 2016. Ullmann's Encyclopaedia of Industrial Chemistry. ISBN: 978-3-527-30673-2. Weinheim: Wiley-VCH.

Viswanadham, R.K., Rowcliffe, D.J., Gurland, J., 1983. Science of Hard Metals. Plenum Press, New York.

Voelter, W., Bayer, E., Barth, G., Bunnenberg, E., Djerassi, C., 1969. Chem. Berichte Journal, Vol. 102, pp. 2003;

Warren, R., Waldron, M. B., 1972. Powder Metallurgy, Vol. 15, No. 30, pp. 166

Wen, C.Y., 1968. Non-catalytic Heterogeneous Solid-fluid Reaction Models. Industrial and Engineering Chemistry, Vol. 60, pp. 34-54.

Westhoff, G., Starr, J.N., 2012. Lactic Acids. Ullmann's Encyclopedia of Chemistry. Weinheim: Wiley-VCH

Witteveen, H. J., Farnau, E. F., 1921. Colours Developed by Cobalt Oxides. Industrial & Engineering Chemistry. 13 (11): 1061–1066.

CHAPTER THREE

MATERIALS AND METHODS

3.1 Introduction

This chapter discusses the basis of the experimental approach, details on how experiments were set up and performed, the materials and equipment used in the study. Analytical techniques and quantitative data analysis employed in the study are discussed to conclude the chapter.

The experimental plan of the study (**Fig.3.1**) was divided into twelve stages. The first stage consisted of cemented tungsten carbide scrap material characterization. The second stage entailed factor range finding trials and reagent selection. The third stage was a kinetic study. The fourth and fifth stages consisted of using insights gained from the second stage to screen factors and optimize leaching conditions respectively. The sixth stage involved the use of optimum conditions obtained from the fifth stage to evaluate the effect of organic acid dosage on sulphuric acid leaching. The recovery of WC as solid particles was done at the seventh stage. Regeneration of the unreacted organic acid was conducted at stage eight. The ninth stage involved leach liquor purification using precipitation and solvent extraction techniques. The recovery of Co in metallic form was carried out at stage ten. Stage eleven involved precipitative recovery of W from raffinate solution. Stage twelve consisted of flowsheet development, mass and energy balance as well as techno-economic evaluation.

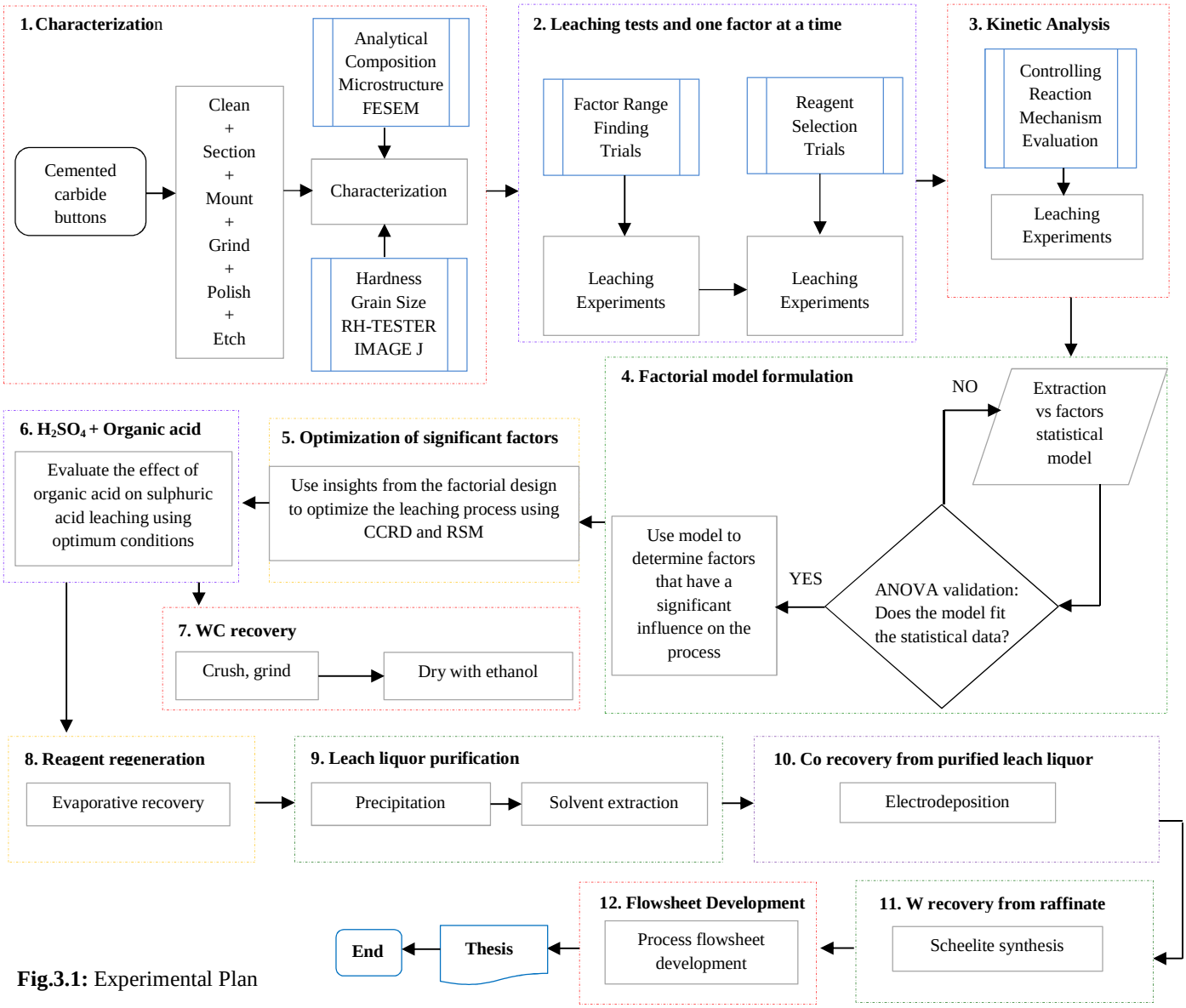

Fig.3.1: Experimental Plan

3.2 Basis of the Experimental Approach

Conventional cemented tungsten carbide scrap recycling techniques discussed in Chapter 2 section 2.3 are based on thermal, physical, chemical, electrochemical and electrolytic means of recovery. Currently, the thermal-based zinc process is widely employed. This process, however, consumes a high amount of electricity, requires the use of costly specialized equipment, and is only focused on the recovery of tungsten powder while ignoring cobalt. Other conventional methods are either energy intensive, require costly equipment, do not fully recover all valuable tungsten carbide constituents, are hazardous and environmentally unfriendly, involve too many

conversion steps or have slow process kinetics (Bhosale, 1990; Katiyar, 2014; Barnard et al, 1971). Thus, this research study aims to address the following shortcomings of conventional techniques: (a) slow process kinetics (b) tungsten passivation (c) discard of valuable constituents as waste (d) high energy consumption and (e) environmental pollution.

The above acknowledged challenges could be addressed by a novel hydrometallurgical approach as detailed below:

From the cobalt Pourbaix diagram in **Figure 3.2**, it can be surmised that the dissolution of cobalt requires oxidative acidic leaching conditions (Garcia et al, 2008) for it to be extracted from the metallic binder phase matrix. It can also be deduced, from the tungsten Pourbaix diagrams in **Figures 3.3** and **3.4**, that tungsten passivates readily at very low pH (Tomlinson and Ayerst, 1989), notably in the same pH region where the cobalt dissolution rate is highest.

The formation of passivating insoluble oxides in WC-Co hardmetals, when exposed to acidic solutions, is a known phenomenon and an area of active research. In their study, Tomlinson and Linzell (1988) reported that tungsten formed thin passivation films over a very wide potential range. A study by Chen (2013) showed that at pH <4.0, tungsten undergoes spontaneous passivation due to the formation of insoluble oxides in the form of WO_2, W_2O_5 and WO_3 (**Figure 3.3**). In an earlier study, Osseo-Asare (1982) revealed that the formation of insoluble oxides, WO_2, W_2O_5 and WO_3, leads to the formation of tungstic acid (H_2WO_4) (**Figure 3.4**), which is much more stable than the oxides. Similar findings on the formation of tungsten precipitates at low pH levels are documented elsewhere in literature (Edtmaier et al, 2005; Bosung and Sunjung, 2016; Lin et al, 1995; Cruywagen et al, 1993).

It is evident that the presence of tungsten in WC-Co hardmetal could be a threat to the process kinetics of cobalt dissolution. Formation of insoluble tungsten oxides and tungstic acid are likely to be an obstruction to the mass transfer of reactants and products within the cemented carbide channels during leaching. Therefore, it is expected that inhibition or elimination of the insoluble tungsten oxides and tungstic acid could allow Co dissolution and mass transfer to occur freely.

It's worth noting, according to **Figure 3.2**, that Co^{3+} is a stable species in the stability region defined by pH <2.0 and Eh >1.75V. However, the presence of Co^{3+} in the leach solution will be

highly unlikely if the Eh is maintained at <1.75V, the region in which Co^{3+} is reduced to Co^{2+}. The refractory carbide phase in the cemented carbide hardmetal (WC-Co) used in the current study is monocrystalline WC and the binder phase is Co metal. The cobalt in the binary phase hard metal, WC-Co, occurs as Co^{2+}.

Worthy of note, are **Figures 3.3** and **3.4**, which show that using an acidic solution is not effective for tungsten leaching. In fact, it is not the intention of this work to leach tungsten into solution, but rather to recover it in form of tungsten monocarbide (WC) as intact particles. Any tungsten co-extracted with Co is unintended and will subsequently be recovered using known chemical means.

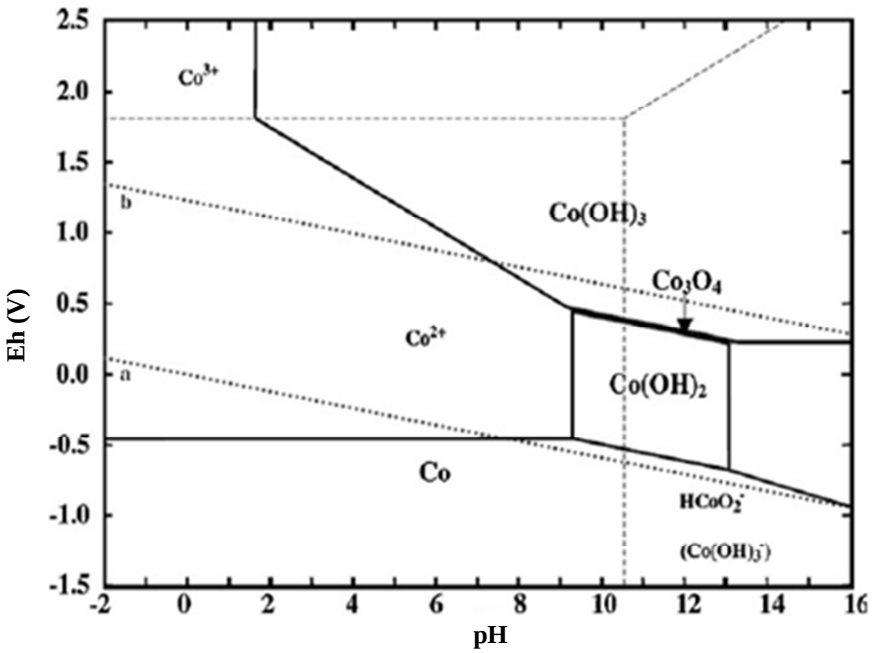

Fig.3.2: Pourbaix diagram for the Cobalt-H_2O system at 25°C; $\{Co^{2+}\} = 10^{-6}$ (Garcia et al, 2008; Pourbaix, 1974)

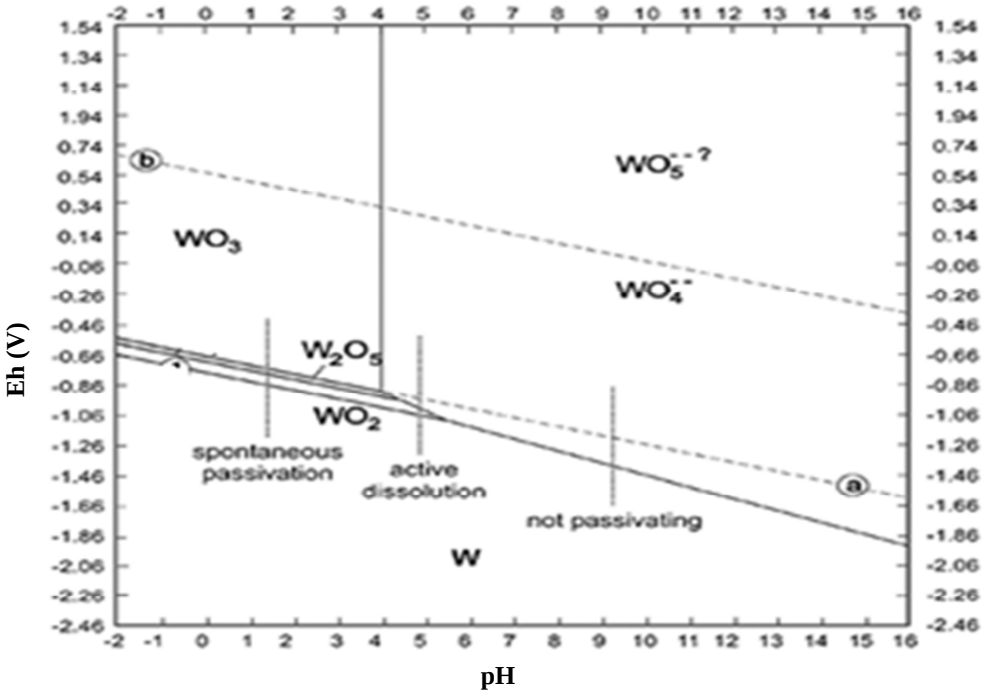

Fig.3.3: Pourbaix diagram for the Tungsten-H_2O system at 25°C; {W} = 10^{-5} (Chen, 2013; Pourbaix, 1974)

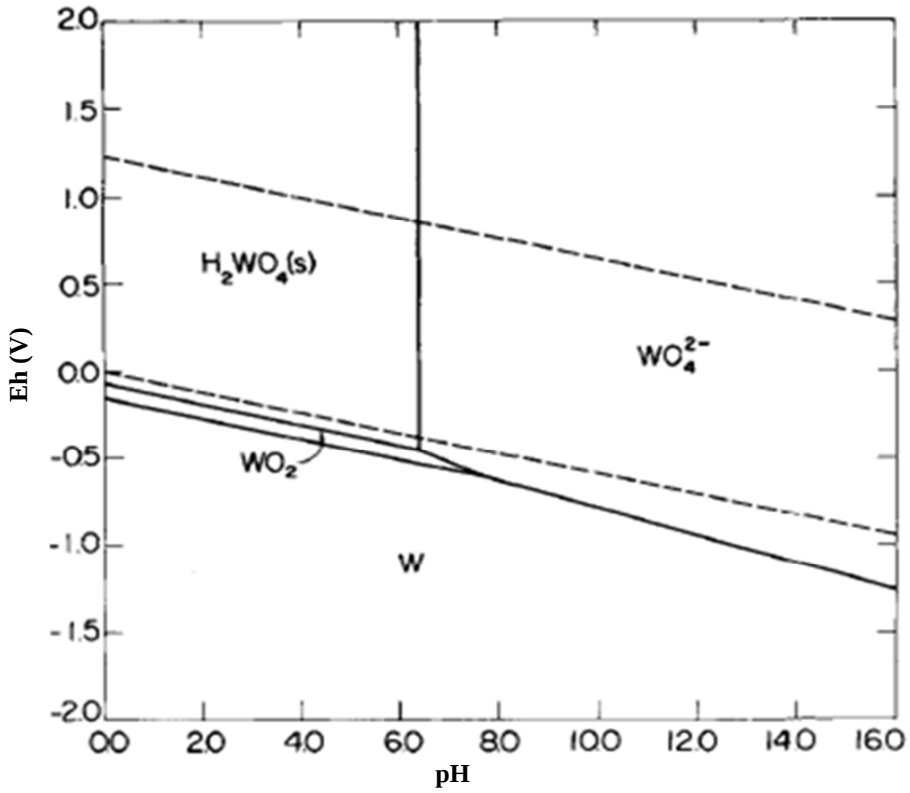

Fig.3.4. Pourbaix diagram for the W-H_2O system at 25°C; {W} = 10^{-3}. (Osseo-Asare, 1982)

According to **Fig.3.2**, it seems possible to dissolve WO_2^{4-} by working at pH 6 to 8. In this same range, Co also dissolves as Co^{2+}. However, working in this pH range has the following disadvantages:

- Slow rate of reaction at pH 6 to 8, compared to pH <4.0 range, due to lower hydronium ion concentration, especially if the reaction mechanism is chemically controlled.
- Lower Co extraction efficiency at pH 6 to 8, compared to pH <4.0 range, due to lower acid concentration.
- Intensified dissolution of tungsten (W) in form of WO_2^{4-} ions. This might adversely affect WC integrity. It is not the intention of the current work to leach tungsten into solution.
- High possibility of cobalt precipitation at pH ≥6.9 (Monhemius, 1977). This might result in poor Co extraction efficiencies.

Organic chelating agents such as acetic, lactic, malic, tartaric, and citric acids are known to form soluble tungsten complex salts (Guedes de Carvalho and Neves, 1992; Van Niekerk and Schoening, 1953). These carboxylic organic acid ligands are known to have a high affinity for complexing and solubilizing metals of the transition series such as Co, W, Fe, Ni, Cu, Pt, Cr, V, Mo, etc.(Dwyer and Mellor, 1964). An example of a tungsten complexation reaction using a lactic acid chelate is shown in **Eqn. 2.4**.

Tungsten lactate may be formed by the reaction between tungsten dioxide (WO_2) and lactic acid chelate in a sodium chloride medium. The formation constant for the tungsten complexation reaction is reported as $1x10^{17.47}$ (Cruywagen et al, 1993). The high magnitude of the formation constant for the tungsten lactate complex, typical of metal chelates, is an indication of a very stable tungsten complex species. The molecular structure of the tungsten lactate complex (tungsten metal chelate) is shown in **Figure 3.5.**

$$WO_2 + 2(C_3H_4O_3^{2-}) = [WO_2(C_3H_4O_3)_2]^{2-} \quad (3.1)$$

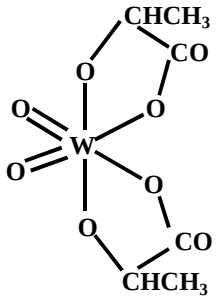

Fig.3.5: Structure of $[WO_2 (C_3H_4O_3)_2]^{2-}$ complex (Cruywagen et al, 1993)

If applied in this way, oxidative reactions that form insoluble tungsten oxides and tungstic acid can be inhibited and a soluble tungsten complex salt can be formed instead (Lin et al, 1995; Guedes de Carvalho and Neves, 1992). This would not only prevent the formation of undesirable tungsten oxides around WC grains but also eliminate or minimize intergranular channel blockage thus preserving the integrity of the WC grains as well as allowing mass transfer to occur unobstructed.

A review of literature has shown that although the organic chelating agents have been proven to be potentially good tungsten complexing agents, and that inorganic acids have also been proven to cause cobalt dissolution, to the best of the authors' knowledge, no published work is available regarding their combined use, in leaching cemented tungsten carbides. However, it is theorized that if a chelating agent achieves metal extraction by the chelate anion complexing with the metal cation, then the equilibrium will be shifted in favour of the metal complex formation; a phenomenon known as metal complexation. Furthermore, an inorganic acid extracts metals by cation displacement from the particle matrix through proton attack, resulting in metal dissolution; a phenomenon known as metal protonation. Once the formation of the tungsten complex has occurred, and the formation of tungsten oxides is inhibited, the passivation effect disappears and the dissolution of cobalt occurs freely. From the two phenomena above, complexation and protonation, it can be ascertained that for the processing of cemented carbide scrap, the combination of an organic chelating agent and an inorganic acid may well be applied to prevent tungsten passivation by complexation as well as to selectively dissolve the cobalt binder phase by protonation, simultaneously.

It is expected that, when subjected to the complexing agent-aided acidic leaching technique, the phases in cemented tungsten carbide will undergo the following possible reactions:

(i) The WC aggregate phase:

$$2WC\text{-}Co + O_{2(g)} + 4H^{+} \rightarrow 2Co^{2+} + 2WC + 2H_2O_{(l)} \quad (3.2)$$

(ii) The cobalt binder phase (matrix):

$$2Co_{(s)} + O_{2(g)} + 4H+ \rightarrow 2Co^{2+} + 2H_2O_{(l)} \quad (3.3)$$

(iii) The 'Co-W-C alloy' binder phase (matrix)

$$2Co_{(s)} + O_{2(g)} + 4H+ \rightarrow 2Co^{2+} + 2H_2O_{(l)} \quad (3.4)$$

$$3W(s) + 4O_{2(g)} + 12H^{+}_{(aq)} \leftrightarrows WO_{2(s)} + 6H_2O_{(l)} + 2W^{6+}_{(aq)} \quad (3.5)$$

$$3WO_{2(s)} + O_{2(g)} + 6H^{+}_{(aq)} \leftrightarrows W_2O_{5(s)} + 3H_2O_{(l)} + W^{6+}_{(aq)} \quad (3.6)$$

$$2W_2O_{5(s)} + O_{2(g)} + 12H^{+}_{(aq)} \leftrightarrows 2WO_{3(s)} + 6H_2O_{(l)} + 2W^{6+}_{(aq)} \quad (3.7)$$

$$WO_{3(s)} + H_2O_{(l)} \leftrightarrows H_2WO_4\ (s) \quad (3.8)$$

The presence of the organic chelating agent will cause the cobalt binder phase to undergo a complexation reaction, as shown below (**Eqn.3.9**), where 'L' is the organic ligand and 'n' is the number of moles.

$$Co\text{-}W\text{-}C + O_2 + 4H^{+} + nL \leftrightarrows CoL_n^{(n-4)-} + WL_n^{(n-4)-} + 2H_2O + C \quad (3.9)$$

In this way,

- Precipitative tungsten reactions 3.2, 3.5 – 3.8 are inhibited or suppressed. What happens if these reactions are allowed to proceed first and then a ligand is added later on is not known. What is known is that all the other tungsten oxides formed are unstable except for tungstic acid which is formed through the last reaction, 3.8.
- Formation of insoluble tungsten oxide films and tungstic acid are prevented.
- Passivation and channel blockage are eliminated or minimized.
- Possible oxidation and degradation of tungsten monocarbide (WC) grains is prevented.

On the basis of these observations, the possibility exists to design a technique wherein the Co is selectively extracted whilst leaving the tungsten monocarbide (WC) intact. It is this possibility which is the focus of this study wherein the process parameters, process kinetics and the physical and chemical properties of cemented carbide during leaching are investigated so as to develop a recycling method which is energy and cost efficient, environmentally-friendly and optimally converts all the scrap metal constituents into valuable products.

Thus, this study investigates the selective dissolution of the Co binder metal and recovery of all valuable constituents from binary-phase cemented carbide (WC-6%wt.Co). The study employed an acid leach process that combines an inorganic acid and an organic chelating agent, in order to provide the basis for overcoming the highlighted issues. In order to achieve this, a statistical Design of Experiments (DOE) method was employed as a research tool to obtain statistically relevant data for modeling optimum leaching conditions. Factor range finding trials were conducted in order to allow for a proper analysis of the influence of process parameters. Reagent selection trials were performed in order to find a suitable lixiviant for selective and effective cobalt dissolution. A conceptual kinetic model was derived in order to describe the dissolution of cobalt out of the hardmetal binder matrix. Furthermore, precipitation, solvent extraction and electrorecovery process techniques were employed for leach liquor purification and resource recovery of WC, Co and W.

A flow diagram of the proposed complexing agent-aided acid leach process is presented in **Figure 3.6.**

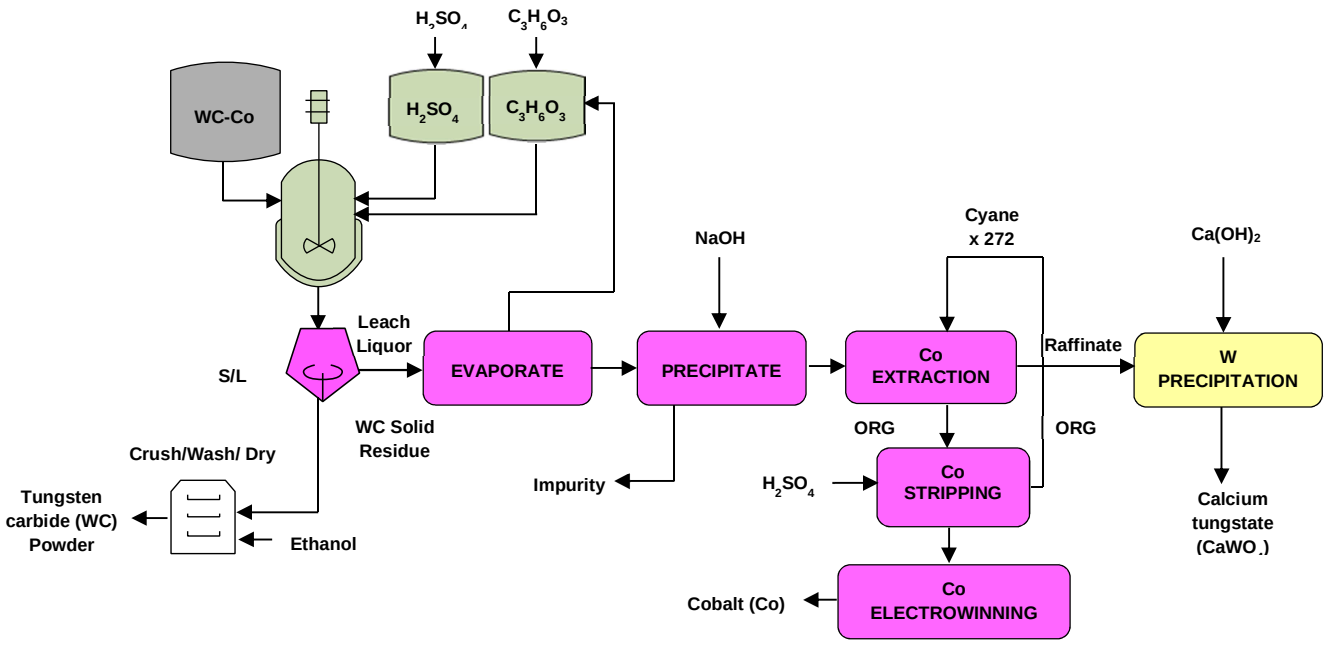

Fig.3.6: A flow diagram of the proposed process for recycling cemented carbide secondary material

The procedure for dosing the two acids, inorganic and organic, entailed mixing the two acids before adding them to the reactor vessel. Previous work regarding the practice of mixing an inorganic and organic acid to form one lixiviant is documented elsewhere (Cruywagen et al, 1993; Lin et al, 1995; Guedes de Carvalho and Neves, 1992).

3.3 Materials

3.3.1 Cemented carbide (WC-6wt.%Co) buttons

The hardmetal used in the current study was purchased from Pilot Tools (Pty) Limited, Denver, South Africa. It was WC-6%wt.Co production scrap buttons, 9.8 mm long and 7.34 mm diameter (**Fig. 3.7**).

Fig.3.7: Production scrap cemented carbide buttons

3.3.2 Tungsten carbide (WC) powder

Tungsten carbide powder (**Figure 3.8**) purchased from Weartech (Pty) Limited, South Africa, was used in the current study to investigate the response characteristics of WC grains to acidic media. The powder was also used to compare to the powder which was generated during recycling. The powder had a purity of 99.9 % and a grain size of 1.13 ± 0.2µm. The powder was used as received without further modification.

Fig.3.8: Cast tungsten carbide powder

The leached WC residue was analyzed for tungstic acid (H_2WO_4) using Raman Spectroscopy. Raman spectra were measured using the 514.5nm line of a Lexel Model 95SHG argon ion laser and Horiba LabRAM HR Raman spectrometer equipped with an Olympus BX41 microscope attachment. The incident beam was focused onto the sample using a 100x LWD objective and the backscattered light was dispersed via 600 lines/mm grating onto a liquid nitrogen cooled CCD detector. The laser power at the sample was kept low (0.4 mW) to minimize the chance of localized heating. Spectra were analyzed using LabSpec v5 software.

3.3.3 Reagents

All reagents used were of analytical grade. The reagents were purchased from Merck and Sigma Aldrich and were used as received without further purification. Distilled water, analytical grade sulphuric acid (98% w/w), lactic acid, tartaric acid, maleic acid, ethanol, Cyanex 272 extractant, Shellsol D70/Shellsol 2375 diluent, Isodecanol (modifier), NaOH, $Ca(OH)_2$ and $CaCl_2$ were used in the leaching, solvent extraction, electrorecovery and precipitation experiments.

3.4 Material Characterization

3.4.1 Metallographic Sample Preparation

The buttons were cleaned ultrasonically with ethanol to remove extraneous material. The metallography and microstructure preparation and analysis were performed as guided by the ASM handbook volume 9 (Aliya, 2004). After cleaning, the cemented carbide button samples were sectioned, mounted, ground and polished, for measuring the hardness and then etched to study the microstructure.

3.4.1.1 Sectioning

Well cleaned buttons were sectioned into two halves each using a precision cutting machine (Model: Secotom-10, Struers, Denmark) (**Figure 3.9**) in preparation for metallography and hardness testing.

Fig.3.9: Precision cutting machine (Secotom-10, Struers)

3.4.1.2 Mounting

Using Polyfast resin, the sectioned buttons were mounted using a hot mounting press (Model: Opal 410, ATA, Germany) (**Figure 3.10**) in preparation for grinding and polishing.

Fig.3.10: Hot mounting press (ATA Opal 410)

3.4.1.3 Grinding and polishing

The mounted button samples were ground and polished using a semi-automatic grinder and polishing machine (Model: Saphir 520, ATA, Germany) (**Figure 3.11**). The samples were ground using 220, 350, 500, 800 and finally 1200 grit paper. The samples were rinsed with water

to remove loose particles and then polished using 1 μm diamond suspension for 5 minutes to obtain a mirror-like finish.

Fig.3.11: Semi-automatic grinder/polisher (Saphir 520)

3.4.1.4 Etching

The polished samples were etched with Murakami reagent for optical imaging and field emission scanning electron microscopy (FESEM) analysis. The composition, preparation and use of the Murakami etchant is listed in **Table 3.1** (ASTM B657-05, 2010). After etching, the samples were rinsed with distilled water and ethanol and then dried using a blow drier.

Table 3.1: Compositions, preparation, and use of the Murakami etchant (ASTM B657-05, 2010)

Etching Technique	Composition of Etchants	Conditions of Etching	Objective of Etching
1	Freshly prepared mixture of equal quantities of 10% (mass/mass) aqueous solutions of $K_3Fe(CN)_6$ (III) (potassium ferricyanide) and potassium or sodium hydroxide ($K_3[Fe(CN)_6]$ in KOH). This is generally referred to as the Murakami solution. 10g of potassium ferricyanide plus 10g of sodium hydroxide in 100mls of distilled water.	Etch at approximately 20°C for 2 to 10 seconds. Flush the test-piece section with water immediately, without removing the oxide layer. Dry the surface carefully with acetone or alcohol without wiping.	Identification of η-phase.
2	Same as 1A	Etch at approximately 20°C for 2 to 4 minutes.	Identification of α, β, and γ-phases.

3.4.2 Metallographic Sample Analysis

3.4.2.1 Optical Light Microscopy

Three etched samples were analyzed for eta phase features by obtaining optical photomicrographs of each sample. The analysis was done using a GX50 inverted metallurgical microscope and SC50 camera coupled with Olympus Imaging Analysis software. The microscope is exhibited in **Figure 3.12**.

Fig.3.12: Light Optical Microscope-GX50

3.4.2.2 Scanning Electron Microscopy (SEM)

High magnification imaging of the microstructure and analysis of the elemental compositions for three button samples was done using a Field Emission Scanning Electron Microscope (FESEM) equipped with an Oxford X-act detector for Energy Dispersive X-ray Spectroscopy (EDS) (Model: Sigma, Carl Zeiss, UK). The average elemental composition was calculated using multiple EDS scans across different regions of the sample. The FESEM apparatus is shown in **Figure 3.13**.

Fig.3.13: Field Emission Scanning Electron Microscope (Zeiss, Sigma)

3.4.2.3 Grain size measurements

The average tungsten carbide grain size was calculated using the intercept technique as per ASTM E112-13 [ASTM, 2013). Image J software version 1.8.0-112 was used in conjunction with the FESEM images to determine the grain sizes of the three etched button samples.

3.4.2.4 Rockwell Hardness

The hardness of three polished samples was measured for hardness using a Rockwell Hardness Tester (Model: 5JR, Wilson Mechanical Instruments Co. Inc., USA) (**Figure 3.14**). A load of 100 gf was applied on the sample with a dwell time of 10 s. At the end of 10 s the hardness of the material was read from the scale on the Tester. The test was performed five times on one sample in order to determine the average hardness. Crushing and pulverization of the button residue skeleton in order to recover WC as recycled powder depends on button hardness. The ability to crush the button after leaching is an indicator of leaching success.

Fig.3.14: Rockwell hardness tester (5JR, Wilson Mechanical Instruments)

3.5 Design of Experiments

One of the key objectives of this study was to identify and attempt to optimize the factors which influence cemented tungsten carbide dissolution. To execute this objective, a statistical Design of Experiments (DOE) method was employed as a research tool to develop an experimentation strategy. The use of DOE has several advantages. It helps to determine important variables that need to be controlled and unimportant variables that may not need to be controlled and provides insight over a range of experimental conditions. Factors of interest are changed in a systematic way so as to ensure reliability and a full evaluation of individual and interaction effects. Therefore, by using a DOE matrix, more precise and useful information is obtained about the studied process. In this study, the factors identified to have a significant influence on the leaching process were optimized and used in subsequent leaching experiments.

In order to explore the possible factor influence on the response (cobalt extraction) and to identify their appropriate upper and lower limits, factors were screened (Chapter 6). A full 2^5 factorial design was employed in identifying the factors with a significant influence on the process. A statistical analysis of the experimental results, using probability plots and Pareto analysis, was used to evaluate the significance of each factor.

After factor screening, optimization of the factors identified as being statistically significant (Chapter 7) was carried out with the purpose of predicting the response values and identification of the optimum response within the experimental range. The optimization experiments were done by using the response surface methodology (RSM) in conjunction with the central composite design (CCRD). The design procedure for RSM used in this study involved three stages as follows: (1) Designing and conducting of experiments (2) Deriving and developing a mathematical model (3) Finding the optimal set of experimental parameters.

The central composite rotatable design (CCRD) was used to design the optimization experiments and the optimal set of parameters was determined graphically using statistical software, Design Expert®11. In the CCRD method, the factorial designs are augmented with axial designs.

A quadratic response surface model of the form,

$$y = \beta_o + \sum_{i=1}^{k} \beta_i x_i + \sum_{i=1}^{k} \beta_{ii} x_i^2 + \sum_{i=1}^{k} \sum_{j=i+1}^{k} \beta_{ij} x_i x_j + \varepsilon \qquad (3.10)$$

was fitted and solved using statistical software, Design Expert®11.

In **Equation 3.1**, y is the predicted response, β_o is the coefficient for intercept, β_i is the coefficient of linear effect, β_{ii} is the coefficient of quadratic effect, β_{ij} is the coefficient of interaction effect, ε is a term that represents other sources of variability not accounted for by the response function, k is the number of variables, x_i and x_j are coded predictor variables for the independent factors (Khuri and Cornel, 1987).

After determination of the coefficients of the regression model, the adequacy of the model was checked using the analysis of variance (ANOVA). To do the analysis, ANOVA uses the following methods:

- Fisher's variance ratio test (F-*test*), *to test evidence of lack of fit and significance of the regression model.*
- Standard errors of model coefficients (t-*test*), *to determine significance of regression coefficients of parameters; intercept term, linear terms, quadratic terms and interaction terms.*
- The coefficient of determination (R^2), *to check model accuracy; comparison between experimental results and predicted values obtained using the refitted model.*
- The absolute average deviation (AAD), *to check model plausibility; if found plausible, then the model can be used to predict response values at any regime in the interval of the experimental design.*

The coefficients of the regression model were estimated by fitting experimental results using Design Expert®11 software.

3.6 Recovery Process Stages

3.6.1 Preliminary 1- Factor range finding trials

Factors that influence a leaching process include: temperature, residence time, reagent concentration, reagent type, solid to liquid ratio, agitation rate, pressure, size of solids, etc. These factors in turn affect chemical kinetics, thermodynamics, fluid mechanics, heat transfer and mass transfer aspects of the leaching process. Due to limited information, in literature, specific to the treatment of binary-phase cemented tungsten carbide leaching tests were performed to determine appropriate factor levels using one factor at a time approach. The chosen factor ranges are presented in **Table 3.2.** The upper limit for the temperature range was set based on the need for a less energy intensive leaching process. The upper limit for the acid concentration range was set based on previous work by Trent (1946) who found that acid leaching of cemented carbides beyond 3M concentration could attack the hard carbide (WC) particles. The authors reported that if the intention of leaching cemented carbides is to recover hard carbide particles, then acid concentration limits should be taken into account.

Table 3.2: Factor values for the range finding trials

Factor		Low	High
1	Temperature (°C)	40	85
2	Leaching time (h)	1	6
3	Acid concentration (M)	0.01	3.00
4	Solid-to-liquid ratio	1:6	1:18
5	Agitation rate (rpm)	0	1000

3.6.2 Preliminary 2- Reagent selection

The insight gained from parameter levels determined in the previous stage was used to test NaOH, H_2SO_4 and organic acids namely lactic, tartaric and maleic acid. The testing of NaOH and H_2SO_4 was meant to identify a better leaching route between the basic and acidic method. Organic acids were tested in order to identify an organic acid with a strong tungsten selectivity and ability to form a soluble and stable tungsten metal complex. The complexation of tungsten by organic ligands is known to aid in suppressing slow and precipitative tungsten reactions in

acidic solutions (Cruywagen et al, 1993; Lin et al, 1995). The precipitative reactions cause poor diffusion and adversely affect mass transfer.

3.6.3 Preliminary 3- Factor screening and process optimization

A combination of insights from stage 1 and stage 2 were used to screen and identify factors that have a significant influence on the cemented tungsten carbide leaching process with the aim of optimizing them. For this, a full factor factorial model involving 5 factors, i.e. temperature, time, acid concentration, solid to liquid ratio and agitation rate was formulated and employed. Insights gained from the full factorial design were utilized to optimize the leaching process using the central composite rotatable design (CCRD) in conjunction with the response surface methodology (RSM) as described in section 3.5.

3.6.4 Resource Recovery

The recovery of WC was performed using optimum leaching conditions obtained from stage 3. An evaporative process was used to regenerate the unreacted organic acid. Impurity removal from the filtrate consisted of adding NaOH to form precipitates. Further purification and upgrading of the cemented carbide leach liquor was performed using solvent extraction resulting in an advance electrolyte and raffinate solution. The pulse electrodeposition method (Metrohm Manual, 2019) was used to recover Co from the purified advance electrolyte using a Potentiostat 208N. The recovery of tungsten from the raffinate solution consisted of adding $Ca(OH)_2$ or $CaCl_2$ to form $CaWO_4$ precipitate (scheelite).

3.6.4.1 Recovery of WC

The recovery of the hard carbide particles from the cemented tungsten carbide leach residue buttons was carried out using a stainless steel ring and puck grinding set (**Figure 3.15**) mounted on a laboratory pulverizer (Model 1MZ-100, JXSC, Jiangxi, China). The residue buttons were placed in between the rings and crushed to powder within a predetermined time. To prevent oxidation, it was necessary to carry out the operation under a protective organic liquid, ethanol. The pulverization conditions are listed in **Table 3.3**. After pulverization, the organic liquid was removed by decantation and the recycled WC powder was dried and characterized using FESEM and XRD analysis. The pulverized WC material was prepared for XRD analysis using a back

loading preparation method. It was analyzed with a Malvern PANalytical Aeris diffractometer with PIXcel detector and fixed slits with Fe filtered Co-Kα radiation. The phases were identified using X'Pert Highscore plus software. The relative phase amounts (weight %) was estimated using the Rietveld method.

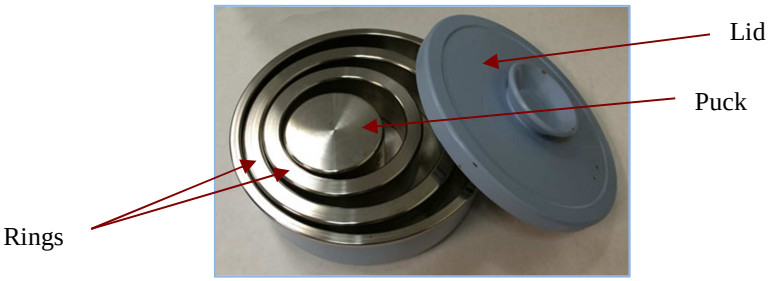

Fig.3.15: Ring and puck grinding set

Fig.3.16: Laboratory pulverizer Model 1MZ-100, JXSC, Jiangxi, China

Table 3.3: Conditions for pulverization of WC residue buttons

Parameter	**Residence time (sec)**	**WC residue weight per run (g)**
Unit value	10-20	60 - 70

3.6.4.2 Reagent Regeneration

An evaporative technique using a distillation rotary evaporator mounted with a reflux condenser (**Figure 3.17**) was used to perform evaporative recovery of lactic acid from the process stream.

The experiments involved placing the leach solution into an eggplant flask, lowering the flask into silicon oil and heating at 125°C for a predetermined period of time. The flask was rotated at 30 rpm. At the end of the experiment, the distillate and residue were collected and characterized using UV-VIS UV-VIS spectroscopy (Model: UV-1800 Shimadzu Spectrophotometer, Kyoto, Japan) and the regeneration efficiency was evaluated. Absorbance was measured at a wavelength of 390nm against the reference solution of 2mL of a 0.2% $FeCl_3$ solution. The reaction acid measurements were performed at 25+/-5°C. The distillation conditions used are listed in **Table 3.4**.

Fig.3.17: Distillation Rotary Evaporator (Laborota 4000)

Table 3.4: Conditions for the evaporative recovery of lactic acid

Parameter	Residence time (hrs)	Temp. (°C)	Solution volume (mL)
Unit value	1 - 3	122	500

3.6.4.3 Precipitative purification

During leaching, Fe impurity levels in the cemented tungsten carbide leach liquor are sometimes noticeably higher than the industry tolerance limit of 1.5ppm required for advance cobalt electrolyte (Sole et al, 2016). In the current study, the removal of Fe impurity from cemented carbide leach liquor consisted of adding NaOH and raising the pH to 3.0 - 7.5. The precipitation technique was based on the Monhemius (1977) diagram for precipitation of metal salts. The precipitation conditions used are presented in **Table 3.5**.

Table 3.5: Conditions for precipitation of Fe, Al and Mn impurities

Parameter	**pH**	**Temp. (°C)**	**Agitation Rate (rpm)**
Unit value	3.0 – 7.5	25	750

3.6.4.4 Solvent extraction

Solvent extraction of Co from the cemented carbide leach liquor was carried out using a separating funnel and an Erlenmeyer flask. A Cyanex 272 extractant and Shellsol D70/Shellsol 2375, an organic diluent were used in the experiments. The use of kerosene as a diluent was also considered. The aqueous and organic phases were mixed at a predetermined ratio, agitated, settled and separated using the afore-mentioned apparatus. The solvent extraction and stripping conditions are shown in **Tables 3.6** and **3.7** respectively. The selection of the conditions was based on literature (Blanchard, 1995; Morin et al., 1996; Fisher and Pavlides, 1998; Sole et al, 2005).

Table 3.6: Conditions for **s**olvent extraction of Co

Parameter	O/A	pH	Extractant conc % (v/v)	Extraction Time (minutes)	Phase Separation Time (minutes)	Temp °C	Agitation rate (rpm)	Extraction stages
Level	3:1	5.0 - 5.6	15	60	15	35	150	3

Table 3.7: Conditions for stripping Co

Parameter	A/O	H_2SO_4 Eluant Acid con (M)	Stripping Time (minutes)	Phase Separation Time (minutes)	Temp °C	Agitation rate (rpm)	Stripping stages
Level	1:1	2	30	15	25	150	3

3.6.4.5 Co electrorecovery

Electrodeposition of cobalt on stainless steel 304L cathode plates was performed using a three electrode electrochemical cell as shown in the schematic set-up in **Figure 3.18**. The surface pre-treatment was achieved by grinding the surface to an 80 grit SiC surface finish and thereafter

activated using a solution with composition 18.5 vol.% HNO_3 – 7.5 vol.% HF – 74 vol.% H_2O for 12.5 minutes. The activation of the steel plate surface with distilled water and acetone (Sharma et al, 2005) was also considered. The electrochemical cell was connected to an Autolab Potentiostat PGSTAT208N as shown in **Figure 3.19**. The Potentiostat was operated by Nova® version 2.1.3 software. Stainless steel plates of 50mm x 50mm x 1mm, placed in a conventional sulphate-sulphuric acid bath comprising of $CoSO_4 \cdot 6H_2O$ at pH3-4 were used to electroplate the 304L stainless steel with cobalt at 60-65°C. To improve the conductivity of the electrolyte, $NaSO_4$ (15gpl) was added (Sharma et al, 2005). The use of $MgSO_4$ (1.6 – 12gpl) was also considered. The distance between the cathode and anode electrodes was maintained at 30mm (Sharma et al, 2005). The Co electroplating conditions are shown in **Table 3.8**. The pulse electrodeposition method was used to achieve the cobalt plating. A Ag/AgCl reference electrode was used to measure the electrochemical potential for applying the cobalt plating with deposition potentials of t_{off} equalling 5 seconds and a steady potential of -0.2 V followed by a t_{on} of 10 seconds and a potential equal to -0.3 V at plating times of 1, 2 and 3 hrs. The choice of the electrochemical potential for plating was based on the cobalt reduction potential of -0.28V while taking into account the ohmic over-potentials that are associated with electro-reduction processes. Ohmic over-potentials are due to the resistance to conduction of ions through the electrolyte, cathode and anode electrodes and contacts between cell components.

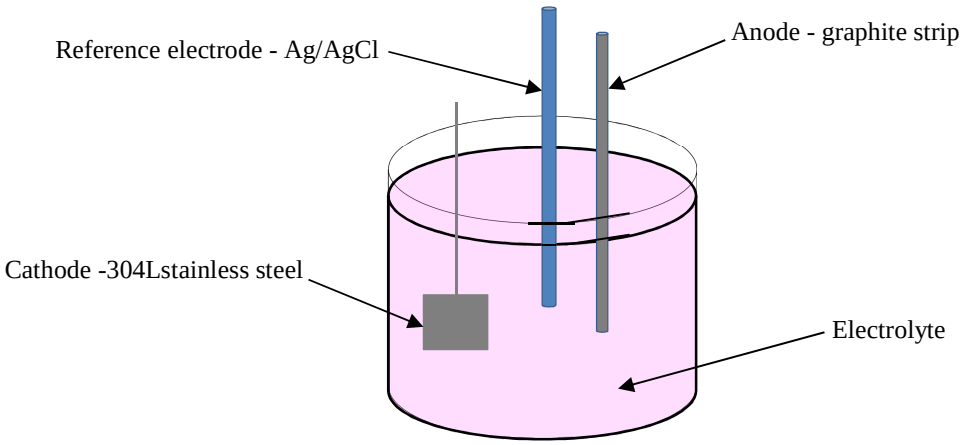

Fig.3.18: Schematic presentation of the electrochemical set-up for the Co electroplating process

Fig.3.19 (a): Potentiostat set-up (PGSTAT208N, Autolab, Metrohm)

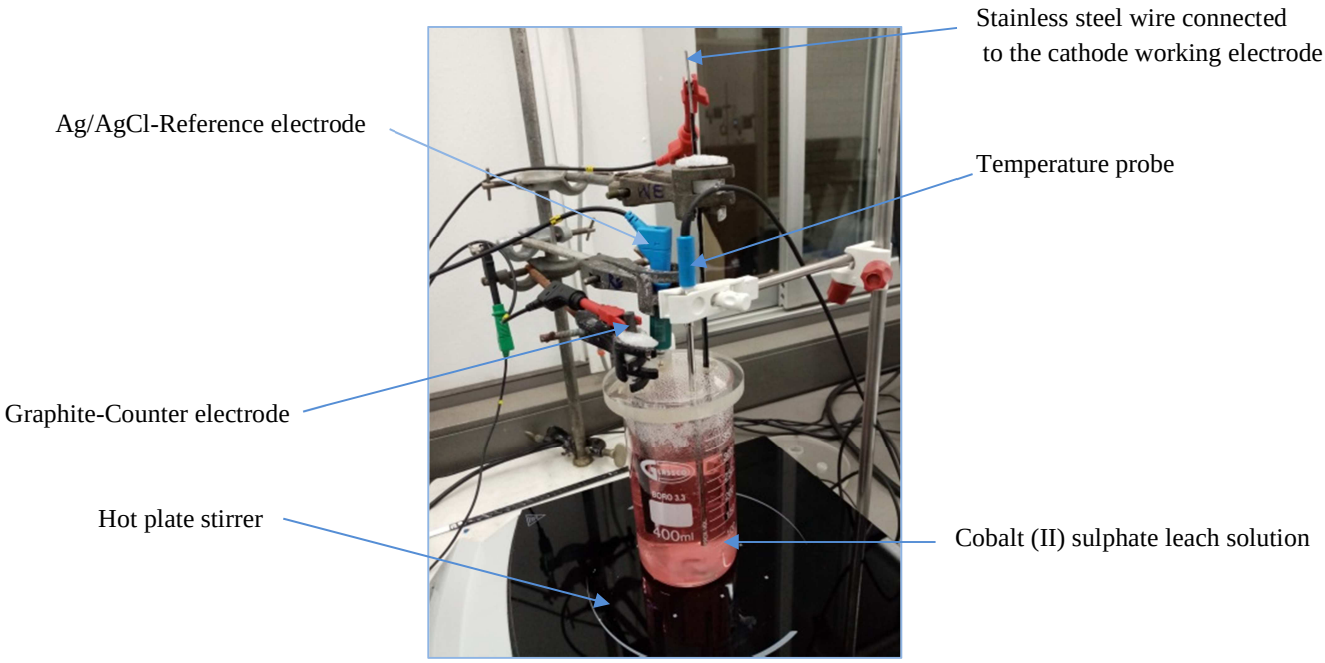

Fig.3.19 (b): Cell set-up used in pulsed electrodeposition (PED)

Table 3.8: Conditions for pulse-electrodeposition of Co using Autolab Potentiostat 208N

Parameter	Current density (A/m^2)	Temp (°C)	Co Feed (gpl)	pH	Current (A)	Potential (V)	Plating time (hrs)	t_{off} (sec)	t_{on} (sec)
Unit value	175-400	60-65	20	3 - 4	1 – 2	-0.28	1-3	5	10
Surface Area	(LxWx2 surfaces ≤ 0.05mx0.05mx2 = 0.005m^2)								

3.6.4.6 Scheelite synthesis

Synthesis of scheelite ($CaWO_4$) was carried out in a 1 L jacketed leaching vessel, an overhead stirrer fitted with an impeller and a thermostatic oil/water bath for external heating of the leaching vessel. A predetermined volume of solution containing tungsten in form of sodium tungstate (Na_2WO_4) was added to the leaching vessel. When the temperature reached the set-point, a specific quantity of precipitant was added to the leaching vessel. After a specified period of time, the slurry was removed from the leaching vessel, washed, filtered, dried and characterized. Characterization of the slurry was carried out using FESEM equipped with an Oxford X-act Energy Dispersive Spectroscopy (EDS) detector (Model: Sigma, Carl Zeiss, UK). The process conditions for scheelite synthesis, shown in **Table 3.9**, were based on literature (Martins et al., 2007; Fan, 1993; Wan et al, 2015).

Table 3.9: Conditions for scheelite ($CaWO_4$) synthesis

Precipitant	Residence time (minutes)	Temp. (°C)	$Ca(OH)_2$ dosage [$Ca(OH)_2$:Na_2WO_4]	$CaCl_2$ dosage [$CaCl_2$:Na_2WO_4]	Agitation Rate (rpm)
$Ca(OH)_2$	150	100	1.4	-	150
$CaCl_2$	20	50	-	1.5-1.7	150

3.7 Leaching Experiments

3.7.1 Experimental Set-up

The leaching set-up consisted of a 2 L leaching vessel, an overhead stirrer fitted with an impeller, a 15 L/min vacuum pump (**Figure 3.20**) for air supply and a thermostatic bath for external heating of the leaching vessel for the necessary temperature.

Fig.3.20: Vacuum pump (Model: N022AN.18, KNF, Germany)

3.7.2 Leaching Experimental Procedure

The leaching set-up consisted of a 1L capacity leaching vessel, an overhead stirrer fitted with an impeller, a reflux condenser, a 15 L/min vacuum pump for air supply and a 40 L thermal water bath for external heating of the leaching vessel (**Fig.3.21**). Leaching consisted of first adding a weighed amount of 15 whole buttons to the leaching vessel then leaching media and agitating the mixture in a constant temperature water bath. The buttons were sitted at the bottom of the leaching vessel. The volume of leaching media added to the leaching vessel was as per the desired predetermined solid-to-liquid ratio. Separate whole button samples were used for each allotted leaching condition.

The kinetic experiments were conducted at predetermined temperatures accompanied with intervallic aliquot sampling of the leach solution. The process conditions for the kinetic study consisted of experimental runs at 50°C, 70°C and 85°C; 2M H_2SO_4 concentration; 1:10 solid to liquid ratio, at an agitation rate of 500rpm. The leached cemented carbide buttons were washed with 200 mL deionized water. The wash water was thereafter mixed with the leach liquor and the volume of the mixed solution was recorded. The mixed solution was analyzed for Co and W using Atomic Absorption Spectrometry (AAS) and Inductively Coupled Plasma-Optical Emission Spectrometry (ICP-OES).

The pH profiles and redox potentials of the leach solution were measured using the Thermo Scientific Orion Star A211 pH Benchtop Meter. The redox potentials readings were obtained using the Ag/AgCl/3M KCl reference electrode and subsequently converted to the standard hydrogen electrode (SHE) by adding 210 mV (Friis et al., 1998). After use the electrode was washed with distilled water and then dried. The electrode was then stored in 3M KCl solution to prevent desiccation.

The leached sample residue was washed with 200 mL distilled water. The wash water was thereafter mixed with the leach liquor and the total volume was recorded. The mixed liquor was set aside for analysis. The WC residue was set aside for material characterization. Filtrates from the leaching process were analysed for Co and W concentration using Atomic Absorption Spectroscopy (Model: Agilent 240FS, Agilent Technologies, USA) and Inductively Coupled

Plasma-Optical Emission Spectrometry (ICP-OES) analyser (Model: SPECTRO GENESIS, Spectro Analytical Instruments, Germany). The experimental set-up is shown in **Figure 3.21**.

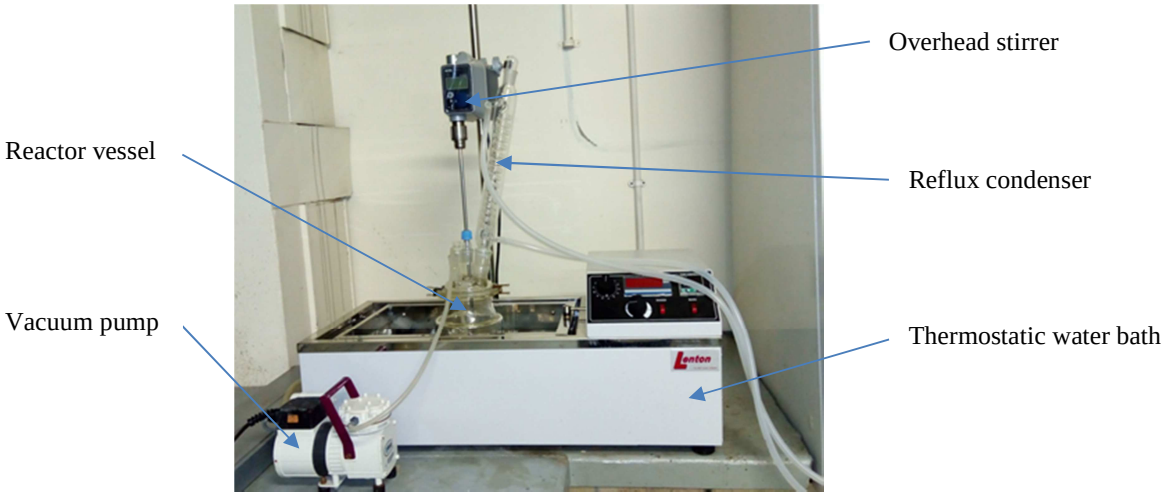

Figure 3.21: Experimental Set-up

3.8 Data Analysis

The data collected from the experiments described in this chapter was used to develop relationships between Co and W extraction and the parameters tested. The tested parameters included: temperature, time, acid concentration, solid to liquid ratio and agitation rate etc. These relationships and the observed results are discussed in the subsequent chapters of this thesis. The extraction efficiency during the leaching of cemented carbide buttons was calculated as a percentage of Co and W in the liquid phase to that in the cemented carbide buttons (sample calculations are illustrated in Appendix A). All results from the experimental testing were recorded. The data in Chapters 6 and 7 was statistically analyzed. Correlations between process variables and conversions were determined graphically, analytically and empirically.

3.9 Summary

This chapter presented details on how experiments were set up and performed, the materials and equipment used and analytical methods employed in the study.

The next chapter describes preliminary laboratory tests and findings. In particular the chapter focuses on reagent selection, factor range finding trials and evaluation of cemented tungsten carbide response characteristics.

3.10 References

Aliya, D., 2004. Metallographic Sectioning and Specimen Extraction, Metallography and Microstructures. ASM Handbook, ASM International, Vol. 9, pp. 229–241.

ASTM Standard B657-05., 2010. Standard Guide for Metallographic Identification of Microstructure in Cemented Carbides, in Annual Book of ASTM Standards, Vol. 02.05, ASTM International, Conshohocken, PA, pp. 404-408.

ASTM., 2013. Standard test methods for determining average grain size, ASTM E112-13, West Conshohocken, PA, ASTM International, pp. 12-14.

Barnard P.G, Starliper A.G, Kenworthy, H., 1971. Reclamation of Refractory Carbides from Carbide Materials. U.S Patent 3, 595, 484.

Bhosale S.N, Mookherjee S, Pardeshi R.M., 1990. Current Practices in Tungsten Extraction and Recovery. High Temperature Materials and Processes, Vol. 9, Issue 2-4.

Blanchard, F., 1995. Kilembe Treating the Stockpiles. Mining Environmental Management, Vol.3, Issue 2, pp. 30–32.

Bosung, S., Sunjung, K., 2016. Cobalt Extraction from Tungsten Carbide-Cobalt (WC-Co) Hard Metal Scraps Using Malic Acid. International Journal of Mineral Processing, Vol.151, pp. 1-7.

Chen, Z.A., 2013. PEC Experiment Standard. Springer, Berlin/New York.

Cruywagen, J.J., Kruger, L., Rohwer, E.A., 1993. Molybdenum (VI) and Tungsten (VI) Complex Formation, Part 5. The Reaction with Lactate in 1.0 mol dm^{-3} Sodium Chloride Medium. Journal of Chemical Society, Dalton Transactions, pp. 105-109.

Cruywagen, J.J., Saayman, L.J., Noven, M.L., 1992. Journal of Crystallographic and Spectroscopic Research, Vol. 22, pp. 737

Dwyer, F.P., Mellor, D.P., 1964. Chelating Agents and Metal Chelates. Academic Press, New York and London

Edtmaier, C., Schiesser, R., Meissl, C., Schubert, W.D., Rock, A., Schoen, A., Zeiler, B., 2005. Selective Removal of the Cobalt Binder in WC-Co Based Hard Metal Scraps By Acetic Acid Leaching. Hydrometallurgy, Vol. 76, pp. 63-71.

Fan, S.S., 1993. The control of calcium tungstate granularity and the recycle of tungsten from the scheelite mother liquor. Rare Met. Cement. Carbides 113, 13–16.

Fisher, K.G., Pavlides, A.G., 1998. The Kasese Cobalt Project. Proceedings Extraction Metallurgy Africa ’98. South African Institute of Mining and Metallurgy, Johannesburg.

Friis, E. P., Andersen, J. E. T., Madsen, L. L.., Bonander, N., Møiler, P., Ulstrup, J., 1998. Dynamics of Pseudomonas Aeruginosa Azurin and its Cys3Ser Mutant at Single Crystal Gold Surfaces Investigated by Cyclic Voltammetry and Atomic Force Microscopy. Electrochimica Acta 43(9), 1114-1122.

Garcia, E.M., Santos, J.S., Pereira, E.C., Freitas, M.B.J.G., 2008. Electrodeposition of Cobalt from Spent Li-ion Battery Cathodes by the Electrochemistry Quartz Crystal Microbalance Technique. Journal of Power Sources, Vol. 185, pp. 549-553.

Guedes de Carvalho, R.A., Neves, O.R., 1992. Leaching of Scheelite (CaWO4) Under Quasi-Stagnant Solution Conditions. Hydrometallurgy, Vol. 28, pp. 45-64.

Inc., New York.

Katiyar, P.K., Randhawa, N.S., Hait, J., Jana, R.K., Singh, K, K., Mankhand, T.R., 2014. An Overview on Different Processes for Recovery of Valuable Metals from Tungsten Carbide Scrap. ICNFMM, Nagpur.

Khuri, A.I., Cornel, J.A., 1987. Response Surfaces: Designs and Analyses. Marcel Dekker,

Kusaka, Y., Yokoyama, K., Sera, Y., Yamamoto, S., Sone, S., Kyono, H., Shirakawa, T., Goto, S., 1986. Respiratory Diseases in Hardmetal Workers: An Occupational Hygiene Study in a Factory. British Journal of Industrial Medicine, Vol. 43, pp. 474-485.

Lin, J.C., Lin, J.Y., Lee, S.L., 1995. Process for Recovering Tungsten Carbide from Cemented Tungsten Carbide Scraps by Selective Electrolysis. US, Patent No. 5,384,016.

Martins, J.I., José, L.F.C., Lima, A., Moreira, S.C.C., 2007. Tungsten Recovery from Alkaline Leach Solutions as Synthetic Scheelite. Hydrometallurgy 85 (2–4), 110–115.

Monhemius, A.J., 1977. Precipitation Diagrams for Metal Hydroxides, Sulfides, Arsenates and Phosphates. Transactions of the Institute of Mining & Metallurgy. Vol. 86, pp. 202-206.

Monhemius, A.J., 1977. Precipitation Diagrams for Metal Hydroxides, Sulfides, Arsenates and Phosphates. Transactions of the Institute of Mining & Metallurgy. Vol. 86, pp. 202-206.

Morin, D., Battaglia, F., Hau, J.M., Ollivier, P., 1996. KCC project: 5% of the world’s cobalt production by means of bioleaching. Chron. Rech. Min. (525).

Osseo-Asare, K., 1982. Solution Chemistry of Tungsten Systems. American Society for Metals and the Metallurgical Society of AIME. Metallurgical transactions B. Vol.13B, pp. 555-564.

Pourbaix, M., 1974. Atlas of Electrochemical Equilibria in Aqueous Solutions, pp. 322-328. National Association of Corrosion Engineers, Houston.

Sharma I.G., Pamela, Alex., Bidaye, A.C., Suri, A.K., 2005. Electro-winning of Cobalt from Sulphate Solutions. Hydrometallurgy, Vol. 80, pp. 132 – 138.

Sole, C.K., Jurrius, Y., Hardwick, E., 2016. Purification of cobalt electrolyte by ion-exchange: Pilot Plat results and preliminary commercial design. Society of chemical industry: IEx 2016 Proceedings-Hydrometallurgy session.

Sole, K.C., Feather, A.M., Cole, P.M., 2005. Solvent extraction in southern Africa: An update of some recent hydrometallurgical developments. Hydrometallurgy, Vol. 78, pp. 52–78.

Tomlinson, W., Ayerst, N., 1989. Anodic Polarization and Corrosion of WC-Co Hard Metals Containing Small Amounts of Cr3C2 and/ VC. Journal of Materials Science, Vol. 24, pp. 2348-2354.

Tomlinson, W.J., Linzell, C.R., 1988. Anodic Polarization and Corrosion of Cemented Carbides with Cobalt and Nickel Binders. Journal of Materials Science, Vol. 23, pp. 914-918.

Trent, E.M., 1946. Process of Separating Hard Constituents from Sintered Hard Metals. US Patent No. 2,407,752.

Van Niekerk, J.N., Schoening, F.R.L., 1953. The crystal structures of nickel acetate, $Ni(CH_3COO)_2 \cdot 4H_2O$, and cobalt acetate, $Co(CH_3COO)_2 \cdot 4H_2O$. Acta Crystallography, Vol.6, pp. 609-612.

Wan, L., Huang, X., Deng, D., Li, H., Chen., Y., 2015. Synthesis of Scheelite from Sodium Tungstate Solution by Calcium Hydroxide Addition. Hydrometallurgy, Vol. 154, pp. 17-19.

Upadhyaya, G.S., 1998. Cemented Tungsten Carbides: Production, Properties and Testing. ISBN 13: 978-0-8155-1417-6, Noyes Publications. New Jersey, USA.

CHAPTER FOUR

PRELIMINARY LEACHING TESTS

4.1 Introduction

The study presented in this Chapter aimed at investigating parameters which promote cobalt dissolution in the WC-6wt%Co button scrap material using an acid leach process. A brief characterization of the material properties of the buttons is presented in the initial part of this chapter. Response characteristics of the buttons during leaching were investigated to understand the limitations of the recovery process.

In order to explore the possible influence of factors on the response (Co extraction) and to find factor ranges (appropriate upper and lower levels), preliminary experimental tests were conducted according to the procedure previously described in Chapter 3 section 3.7. The parameters investigated included leaching temperature, leaching time, acid concentration, solid to liquid ratio and agitation rate.

With the intention of investigating the possible influence of different leaching media on the response and to select the appropriate lixiviants, preliminary reagent selection trials were conducted. The lixiviants tested were sulphuric acid, sodium hydroxide, lactic acid, tartaric acid and maleic acid. The understanding obtained from these preliminary experiments was used as a basis for the kinetic study, screening, optimization, purification and recovery investigations that follow in subsequent chapters.

4.2 Characterization of WC-6wt%Co scrap buttons

Figure 4.1 shows the microstructure of the buttons where tungsten is present in the cemented carbide in the form of tungsten monocarbide grains (WC) and cobalt in the form of a metallic binder matrix. The term “cemented” refers to the tungsten carbide (WC) grains being captured in the cobalt metallic binder phase and “cemented” together, forming a covalent bond between the two phases (General Carbide, 2016). Using multiple EDS scans across different regions of the sample, the average elemental composition of cemented carbide was calculated as 85.95wt.% tungsten, 8.77wt.% carbon and 5.28wt.% cobalt (**Table 4.1**).

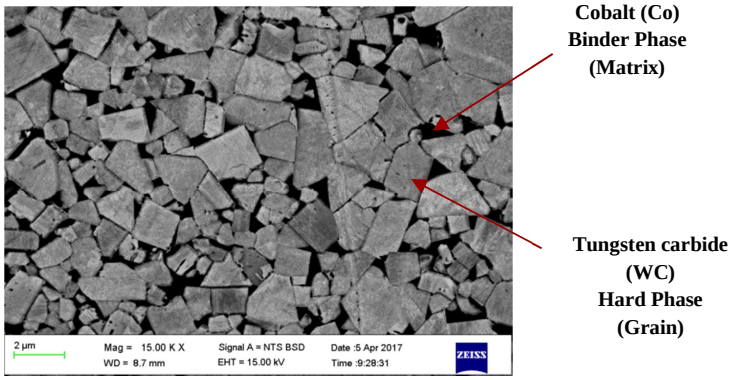

Fig.4.1: Microstructure of cemented tungsten carbide (WC-6wt.%Co)

Table 4.1: Cemented tungsten carbide composition

Element	Weight (%)
Carbon (C)	8.77
Cobalt (Co)	5.28
Tungsten (W)	85.95
Total	100

Grain sizes of typical cemented tungsten carbide cobalt grades are presented in **Table 4.2**. The average WC grain size of the buttons used in the current study was measured as 1.13 ± 0.2µm and which falls within the 'fine' size classification of the industry standard specification reflected in Table 4.2 (Sandvik, 2005). The WC grain size influences the distribution structure of the cobalt binder phase matrix, which exists as a continuous cobalt network with fluctuating width of the branches widely described as the 'mean linear intercept' or 'mean free path' (Exner, 1979). The average button hardness was measured as 62.5 ±5.6 HRC. According to Sandvik (2020), cemented tungsten carbide hardness is inversely related to the binder content and WC grain size. Cemented carbide hardness increases with decreasing binder content and decreasing WC grain size.

Table 4.2: Cemented tungsten carbide (WC-Co) grain size (Sandvik, 2005)

Pilot Tools Cemented Carbide Average Grain Size (µm)				1.13				
Industry Standard Grain Size (µm)	>0.2	0.2-0.5	0.5-0.9	1.0-1.3	1.4-2.0	2.1-3.4	3.5-5.0	>5.0
Classification	Nano	Ultra-Fine	Sub-micron	Fine	Medium	Medium Course	Course	Extra Course

Figure 4.2 shows the optical photomicrograph of an etched cemented tungsten carbide sample. Using Olympus GX51 microscope, results showed that the eta (η) phase was absent.

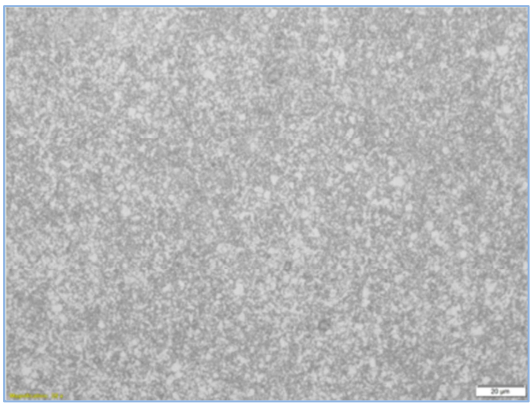

Fig.4.2: Microstructure of cemented tungsten carbide (WC-6wt.%Co) showing that eta (η) phase is absent; light Murakami etching (10s), x500.

4.3 Leaching Tests

The leaching tests consisted of reacting WC-6wt%Co button scrap with different lixiviants. The lixiviants tested included: alkaline, organic and inorganic acidic solutions. A brief description of the dissolution reactions possible with each lixiviant is given first followed by the experimental results and analyses.

4.3.1 Alkaline leaching

The extraction of Co from cemented carbide using caustic leaching consisted of reacting NaOH solution with cemented carbide button samples. The possible dissolution of Co and W from cemented carbide was based on the thermodynamic feasibility of hardmetals in aqueous alkaline solutions as described by Chen (2013). The following are the possible reactions:

$$2Co_{(s)} + O_{2\,(g)} + 4OH^- \leftrightarrows 2Co(OH)_2 + 4e^- + 2H_2O_{\,(l)} \quad (4.1)$$

$$WC + O_2 + 4OH^- \leftrightarrows WO_4^{2-} + C + 2e^- + 2H_2O_{(l)} \quad (4.2)$$

4.3.2 Organic Acid Leaching

The extraction of Co from cemented carbide using organic acid leaching was carried out by reacting lactic, maleic and tartaric acid solutions with cemented carbide button samples. The dissolution of Co from cemented carbide was based on the oxidation potential of metals

(Bronsted, 1931) and the thermodynamic feasibility of hardmetals in aqueous alkaline solutions as described by Chen (2013). Metal dissolution by organic acid ligands is exemplified by the complexation reaction of Co and W with a lactic acid ligand as shown in **Eqns. 4.3** and **4.4**.

$$Co + 2C_3H_5O_3^{-1} + 2H^+ + O_2 = C_3H_{10}CoO_6 + H_2O \quad (4.3)$$

$$WO_2 + 2(C_3H_4O_3^{2-}) = [WO_2(C_3H_4O_3)_2]^{2-} \quad (4.4)$$

4.3.3 Inorganic Acid Leaching

The extraction of Co from cemented carbide using an inorganic acidic solution was carried out by reacting sulphuric acid solution with cemented carbide button samples. The dissolution of Co and W metals was based on the oxidation potential of metals (Bronsted, 1931) and thermodynamic feasibility of hardmetals in aqueous acidic media as described by Garcia and co-researchers (2008). The following are the possible reactions:

$$2Co_{(s)} + O_{2\,(g)} + 4H^+ \leftrightarrows 2Co^{2+} + 2H_2O_{(l)} \quad (4.5)$$

$$3WC + 4O_2 + 12H^+ \leftrightarrows WO_2 + 6H_2O + 3C + 2W^{6+} \quad (4.6)$$

$$3WO_2 + O_2 + 6H^+ \leftrightarrows W_2O_5 + 3H_2O + W^{6+} \quad (4.7)$$

$$2W_2O_5 + O_2 + 12H^+ \leftrightarrows 2WO_3 + 6H_2O + 2W^{6+} \quad (4.8)$$

4.4 Results and Discussion

4.4.1 Cemented Carbide Dissolution Behaviour in Acidic and Alkaline Media

Co and W dissolution as a function of acidic and basic media type is illustrated in **Figure 4.3**. Experimental results in **Fig.4.3** show that leaching of cemented carbide using sulphuric acid gave a maximum Co extraction of 8.7% in 6 hrs compared to 1.13% Co extraction in NaOH. In acidic solutions, W showed stable passivity, whereas Co readily dissolved; the situation observed in alkaline media is vice versa. The results are in agreement with Chen (2013) who suggests that W passivates in acidic media due to formation of insoluble tungsten oxides like WO_2, W_2O_5 and WO_3. The insoluble oxides form a non-reactive layer that protects W from further reactions. Tomlinson and Ayerst (1989) made a similar observation about W passivation in acidic solutions. According to Garcia and co-researchers (2008), the passivation of cobalt in alkaline solutions is due to the precipitation of cobalt to form cobalt hydroxide ($Co(OH)_2$). The authors observed that the cobalt precipitate hinders further cobalt reactions thus, causing passivation. Sulphuric acid was found to have superior dissolution ability for Co, whereas NaOH showed little effect.

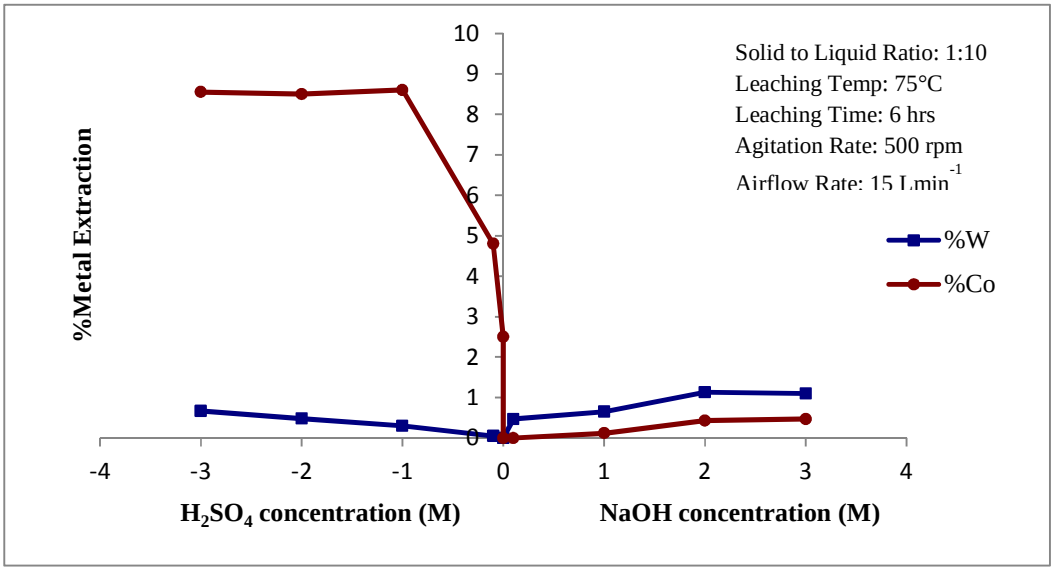

Fig.4.3: Co and W dissolution as a function of acidic and basic concentration

4.4.2 Cemented Carbide Dissolution Behaviour in Inorganic and Organic Acidic Media

4.4.2.1 Inorganic Acid Leaching

The dissolution of Co and W as a function of sulphuric acid concentration is presented in **Figure 4.4**. Inorganic (mineral) acids extract metals by cation displacement from the metal containing particle. For hardmetals, Co^{2+} ion is displaced from the binder matrix and W^{6+} ion from the WC aggregate phase. The hydronium (H^{+}) ion reacts with Co and W, causing the metals to become ionized thus inducing metal dissolution (Bronsted, 1931). As seen in the figure, sulphuric acid concentration has a much stronger effect on Co dissolution than it has on W. An increase in sulphuric acid concentration dramatically enhanced Co extraction from 2.6% to a maximum of 8.7% at 1.0M within 6hrs of leaching. Further increase in acid concentration beyond 1.0M did not yield any significant change in Co dissolution. This could possibly be attributed to the formation of some insoluble tungsten precipitates. Further test work discussed in section 4.6.6 entailed exploring the effect of acid solutions on mono tungsten carbide (WC) grains. The WC grains, in form of powder, were reacted with sulphuric acid. The Raman spectroscopy results showed a substantial formation of tungstic acid. This result was found to be consistent with similar observations suggested by some authors (Edtmaier et al, 2005; Chen, 2013; Osseo-Asare, K., 1982; Bosung and Sunjung, 2016). The authors further suggest that the tungstic acid

precipitates create a blockage within the cemented carbide channels hence hindering the mass transfer of reactants and products.

The co-dissolution of tungsten was found to be up to a maximum of 0.4% extraction, suggesting that tungsten dissolution is inhibited in acidic environment. In acidic solutions W shows stable passivity, whereas Co readily dissolves. However, the co-dissolution of tungsten is associated with the formation of insoluble W precipitates as suggested by several authors (Edtmaier et al, 2005; Chen, 2013; Osseo-Asare, K., 1982; Bosung and Sunjung, 2016). These precipitates are postulated to be a possible interference to Co dissolution rates.

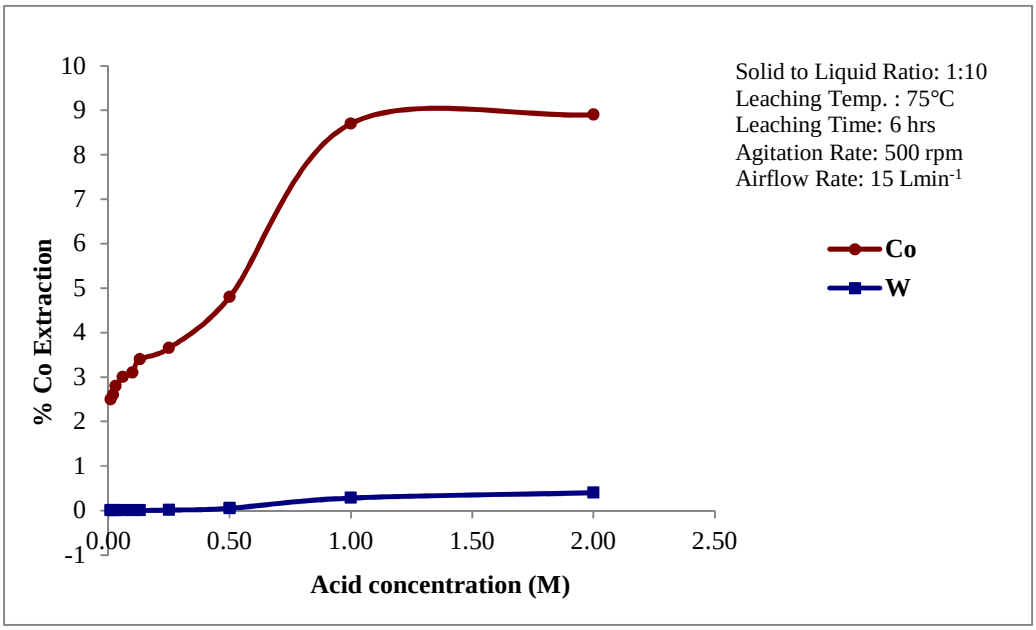

Fig.4.4: Co and W dissolution as a function of sulphuric acid concentration

4.4.2.2 Organic Acid Leaching

Cobalt and tungsten dissolution as a function of organic acid type at different acid concentrations is presented in **Figures 4.5** and **4.6** respectively. Organic acids achieve metal extraction by the anion ($RCOO^-$) complexing with Co^{2+} or W^{6+} cation through proton removal from the organic acid and shifting the equilibrium in favour of the metal complex. Three types of organic acids, lactic, maleic and tartaric, were tested at acid concentrations of 0.01M, 0.1M, 0.25M and 0.5M in order to determine the ability of the acids to extract Co and W from cemented carbide hardmetal. Results in **Fig.4.5** show that, within 6hrs of leaching, lactic, maleic and tartaric acids were able

to extract up to a maximum of 2.8%, 2.3% and 2.1% Co respectively. The decrease in Co extraction efficiencies with increasing acid concentration might be attributed to excess acid resulting in high solution viscosity and poor diffusion. Among the three organic acids tested, lactic acid showed the strongest effect on Co dissolution. The order of effectivity in Co dissolution by the organic acids was found to be lactic>maleic>tartaric acid.

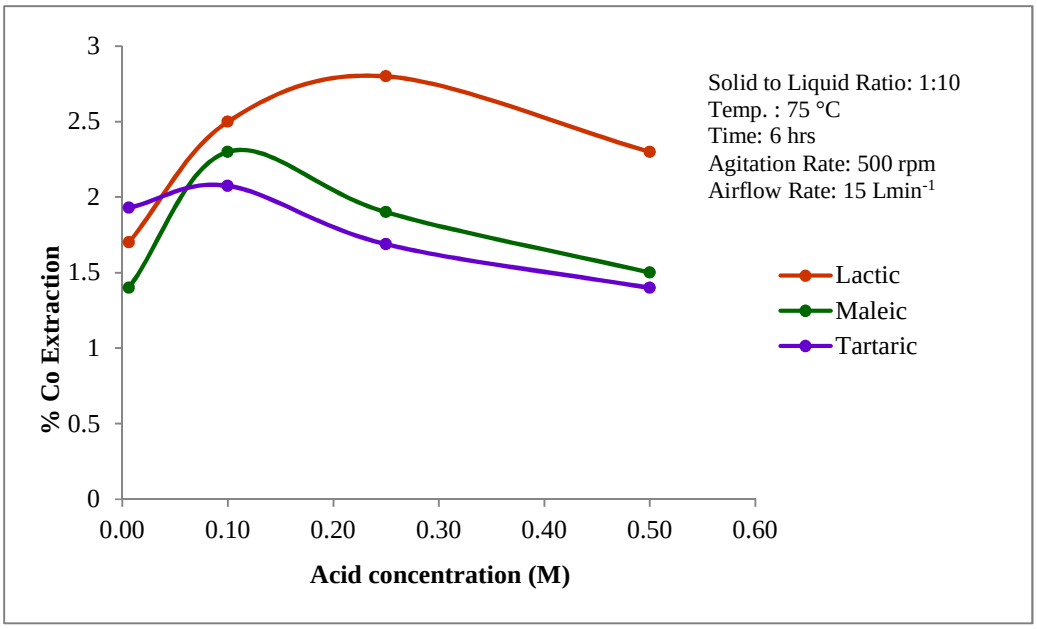

Fig.4.5: Co dissolution as a function of organic acid type

Results in **Figure 4.6** show that, within 6hrs of leaching, lactic, maleic and tartaric acids were able to extract up to a maximum of 0.16%, 0.10% and 0.11% W respectively. The order of effectivity in W dissolution was found to be lactic>tartaric>maleic acid. Although lactic and tartaric acids had a stronger effect on W dissolution than maleic acid, lactic and maleic acid had a wider acid range for tungsten dissolution compared to tartaric acid. This characteristic might be attributed to the possibility that lactic and maleic acid have a higher affinity for W^{+6} ions over a wide acid range where they form more stable tungsten complex salts than tartaric acid. In terms of tungsten complexation and tungsten salt complex stability, lactic acid was found to give the best performance among the three organic acids and was, therefore, adopted for use in all subsequent experiments.

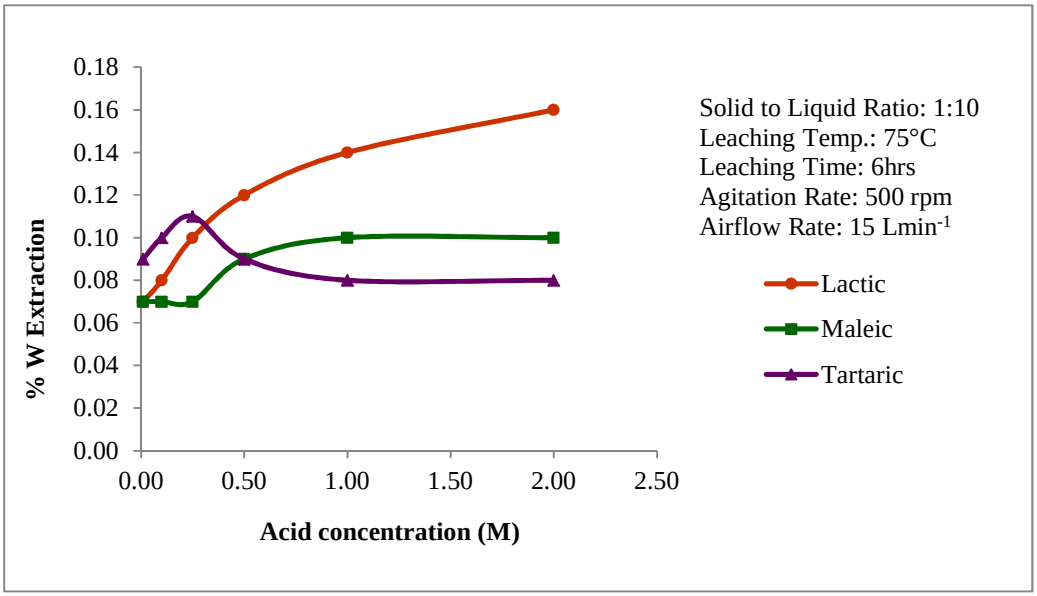

Fig.4.6: W dissolution as a function of organic acid type

4.4.2.3 Organic vs Inorganic Acid Leaching: Cobalt Dissolution

A comparison of cobalt dissolution as a function of acid type is illustrated in **Figure 4.7**. The figure shows a comparison of sulphuric acid performance against lactic, tartaric and maleic acid. As seen in the figure, sulphuric acid has a much stronger effect on cobalt dissolution compared to all the three organic acids. The difference between inorganic and organic acid extractions might be explained by the fact that inorganic acids deprotonate and dissociate more easily than organic acids and are therefore more effective in metal ionization (Housecroft, 2008; Earnshaw and Greenwood, 1997; Bronsted, 1931).

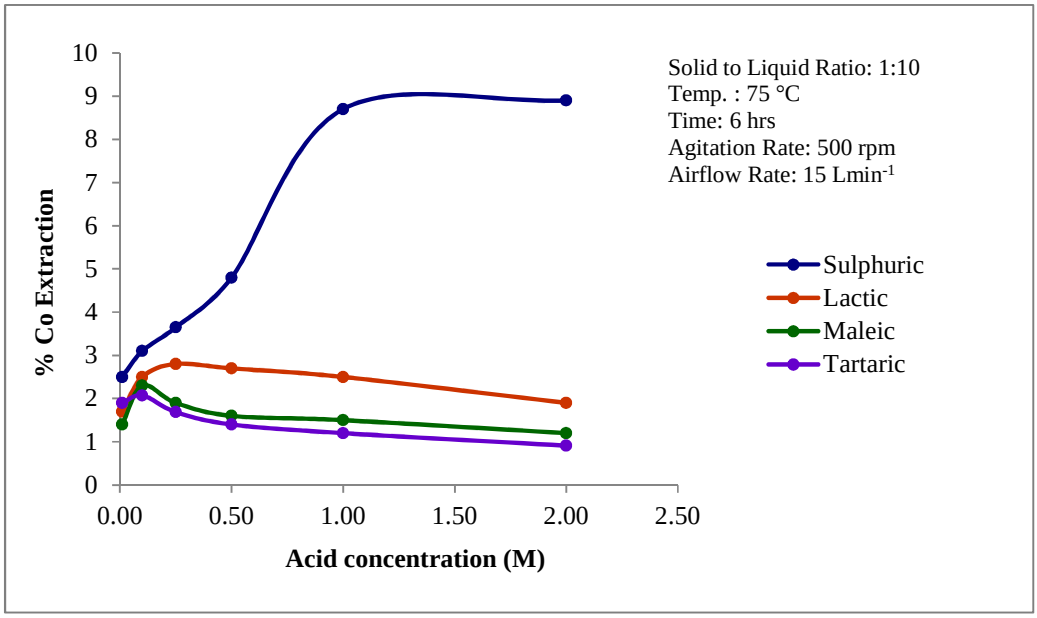

Fig.4.7: Co dissolution as a function of acid type

4.4.2.4 Organic vs Inorganic Acid Leaching: Tungsten Dissolution

A comparison of tungsten dissolution as a function of acid type is exhibited in **Figure 4.8**. As seen in the figure, lactic, tartaric and maleic acid can solubilize tungsten to form soluble and stable tungsten salts. The figure also shows that sulphuric acid has a stronger effect on tungsten dissolution compared to organic acids. Though higher than the rest, tungsten extraction by sulphuric acid, at 0.40% extraction, is quite low and is not expected to have a significant adverse effect on WC grains and therefore not a threat to WC grain integrity.

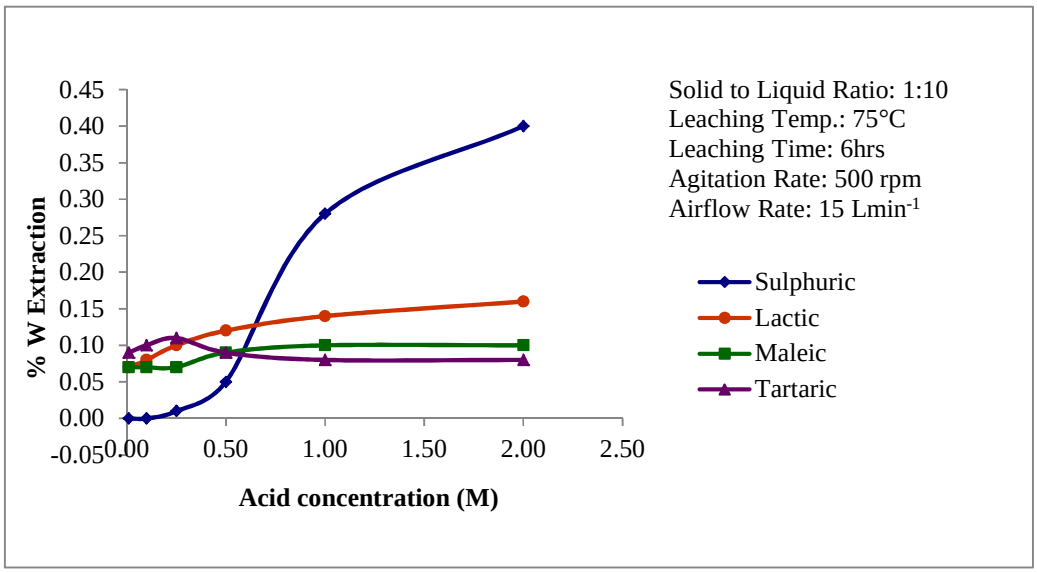

Fig.4.8: W dissolution as a function of acid type

4.5 Effect of Parameters on Cemented Carbide Dissolution Behaviour in Acidic Media

Based on results from the foregoing preliminary leaching tests, the acidic route was found to be the best approach for processing cemented carbide scrap material. Therefore, in order to investigate the effect of different parameters on cemented carbide dissolution, experiments were performed using sulphuric acid. The studied parameters included: leaching temperature, leaching time, acid concentration, solid to liquid ratio and agitation rate.

4.5.1 Effect of Leaching Temperature

Temperature is an important parameter that governs the rate at which reactions take place. This is because at higher temperature molecule collision frequency is greater and the proportion of molecules with sufficient energy to react is significantly higher. Although collision frequency is greater at higher temperatures, this alone contributes only a very small proportion to the increase in the rate of reaction (Housecroft, 2008; Earnshaw and Greenwood, 1997).

To investigate the effect of temperature on the dissolution of Co and W, experiments were carried out from 40°C to 85°C. As shown in **Figure 4.9**, temperature has a strong effect on the

dissolution of Co, whereas the effect on W dissolution is very little. With increasing temperature from 40 to 85°C, the dissolution of Co dramatically increased from 3.8% to 9.6% extraction within 6hrs of leaching time. This is because molecules at higher temperature have more thermal energy required for effective reaction. However, the dissolution of W increased marginally from 0.34% to 0.45% extraction. The highest Co extraction of 9.6% was observed at 85°C indicating that, at this temperature, there's a higher ionization of Co ions. On the other hand, the low dissolution of W^{6+} ions seems to indicate that high temperature has little effect on the ionization of W ions. The resistance to W ionization could be attributed to the strong covalent bonds formed by the 5d electrons in tungsten atoms (Lassner and Schubert, 1999).

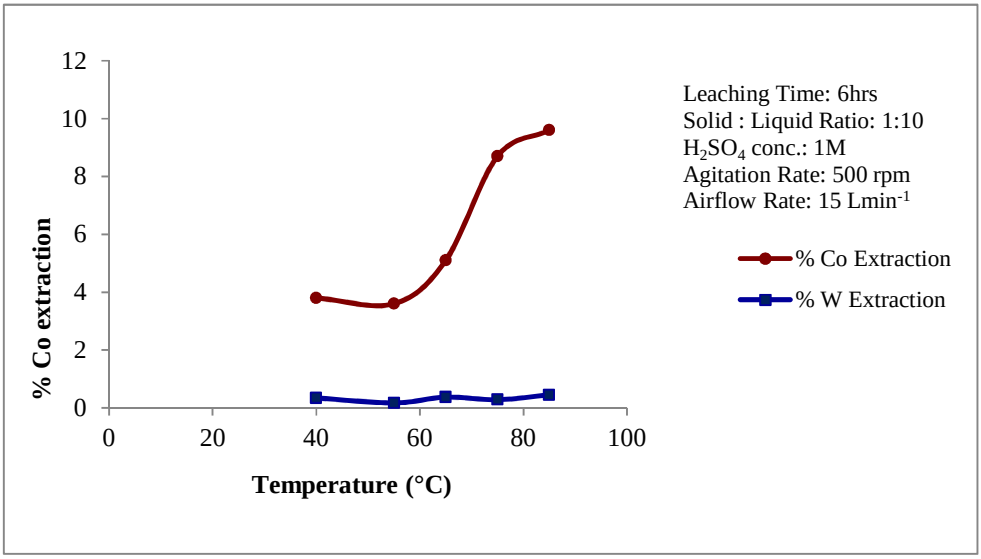

Fig.4.9: Co and W dissolution as a function of leaching temperature

4.5.2 Effect of Acid Concentration at Different Temperatures

The concentration of hydronium ions in acid is an important factor to be considered for effective metal dissolution.

To investigate the effect of acid concentration at different temperatures, experiments were carried out from 0.01M to 3M acid concentration at 75°C and 85°C respectively. The results in **Figure 4.10** show that the dissolution of Co at 75°C increased sharply from 0.01M to a maximum of 8.7% at 1M. This is because the hydronium ion reacts with metal causing it to

undergo oxidation thus inducing metal dissolution (Bronsted, 1931; Garcia et al, 2008). In addition, the initial hydronium ions provide the necessary driving force needed to overcome the resistances to mass transfer between the aqueous phase and the solid metal phase. When the concentration of reactants increases, more molecules or ions interact to form new compounds, and the rate of reaction increases (Levenspiel, 1972; Kumar et al., 2010). However, beyond 1M, Co dissolution slightly decreased with increasing concentration. The decrease in Co dissolution at higher acid concentration could be attributed to increased hydronium ion concentration leading to intensified formation of insoluble tungsten oxides and tungstic acid (Edtmaier et al, 2005; Chen, 2013; Osseo-Asare, K., 1982; Bosung and Sunjung, 2016). The insoluble tungsten oxides or tungstic acid cause poor diffusion. It seems increasing acid concentration produces two effects simultaneously. An increase in the hydronium ion enhances the dissolution of Co on one hand, but intensifies the formation of tungstic acid precipitates on the other. The precipitates hinder mass transfer within cemented carbide channels thus decreasing the rate of Co dissolution.

Further test work entailed exploring the effect of acid concentration at a higher temperature (**Figure 4.10**). Results showed a substantial increase in Co extraction of up to 17.9%. The increase in temperature may have been helpful in breaking down obstructive precipitates or passivation layers due to elevated localized temperatures thus, enhancing the rate of Co dissolution.

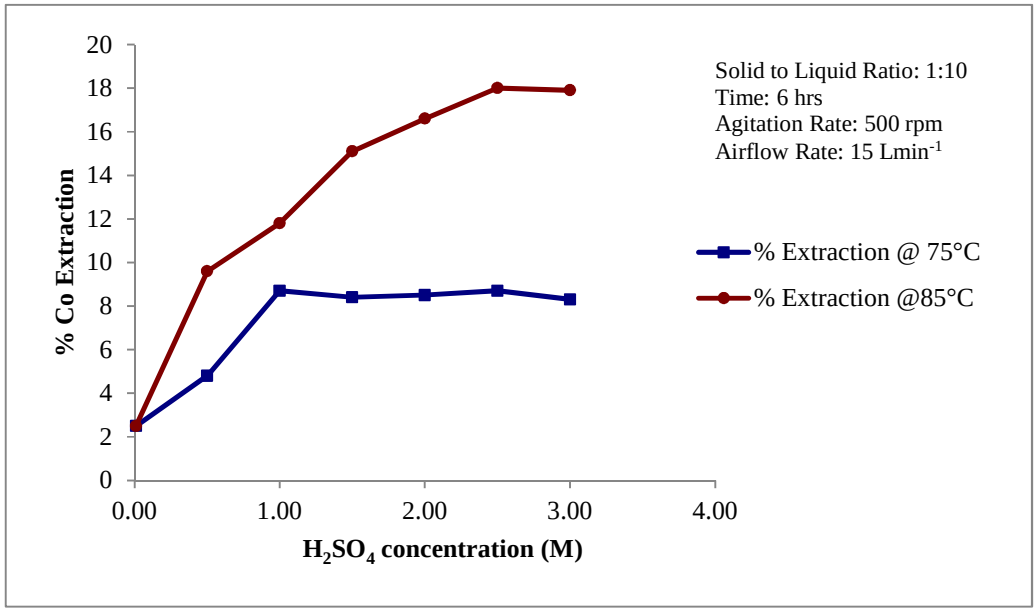

Fig.4.10: Co and W dissolution as a function of acid concentration at different temperatures

4.5.3 Effect of Solid-to-Liquid Ratio

Solid-to-liquid ratio is an important factor that has an effect on optimum contact between solids and fluids. It is an important physical property for characterizing a chemical reaction system.

The effect of solid-to-liquid ratio on Co and W dissolution is presented in **Figure 4.11**. Results for Co dissolution show a maximum solid-to-liquid ratio of 1:10 with much lower extractions on either side. The solid-to-liquid ratio is a representation of the ratio of weight of solids to volume of acid. A decrease in solid-to-liquid ratio therefore implies an increase in acid volume while the amount of solids remains constant. Increased acid volume creates a less dense mixture and makes more surface area available for optimum contact between reactants. An increase in surface areas available for contact, in particular for heterogeneous systems, leads to optimum reaction rates. In this case, increased available surface area for contact and increased hydronium ions due to increased solution volume intensified the formation of tungstic acid precipitates thus, causing poor diffusion. The decreased Co extraction due to increased solid-to-liquid ratio was likely caused by the increased density of the reactant mixture. The dense mixture may have deprived the cemented carbide buttons sufficient hydronium ions for more Co dissolution.

The results for W dissolution presented in **Figure 4.11** show a different trend to that of Co. The figure shows that W dissolution decreased with increase in solid-to-liquid ratio from 1.1% at 1:18 to 0.2% at 1:6. Lower solid-to-liquid ratios seemed to promote W dissolution. The upward trend in W dissolution with decrease in solid-to-liquid ratio was an indication that the metal's dissolution is not affected by the formation of tungsten precipitates in the same way that Co is.

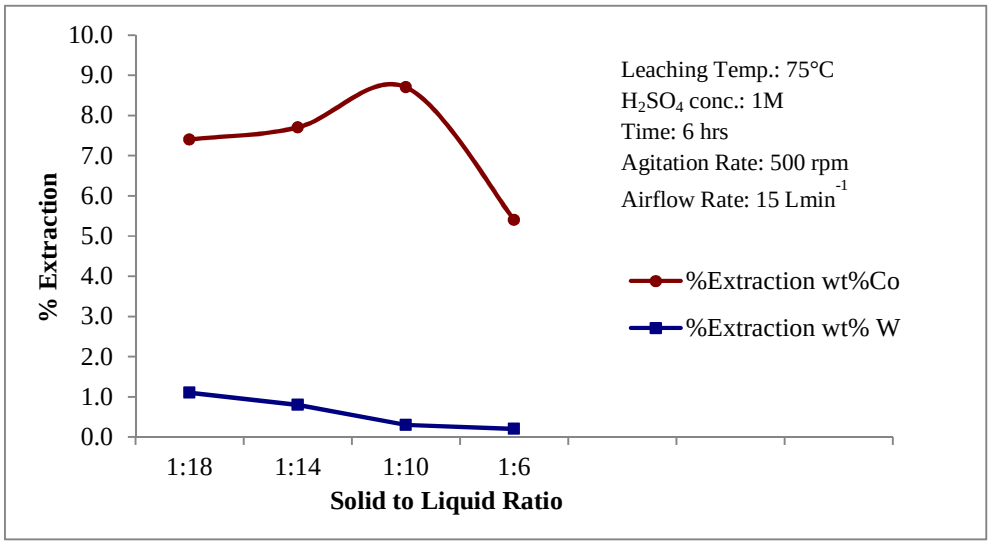

Fig.4.11: Co and W dissolution as a function of solid to liquid ratio

4.5.4 Effect of Agitation Rate

Agitation is an important parameter that promotes mass transfer. Whereas diffusion is a movement of molecules within the bulk fluid, agitation moves the whole mass of the bulk fluid. It is a mechanical mass transfer of the bulk fluid that, in heterogeneous systems, enables recurring solid-fluid surface contact (Levenspiel, 1972).

Experiments were performed to study the effect of agitation rate. The results in **Figure 4.12** show that with increasing agitation rate, the dissolution of Co improved from 7.4% to a maximum of 9.3% at 750rpm. Upon further increase in the agitation rate, Co extraction decreased slightly. High agitation rates enhance mass transfer in viscous solutions. In this study, the solution was not viscous. Therefore, an increase in agitation seemed to have a limiting effect on Co dissolution beyond 750 rpm. The agitation variable did not seem to have a significant effect on tungsten dissolution.

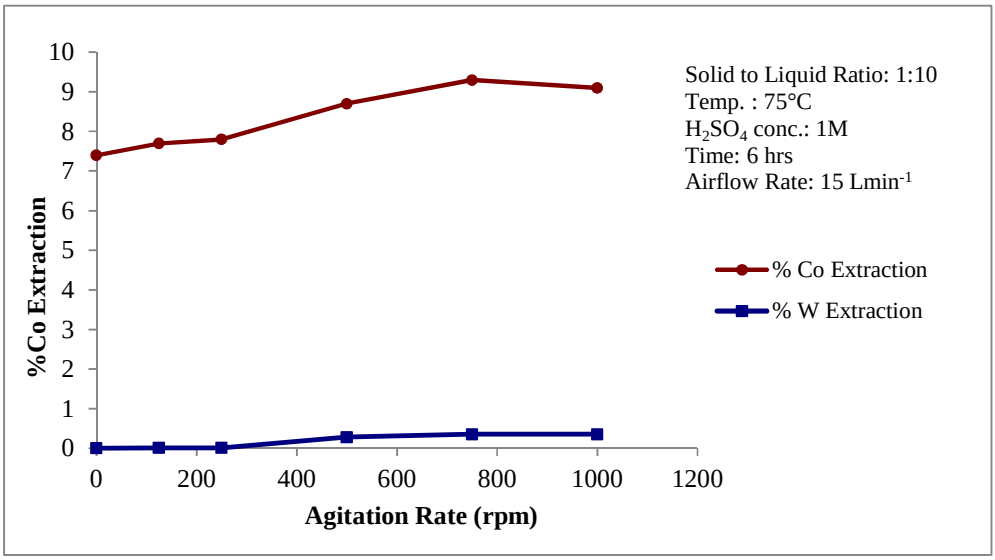

Fig.4.12: Co and W dissolution as a function of agitation rate

4.5.5 Effect of Leaching Time

Leaching time is an important factor that has an effect on the duration of a dissolution reaction. It provides information of the minimum time required for considerable dissolution to take place. It also provides information on the possible diffusion control mechanism for the metal ion as it moves from the reaction surface to the bulk solution (Levenspiel, 1972).

To study the effect of leaching time on Co and W dissolution, experiments were conducted at leaching times ranging from 0.25 days to 10.5 days. Co and W dissolution as a function of leaching time is presented in **Figure 4.13.** A Co extraction of 29.4% was obtained after 1 day and 99.6% after 10.5 days. The data shows a relatively high Co extraction rate in the first 100 h and a much lower rate thereafter. The reduced rate could possibly be attributed to the formation of some insoluble tungsten oxides. The profile is distended by virtue of the fact that the reaction follows a shrinking core model (SCM) of attack. As leaching progresses to the inner core of the solid cemented carbide piece, there is less and less available unreacted surface area for contact and reaction. The SCM profiles and the specific times at which they were taken are indicated in **Figure 4.13**. The data further shows a W co-extraction of up to 10% in 10.5 days. Tungsten showed low dissolution and stable passivity, whereas Co readily dissolved. This could be attributed to the fact that tungsten, in its most common oxidation state of +6, has a higher reduction potential of -0.09V (Charlot, 1971; Haynes et al, 2017) compared to -0.28V for cobalt

(Charlot, 1971; Haynes et al, 2017). In addition, tungsten readily forms a protective and refractory passivation layer (Chen, 2013; Kellner et al, 2009) which slows down prolonged dissolution.

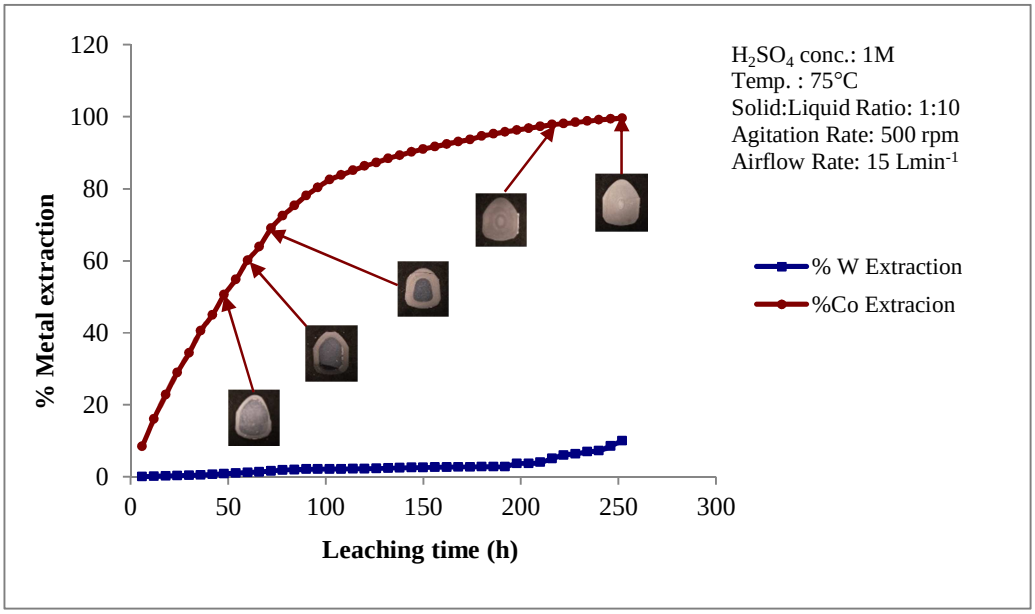

Fig.4.13: Co and W dissolution as a function of leaching time

The cemented carbide leaching progression is illustrated in the line-scan shown in **Figure 4.14**. The two differently shaded areas of the line scan show evidence of progressive leaching from left to right. The figure also shows three elements of interest, Co, W, C, and the effect on them as leaching progresses. The results showed that after 24 hrs of leaching, Co was depleted in the light grey area but unaffected in the non-leached dark grey area, whereas tungsten remained relatively the same throughout.

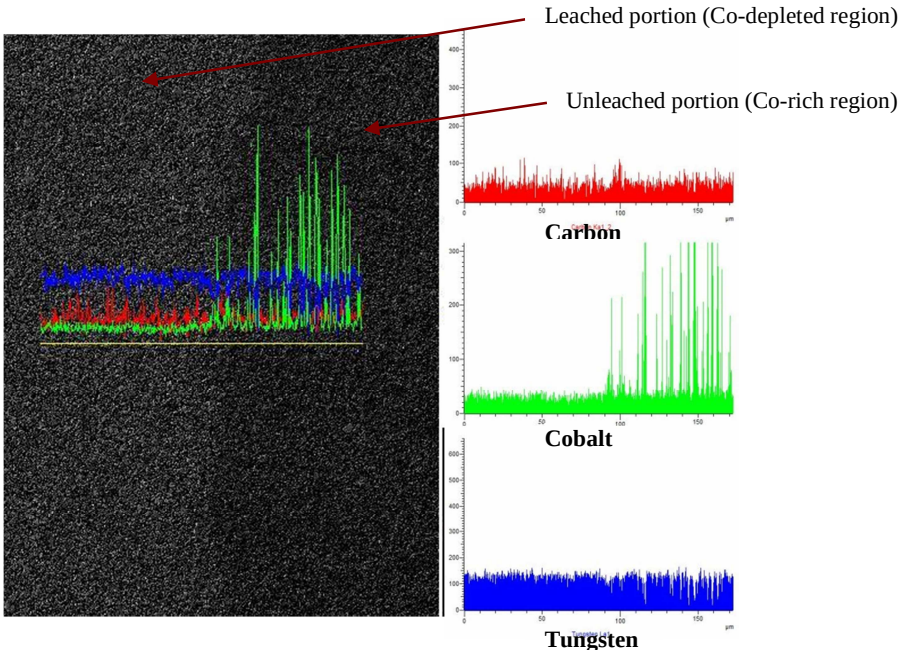

Fig.4.14: Line-scan of leached cemented tungsten carbide (after 24 hrs of leaching in 1M H_2SO_4) using Field Emission Scanning Electron Microscope (FESEM)

The cemented carbide leaching progression is exhibited in the micrograph images shown in **Figure 4.15.** The dark area is Co rich and the light areas are Co depleted. The results in the images show further evidence of progressive leaching form the outer core to the inner core of the cemented carbide button as per the shrinking core model.

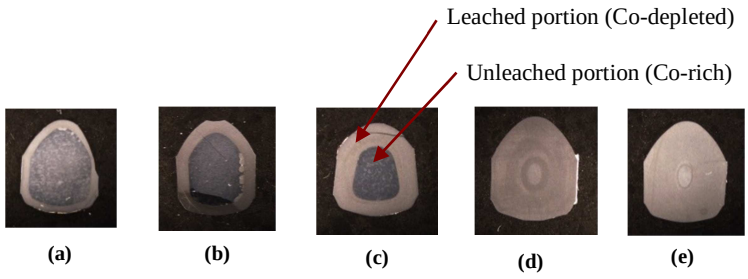

Fig.4.15: Cemented tungsten carbide leached with 1M H_2SO_4 after:

(a) 2 days, (b) 2.5 days, (c) 3 days, (d) 9 days and (e) 10.5 days

The XRD pattern of the WC residue is shown in **Figure 4.16**. The XRD analysis was used to confirm that Co was successfully leached out of cemented carbide after sulphuric acid leaching. The peaks are characteristic of the WC also known as Qusongite. The figure further shows Fe presence in the residue. This could have come as a result of residue contact with reactor vessel accessories. The XRD analysis also shows that the chemical composition of the residue is 99.0% Qusongite. This therefore, confirms that Co was successfully extracted from cemented carbide through acid leaching.

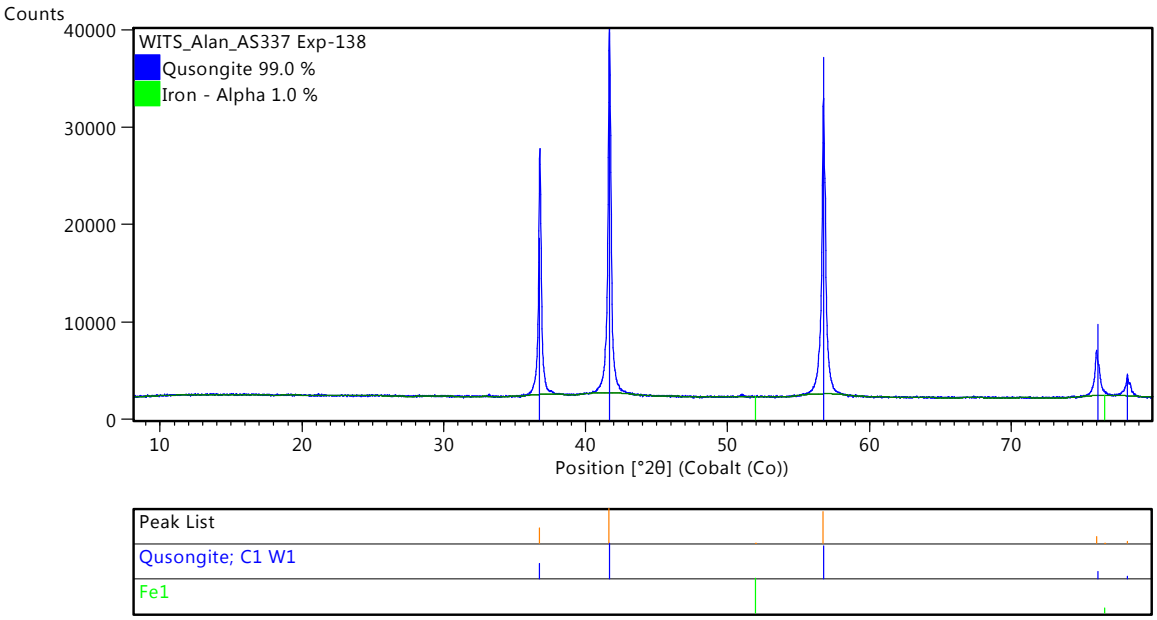

Fig.4.16: An XRD pattern of WC powder residue leached at 1M H_2SO_4 and 75°C, 1:10 solid to liquid ratio and agitation rate of 500 rpm.

The chemical composition of the leach liquor extracted within the 10.5 days leaching time is shown in **Table 4.3**. The chemical composition showed Fe as the major impurity suggesting that leach liquor purification was necessary before electrorecovery of Co. The impurities are possibly from the acidic contact with some metallic components of the reaction vessel. The presence of W suggested that its recovery was an important factor to consider.

Table 4.3: Chemical composition of cemented carbide (WC-6%wt.Co) leach liquor

Element	Al	Ca	Co	Cu	Fe	K	Mg	Ni	W	pH
Conc (ppm)	0.4	0.1	130.8	0.4	58.4	0.4	1.0	7.8	1.3	1.0

4.6 Eh-pH Profiles for the Cemented Tungsten Carbide Leaching Process

The thermodynamic feasibility of hardmetals in aqueous media requires oxidative acidic conditions. To investigate and evaluate these conditions, experiments were performed at a sulphuric acid concentration of 1M, a temperature of 75°C, a solid to liquid ratio of 1:10 for 6 h while stirring at 500rpm. Atmospheric air, pumped into the leach solution mixture at 15Lmin^{-1} using a vacuum pump, was used as the oxidant. Eh and pH values were measured during the leaching process and are presented in **Figure 4.17**. The results in the figure showed that, despite a slight decrease over time, the Eh and pH values were well within the required oxidative acidic dissolution range of -0.5<Eh <1.8 and pH <4 (Garcia et al, 2008) respectively. The slight decrease in pH with increasing leaching time was likely due to the increase in hydronium (H_3O^+) ions resulting from the two-stage dissociation behaviour of sulphuric acid (Pavlov, 2017). When mixed with water, sulphuric acid dissociates in two degrees. The first degree of dissociation of H_2SO_4 can be expressed by the equation (Pavlov, 2017):

$$H_2SO_4 + H_2O = H_3O^+ + HSO_4^- \quad (4.9)$$

The first dissociation constant is equal to: $k_1 = 1x10^3$ as determined by Young (1951). This value indicates that the first dissociated sulphuric acid is a strong acid and the equilibrium maintains, but a very small amount of non-dissociated H_2SO_4 (Pavlov, 2017).

In the second degree of dissociation, the hydrogen sulphate anion ($H_SO_4^-$) dissociates further into sulphate ions and even more hydronium ions. The second degree of dissociation can be expressed by the equation:

$$HSO_4^- + H_2O = H_3O^+ + SO_4^{2-} \quad (4.10)$$

The second dissociation constant is equal to: $k_2 = 1.02\ x10^{2-}$ (Pavljuk et al, 1972; Covington et al, 1965). Although in the second degree of dissociation, the acid behaves like a weak acid, sulphuric acid is a strong acid and so it ionizes completely with little or no chance of reversibility

(Pavlov, 2017). In the second dissociation where SO_4^{2-} ions are released to form cobalt sulphate, more hydronium ions are equally released resulting in a decrease in pH. A comparison between the two dissociation constants shows that the first dissociation releases more hydronium ions than the second.

Based on the cobalt Pourbaix diagram (Garcia et al, 2008; Pourbaix, 1966), and as discussed in Chapter 2 section 2.10, cobalt reduction is represented by the reaction:

$$Co^{2+} + 2e^- = Co_{(s)} \qquad E^o = -0.28V \qquad (4.1)$$

And the reaction for oxygen reduction is presented as:

$$2H^+ + 0.5O_{2(g)} + 2e^- = H_2O \qquad E^o = 1.23V \qquad (4.12)$$

The overall chemical reaction for the thermodynamic stability of cobalt in aqueous solution is, therefore, presented as:

$$Co + 0.5O_2 + 2H^+ = Co^{2+} + H_2O \qquad E^\circ = 1.51V \qquad (4.13)$$

The above equation shows that cobalt dissolution is thermodynamically possible under oxidizing conditions (Pourbaix, 1966).

The results in **Figure 4.17** show a slight decrease in Eh with increasing leaching time suggesting a decrease in the oxidative strength of the leaching system. The decrease in Eh may have resulted from a decrease in oxygen solubility in the solution mixture as leaching progressed.

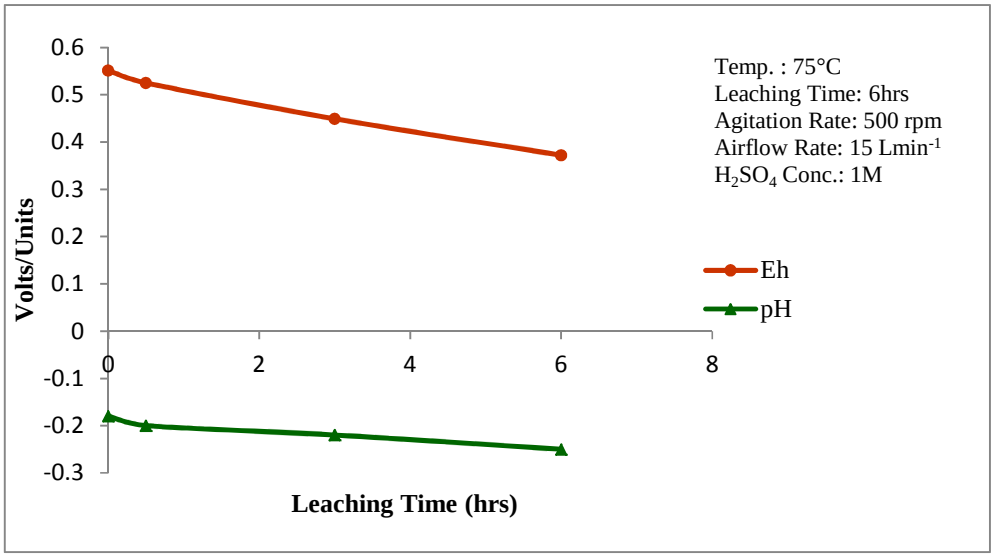

Fig.4.17: Eh and pH as a function of time

To maintain an oxidative environment, atmospheric air was pumped into the leach solution mixture at 15Lmin^{-1} using a vacuum pump. The dissolved oxygen in the leach solution before and after air supply is illustrated in **Table 4.4**. The table shows an increase in dissolved oxygen from 10.1% (0.92mg/L) to 62.4% (5.41mg/L) after air supply. It was inferred from the results in the table that the air supply at 15Lmin^{-1} was sufficient to provide an oxidative environment as confirmed by the results in **Figure 4.17**.

Table 4.4: Dissolved oxygen in 1M H_2SO_4 solution before and after bubbling atmospheric air

	BEFORE		**AFTER**	
Temp (°C)	26.6		26.6	
Oxygen conc.	**%**	**mg/L**	**%**	**mg/L**
Run 1	10.5	0.96	63.6	5.46
Run 2	9.7	0.88	61.2	5.36
Average	10.1	0.92	62.4	5.41

4.7 Investigating the Behaviour of WC Grains in Acidic Media

A study to investigate the possible formation of tungstic acid (H_2WO_4) within cemented tungsten carbide channels during acidic leaching consisted of reacting tungsten carbide powder with sulphuric acid. The tungsten carbide (WC) powder used in the experiment had similar chemical properties as the tungsten monocarbide (WC) grains in the cemented carbide button sample described in Chapter 3 section 3.2.1. The possible formation of tungstic acid was based on the thermodynamic feasibility of hardmetals in aqueous acidic media as proposed by Osseo-Asare (1982). The following are the possible reactions leading to the formation of tungstic acid:

$$3WC + 4O_2 + 12H^+ \leftrightarrows WO_2 + 6H_2O + 3C + 2W^{6+} \quad (4.14)$$

$$3WO_2 + O_2 + 6H^+ \leftrightarrows W_2O_5 + 3H_2O + W^{6+} \quad (4.15)$$

$$2W_2O_5 + O_2 + 12H^+ \leftrightarrows 2WO_3 + 6H_2O + 2W^{6+} \quad (4.16)$$

$$WO_3 + H_2O \leftrightarrows H_2WO_4 \text{ (tungstic acid)} \quad (4.17)$$

4.7.1 The Effect of Acidic Media on WC grains

To study the effect of acidic solutions on WC grains, two sets of experiments were performed at a solid to liquid ratio of 1:10, an agitation rate of 500rpm and a leaching time of 6h. The first set involved using 1M and 2.5M sulphuric acid concentrations and leaching WC grains at 75 and 85°C. The second experiment consisted of adding 5% (v/v) lactic acid to 2.5M sulphuric acid and leaching at 85°C.

The Raman spectra for the leached WC powder residue are presented in **Figure 4.18**. The spectra show certain characteristics about the WC powder samples leached at different conditions. Leaching with 1M and 2.5M sulphuric acid concentration at 75°C and 85°C led to a more crystalline phase characterized by broad and sharp peaks (AS514B-g, AS516b and AS517b) that could be ascribed to the presence of tungstic acid (H_2WO_4).

Confirmation of the presence of tungstic acid in the leached WC residue sample was indicated by peaks at 950cm^{-1}Raman Shift which conformed to standard Raman spectra for tungstic acid (Suzuki et al, 2017). These findings support previously reported data (Edtmaier et al, 2005; Chen, 2013; Osseo-Asare, K., 1982; Bosung and Sunjung, 2016). It is interesting to note that with the addition of 5% (v/v) lactic acid to 2.5M sulphuric acid leach solution, a diminished tungstic acid peak (AS518-d) is observed. The diminished peak was associated with the addition of lactic acid to the leach solution. The lactic acid may have reacted with W^{6+} ions to form a soluble and stable tungsten lactate salt complex thus, suppressing the tungstic acid forming reactions. Tungstic acid is a precipitate and as such, it tends to cause channel blockage when formed inside cemented carbide solid pieces during leaching. For this reason, the formation of tungstic acid during leaching of cemented carbide is undesirable.

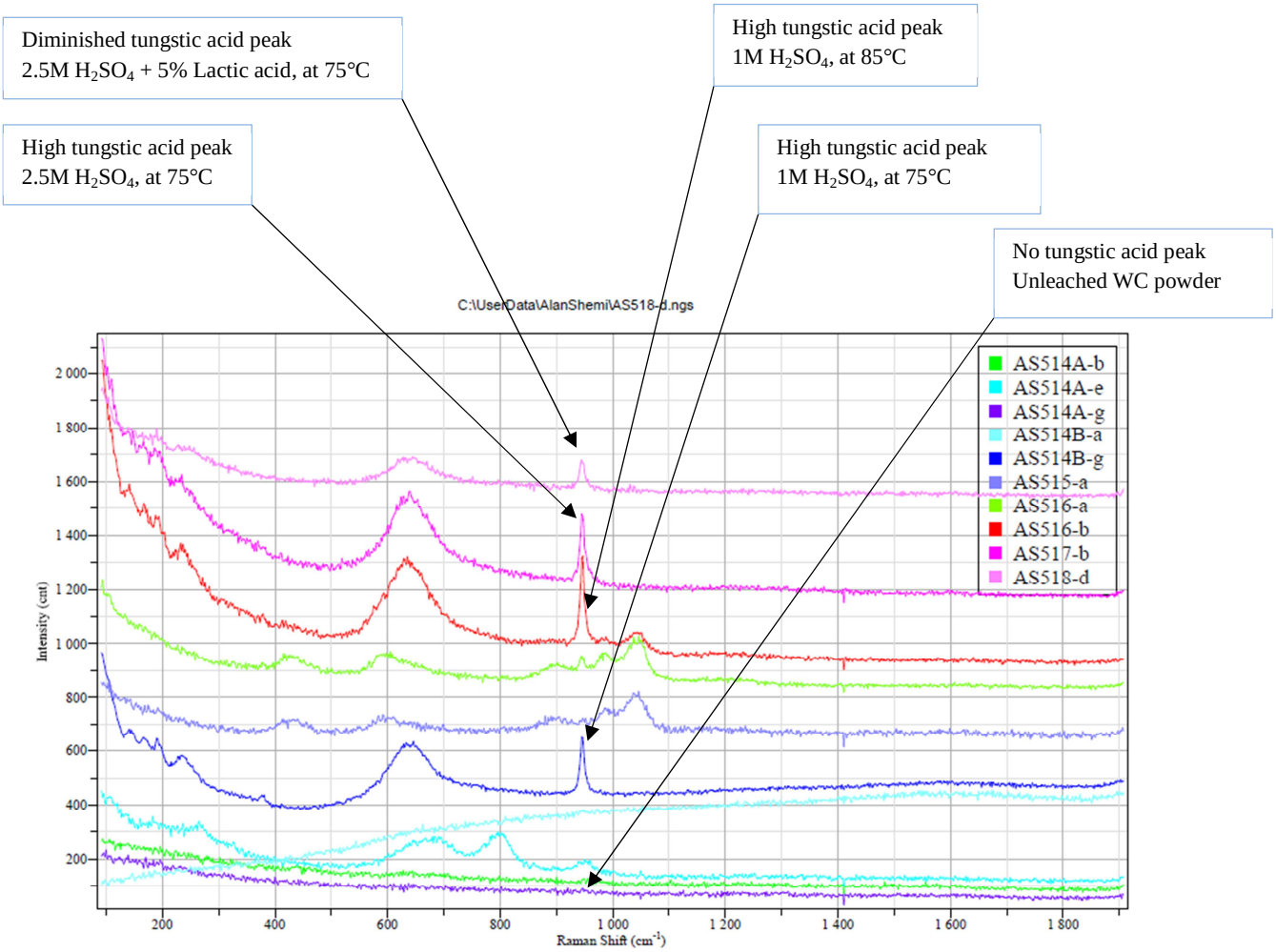

Fig.4.18: Raman spectra for leached WC powder residue

4.8 Summary

In order to identify suitable aqueous media for Co extraction from hardmetal scrap, preliminary leach tests were initially performed using alkaline, organic and inorganic lixiviants. Follow up preliminary tests were also conducted in order to explore the possible influence of factors on the response (Co extraction) and to identify their appropriate upper and lower levels. The study also looked at the possible occurrence of eta phase in the cemented tungsten carbide scrap material, the Eh and pH profiles as well as the effect of acidic media on WC grains.

- Optical photomicrograph results showed no evidence of eta (η) phase occurrence in the cemented tungsten carbide material used in the current study.

- Co extraction from cemented carbide is favoured more in acidic than in alkaline media whereas tungsten extraction is better in alkaline than acidic media.
- A comparison between acid and alkaline media showed that the acidic media is a better leaching route for the selective dissolution of Co from the cobalt binder phase matrix.
- A comparison between inorganic and organic acid showed that inorganic acid media had a stronger effect on Co dissolution from cemented carbide than organic acids due to better inorganic acid deprotonation and dissociation properties. Leaching with sulphuric acid gave a maximum Co extraction of 8.7% in 6hrs compared to 2.8%, 2.3% and 2.1% Co extraction from lactic, maleic and tartaric acid respectively. Sulphuric acid was therefore adopted as the pertinent leaching lixiviant
- Results showed that Co extraction from cemented carbide buttons using sulphuric acid is possible up to 99.6% in 10.5 days using 1M H_2SO_4, at 75°C, 1:10 solid liquid ratio and 500 rpm agitation rate.
- A comparison among the three organic acids showed that lactic acid had the strongest effect on Co and W dissolution thus showing stronger Co and W metal complexation ability. The order of effectivity for Co dissolution by organic acids was lactic>maleic>tartaric acid and lactic>tartaric>maleic acid for W dissolution. Lactic acid was therefore adopted as the pertinent complexation agent.
- The factor range finding trials revealed that all the five process parameters tested had a noticeable influence on the Co dissolution process with clearly identifiable lower and upper levels.
- Results for Eh and pH profiles showed that appropriate oxidative acidic conditions for Co dissolution within the region of $-0.5<Eh<1.8$ and $pH<4.0$ are both attainable and sustainable.
- Raman spectroscopy results showed that WC grains, when exposed to acidic media, react to form tungstic acid (H_2WO_4) precipitates. However, a diminished tungstic acid peak seemed to indicate that addition of an organic ligand can suppress the precipitate forming reactions.

In the next Chapter, an attempt is made to derive a conceptual kinetic model that describes Co dissolution out of cemented tungsten carbide hardmetal.

4.9 References

Bhosale, S.N., Mookherjee, S., Pardeshi, R.M., 1990. Current Practices in Tungsten Extraction and Recovery. High Temperature Materials and Processes, Vol. 9, Issue 2-4.

Bosung, S., Sunjung, K., 2016. Cobalt Extraction from Tungsten Carbide-Cobalt (WC-Co) Hard Metal Scraps Using Malic Acid. International Journal of Mineral Processing, Vol. 151, pp. 1-7.

Bronsted, J.N., 1931. On The Dissolution of Metals in Acids. Journal of American Chemistry Society. Vol.53, Issue 10, pp. 3624-3644. https://doi.org/10.1021/ja01361a006.

Charlot, G., 1971. Selected Constants, Oxidation and Reduction Potentials of Inorganic Substances in Aqueous Solution. Butterworths, London.

Chen, Z.A., 2013. PEC Experiment Standard. Springer, Berlin/New York.

Earnshaw, A., Greenwood, N.N., 1997. Chemistry of the Elements (2nd Ed.). Butterworth-Heinemann, Oxford.

Edtmaier, C., Schiesser, R., Meissl, C., Schubert, W.D., Rock, A., Schoen, A., Zeiler, B., 2005. Selective Removal of the Cobalt Binder in WC-Co Based Hard Metal Scraps By Acetic Acid Leaching. Hydrometallurgy, Vol. 76, pp. 63-71.

Exner, H.E., 1979. Physical and Chemical Nature of Cemented Carbides. International Metals Reviews, Vol. 4, pp. 149-173.

Freemantle, C., Sacks, N., 2015. Recycling of Cemented Tungsten Carbide Mining Tool Scrap. The Journal of the South African Institute of Mining and Metallurgy, Vol. 115, pp. 1207-1213.

Garcia, E.M., Santos, J.S., Pereira, E.C., Freitas, M.B.J.G., 2008. Electrodeposition of Cobalt from Spent Li-ion Battery Cathodes by the Electrochemistry Quartz Crystal Microbalance Technique. Journal of Power Sources, Vol. 185, pp. 549-553.

General Carbide., 2016. Designer's Guide to Tungsten Carbide. http://www.generalcarbide.com. Retrieved, 25 June 2016.

Haynes, W.M., Lide, D.R., Bruno, T.J., 2017. Handbook of Chemistry and Physics. CRC Press, New York.

Housecroft, C.E., Sharpe, A.G., 2008. Inorganic Chemistry (3rd Edn.). Pearson, England.

Katiyar, P.K., Randhawa, N.S., Hait, J., Jana, R.K., Singh, K.K., Mankhand, T.R., 2014. An Overview on Different Processes for Recovery of Valuable Metals from Tungsten Carbide Scrap. ICNFMM, Nagpur.

Lassner, E., Schubert, W.D., 1999. Tungsten: Properties, Chemistry, Technology of the Element, Alloys and Chemical Compounds. Kluwer Academic/Plenum Publishers, New York

Levenspiel, O., 1972. Chemical Reaction Engineering. John Willey and Sons, New York.

Osseo-Asare, K., 1982. Solution Chemistry of Tungsten Systems. American Society for Metals and the Metallurgical Society of AIME. Metallurgical transactions B. Vol. 13B, pp. 555-564.

Pourbaix, M., 1966. Atlas of Electrochemical Equilibria in Aqueous Solutions. Franklin, J.A. Translation, Pergamon, Oxford.

Sandvik., 2005. Types of Cemented Carbide. http://www.hardmaterials.sandvik.com. Retrieved, 4 March 2020.

Sandvik., 2020. Understanding Cemented Carbide. http://www.hardmaterials.sandvik.com. Retrieved, 5 March 2020.

Suzuki, A., Tomita, O., Higashi, M., Abe, R., 2017. Tungstic Acids H_2WO_4 and H_4WO_5 as Stable Photocatalysts for Water Oxidation under Visible Light. Journal of Materials Chemistry A. Vol. 5, pp.10280–10288.

Tomlinson, W., Ayerst, N., 1989. Anodic Polarization and Corrosion of WC-Co Hard Metals Containing Small Amounts of Cr3C2 and/ VC. Journal of Materials Science, Vol. 24, pp. 2348-2354.

Vanderpool, C.D., 1983. Electrolytic Disintegration of Sintered Metal Carbides. US Patent No. 4,385,972.

Kellner, F.J.J., Hildebrand, H., Virtanen, S., 2009. Effect of WC grain size on the corrosion behaviour of WC-Co based hardmetals in alkaline solutions.

Pavlov, D., 2017. Lead – Acid Batteries: Science and Technology (2nd Ed.)

Young, T.F., 1951. Rec. Chem. Prog. Vol. 12, pp. 81.3

Pavljuk, L.A., Smoljakov, B.S., Krjukov, P.A., 1972. hr Izv. Sib. Otd. Akad., Nauk SSSR, Vol. 3, pp.3.

Covington, A.K., Dobson, J.V., Wynne-Jones, W.F.K.., 1965. Trans. Faraday Soc. Vol.61, pp. 2050-2057.

CHAPTER FIVE

KINETIC STUDY

5.1 Introduction

The purpose of a kinetic study, inter alia, is to determine the predominant controlling reaction mechanisms of a process. A kinetic study makes use of mathematical modeling of fluid-solid systems using models like the shrinking core model (SCM) to interpret experimental results and to gain insight into reaction mechanisms (Levenspiel, 1972). The SCM is widely used to model fluid-solid reactions such as the leaching of metals from minerals or metal-containing materials. In the SCM, it is assumed that the solid particle is spherical and it reacts with the fluid isothermally. Also, the concentration of the reacting fluid is assumed to be constant or in excess (Gbor and Jia, 2004). For heterogeneous systems, reaction kinetics is based on the shrinking core model (Levenspiel, 1972; Smith, 1981; Han, 2002). This is the most widespread and realistic model describing fluid-solid reaction kinetics of dense (non-porous) particles. Examples of fluid-solid reactions include, the oxidation of sulphide minerals to yield oxides by reducing gases, and the extraction of metals from ores using acids (Levenspiel, 1972). One of the convincing ways of finding out the mechanism controlling the shrinkage processes is the use of activation energies (Gbor and Jia, 2004). In order to gain a fuller understanding of a process, some authors (Gurmen and Friedrich, 2005; Potgieter, et al, 2006) have opted to use the SCM and activation energy model jointly.

The main aim of this kinetic study was to derive a conceptual reaction kinetic model that describes the dissolution of the cobalt out of the hardmetal buttons. The conceptual kinetic model for the co-dissolution of tungsten was also derived and evaluated. The experimental kinetic data for determining the reaction mechanisms was collected by running kinetic experiments. The factor levels used in this study were chosen based on the findings from the preliminary leaching tests discussed in Chapter four. The experimental procedure followed in this chapter is described in Chapter 3 section 3.7.2.

5.2 Shrinking Core Rate Controlling Mechanisms

The analysis of Co and W dissolution rates from WC-6wt%Co buttons was based on the shrinking core model under the assumption that the material consists of homogeneous solid particles that react isothermally with the fluid media (Gbor and Jia, 2004; Levenspiel, 1972).

To determine the rate controlling regime for metal dissolution, experimental results at different temperatures were plotted in terms of the standard equations of the shrinking core model. The reaction kinetic models are displayed in **Table 5.1**. The models are represented by linear kinetic equations, $x = kt$, for film diffusion control; $1- (1-x)^{1/3} = kt$, for chemical reaction control and $1-3(1-x)^{2/3} + 2(1-x) = kt$, for product layer (ash) diffusion control, where x is the conversion, t is the time (s) and k is the reaction rate constant (s^{-1}). All the kinetic experiments were conducted with 2M acid concentration and 1:10 solid-to-liquid ratio. The dissolution rates of both Co and W were investigated with a view to understanding the dissolution characteristics of the hardmetal buttons.

Table 5.1: Shrinking Core Models (Levenspiel, 1972)

Regime	Liner Kinetic Equation
Film diffusion control	$x = kt$
Chemical reaction control	$1- (1-x)^{1/3} = kt$
Product (ash) diffusion control	$1-3(1-x)^{2/3} + 2(1-x) = kt$

5.2.1 Cobalt Dissolution

The kinetic equations for Co dissolution, as a function of time, at 50°C were plotted and are presented in **Figures 5.1** to **5.3**.

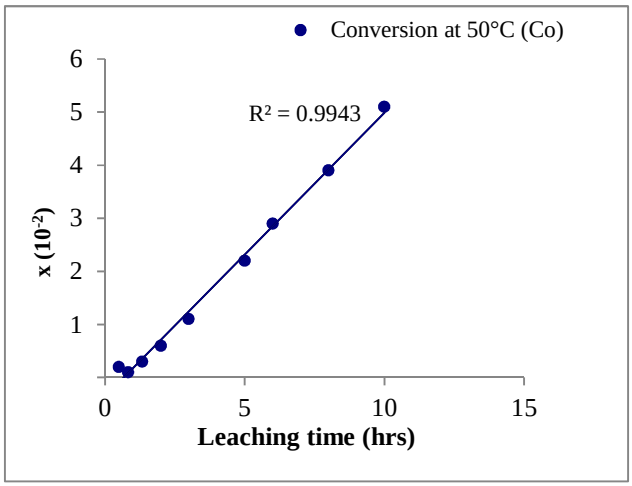

Fig.5.1: Plot of x versus time for Co dissolution at 50°C

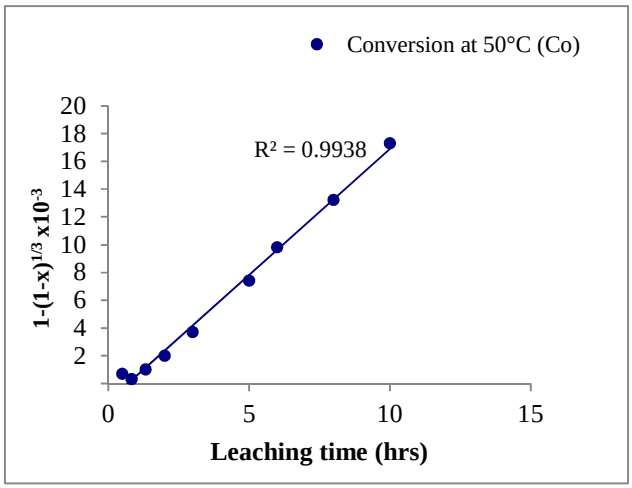

Fig.5.2: Plot of 1- $(1-x)^{1/3}$ versus time for Co dissolution at 50°C

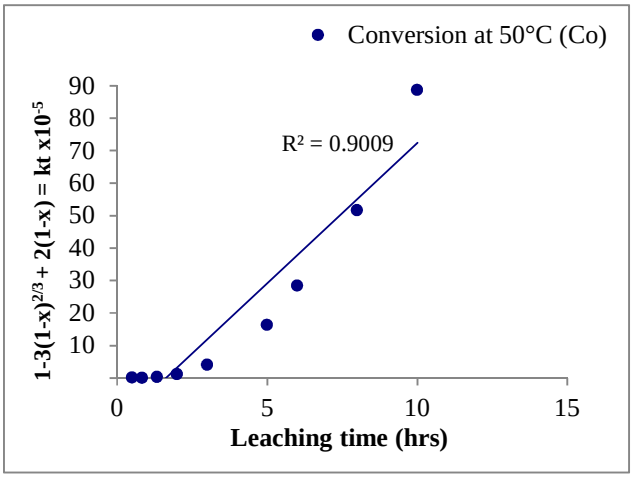

Fig.5.3: Plot of 1- $3(1-x)^{2/3}$ + 2(1-x) versus time for Co dissolution at 50°C

The kinetic equations for Co dissolution as a function of time at 70°C were plotted and are exhibited in **Figures 5.4** to **5.6**

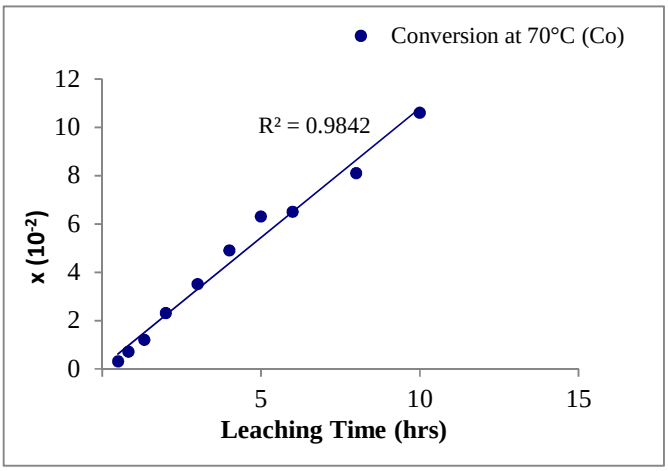

Fig.5.4: Plot of x versus time for Co dissolution at 70°C

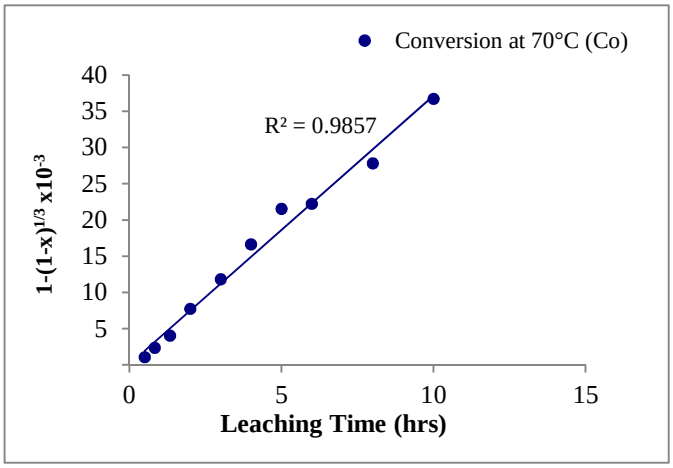

Fig.5.5: Plot of 1- $(1-x)^{1/3}$ versus time for Co dissolution at 70°C

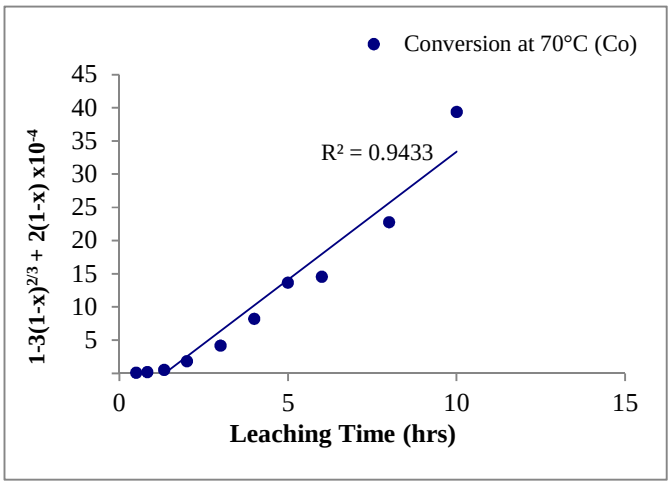

Fig.5.6: Plot of 1- $3(1-x)^{2/3}$ + 2(1-x) versus time for Co dissolution at 70°C

The kinetic equations for Co dissolution as a function of time at 85°C were plotted and are illustrated in **Figures 5.7** to **5.9**.

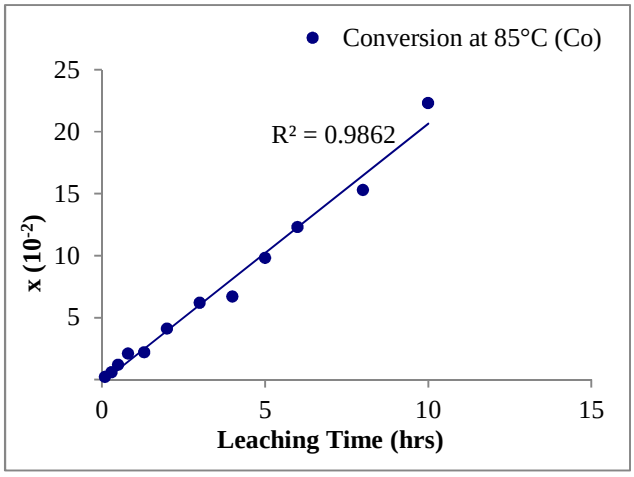

Fig.5.7: Plot of x versus time for Co dissolution at 85°C

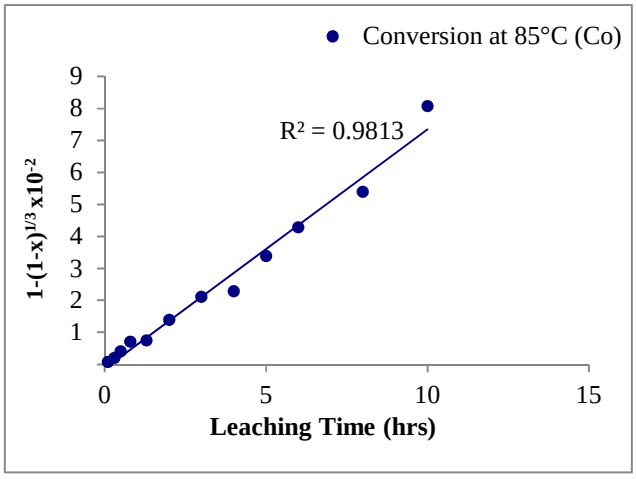

Fig.5.8: Plot of 1- $(1-x)^{1/3}$ versus time for Co dissolution at 85°C

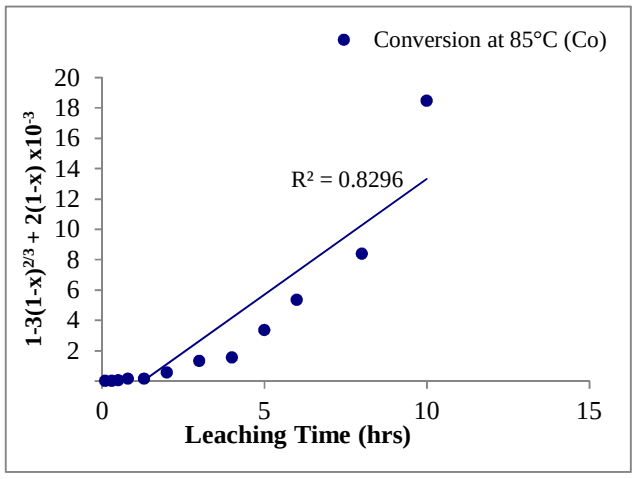

Fig.5.9: Plot of 1- $3(1-x)^{2/3}$ + 2(1-x) versus time for Co dissolution at 85°C

From the analysis of the forgoing kinetic plots, it was found that the Co dissolution rate at 50°C, 70° and 85°C was well expressed by the rate equations based on thin film diffusion and a surface reaction controlled process represented by the kinetic equations $x = kt$ and $1- (1-x)^{1/3} = kt$ respectively. The strong correlation coefficients of 90.09%, 94.33% and 82.96% in **Figures 5.3, 5.6** and **5.9**, respectively, indicate that a process controlled by diffusion through surface layers, though not dominant, is strongly associated (Taylor, 1990; Weber and Lamb, 1970; Mason et al, 1983) with the Co dissolution process.

In their kinetic study, Gurmen and Friedrich (2005) found that Co dissolution from cemented tungsten carbide was a product layer diffusion controlled process. This is in contrast to results obtained from the current study. The difference in the two results may have arisen from the fact that Gurmen and Friedrich (2005) used pulverized material whereas the material used in the current study is a solid mass of button inserts. The small particle size, higher surface area available for reaction and mineral liberation may have favoured a product layer controlled process.

5.2.2 Tungsten Dissolution

To determine the reaction controlling mechanism for tungsten dissolution from the WC-6wt%Co, experimental results at different temperatures were plotted in terms of the standard equations of the shrinking core model. The kinetic equations for W dissolution as a function of time at 50°C were plotted and are presented in **Figures 5.10** to **5.12**.

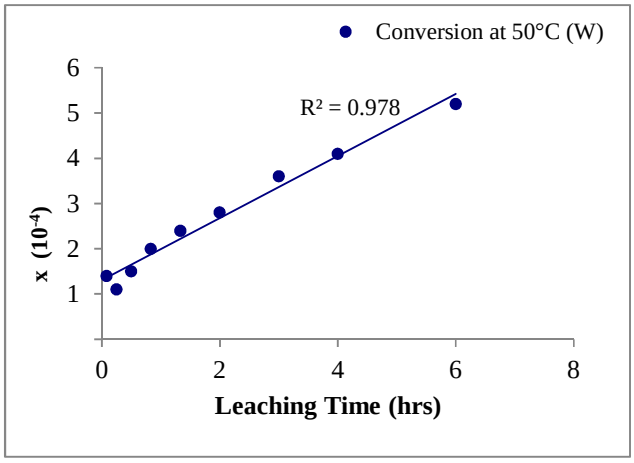

Fig.5.10: Plot of x versus time for W dissolution at 50°C

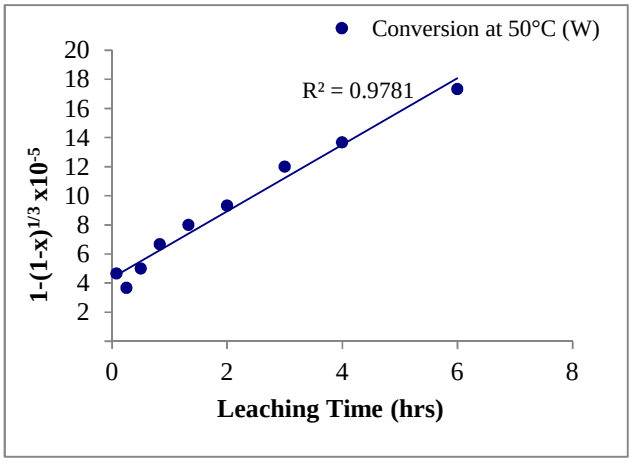

Fig.5.11: Plot of 1- $(1-x)^{1/3}$ versus time for W dissolution at 50°C

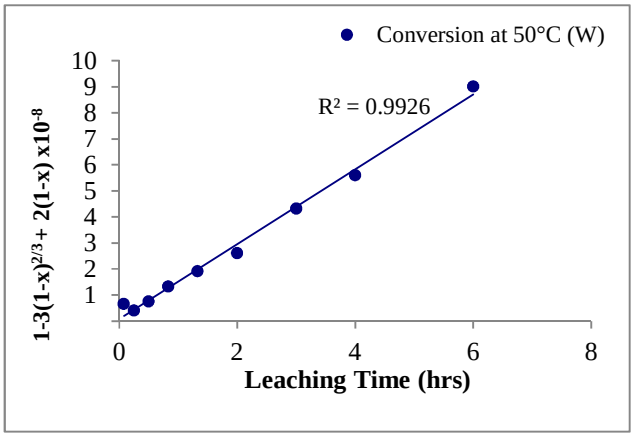

Fig.5.12: Plot of 1- $3(1-x)^{2/3}$ + 2(1-x) versus time for W dissolution at 50°C

The kinetic equations for tungsten dissolution as functions of time at 70°C were plotted and are exhibited in **Figures 5.13** to **5.15**.

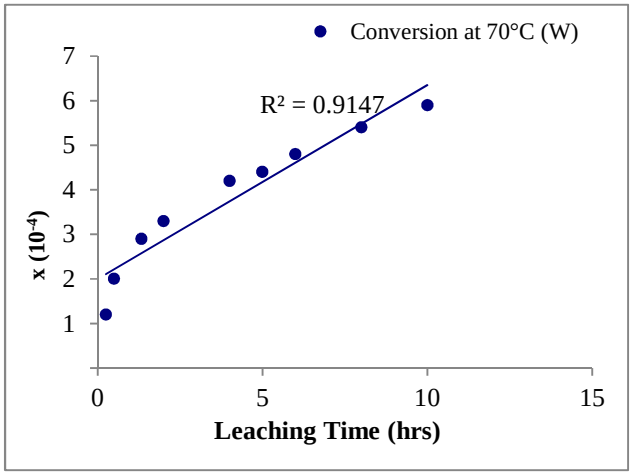

Fig.5.13: Plot of x versus time for W dissolution at 70°C

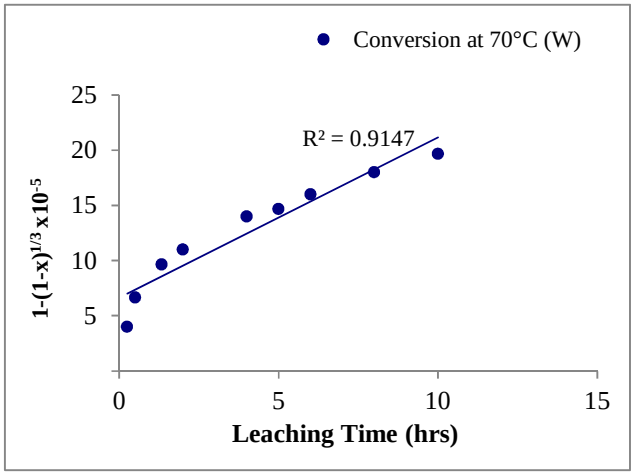

Fig.5.14: Plot of 1- $(1-x)^{1/3}$ versus time for W dissolution at 70°C

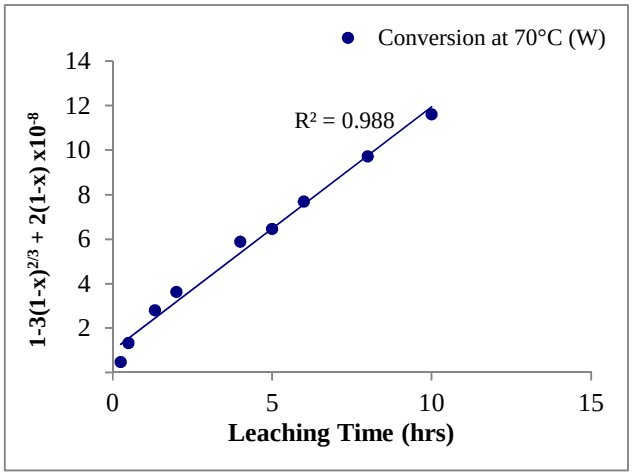

Fig.5.15: Plot of 1- $3(1-x)^{2/3}$ + 2(1-x) versus time for W dissolution at 70°C

The kinetic equations for tungsten dissolution as a function of time at 85°C were plotted and are shown in **Figures 5.16** to **5.18**.

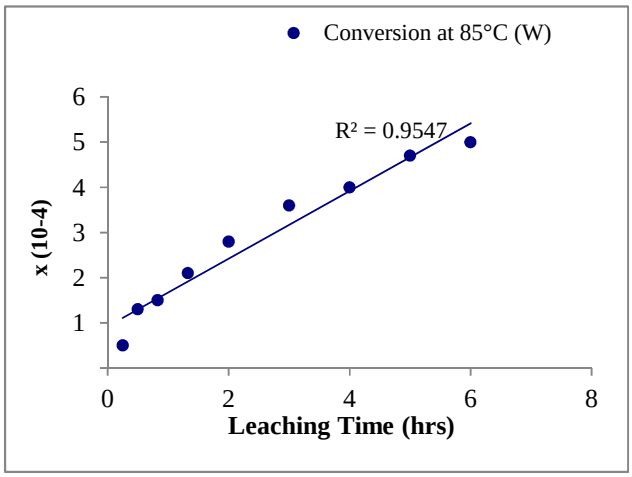

Fig.5.16: Plot of x versus time for W dissolution at 85°C

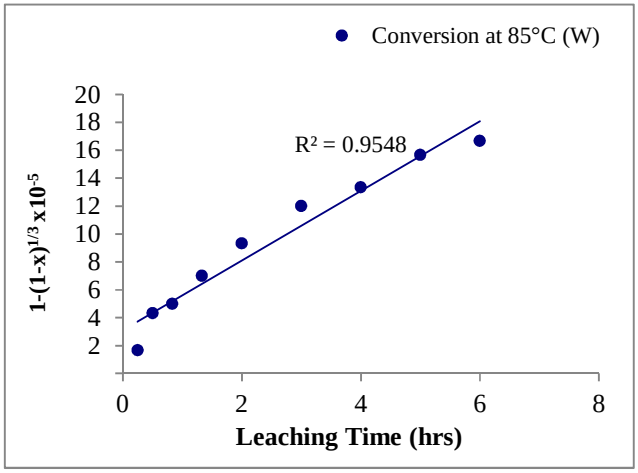

Fig.5.17: Plot of 1- $(1-x)^{1/3}$ versus time for W dissolution at 85°C

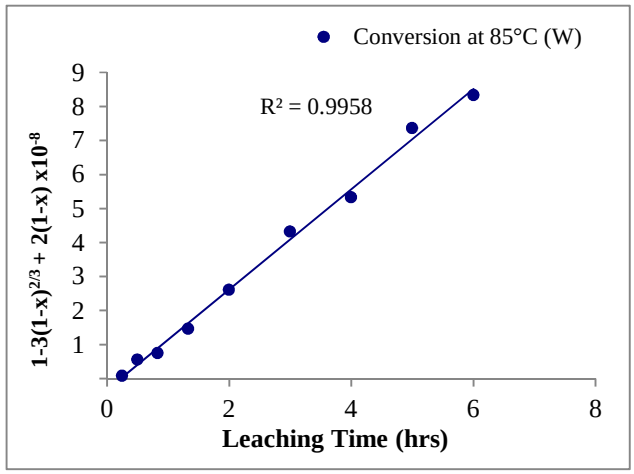

Fig.5.18: Plot of 1- $3(1-x)^{2/3}$ + 2(1-x) versus time for W dissolution at 85°C

From the analysis of the forgoing kinetic plots, it was found that the W dissolution rate at 50°C was well expressed by the rate equation based on thin film diffusion, a surface reaction controlled process and a process controlled by diffusion through surface layers represented by the kinetic equations $x = kt$, $1- (1-x)^{1/3} = kt$ and $1-3(1-x)^{2/3} + 2(1-x) = kt$ respectively. At higher temperatures (70–80°C), W dissolution was well expressed by the rate equation based on a process controlled by diffusion through surface layers represented by the kinetic equation $1-3(1-x)^{2/3} + 2(1-x) = kt$. Film diffusion and chemical reaction mechanisms were, by virtue of their strong correlation coefficients (Taylor, 1990; Weber and Lamb, 1970; Mason et al, 1983), found to be highly associated with the W dissolution process at all the three temperature levels.

Gbor and Jia (2004) have suggested that the magnitude of activation energy can provide a more positive evidence for the reaction and diffusion controlled regimes. In the section that follows, an attempt was made to use activation energy as an alternative technique for examining rate controlling reaction mechanisms.

5.3 Determination of Activation Energies

Activation energy models are often employed in conjunction with SCM in order to gain a fuller understanding of the process being investigated.

A quantitative relationship between the rate constant (k) and temperature (T) is given by the Arrhenius equation (**Eq. 5.1**) below:

$$k = Ae^{-\frac{Ea}{RT}} \qquad (5.1)$$

Where A is the frequency factor, E_a is the activation energy, R is the gas constant = 8.314 ($J \cdot mol^{-1} \cdot K^{-1}$) and T is the absolute temperature in Kelvin (K).

For a process run at two known temperatures and/or rate constants, **Equation 5.2** (Laidler, 1984; Logan, 1982; Chang, 2005; Segal, 1975) may be used to determine activation energy (E_a).

$$\ln k_2 - \ln k_1 = \frac{Ea}{R}\left(\frac{1}{T_1} - \frac{1}{T_2}\right) \qquad (5.2)$$

5.3.1 Cobalt dissolution

Kinetic experiments were performed according to the procedure described in chapter 3 section 3.7.2. Cobalt dissolution in the leaching process was considered to proceed according to the following reaction:

$$2Co + O_2 + 2H_2SO_4 \leftrightarrows 2CoSO_4 + 2H_2O \qquad (5.3)$$

The changing rate in cobalt dissolution was observed at three different temperatures, 50°C, 70°C and 85°C, by monitoring the concentration of cobalt sulphate [$CoSO_4$] with change in time. **Figure 5.19** shows the variation of cobalt sulphate concentration as a function of leaching time.

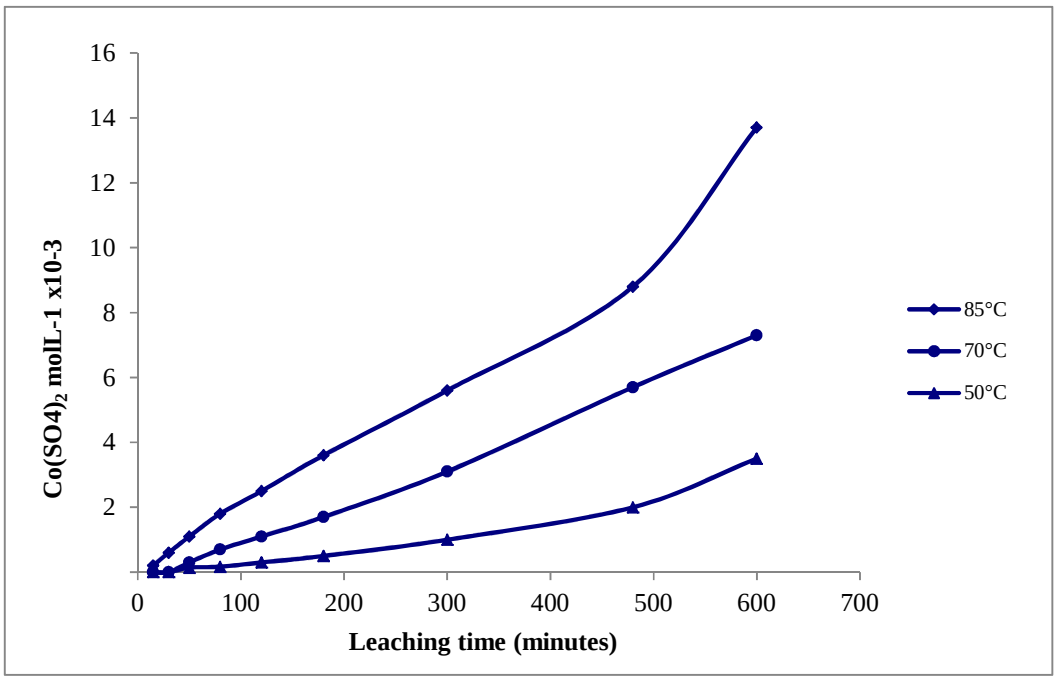

Fig.5.19: Variation of cobalt sulphate [$CoSO_4$] concentration with time at different temperatures

The rate of reaction at any instant in time was determined by measuring the slopes of each curve at that particular time using the graphs in **Figure 5.19**. The slope at any given point also corresponds to the rate of reaction at an instant of concentration. The rates of reaction were then plotted against concentration for each curve as shown in **Figures 5.20** to **5.22**. The three curves depict a variation of rate of reaction as a function of Co sulphate concentration at 50°C, 70°C and 85°C.

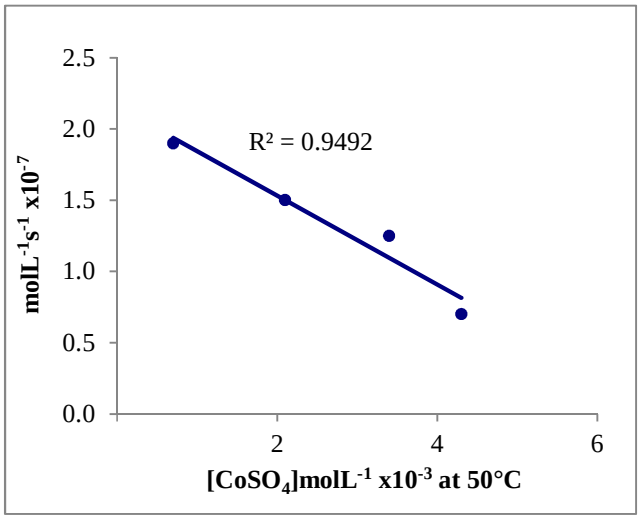

Fig.5.20: Variation of rate of reaction with cobalt sulphate conc. at 50°C

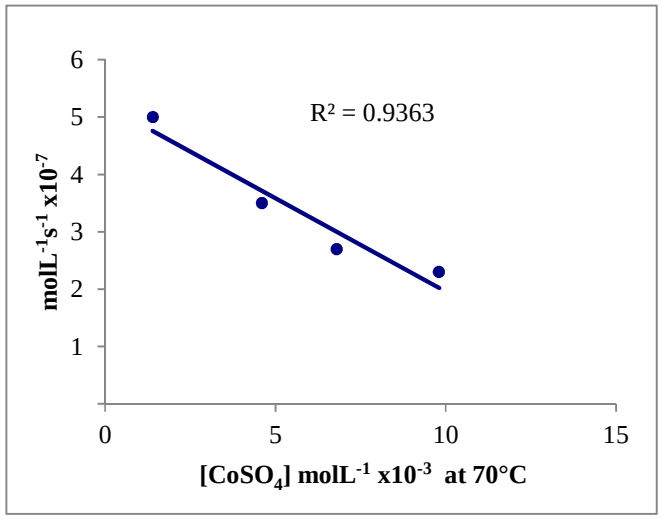

Fig.5.21: Variation of rate of reaction with cobalt sulphate conc. at 70°C

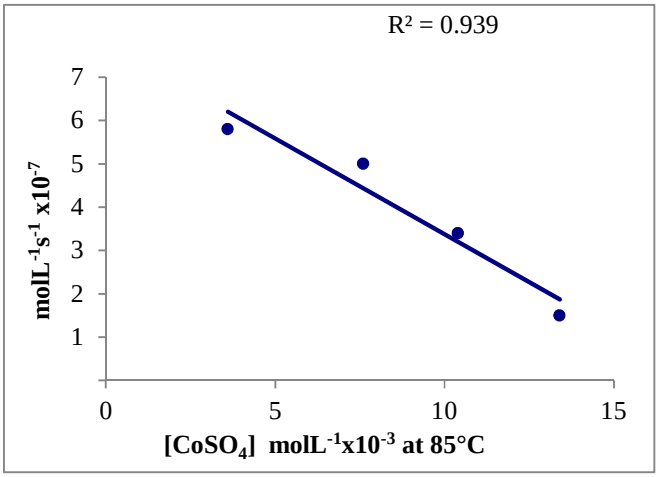

Fig.5.22: Variation of rate of reaction with cobalt sulphate conc. at 85°C

From the slopes of the rate of reaction versus concentration shown in **Figures 5.20** to **5.22**, cobalt dissolution rate constants k_1 at 50°C, k_2 at 70°C and k_3 at 85°C were determined as 1.2 x $10^{-5}s^{-1}$, 4.7 x$10^{-5}s^{-1}$ and 6.0 x10^{-5} s^{-1} respectively and were plotted against 1/T (Arrhenius plot) presented in **Figure 5.23**. The plot shows the effect of temperature on the rate constant for the cobalt dissolution reaction. It can be seen from the plot that the cobalt dissolution rate constant increased with increasing temperature from 50°C (323 K) to 85°C (358K).

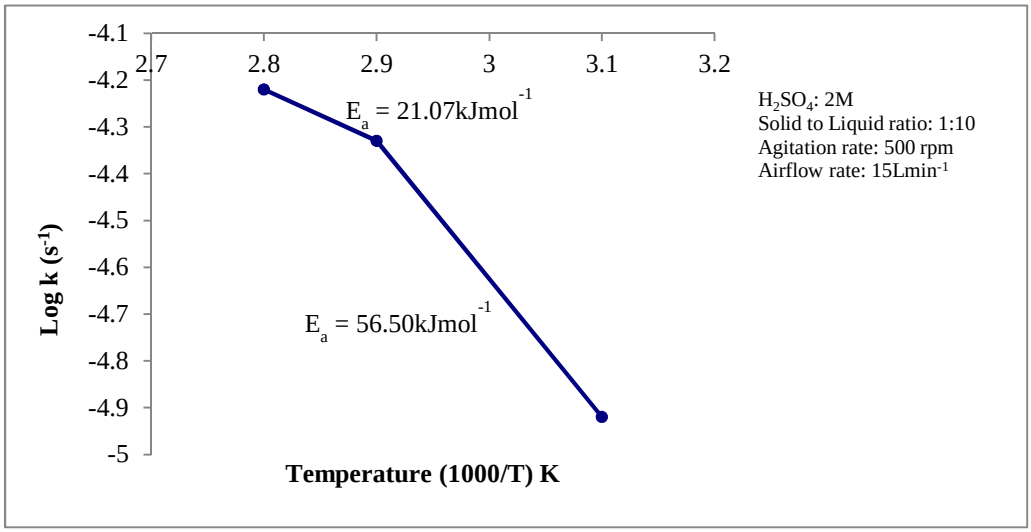

Fig.5.23: Variation of Co dissolution rate constant (k) with temperature

From the slopes of the plot in **Figure 5.23** and using the Arrhenius relationship (**Eq. 5.2**), the activation energy of the Co dissolution reaction (E_a) was calculated as 56.50kJmol^{-1} for the lower temperature range (50-70°C), 21.07 kJmol^{-1} for the higher range (70°C-85°C) and 44.70 kJmol^{-}1 for the overall range (50°C- 85°C). Based on activation energies for rate controlling mechanisms displayed in **Table 5.2** (Habashi, 1969; Potgieter et al., 2006; Sohn and Wadsworth, 1979; Gurmen, 2005), the results indicate that the Co dissolution reaction was a mixed control of chemical reaction and film diffusion. A chemical reaction controlled process is highly influenced by temperature which aids the reaction rate (Levenspiel, 1972).

Diffusion controlled reactions are reactions that occur so quickly that the reaction rate is the rate of transport of the reactants through the reaction medium (Atkins, 1998). Under film diffusion control, the formation of products from the activated complex is much faster than the diffusion of reactants. In the case of fluid-solid systems, the diffusion of reactants in a film diffusion-controlled reaction can be enhanced by stirring or agitation (Atkins, 1998; Levenspiel, 1972).

Table 5.2: Activation Energies for Rate Controlling Mechanisms (Habashi, 1969; Potgieter et al., 2006; Sohn and Wadsworth, 1979)

Regime	Activation Energy
Product (Ash) diffusion control	< 20 $kJmol^{-1}$
Film diffusion control	20 - 50 $kJmol^{-1}$
Chemical reaction control	> 50 $kJmol^{-1}$

5.3.2 Tungsten dissolution

From the kinetics experiment, W dissolution in sulphuric acid solution was considered to proceed according to the following possible reactions:

$$3WC + 4O_2 + 12H^+ \leftrightarrows WO_2 + 6H_2O + 3C + 2W^{6+} \quad (5.3)$$

$$3WO_2 + O_2 + 6H^+ \leftrightarrows W_2O_5 + 3H_2O + W^{6+} \quad (5.4)$$

$$2W_2O_5 + O_2 + 12H^+ \leftrightarrows 2WO_3 + 6H_2O + 2W^{6+} \quad (5.5)$$

The changing rate in W dissolution was observed at three different temperatures, 50°C, 70°C and 85°C by monitoring the concentration of tungsten in solution with change in time as shown in **Figure 5.24**.

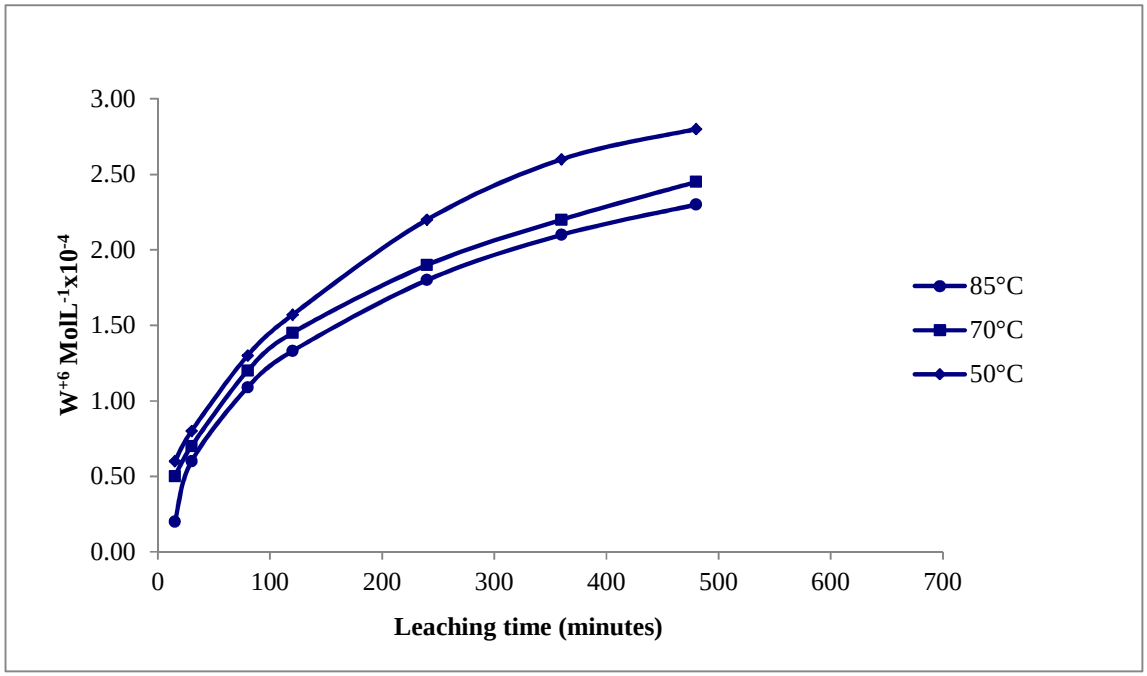

Fig.5.24: Variation of tungsten concentration with time at different temperatures

The rate of reaction at any instant in time was determined by measuring the slopes of each curve at that particular time using the graphs in **Figure 5.24.** The rates of reaction were then plotted against concentration for each curve as shown in **Figures 5.25** to **5.27**.

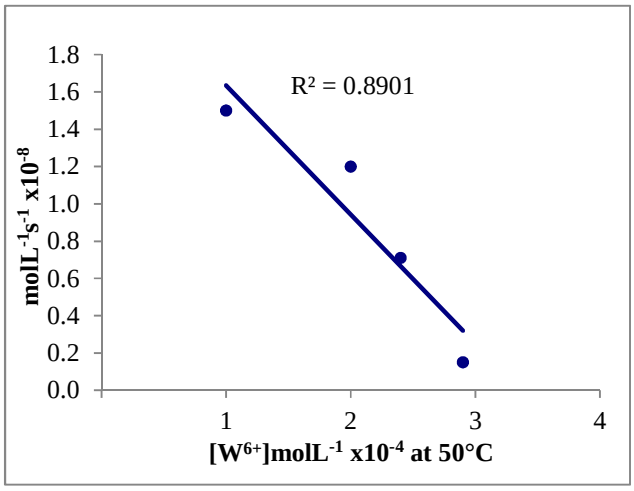

Fig.5.25: Variation of rate of reaction with tungsten conc. at 50°C

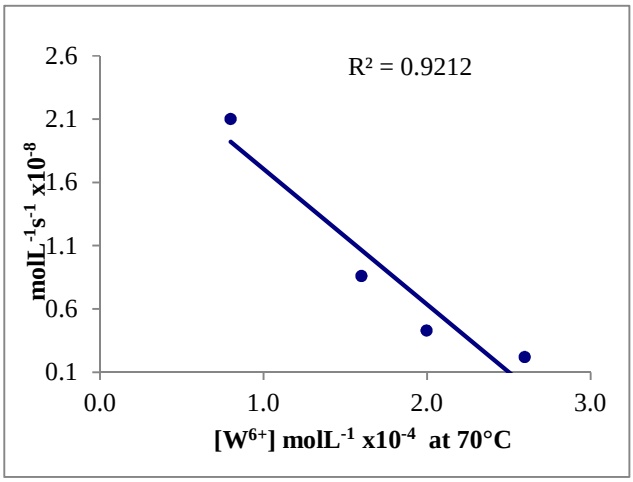

Fig.5.26: Variation of rate of reaction with tungsten conc. at 70°C

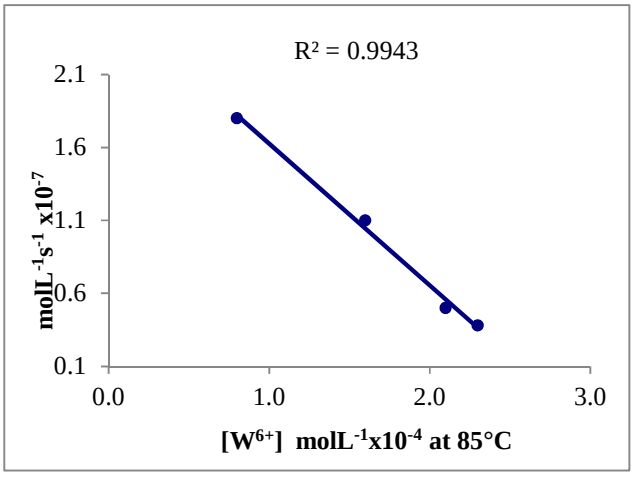

Fig.5.27: Variation of rate of reaction with tungsten conc. at 85°C

From the slopes of the rate of reaction versus concentration shown in **Figures 5.25** to **5.27**, W dissolution rate constants k_1 at 50°C, k_2 at 70°C and k_3 at 85°C were determined as 5.5 x $10^{-5}s^{-1}$, $6.25x10^{-5}s^{-1}$ and $10.41x10^{-5}$ s^{-1} respectively and were plotted against 1/T (Arrhenius plot) presented in **Figure 5.28**. The plot shows the effect of temperature on the rate constant for the reaction. It can be seen from the plot that the W dissolution rate constant increased with increasing temperature from 50°C (323 K) to 85°C (358K).

Using the Arrhenius relationship (**Eq. 5.2**) and from the slopes of the plots in **Figure 5.28**, the activation energy of the reaction (E_a) was calculated as 5.7kJmol^{-1} for the lower temperature range (50°C-70°C), 42.13 kJmol^{-1} for the higher range (70°C-85°C) and 17.87 kJmol^{-1} for the overall range (50-85°C). Based on activation energies for rate controlling mechanisms displayed in **Table 5.2** (Habashi, 1969; Potgieter et al., 2006; Sohn and Wadsworth, 1979; Gurmen, 2005), the results indicate that the W dissolution reaction was a mixed control of product layer diffusion and film diffusion.

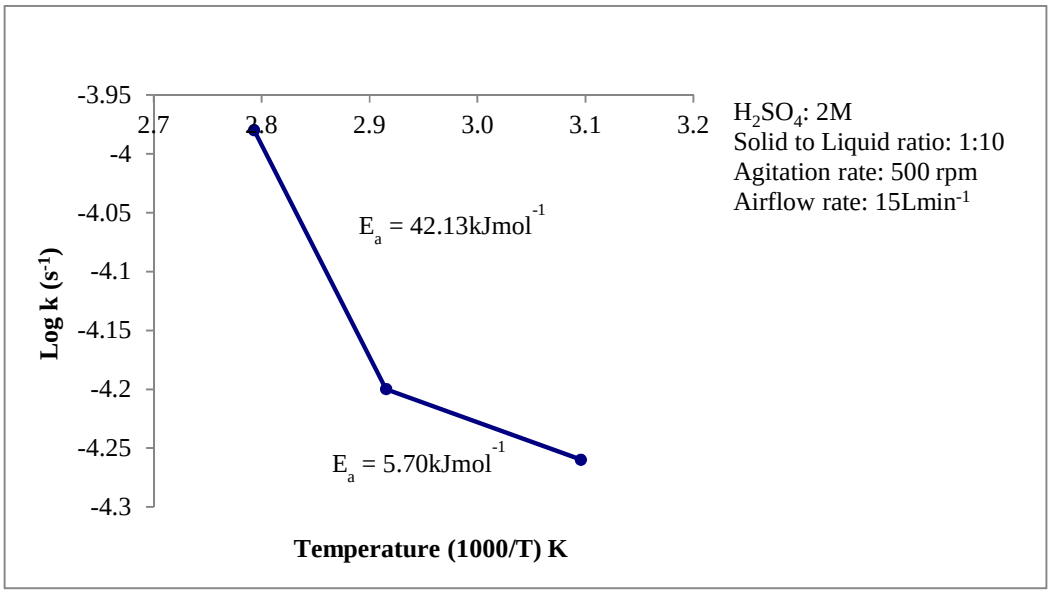

Fig.5.28: Variation of rate constant (k) with temperature

Product layer diffusion reactions are associated with the formation of an ash layer around the reacting solid particle. The ash layer tends to inhibit the mass transfer of reactants. The mass transfer of reactants in a product layer diffusion-controlled reaction can be enhanced by stirring or agitation (Atkins, 1998; Levenspiel, 1972). Tungsten reactions in acidic media have a tendency of forming precipitates as suggested by several authors (Edtmaier et al, 2005; Bosung and Sunjung, 2016; Lin et al, 1995; Cruywagen et al, 1993). This was demonstrated and is discussed in Chapter 4 section 4.7.1.

5.4 Summary

The main purpose of the kinetic study was to derive a conceptual reaction kinetic model that describes the dissolution of cobalt out of the cemented carbide hardmetal.

The Co dissolution process in cemented tungsten carbide buttons (**Fig.5.19**) follows the kinetic models $x = kt$ and $1- (1-x)^{1/3} = kt$, and the apparent activation energy is determined to be 56.70kJmol^{-1} for the lower temperature range (50°C - 70°C) and 21.07kJmol^{-1} for the higher temperature range (70°C-85°C). This indicates that the leaching process of cobalt from cemented carbide scrap is a mixed control of chemical reaction and thin film diffusion. **Fig.4.12** in the preliminary results shows that agitation rate has an effect on the rate of Co dissolution.

Although the formation of a product layer is suggested in earlier chapters and is strongly evident in the kinetic study, the product layer was, however, not found to be in control of the Co dissolution process. The W dissolution process in cemented tungsten carbide buttons (**Fig.5.24**) follows the kinetic models $x = kt$, $1- (1-x)^{1/3} = kt$ and $1-3(1-x)^{2/3} + 2(1-x) = kt$, and the apparent activation energy is determined to be 5.70 kJmol^{-1} for the lower temperature range (50°C - 70°C) and 42.13kJmol^{-1} for the higher temperature range (70°C-85°C). This indicates that the co-dissolution of W from cemented carbide buttons is a mixed control of thin film diffusion, chemical reaction and product layer diffusion.

The next chapter is focused on the formulation and use of a full factorial model design in order to identify factors which significantly influence the cemented carbide leaching process. The design of the model is based on insights gained from preliminary tests discussed in Chapter 4.

5.5 References

Atkins, P.,1998. Physical Chemistry (6th ed.). New York: Freeman. pp. 825–8

Bosung, S., Sunjung, K., 2016. Cobalt Extraction from Tungsten Carbide-Cobalt (WC-Co) Hard Metal Scraps Using Malic Acid. International Journal of Mineral Processing, Vol. 151, pp. 1-7

Chang, R., 2005. Physical Chemistry for the Biosciences. University Science Books, Sausalito (CA), pp. 311-347.

Cruywagen, J.J., Kruger, L., Rohwer, E.A., 1993. Molybdenum (VI) and Tungsten (VI) Complex Formation, Part 5. The Reaction with Lactate in 1.0 mol dm-3 Sodium Chloride Medium. Journal of Chemical Society, Dalton Transactions, pp. 105-109.

Edtmaier, C., Schiesser, R., Meissl, C., Schubert, W.D., Rock, A., Schoen, A., Zeiler, B., 2005. Selective Removal of the Cobalt Binder in WC-Co Based Hard Metal Scraps By Acetic Acid Leaching. Hydrometallurgy, Vol. 76, pp. 63-71

Gbor, P.K., Jia, C.Q., 2004. Critical Evaluation of Coupling Particle Size Distribution with the Shrinking Core Model. Chemical Engineering Science, Vol. 59, pp. 1979-1987.

Gurmen, S., Friedrich, B., 2005. Recovery of Cobalt Powder and Tungsten Carbide from Cemented Carbide Scrap - Part I: Kinetics of Cobalt Acid Leaching. World of Metallurgy-ERZMETALL. Vol. 57, pp. 143-147.

Habashi, F., 1968. Principles of Extractive Metallurgy: General principles, Vol. 1. Gordon and Breach, New York, pp. 143.

Sohn, H. Y., Wadsworth, E. M., 1979. Rate Processes of Extractive Metallurgy, Plenum Press, New York, 141-143.

Laidler, K., 1984. Development of the Arrhenius Equation. Journal of Chemical Education, 61(6), pp. 494.

Levenspiel, O., 1972. Chemical Reaction Engineering. John Willey and Sons, New York.

Lin J.C, Lin J.Y, Lee S.L., 1995. Process for Recovering Tungsten Carbide from Cemented Tungsten Carbide Scraps By Selective Electrolysis. US, Patent No. 5,384,016. 24 June 1995.

Logan, S.R., 1982. The Origin and Status of the Arrhenius Equation. Journal of Chemical Education, 59(4), pp. 279.

Mason, R.O., Lind, D.A., Marchal, W.G., 1983. Statistics: An Introduction. New York. Harcourt Brace Jovanovich, Inc. pp. 368-383.

Potgieter, J.H., Kabemba, M.A., Teodorovic, A., Potgieter-Vermaak, S.S., Augustyn, W.G., 2006. An Investigation into the Feasibility of Recovering Valuable Metals from Solid Oxide Compounds by Gas Phase Extraction in a Fluidized Bed. Minerals Engineering, Vol. 19, pp. 140-146.

Segal, I.H., 1975. Enzyme Kinetics: Behaviour and Analysis of Rapid Equilibrium and Steady State Enzyme Systems. John Wiley and Sons, New York. pp. 931-933.

Taylor, R., 1990. Interpretation of the Correlation Coefficient : A Basic Review. JDMS I: 35-39.

Weber, J.C., Lamb, D.R., 1970. Statistics and Research in Physical Education, St. Louis: C.V, Mosby.

Smith, J.M., 1981. Chemical Engineering Kinetics. McGraw Hill, New York.

Han, K. N., 2002. Fundamentals of Aqueous Metallurgy. Society for Mining, Metallurgy, & Exploration Inc, Colorado.

CHAPTER SIX

IDENTIFICATION OF INFLUENTIAL FACTORS

USING DESIGN OF EXPERIMENTS (DOE)

6.1 Introduction

The success of leaching metals from minerals or metal-containing materials largely depends on the selection of suitable process parameters at which the metal extraction efficiency, as a measured response, is optimal. Experimental techniques for obtaining optimum results require the use of a combination of factorial designs and response surface methodologies. Factorial designs, as described by Montgomery (2005) and Box et al (1978), are diagnostic experiments that are employed as a characterization or screening tool for evaluating the influence of main factors on a process.

Despite extensive studies on the various techniques of recycling cemented tungsten carbide-cobalt secondary material, literature is limited regarding leaching models that are specific to the extraction of cobalt from these hardmetals using sulphuric acid. The main purpose of this study, therefore, was to investigate and identify factors that significantly influence the leaching of cemented carbide hardmetal. The study employed a statistical Design of Experiments (DOE) method as a research tool to develop an experimentation strategy for determining the significant factors affecting cemented carbide leachability with sulphuric acid. The significance of each factor and associated interactive effects were evaluated using a two-level five-factor full factorial statistical design of experiments (2^5) and percent (%) cobalt extraction was taken as the measured response or desired goal. Once the significant factors are identified, they can be optimized while the non-significant factors are kept at cost effective levels. Identification of influential factors is essential for process optimization and cost control. The experimental procedure followed in this chapter is described in Chapter 3 sections 3.5 and 3.7.2.

6.2 Factors and Factor Levels in Experiments

Statistical design of experiments (DOE) was employed to study the leaching behaviour of cemented tungsten carbide using a 2^5 full factorial design. In this work, the choice of factors and their levels was based on preliminary experiments.

Experimental design factors were classified as controlled factors and held constant factors. The controlled factors presented in **Table 6.1** were the factors selected for investigation. The held constant factor such as oxygen flowrate is a factor that may have an influence on the response but is of no particular interest in the current study so it was held constant at 15 $Lmin^{-1}$. Factors were studied with their codified values of -1 and +1. The coded and physical values are given in **Table 6.2**. The levels of controlled variables in coded units (Box et al., 1978) were obtained using the following formula:

$$\boldsymbol{coded\ value} = \frac{\boldsymbol{X - X_0}}{\boldsymbol{0.5(X_2 - X_1)}} \qquad (6.1)$$

Where, X = physical value, X_0 = mean, X_1 = lowest, X_2 = highest

Table 6.1: Experimental factors and levels for controlled factors

Controlled Factors	Level 1 (-1)	Centre Point (0)	Level 2 (+1)
Temperature (°C)	68	75	82
Leaching time (hrs)	6	8	10
Acid Concentration (M)	1	1.5	2
Solid to Liquid ratio	1:10	1:12	1:14
Agitation Rate (rpm)	500	645	790

6.3 Methodology for data analysis

Experimental results were analyzed statistically by using normal probability plot of effects, Pareto chart, residuals analysis and centre points (Daniel, 1959; Design Expert®11 manual, 2019).

6.3.1 Pareto Chart

Plotting the effects on a Pareto chart (Tague, 2004; Wilkinson, 2006) provides an alternative and equally effective way of helping with selection of significant factors. The Pareto chart is based on an algorithm that produces a statistically-based acceptance limit of significance represented by horizontal bar graphs. The statistical technique, based on the Pareto principle of the vital few, is used for a selection of the "vital few" factors that produce the significant overall effect. The critical value line that cuts across the bar graphs serves to separate the vital from the non-vital effects.

6.3.2 Normal Probability Plot of Effects

In the assessment of effects from unreplicated factorials, occasionally real and meaningful higher order interactions occur and therefore it is necessary to allow for selection. A method (Daniel, 1959) by which effects are plotted on a normal probability plot often provides an effective way of helping with selection. If the effects had occurred simply as the result of random variation about a fixed mean, and the changes in levels of the independent variables had had no real effect at all on the aluminium extraction, then all the 31 main effects and interactions would be distributed about zero (normal distribution). They would therefore, plot on a normal probability plot as a straight line. To see whether they do, the 31 main effects are ordered in increasing order and plotted with an appropriate scale. The scale is obtained by employing the generalized equation:

$$\boldsymbol{P = (i - 0.5) * \frac{100}{m}} \qquad (6.2)$$

Where,

m = total number of effects, P = Probability points, i = Order number

6.3.3 Graphical Residual Analysis

Normal plotting of residuals provides a diagnostic check for any tentatively entertained model (Box et al., 1978). The normal probability plots of the residuals for the data tests the theory that the residuals have a normal distribution. This should be a straight line if the residuals have a normal distribution. A plot of residuals versus the predicted values (fitted model values) is a test of the theory that the variations are the same in each group. Studentized 'deleted' residuals were

calculated for each run in order to remove undue influence from outliers. A Studentized residual, therefore, is evaluated based on the predicted value when the value itself is excluded from the analysis. The residuals were calculated using the following equation:

$$Residual = \frac{R_{i,observed} - R_{i,predicted}}{\sigma_{i,residual}} \quad (6.3)$$

Where, $R_{i,\ observed)}$ is the i^{th} observation (extraction) in the experimental data, $R_{i,\ predicted}$ is the predicted value of the response from the fitted model, $\sigma_{i,\ residual}$ is the standard deviation of all residuals from the regression analysis that deleted the i^{th} observation.

6.3.4 Test for Curvature

The check for local planarity is supplied by comparing $Y_{f,}$ the average of the factorial points, with Y_c, the average at the centre of the design. By thinking of the design as sitting on a saucer like surface, it is seen that $Y_f - Y_c$ is a measure of the overall curvature of the surface (Box et al., 1978). If Y_c is the average cobalt extraction of total runs at the centre and Y_f the average cobalt extraction of the total runs at the factorial points under study, then, if the difference is small then the centre points lie on or near the plane passing through the factorial points and hence there's no quadratic curve and no curvature. However, if $Y_f - Y_c$ is large, then quadratic curvature is present (Montgomery, 2005).

6.4 DOE Results

6.4.1 Identification of Significant Factors

Cobalt extraction results from experimental runs for the 2^5 full factorial design with codified and actual values are given in **Table 6.2**.

The cobalt extraction in the sulphuric acid leaching of cemented carbide presented in **Table 6.2** was calculated as a percentage of cobalt in leach liquor to that in the unprocessed cemented carbide.

Table 6.2: Cobalt extraction results for the 2^5 full factorial design

Standard Run Order	Random Run Order	Controlled Factors					Co Extraction (%)
		A	B	C	D	E	
1	5	-1	-1	-1	-1	-1	7.0
2	10	+1	-1	-1	-1	-1	11.5
3	15	-1	+1	-1	-1	-1	10.1
4	20	+1	+1	-1	-1	-1	18.2
5	1	-1	-1	+1	-1	-1	8.3
6	30	+1	-1	+1	-1	-1	17.6
7	14	-1	+1	+1	-1	-1	12.3
8	32	+1	+1	+1	-1	-1	23.0
9	19	-1	-1	-1	+1	-1	7.2
10	2	+1	-1	-1	+1	-1	11.8
11	21	-1	+1	-1	+1	-1	10.8
12	29	+1	+1	-1	+1	-1	17.8
13	28	-1	-1	+1	+1	-1	8.1
14	7	+1	-1	+1	+1	-1	15.4
15	3	-1	+1	+1	+1	-1	12.8
16	27	+1	+1	+1	+1	-1	23.0
17	26	-1	-1	-1	-1	+1	6.5
18	31	+1	-1	-1	-1	+1	8.2
19	9	-1	+1	-1	-1	+1	11.3
20	4	+1	+1	-1	-1	+1	18.1
21	11	-1	-1	+1	-1	+1	8.1
22	24	+1	-1	+1	-1	+1	15.4
23	25	-1	+1	+1	-1	+1	13.4
24	22	+1	+1	+1	-1	+1	21.9
25	23	-1	-1	-1	+1	+1	8.3
26	17	+1	-1	-1	+1	+1	11.3
27	16	-1	+1	-1	+1	+1	7.1
28	13	+1	+1	-1	+1	+1	11.4
29	12	-1	-1	+1	+1	+1	17.4
30	6	+1	-1	+1	+1	+1	15.6
31	18	-1	+1	+1	+1	+1	13.5
32	8	+1	+1	+1	+1	+1	22.4

The actual factor levels coded as values of (-1) and (+) in the table are as follows:

A (Temperature): 68°C (-1) and 82°C (+1); B (Leaching time): 6hrs (-1) and 10hrs (+1);

C (Acid concentration): 1M (-1) and 2M (+1); D (Solid: Liquid ratio): 1:10(-1) and 1:14(+1)

E (Agitation rate): 500rpm (-1) and 790rpm (+1)

6.4.1.1 Pareto Chart

The experimental data given in **Table 6.2** was used to estimate the main and interaction effects presented in **Figure 6.1**.

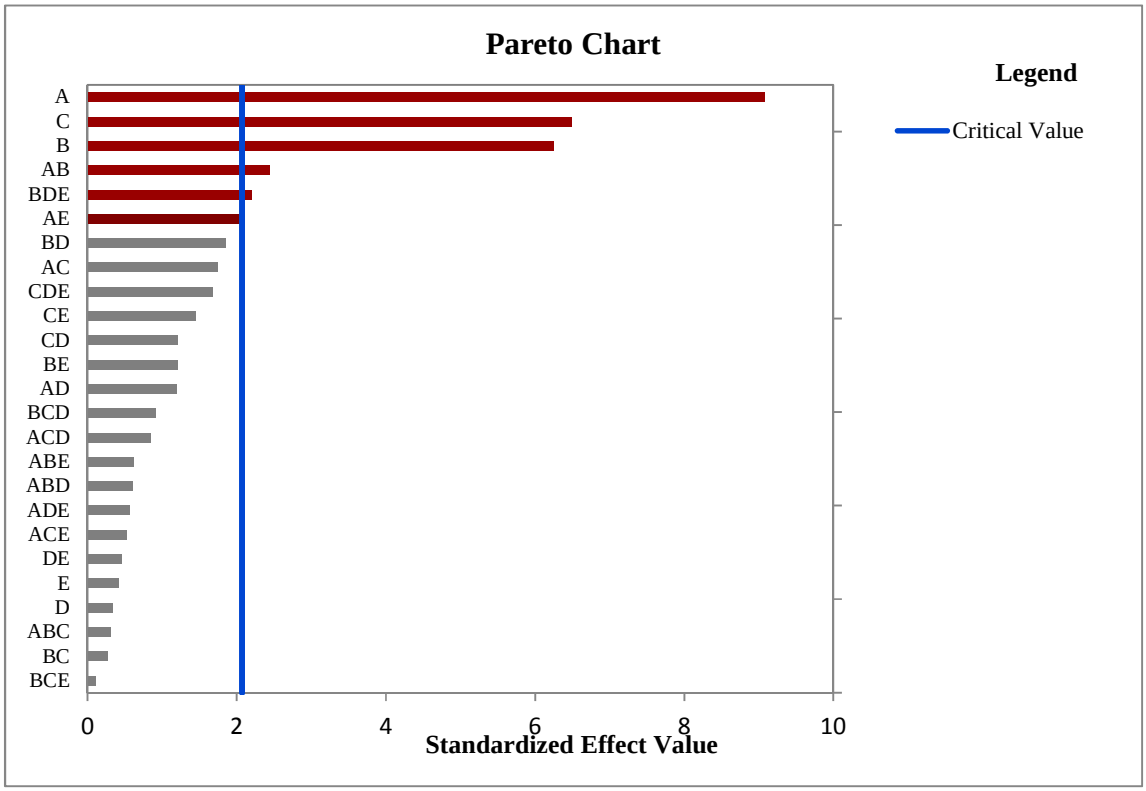

Fig.6.1: Pareto chart showing significance of main and interactive effects of: **t**emperature, leaching time, acid concentration, solid-to-liquid ratio and agitation rate

Standardized effect values at or beyond the critical value line indicate that the terms are significant and those below the line are not significant. In this case the main effects A, B, C and interaction effects AB, AE and BDE are significant.

6.4.1.2 Normal Probability Plot

The experimental data given in **Table 6.2** was also used to estimate the main and interaction effects presented in **Figure 6.2**.

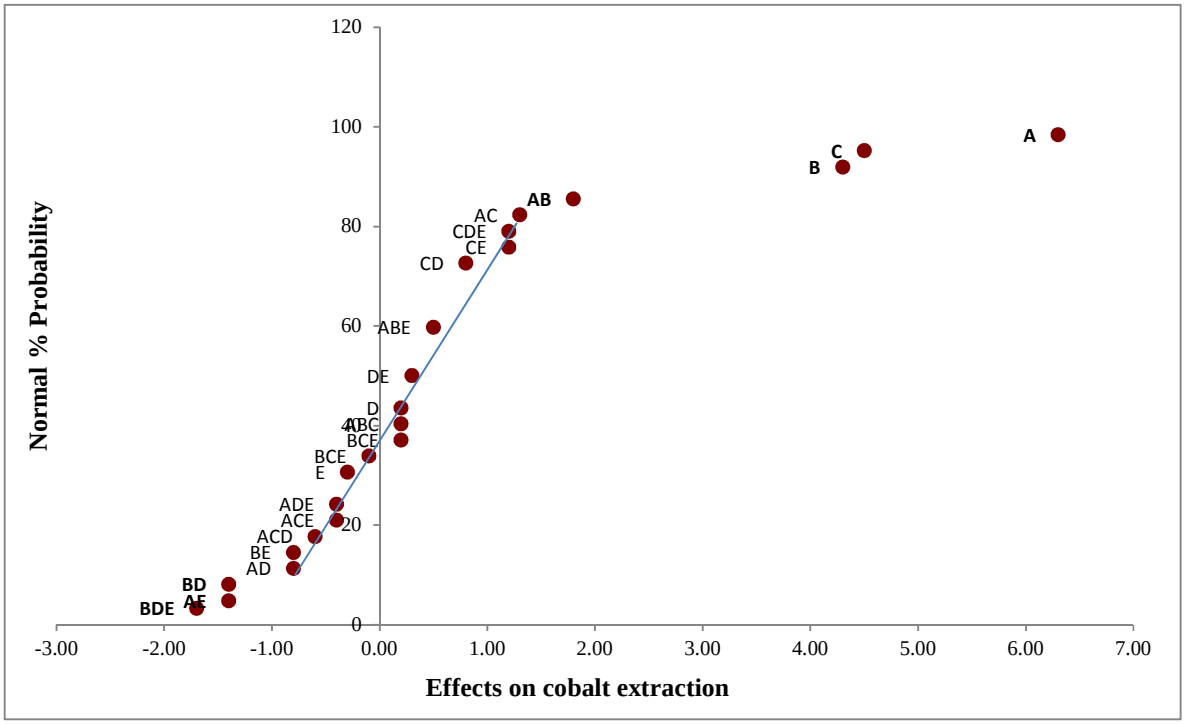

Fig.6.2: Normal probability plot

The main and interaction effects presented in **Figure 6.2** were estimated using experimental data and the normal probability plot of effects was used to determine the significant effects. Analysis of the figure showed effects which were roughly normal and were distributed about the zero mean. They plotted on a normal probability graph as a straight line. Beginning with effects with magnitudes close to zero, 16 of the estimates, fitted reasonably well on a straight line. Those corresponding to temperature (A), leaching time (B), acid concentration (C), temperature and time interaction (AB), time and solid to liquid ratio interaction (BD), temperature and agitation rate interaction (AE) and time, solid to liquid ratio and agitation rate interaction (BDE) did not fit on the straight line. The effects that did not fit on the straight are not easily explained as chance occurrences, they are interpreted to mean that they are statistically significant (Box et al., 1978; Montgomery, 2005).

A first order polynomial model between the factors and the response was developed to illustrate the dependence of the response on the more significant factors. The model is expressed below as:

$$R = 13.27 + 3.14X_A + 2.17X_B + 2.24X_C + 0.8937X_AX_B - 0.7188X_AX_E - 0.8562X_BX_DX_E \quad (6.4)$$

Where R is the cobalt extraction, X_A, X_B, X_C, X_D and X_E are predictor variables which take the value of -1or +1 (low or high). In **Eq. (6.5)**, the positive signs in the prediction model indicate that in order to maximize acid leaching of cemented carbide, these factors must be kept at high levels. The negative signs indicate that these factors must be kept at low levels. For example, solid to liquid ratio and agitation rate must be kept at low levels.

6.4.1.3 Test for Curvature

The cobalt extraction results for centre points for the full factorial design (2^5) are presented in **Table 6.3.**

Table 6.3: Cobalt extraction results for center point replicates for the 2^5 full factorial

Run	Control Factors					Cobalt Extraction (%)
	A	B	C	D	E	
1	0	0	0	0	0	10.1
2	0	0	0	0	0	8.4
3	0	0	0	0	0	9.4
4	0	0	0	0	0	8.2
5	0	0	0	0	0	10.2
6	0	0	0	0	0	8.3
7	0	0	0	0	0	9.7

The actual factor levels coded as values of (0) in the table are centre point values and are as follows:
A (Temperature): 75° C (0); B (Leaching time): 8hrs (0); C (Acid concentration): 1.5M (0);
D (Solid: Liquid ratio): 1:12(0); E (Agitation rate): 645rpm (0)

The observed cobalt extractions at the seven centre points were: 10.1%, 8.4%, 9.4%, 8.2%, 10.2%, 8.3% and 9.7%. The average of these points is 9.2%. The average of the 32 factorial points of the 2^5 factorial design in **Table 3.2** is 13.3%. Since the two averages are not similar (difference of 3.6%), it is clear that the planar model may not be adequate. In other words

curvature is most likely present. The presence of cross products (significant interaction effects) in the fitted model, in **Eq. (6.5)**, further suggests the presence of curvature.

6.4.1.4 Graphical Residual Analysis

The normal plot of residuals is presented in **Figure 6.3**. All residuals lie on a straight line with a correlation coefficiency of 92.45% as illustrated in the figure showing that the residuals were distributed normally. A plot of residuals versus predicted extraction presented in **Figure 6.4** is a test of the assumption that the variations are the same in each group. All residuals fall within the upper and lower boundaries. Since the residuals were distributed normally with constant variance, mean zero and independently, as shown in **Figure 6.3** and **Figure 6.4**, it can be concluded that **Eq. (1.3)** fitted the experimental data well.

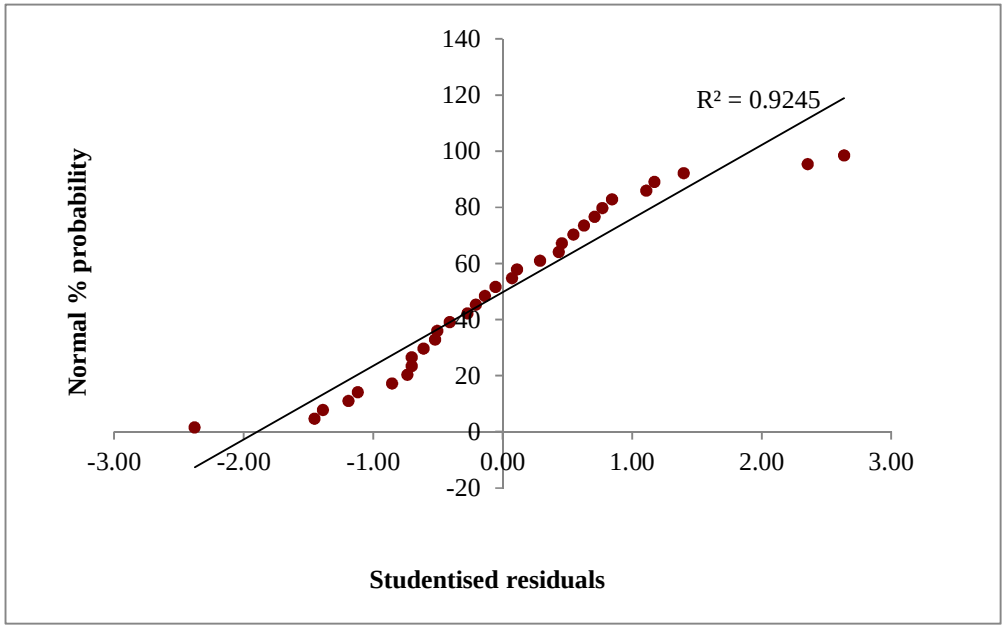

Fig.6.3: Normal plot of residuals

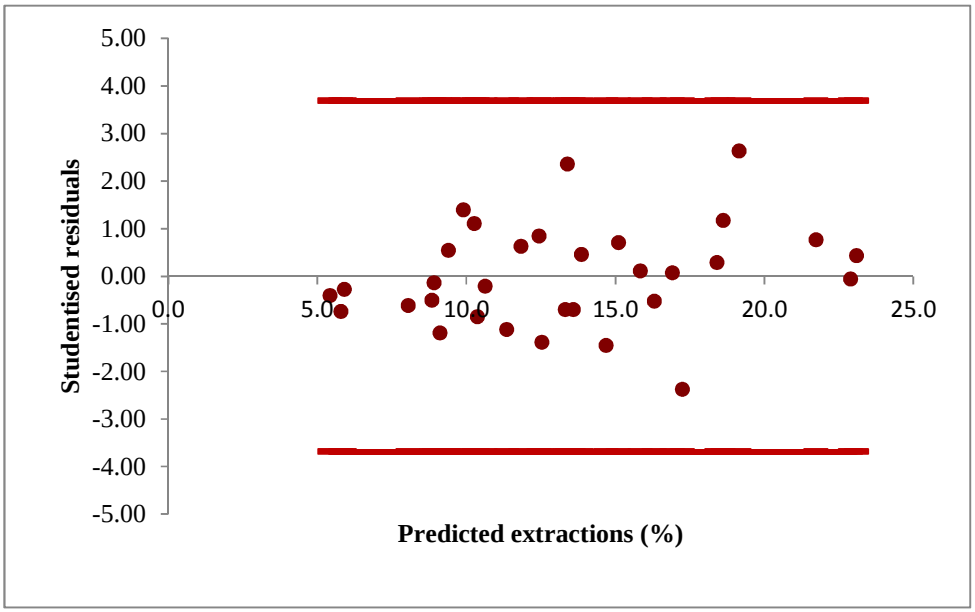

Fig.6.4: Plot of residuals versus predicted extractions

6.4.2 Influence of Factors on Co extraction

The main effect of a variable should be individually interpreted only if there's no evidence that the variable interacts with other variables. When there's evidence of one or more such interaction effects, the interacting variables should be considered jointly (Box et al., 1978). In this study the interaction amongst all tested variables was found to be statistically significant except for acid concentration. In the current study, both cases applied. Therefore, all the factors were first interpreted individually and the interacting variables were interpreted jointly.

6.4.2.1 Effect of Leaching Temperature

The effect of leaching temperature is illustrated in **Figure 6.5**. The figure shows Co extraction as a function of temperature at 68°C and 82°C as the low (-1) and high (+1) factor levels respectively. Co extraction increased proportionally with increase in temperature. A higher Co extraction of 15.3% was obtained at 82°C while 10.1% was obtained at 68°C. The high Co extraction at higher temperature could be explained with reference to the activation energy results obtained in the kinetic study in Chapter 5 section 5.3.1. The lower activation energy (21.07kJmol^{-1}) barrier at higher temperature may have been helpful in breaking down any obstructive passivation layer hence enhancing the reaction rate of Co dissolution.

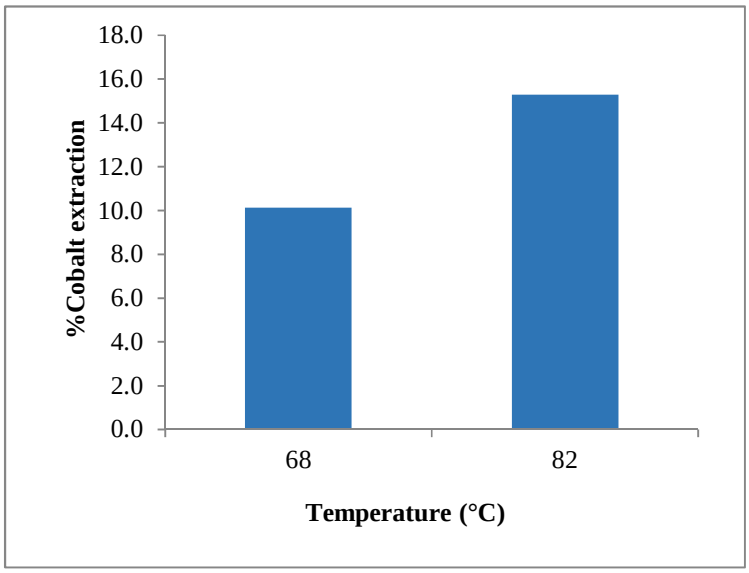

Fig.6.5: Effect of temperature on Co extraction (from the full 2^5 factorial designs)

6.4.2.2 Effect of Leaching Time

The effect of leaching time is exhibited in **Figure 6.6**. The figure shows Co extraction as a function of leaching time of 6hrs and 10hrs as the low (-1) and high (+1) factor levels respectively. The dissolution of Co increased with increase in leaching time. A higher Co extraction of 15.4% was achieved after 10hrs of leaching whereas 11.1% was obtained after 6hrs. The increased extraction with longer leaching time signified the fact that adequate leaching time is necessary to overcome resistance to mass transfer of reactants and products caused by insoluble formations like tungstic acid that may have caused obstruction.

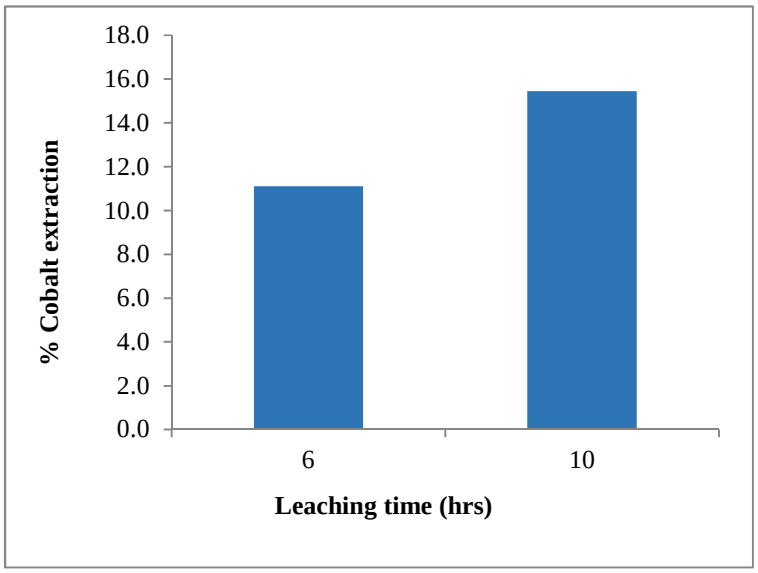

Fig.6.6: Effect of leaching time on Co extraction (from the full 2^5 factorial design)

6.4.2.3 Effect of Acid Concentration

The effect of acid concentration is displayed in **Figure 6.7**. The figure shows Co extraction as a function of acid concentration at 1M and 2M as the low (-1) and high (+1) factor levels respectively. Results in **Figure 6.7** show that Co extraction increased proportionally with increase in acid concentration. A higher Co extraction of 15.5% was obtained at 2M whereas 11.0% was obtained at 1M. This is in contrast with results obtained in Chapter 4 section 4.5.2, for the effect of acid concentration on Co extraction at lower temperatures, but in agreement with the results for the effect of acid concentration at higher temperatures. As observed in Chapter 4, high acid concentrations at low temperatures intensify the precipitative formation of insoluble tungstic acid which cause low mass transfer rates of reactants and products thus decreasing Co extraction efficiencies. However, in the current case, the variation of temperature in the factorial design of the screening experiments may have helped in the breaking down of any obstructive tungstic acid precipitates hence increasing Co extraction at higher acid concentration as displayed in **Figure 6.7**. This suggests an interaction between temperature and acid concentration (AC) as displayed in the Pareto chart in **Figure 6.1**. While the interaction was not picked up as being statistically significant, it is, nevertheless, scientifically important to the cemented carbide dissolution process.

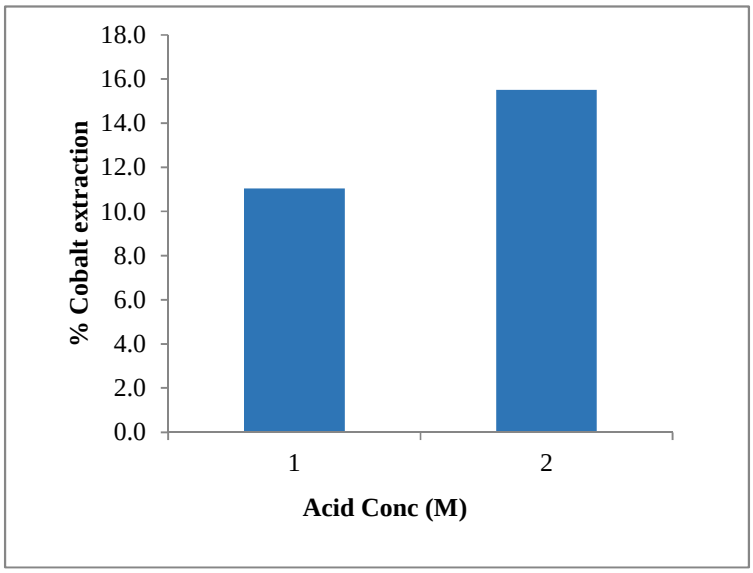

Fig.6.7: Effect of acid concentration on cobalt extraction (from the full 2^5 factorial design)

6.4.2.4 Effect of Solid-to-Liquid Ratio

The effect of solid to liquid ratio is presented in **Figure 6.8**. The figure shows Co extraction from cemented carbide at solid to liquid ratios of 1:14 and 1:10 which are low (-1) and high (+1) levels respectively. Higher Co extraction was attained at the lower solid to liquid ratio of 1:14 than at the higher solid to liquid ratio of 1:10. This is in contrast with results obtained earlier in preliminary experiments discussed in Chapter 4 section 4.5.3 which showed lower Co extraction at lower solid to liquid ratio of 1:14. As observed in Chapter 4, lower solid to liquid ratios intensify the formation of tungstic acid precipitates thus causing poor diffusion which in turn lead to decreased extraction efficiencies. However, in the current case, the variation of temperature in the factorial design of the screening experiments may have assisted in the breaking down of any obstructive precipitates, thus enhancing Co extraction at the lower solid to liquid ratio as shown in **Figure 6.8**. This suggests an interaction between temperature and solid to liquid ratio (AD) as displayed in the Pareto chart in **Figure 6.1**. Although this interaction was not picked up as being statistically significant, it is, however, scientifically important to the cemented carbide dissolution process.

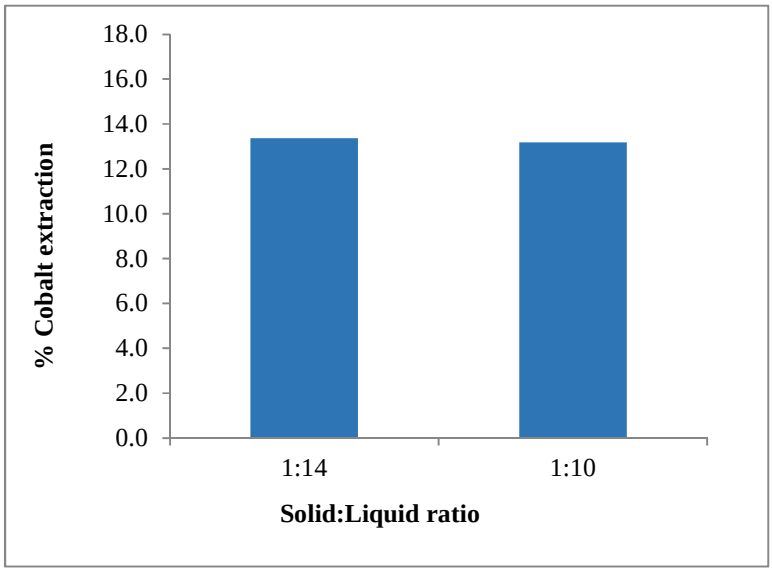

Fig.6.8: Effect of solid to liquid ratio on cobalt extraction (from the full 2^5 factorial design)

6.4.2.5 Effect of Agitation Rate

The effect of agitation rate is presented in **Figure 6.9**. The figure shows Co extraction as a function of agitation rate at 500rpm and 790rpm as the low (-1) and high (+1) factor levels respectively. Co extraction deceased slightly with increase in agitation rate. A higher Co extraction of 13.4% was obtained at 500rpm while 13.1% was obtained at 790rpm. High mass transfer speed may not have allowed optimum solid-fluid contact with the unreacted part of the bulk solution, thus adversely affecting leaching efficiencies. Results obtained earlier, in Chapter 4 section 4.5.4, are in agreement with this trend. The results indicate that there's an optimum agitation rate at which Co extraction occurs and beyond which leaching efficiencies start decreasing.

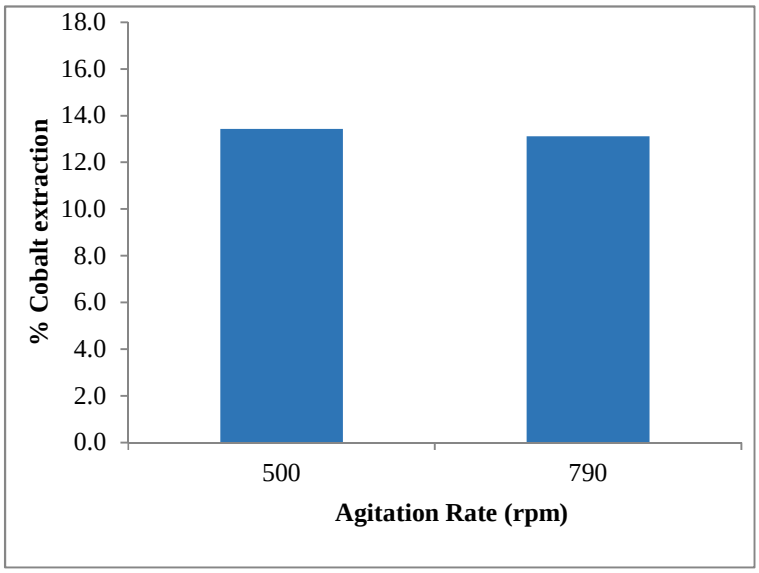

Fig.6.9: Effect of agitation rate on cobalt extraction (from the full 2^5 factorial design)

6.4.2.6 Effect of Factor Interaction

An interaction of factors is a relationship where the effect that a factor has on the product or process is altered due to the presence of one or more factors and often times, interaction effects have more impact on the results than individual factors.

In the current study, factor interaction effects were normally distributed with mean zero and fell along a straight line on the plot shown in **Figure 6.2**. In the ranges studied, the interaction between variables AB (temperature and leaching time), AE (temperature and agitation rate) and BDE (leaching time, solid to liquid ratio and agitation rate), was observed to be statistically significant. The three significant factor interactions are presented in **Figure 6.10** below. The interacting variables were interpreted jointly.

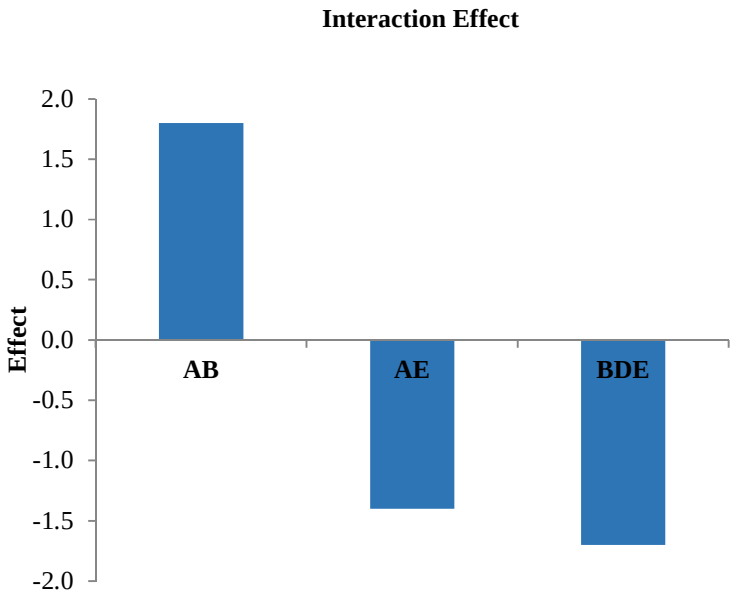

Fig.6.10: Interaction effects of significant factors from the full 2^5 factorial design.

6.4.2.6.1 Interaction effect of temperature (A) and leaching time (B)

A joint analysis of the effect of leaching temperature and leaching time presented in **Figures in 6.5** and **6.6** shows that both factors had a similar positive effect on Co dissolution. Therefore, the combined effect was a positive influence on Co dissolution as shown in **Figure 6.10**. This means that in order to maximize Co dissolution, both leaching temperature and leaching time must be kept at high levels.

6.4.2.6.2 Interaction effect of temperature (A) and agitation rate (E)

A joint examination of the effect of leaching temperature and agitation rate exhibited in **Figures in 6.5** and **6.9** shows that the two factors had different effects on Co dissolution. Whereas high temperature promoted Co dissolution, the negative effect of a high agitation rate outweighed the positive impact of temperature and the net effect, as shown in **Figure 6.10**, was a negative impact on Co dissolution. This implies that that in order to maximize Co dissolution, temperature must be kept at a high level and the agitation rate must be kept at a low level.

6.4.2.6.3 Interaction effect of leaching time, solid: liquid ratio and agitation rate

A joint analysis of the effect of leaching time, solid to liquid ratio and agitation rate presented in **Figures 6.6, 6.8** and **6.9** shows that the three factors have different effects on Co dissolution. Whereas long leaching time promoted Co dissolution, the negative effect of a high solid to liquid ratio and agitation rate counteracted the positive impact of long leaching time as shown in **Figure 6.10**. Therefore, in order to maximize Co dissolution, leaching time must be kept at a high level whereas solid to liquid ratio and agitation rate must be kept at low levels.

6.5 Summary

The purpose of the screening or diagnostic two-level full factorial design discussed in this chapter was to obtain experimental data to serve as the beginning step to the final optimization that is presented in the next chapter (Chapter 7). Five factors: temperature, leaching time, acid concentration, solid to liquid ratio and agitation rate were screened. Using a full five factor factorial design (2^5), all the five factors were tested and their influence on the Co dissolution process was evaluated.

- Three main factors found to have a significant influence on the Co dissolution process were temperature, leaching time and acid concentration. These three factors are key to the optimization of the Co dissolution process.
- Three factor interactions found to have a significant effect on Co dissolution were leaching temperature and leaching time (AB); leaching temperature and agitation rate (AE); leaching time, solid to liquid ratio and agitation rate (BDE).
- The interaction variables, leaching temperature and leaching time (AB) had a positive effect on the Co dissolution process. A joint analysis of the interaction showed that both factors must be kept at high levels in order to maximize Co dissolution.
- Interaction variables, leaching temperature and agitation rate (AE) had a negative effect on the Co dissolution process. A joint analysis of the interaction showed that, in order to maximize Co dissolution, leaching temperature must be kept at a high level and agitation rate at a lower level.
- Interaction variables, leaching time, solid to liquid ratio and agitation rate (BDE) also had a negative impact on the Co dissolution process. A joint analysis of the results showed that, in

order to maximize Co dissolution, leaching time must be kept at a high level whereas solid to liquid ratio and agitation rate must be kept at low levels.

- Analysis of the normal probability plot and Pareto chart results revealed that temperature had the strongest impact on the Co extraction process compared to acid concentration and leaching time. It is evident from the results that Co dissolution from cemented carbide (WC-6wt.%Co) is predominantly a temperature driven process.

The next chapter is focused on the modeling of optimum conditions required for cemented carbide (WC-6wt.%Co) leaching based on the three significant factors identified in this chapter.

6.6 References

Barnard, P.G., Starliper, A.G., Kenworthy, H., 1971. Reclamation of Refractory Carbides from Carbide Materials. U.S Patent 3, 595, 484. 27 July 1971.

Barrentine, L.B., 1999. An Introduction to Design of Experiments: A Simplified Approach. ASQ Quality Press, Wisconsin.

Bhosale, S.N., Mookherjee, S., Pardeshi, R.M., 1990. Current Practices in Tungsten Extraction and Recovery. High Temperature Materials and Processes, Vol. 9, Issue 2-4.

Bosung, S., Sunjung, K., 2016. Cobalt Extraction from Tungsten Carbide-Cobalt (WC-Co) Hard Metal Scraps Using Malic Acid. International Journal of Mineral Processing, Vol. 151, pp. 1-7.

Box, G.E.P., Hunter, W.G., Hunter, J.S., 1978. Statistics for Experimenters: An Introduction to Design, Data Analysis and Model Building. John Wiley and Sons, New York.

Bronsted, J.N., 1931. On The Dissolution of Metals in Acids. Journal of American Chemitry Society. Vol.53, Issue 10, pp. 3624-3644. https://doi.org/10.1021/ja01361a006.

Chen, Z.A., 2013. PEC Experiment Standard. Springer, Berlin/New York.

Daniel, C., 1959. Use of half normal plots in interpreting factorial two level experiments. Technometrics 1 (4), 311–341.

Design Expert® 11 Manual., 2019. Internet Version <http://www.statease.com>. Stat-Ease, Incorporation, Minneapolis. Retrieved 10 November 2019.

Edtmaier, C., Schiesser, R., Meissl, C., Schubert, W.D., Rock, A., Schoen, A., Zeiler, B., 2005. Selective Removal of the Cobalt Binder in WC-Co Based Hard Metal Scraps By Acetic Acid Leaching. Hydrometallurgy, Vol. 76, pp. 63-71

Exner, H.E., 1979. Physical and Chemical Nature of Cemented Carbides. International Metals Reviews, Vol. 4, pp. 149-173.

Garcia, E.M., Santos, J.S., Pereira, E.C., Freitas, M.B.J.G., 2008. Electrodeposition of Cobalt from Spent Li-ion Battery Cathodes by The Electrochemistry Quartz Crystal Microbalance Technique. Journal of Power Sources, Vol. 185, pp. 549-553.

Gurmen, S., 2005. Recovery of Nano-Sized Cobalt Powder from Cemented Carbide Scrap. Turkish Journal of Engineering and Environmental Science. Vol.29, pp. 343-350.

Katiyar, P.K., Randhawa, N.S., Hait, J., Jana, R.K., Singh, K,K., Mankhand, T.R., 2014. An Overview on Different Processes For Recovery of Valuable Metals From Tungsten Carbide Scrap. ICNFMM, Nagpur.

Levenspiel, O., 1972. Chemical Reaction Engineering. John Willey and Sons, New York.

Montgomery, D.C., 1976. Design and Analysis of Experiments. John Wiley and Sons, New York.

Montgomery, D.C., 2005. Design and Analysis of Experiments. John Wiley and Sons, New Jersey.

Osseo-Asare, K., 1982. Solution Chemistry of Tungsten Systems. American Society for Metals and the Metallurgical Society of AIME. Metallurgical transactions B. Vol.13B, pp. 555-564.

Rudiger, O., Hirschfeld, D., Hoffmann, A., Kolaska, J., Ostermann, G., Willbrand, J., 1971. Composition and Properties of The Binder Metal in Cobalt Bonded Tungsten Carbide in: Modern Developments in Powder Metallurgy, H.H. Hausner (ed.). pp. 215-224.

Tague, N.R., 2004. The Quality Toolbox, Second Edition, ASQ Quality Press, Wisconsin.

Tomlinson W, Ayerst N (1989) Anodic Polarization and Corrosion of WC-Co Hard Metals Containing Small Amounts of Cr3C2 and/ VC. Journal of Materials Science, Vol. 24, pp. 2348-2354.

Trent E.M (1946) Process of Separating Hard Constituents from Sintered Hard Metals. US Patent No. 2,407,752. 17 September 1946.

Wilkinson, L., 2006. Revising the Pareto chart. American Statistician, Vol. 60, No.4, pp. 332-334.

CHAPTER SEVEN

OPTIMIZATION OF SIGNIFICANT FACTORS

USING RSM AND CCRD

7.1 Introduction

Designing systems and products requires a deep understanding of influences that achieve a desirable performance. Based on this understanding, modeling and optimization of system influences to increase performance efficiency is extremely important. This, coupled with the need for an efficient and systematic decision-making approach, drives the need for optimization strategies (Biegler, 2010). Optimization may be defined as finding an alternative with the most cost effective or highest achievable performance under the given constraints, by maximizing desired factors and minimizing undesired ones. The main objective in process optimization is maximization of yield, minimization of variability and overall process improvement (Design Expert®11 manual, 2019).

The main aim of this study was to determine and evaluate the conditions that maximize the recovery of Co from hardmetals. In this study, a statistically-based optimization approach called response surface methodology (RSM) was used in conjunction with the central composite rotatable design (CCRD) in order to model and optimize hardmetal leaching conditions. Response surface methodology is a famous technique used to find optimal conditions by using a quadratic polynomial regression model and is applied after diagnostic or screening experiments (Box et al., 1978). The CCRD is an experimental design used to collect data for building a second order (quadratic) model for the response variable. This chapter used insights gained from the diagnostic or screening experiments conducted in Chapter six to optimize the process conditions for cemented tungsten carbide-cobalt dissolution. The factors identified as being statistically significant in the screening experiments, leaching temperature, leaching time and acid concentration were separated for optimization and the non-significant factors, solid-to-liquid ratio and agitation rate, were kept constant. The experimental procedure followed in this chapter is described in Chapter 3 sections 3.5 and 3.7.2.

7.2 Derivation of the model

Experimental results shown in **Table 7.1** were collected by using the central composite rotatable design (CCRD). The results were used for fitting the second order response and estimating the coefficients of the regression model.

Table 7.1: Observed values for the Co extraction

Factor Levels						Co Extraction (%)	Standard Run
Coded			Actual				
A Temp	B Time	C Acid Conc	A Temp (°C)	B Time (hrs)	C Acid Conc (M)		
-1	-1	-1	65	6	1	6.9	1
+1	-1	-1	82	6	1	13.0	2
-1	+1	-1	65	10	1	11.4	3
+1	+1	-1	82	10	1	21.1	4
-1	-1	+1	65	6	2	8.4	5
+1	-1	+1	82	6	2	16.9	6
-1	+1	+1	65	10	2	13.6	7
+1	+1	+1	82	10	2	24.5	8
-1.682	0	0	60	8	1.5	8.7	9
+1.682	0	0	87	8	1.5	21.6	10
0	-1.682	0	74	4	1.5	7.6	11
0	+1.682	0	74	12	1.5	21.7	12
0	0	-1.682	74	8	0.6	10.7	13
0	0	+1.682	74	8	2.4	16.6	14
0	0	0	74	8	1.5	15.0	15
0	0	0	74	8	1.5	14.2	16
0	0	0	74	8	1.5	15.6	17
0	0	0	74	8	1.5	15.0	18
0	0	0	74	8	1.5	15.3	19
0	0	0	74	8	1.5	14.8	20

The fitted second order model was obtained as:

$$\hat{y} = 14.98 + 4.17x_1 + 3.60x_2 + 1.53x_3 + 0.750x_1x_2 + 0.450x_1x_3 + 0.025x_2x_3 + 0.064x_1^2 - 0.113x_2^2 - 0.467x_3^2 \quad \textbf{(7.1)}$$

Where,

x_1= temperature, x_2 = time and x_3 = acid concentration

Within predictor variable limits:

$$-\lambda \le x_i \le +\lambda; i = 1, 2, 3$$

Where x_i are coded predictor variables and $\lambda = 2^{(k-q)1/4} = 1.682$ (for k = 3, q = 0) is the distance of the axial points from the centre of the CCRD that gives the limits of the valid region under experimentation.

7.2.1 Checking the Adequacy of the Developed Model

The adequacy of the fitted model was carried out using the analysis of variance (ANOVA) shown in **Table 7.2.**

Table 7.2: ANOVA for Quadratic model

Source	Terms	Sum of Squares	Degrees of Freedom	Mean Square	F-value	P-value
Model		455.23	9	50.58	80.67	<0.0001
	x_1	237.03	1	237.03	378.02	<0.0001
	x_2	176.62	1	176.62	281.69	<0.0001
	x_3	32.05	1	32.05	51.12	<0.0001
	x_1x_2	4.510	1	4.510	7.18	0.0231
	x_1x_3	1.62	1	1.62	2.58	0.1391
	x_2x_3	0.0050	1	0.0050	0.0080	0.9306
	x_1^2	0.0582	1	0.0582	0.0929	0.7668
	x_2^2	0.1847	1	0.1847	0.2946	0.5992
	x_3^2	3.14	1	3.14	5.01	0.0492
Residual		6.27	10	0.6270		
Lack of fit		5.14	5	1.03	5.46	0.0608
Pure error		1.13	5	0.2257		
Cor Total		461.50	19	-		

For each source of terms, the probability (P-value) was examined to see if it fell below the chosen statistical significance level. For a statistical significance with a confidence level limit of 95%, the probability (P-value) was examined against a factor of 0.05 (5%). P-values less than 0.05 indicate model terms are significant. In this case, x_1, x_2, x_3, x_1x_2, x_3^2 were found to be significant model terms. Values greater than 0.1 indicate model terms are not significant.

The Model P value of <0.0001 and Model F-value of 80.67 implies the **model** is significant.
The Lack of Fit **F-value** of 5.46 implies the Lack of Fit is not significant. Non-significant Lack of Fit is good. It shows that the model fits.

To obtain a simple and yet realistic model, the fitted model was re-fitted using only the variable terms that were significant and is presented in **Table 7.3**.

Table 7.3: ANOVA for the re-fitted Quadratic model

Source	Terms	Sum of Squares	Degrees of Freedom	Mean Square	F-value	P-value
Model		454.96	6	75.83	150.70	<0.0001
	x_1	237.03	1	237.03	471.06	<0.0001
	x_2	176.62	1	176.62	351.01	<0.0001
	x_3	32.05	1	32.05	63.70	<0.0001
	x_1x_2	4.50	1	4.50	8.94	0.0104
	x_1x_3	1.62	1	1.62	3.22	0.0960
	x_3^2	3.14	1	3.14	6.23	0.0268
Residual		6.54	13	0.5032		
Lack of fit		5.41	8	0.6766	3.00	0.1209
Pure error		1.13	5	0.2257		
Cor Total		461.50	19	-		

The lack of fit for the re-fitted model was examined using the probability value (P-value), given as 0.1209 in the table. This is greater than 0.05, indicating that the model does not present any evidence of lack of fit. The significance of the re-fitted regression model was also examined using the probability value (P-value). The obtained value of <0.0001 is less than 0.05, indicating that the regression model is significant at a confidence level limit of 95%. In this case, x_1, x_2, x_3, x_1x_2, x_3^2 are significant model terms. Values greater than 0.1 indicate model terms are not significant. The model term $\boldsymbol{x_1x_3}$ is less than 0.1. It is within acceptable limits and therefore it is retained based on the experimenter's discretion.

The Fit Statistics for the re-fitted model are listed in **Table 7.4.**

Table 7.4: Fit Statistics for the re-fitted model

Std. Dev.	0.7094		**R^2**	0.9858
Mean	14.63		**Adjusted R^2**	0.97934
C.V%	4.85		**Predicted R^2**	0.9598
			Adequacy Precision	44.2946

The Fit Statistics, presented in **Table 7.4**, show a low standard deviation value of 0.71 and a high R-squared value of 98.58%. This indicates that the model is statistically plausible to define the true behaviour of the experimental system. The adequacy precision ratio measures the signal to noise ratio. A ratio greater than 4 is desirable. The ratio of 44.29 indicates an adequate signal and therefore this model can be used to navigate the design space. This means that the cobalt extraction values at any regime in the interval of the experiment design can be calculated from **Equation 7.2**.

Final Equation in terms of coded factors

The final equation of the re-fitted model in terms of coded factors is:

$$\hat{y} = 14.95 + 4.17x_1 + 3.60x_2 + 1.53x_3 + 0.75x_1x_2 + 0.45x_1x_3 - 0.46x_3^2 \quad (7.2)$$

The equation in terms of coded factors can be used to make predictions about the response (% Co extraction) for given levels of each factor. In **Equation 7.2**, the negative sign in the prediction model equation indicates that in order to maximize leaching of Co from cemented carbide, these factors must be kept in low levels. The positive signs mean that the factors must be kept at high levels. The coded equation is useful for identifying the relative impact of the factors by comparing the factor coefficients. The coefficient estimate represents the expected change in response per unit change in factor value when all remaining factors are held constant. The intercept is the overall average response of all the runs. The coefficients are adjustments around that average based on the factor settings (Design Expert®11 manual, 2019).

Final Equation in terms of actual factors

The final equation of the re-fitted quadratic model in terms of actual factors is:

$$\hat{y} = -6.605 - 0.022(Temp) - 1.445(Time) + 0.829(Acid\ conc) + 0.044(Temp)(Time) + 0.106(Temp)(Acid\ conc) - 1.849(Acid\ conc)^2) \quad \textbf{(7.3)}$$

Equation 7.3 in terms of actual factors can be used to make predictions about the response for given levels of each factor. Here, the levels should be specified in the original units for each factor. For example, temperature (degrees centigrade); time (hours); acid concentration (Molarity). This equation should not be used to determine the relative impact of each factor because the coefficients are scaled to accommodate the units of each factor and the intercept is not at the centre of the design space.

7.2.2 Statistical Properties of the Model

7.2.2.1 Normal Plot of Residuals

A residual is the difference between the observed value and the predicted value. The normal probability plot of residuals is a graphical technique to identify substantive departures from normality. This includes identifying outliers, skews, etc. If the plot is close to a straight line, the data is normally distributed. Deviations from a straight line suggest departures from normality (Design Expert®11 manual, 2019).

Figure 7.1 is a normal plot of residuals. As illustrated in the figure, all residues lie close to the straight line with a linear correlation coefficient of 95.63%, which shows that the residuals were distributed normally.

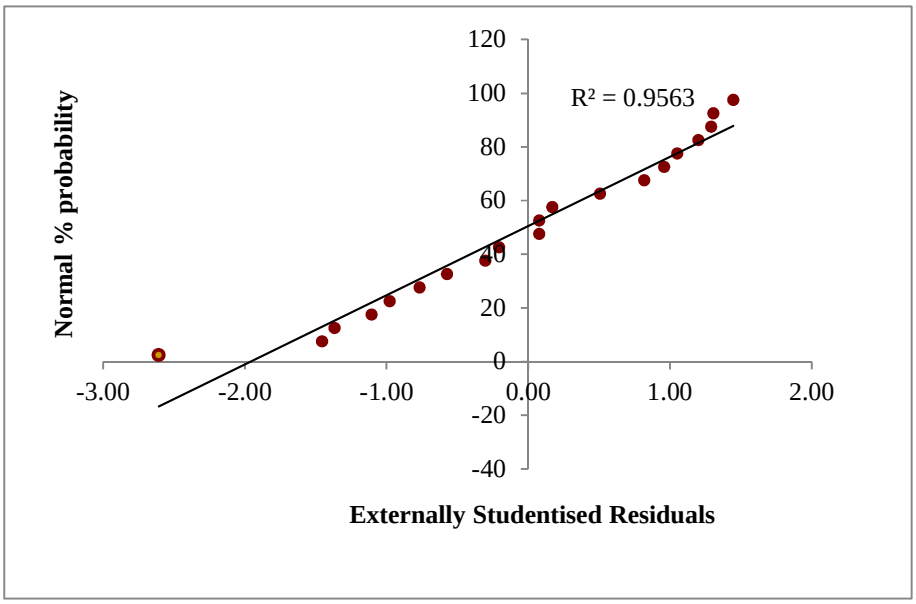

Fig.7.1: Normal plot of residuals

7.2.2.2 Residuals vs Run

Figure 7.2 is a plot of residuals vs run number. The plot can be used to check on runs that appear to be outliers (Design Expert®11 manual, 2019) like the run highlighted in **Figure 7.1**. Although the highlighted run does differ more from its predicted value than any other, **Figure 7.2** shows that there's no cause for alarm because it is within the upper and lower control limits.

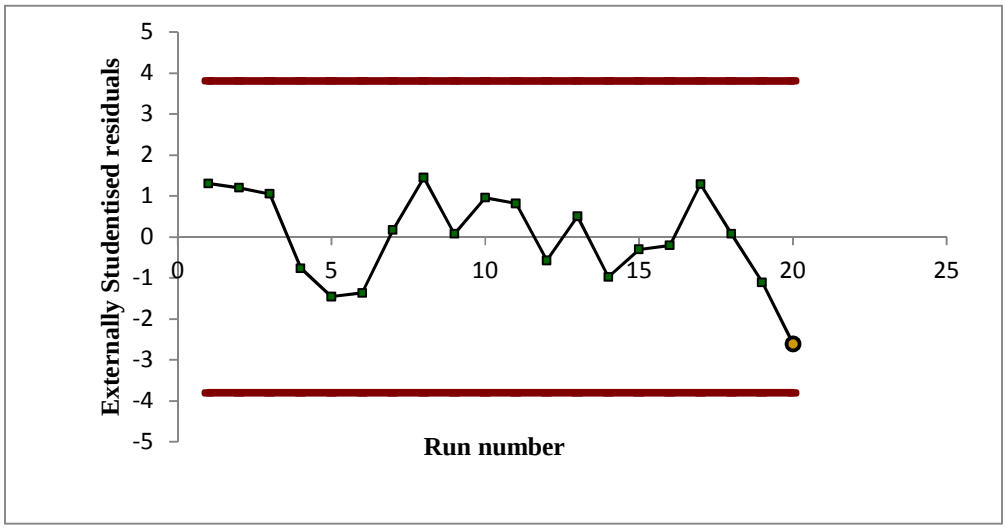

Fig.7.2: Residuals vs run

7.2.2.3 Predicted vs Observed

Experimental results and predicted values, obtained using the re-fitted model, are given in **Table 7.5**. The relationship between experimental and predicted Co extraction is presented in **Figure 7.3**. The figure shows that the predicted values are reasonably comparable to the experimental values with the linear correlation coefficient (R^2) of 0.9858. Statistically, this means that 98.6 % of the sample variation can be explained by the independent variables.

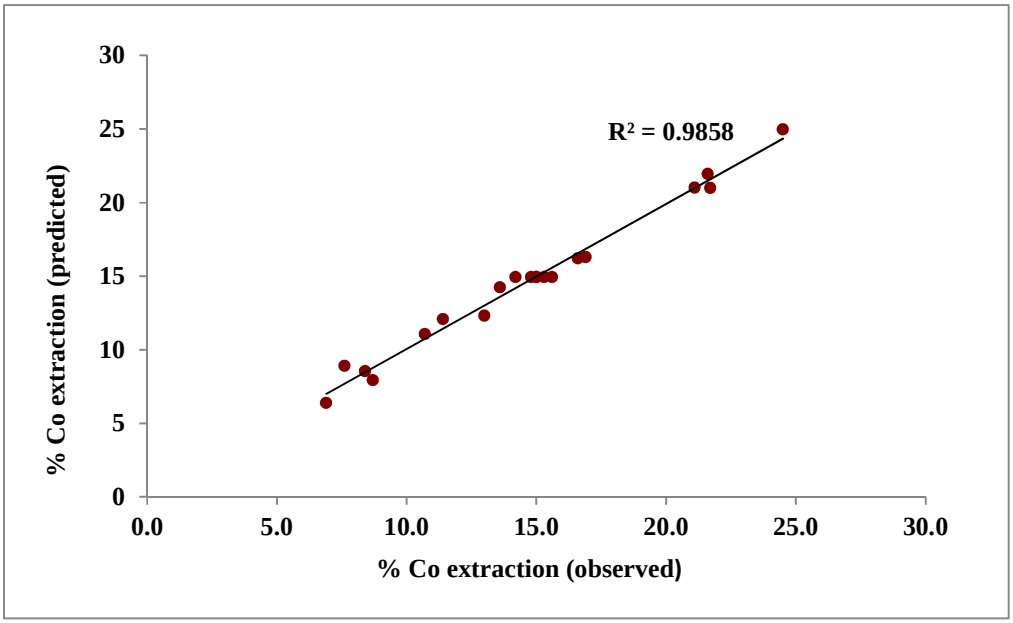

Fig.7.3: Relationship between experimental (observed) and predicted cobalt extraction

Table 7.5: Observed and predicted values for cobalt extraction

Factor Levels						Cobalt Extraction (%)		Standard Run
Coded			Actual			Observed	Predicted	
A (Temp)	B (Time)	C Acid Conc (M)	A Temp (°C)	B Time (hrs)	C Acid Conc (M)			
-1	-1	-1	65	6	1	6.9	6.4	1
+1	-1	-1	82	6	1	13.0	12.3	2
-1	+1	-1	65	10	1	11.4	12.1	3
+1	+1	-1	82	10	1	21.1	21.0	4
-1	-1	+1	65	6	2	8.4	8.6	5
+1	-1	+1	82	6	2	16.9	16.3	6
-1	+1	+1	65	10	2	13.6	14.3	7
+1	+1	+1	82	10	2	24.1	25.0	8
-1.682	0	0	60	8	1.5	8.7	7.9	9
+1.682	0	0	87	8	1.5	21.6	22.0	10
0	-1.682	0	74	4	1.5	7.6	8.9	11
0	+1.682	0	74	12	1.5	21.7	21.0	12
0	0	-1.682	74	8	0.6	10.7	11.1	13
0	0	+1.682	74	8	2.4	16.6	16.2	14
0	0	0	74	8	1.5	15.0	15.0	15
0	0	0	74	8	1.5	14.2	15.0	16
0	0	0	74	8	1.5	15.6	15.0	17
0	0	0	74	8	1.5	15.0	15.0	18
0	0	0	74	8	1.5	15.3	15.0	19
0	0	0	74	8	1.5	14.8	15.0	20

7.2.2.4 Perturbation Plot

A perturbation plot (**Figure 7.4**) shows all variable factors on one response plot. The plot provides silhouette views of the response surface. For response surface designs, the perturbation plot shows how the response changes as each factor moves from the chosen reference point, with all other factors held constant at the reference value. The reference point is at the middle of the design space, coded zero level of each factor (Design Expert®11 manual, 2019). In this case, at the center point, it can be seen that factor C (acid conc.) produces a relatively small effect, compared to factor A (temperature) and factor B (time), as it changes from the reference point.

This is in agreement with the earlier observation made in the preliminary tests in section 4.6.3.1 **Figure 4.4** where it was noted that increase in acid concentration did not yield a significant change in Co dissolution.

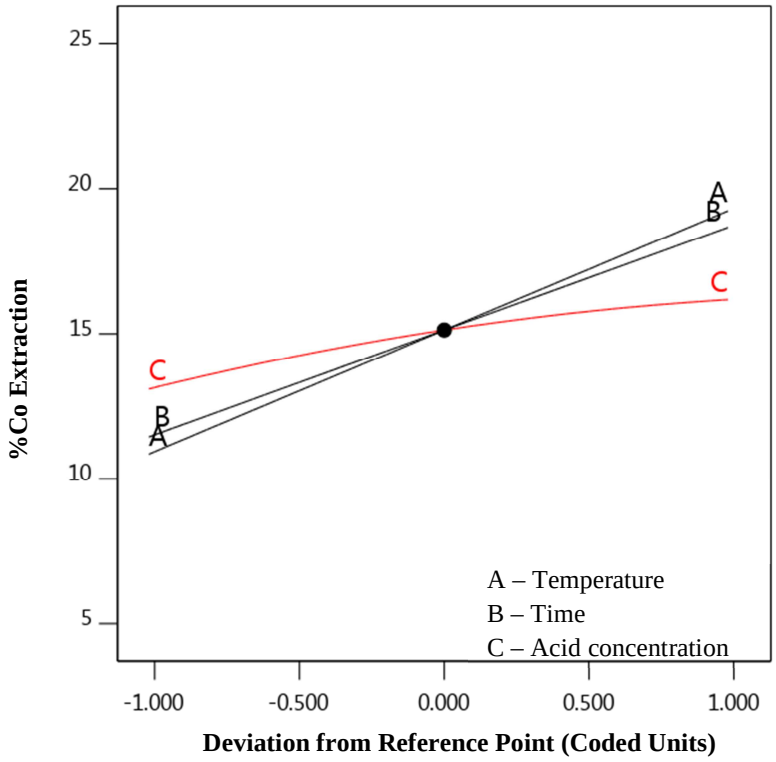

Fig.7.4: Perturbation plot for factors A (temperature), B (time) and C (acid conc.)

7.2.2.5 Three-Dimensional Surface Plot

A response can be displayed in a three-dimensional (3D) view. The 3D surface plot shows how the response (Co extraction) varies as a function of two factors, A and C, in **Figure 7.5 (a)**; A and B in **Figure 7.5 (b)**. The surface plot displays coordinates as actual or coded design points. The 3D response surface plot presents a compelling picture of how the response (% Co extraction) can be maximized. In both 3D views, where the response varies as a function of two factors, temperature showed a much stronger impact on the Co extraction efficiency.

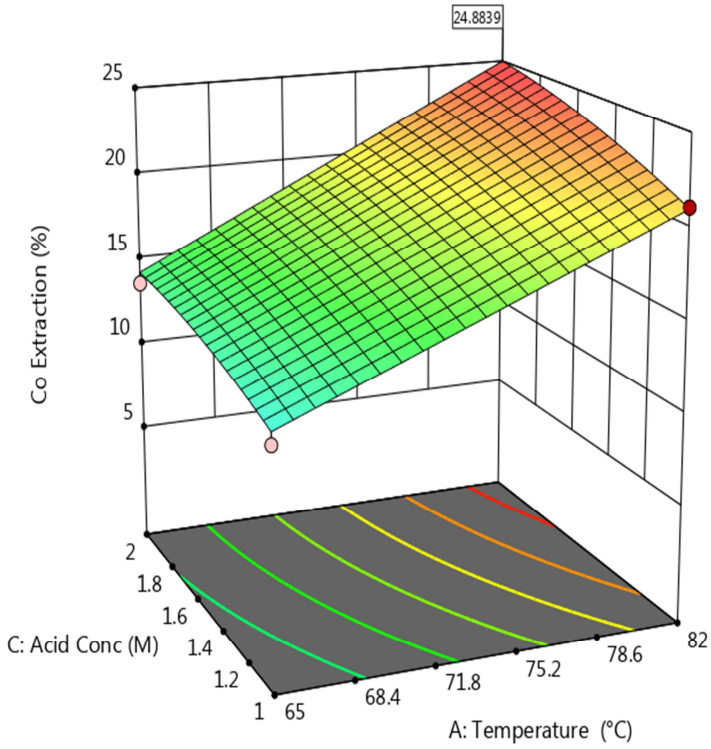

Fig.7.5 (a): 3D surface plot (acid conc vs temp)

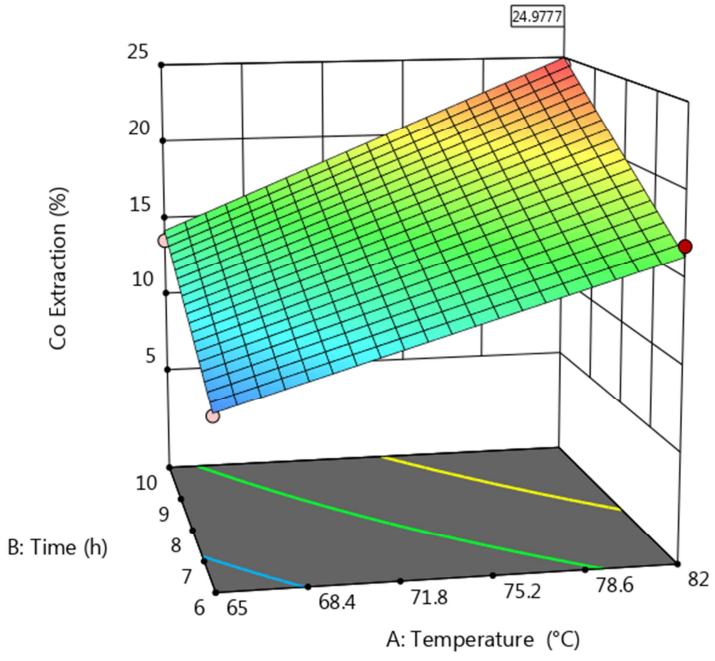

Fig.7.5 (b): 3D surface plot (time vs temp)

7.3 Determination of Optimum Conditions

The major objective of the study described in this chapter was to determine the conditions that maximize cobalt extraction from the binary-phase cemented carbide (WC-6%wt.Co). After the model was checked for adequacy of fit in the region defined by the coordinates of the design and was found to be adequate, the model was used to locate the point of maximum response.

For quadratic regression models, the point for which the response is optimized is the point at which the partial derivatives $\frac{\partial \hat{y}}{\partial x_1}, \frac{\partial \hat{y}}{\partial x_2}, \ldots \frac{\partial \hat{y}}{\partial x_k}$, are all *equal to zero*. This point is called the *stationary point*. The stationary point may be a point of maximum response, minimum response or a saddle point. These conditions are easy to identify in the case of two factor experiments, by the inspection of contour plots. When more than two factors exist in an experiment, a mathematical or numerical solution for the location of the stationary point can be used (Khuri and Cornell, 1987. In the current study, a numerical solution was employed in locating the points at which the response was optimum.

7.3.1 Numerical Optimization

Numerical optimization will maximize, minimize, or target a desired response by setting optimization criteria for all variable factors and the response. Factor ranges are restricted to coded factorial levels of +1 to -1. This is the region for which this experimental design provides the most precise predictions (Design Expert®11 manual, 2019). Response ranges are based on the experimenter's discretion. For process yield, response ranges are often set close to 100% but could be lower depending on process limitations.

Figure 7.6 is the numerical optimization view for optimum actual factor levels and optimum Co extraction response. Factor desirability levels that give the optimum response are shown in **Figures 7.7 (a) and 7.7 (b)**. Desirabilities range from zero to one for any given response. A value of one represents the ideal case. A zero indicates that the response falls outside desirable limits.

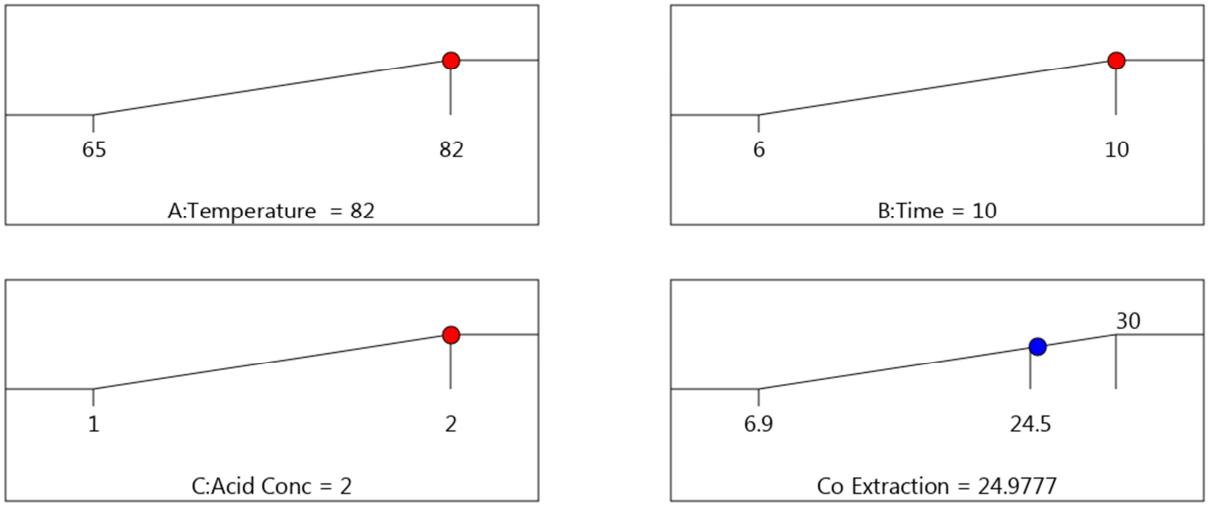

Fig. 7.6: Numerical optimum levels for factors A, B, C and the Co extraction response

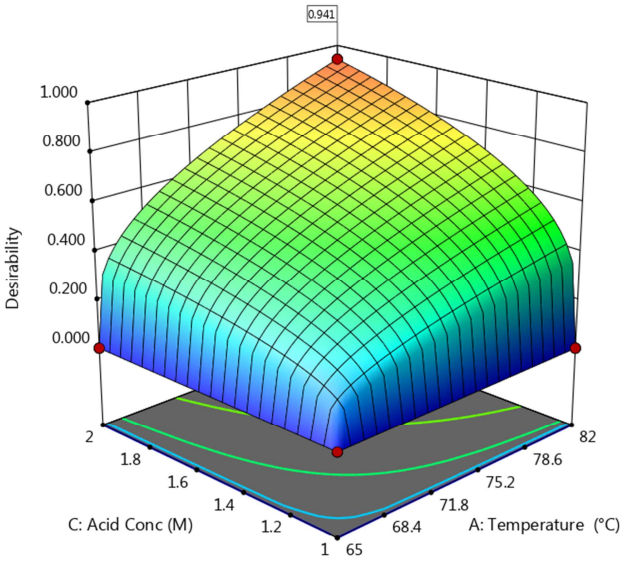

Fig.7.7 (a): Factor desirability levels (acid, temp)

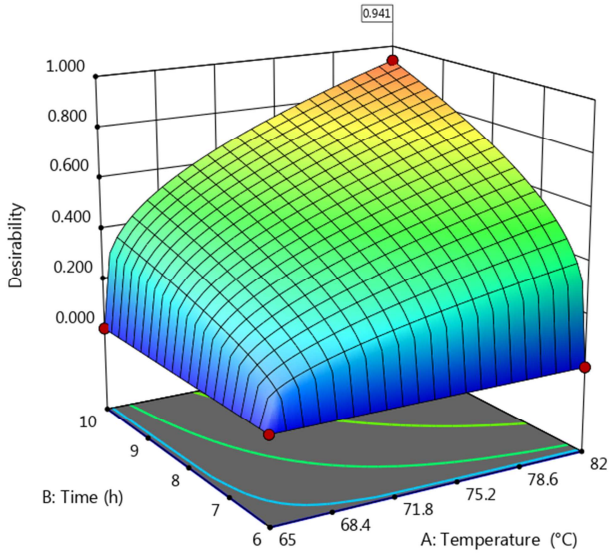

Fig.7.7 (b): Factor desirability levels (time, temp)

Factor desirability levels that give the optimum response were found to be 0.941, in both cases, suggesting that the levels were well within desirable limits.

Analysis of **Figure 7.6** shows that the coded values are $x_1 = 1$, for optimum temperature; $x_2 = 1$ for optimum time and $x_3 = 1$ for optimum acid concentration. The actual values are 82°C for optimum temperature, 10hrs for optimum time and 2M for optimum acid concentration.

Using coded values in **Equation 7.2**,

Predicted Co extraction, $\hat{y}$ = **24.99% ~ 25.0%**

Using actual values in **Equation 7.3,**

Predicted Co extraction, $\hat{y}$ = **24.98% ~ 25.0%**

7.3.2 Confirmatory Experiments

In order to test the validity of the optimized conditions given by the model, replicated experiments were carried out with parameters suggested by the model. The conditions used in the confirmatory experiments were as follows: temperature (82°C), time (10hrs) and acid concentration (2M).

The Co extraction after leaching at a solid to liquid ratio of 1:10 and agitation rate of 750rpm was found to be 24.13% (**Table 7.6**), which is consistent with the model. With an error margin of 0.90% between the predicted value and the confirmatory test value, the model fits the experimental data very well, and can therefore be considered to be acceptably valid.

Table 7.6: Cobalt extraction at optimum leaching conditions

Parameter	Temperature (°C)	Time (hrs)	Acid Concentration (M)	% Co Extraction
Model	82	10	2	25.0
Confirmatory tests	82	10	2	24.13

The optimum cemented carbide leaching conditions are illustrated in **Table 7.7** and modeled in **Equation 7.4**. These conditions represent an optimized sulphate system for leaching binary-phase cemented carbide. The model can be used as a predictive tool within the limits of the valid region. The model shows the predicted response (**Y**), the intercept, the linear effect, the interaction effect and the quadratic effect.

Table 7.7: Final optimum Leaching conditions

Temperature	82°C
Time	10hrs
H_2SO_4 concentration	2M
Solid to Liquid Ratio	1:10
Agitation Rate	750rpm
Predicted Co Extraction	25.0%

$$Y = 14.95 + (4.17x_1 + 3.60x_2 + 1.53x_3) + (0.75x_1x_2 + 0.45x_1x_3) - 0.46x_3^2 \quad \textbf{(7.4) (Predictive model)}$$

Although the above model may not be used to make predictions outside its valid region, the optimum conditions could be employed to test the effect of lactic acid dosage, H_2O_2 dosage, HCl dosage, HNO_3 dosage and effect of higher temperature. In the current study, the optimum conditions were used to determine the extent of Co extraction and associated recycle time, effect of lactic acid dosage and effect of higher temperature.

7.4 Testing the sulphate leaching system

7.4.1 Extent of Co dissolution and recycle time

To study the extent of Co dissolution and recycle time under optimum conditions, experiments were carried out at optimum leaching conditions displayed in **Table 7.10** and compared against the Co extraction profile obtained under non-optimum conditions. The results are displayed in **Figure 7.8**. The figure shows that, under non-optimum conditions, 97.8% Co was extracted in 9 days whereas 97.6% could be extracted in 4.2 days under optimum conditions. The results demonstrate that under optimum conditions, almost the same amount of Co could be extracted in approximately half the time required under non-optimum conditions.

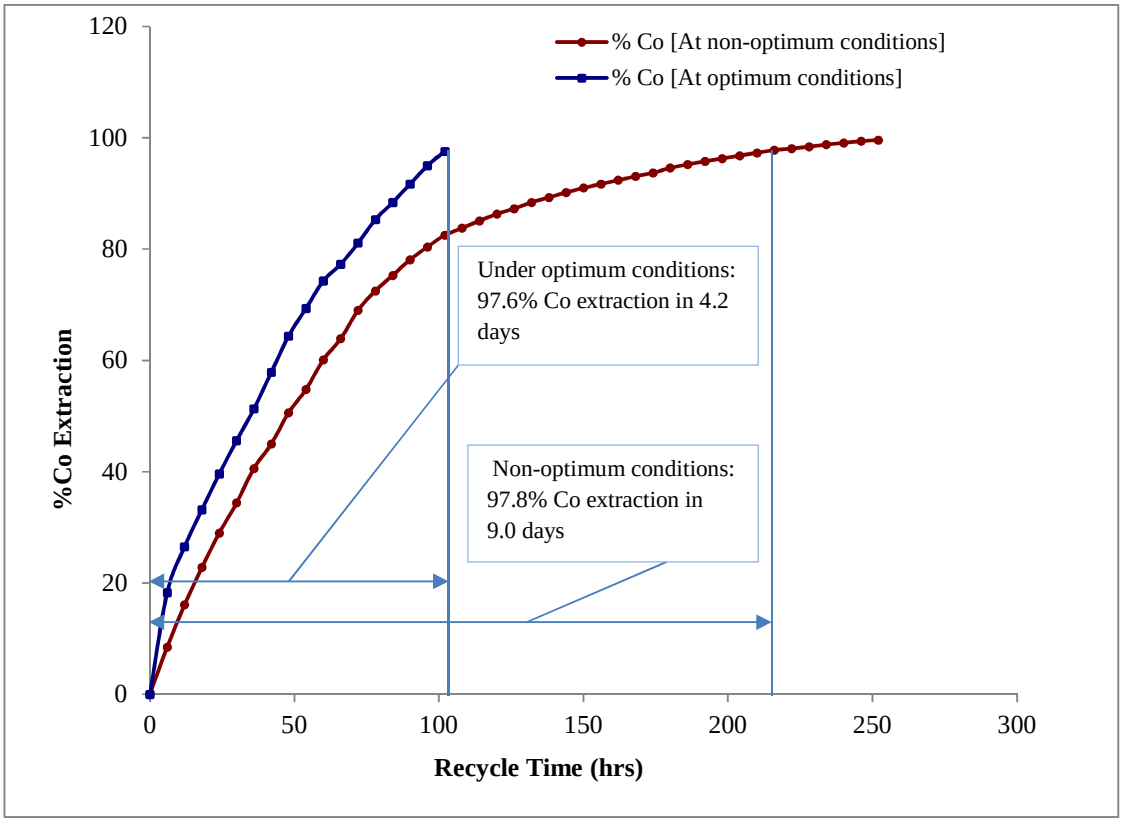

Fig.7.8: Co dissolution as a function of time

7.4.2 Effect of lactic acid dosage

To investigate the effect of lactic acid dosage on Co dissolution under optimum conditions, experiments were performed using a lactic acid dosage of 5% (v/v) and 10% on the sulphate system. The results are exhibited in **Figure 7.9**. The figure shows that 5% lactic acid dosage performed better than the 10% dosage but both lactic acid dosages were outperformed by sulphuric acid leaching without any dosage. Analysis of the figure shows that when dosed with lactic acid, the organic ligand has a noticeable effect in the initial stages. Lactic acid at 5% dosage the system performed better than sulphuric acid alone in the first 1 hour. At 10% lactic acid dosage, the system performed better in the first 30 minutes. The initial good performance of the lactic acid dosed system seems to indicate that the organic ligand was more effective on the surface of the cemented carbide solid pieces but became ineffective as leaching progressed below the surface region into the inner core. The decrease in Co extraction efficiencies with

increasing time might be attributed to high solution viscosity and poor diffusion in the minute channels within the solid mass of cemented carbide pieces.

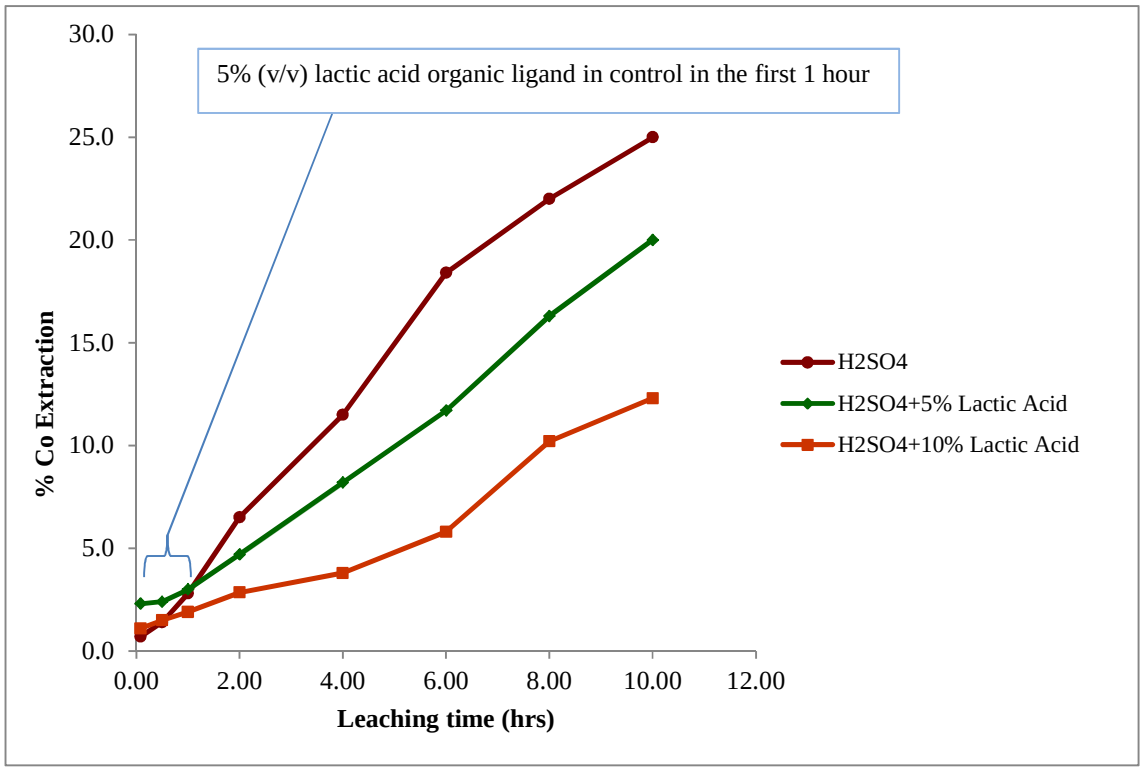

Fig.7.9: Leaching Profiles of H_2SO_4 vs [H_2SO_4 + 5% (v/v) Lactic Acid]

7.4.3 Effect of higher temperature

To investigate the effect of leaching at different temperatures under optimum conditions, experiments were carried out from at 82°C and 92°C. The results in **Figure 7.10** show that the dissolution of Co at 92°C using sulphuric acid only increased sharply and gave a Co extraction of 31.7% compared to 25.0% at 82°C. Results further show that higher temperature did not improve Co extraction much for the leaching solution with a 5% lactic acid dosage. It is evident that temperature has a stronger effect on Co extraction than lactic acid dosage.

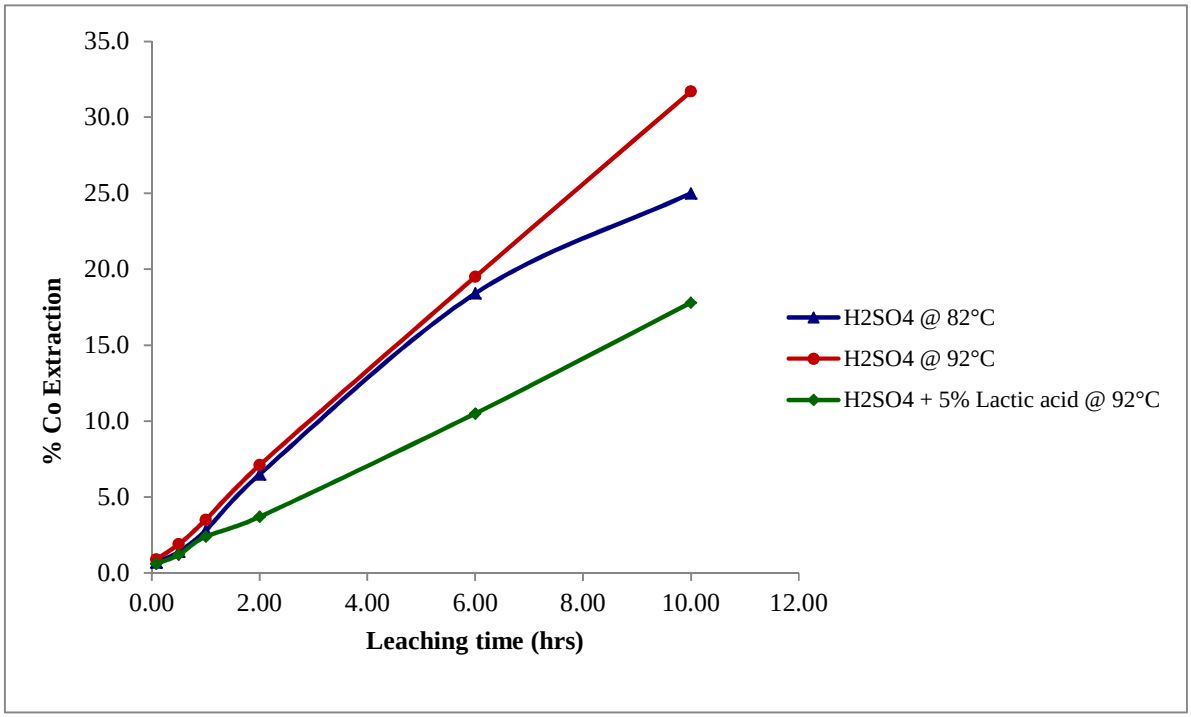

Fig.7.10: Leaching Profiles at different temperatures

7.4.5.4 Co extraction and associated recycle times

A comparison of Co extraction efficiencies and associated recycle times for the current study and other cemented carbide leaching systems is presented in **Table 7.11**. Projections from the current study show that relatively higher Co extractions within shorter recycle times are attainable with the sulphate system and could even perform better than other systems shown in **Table 7.8**. However, this might require much lower lactic acid dosages as clearly seen in **Figure 7.9**.

Table 7.8: Co extraction efficiencies and associated recycle (leaching) time

Processing Method	Temperature (°C)	Co Extraction Efficiency (%)	Associated recycle time (days)	Material Type
Acetic acid system	40-80	85.0	4.6	Ternary phase cemented carbide-solid mass (Edtmaier et al, 2005)
Acetic acid system	80	-	21	Zinc recycling process rejects-solid mass (Freemantle and Sacks, 2015)
HCl system	110	-	1	Hardmetal scrap (Kojima et al, 2005)
HNO_3 system	25	91.5	0.08	Cemented carbide scrap-powder (<90μm) (Gurmen and Friedrich, 2005)
Malic acid system	70	98.0	6	Pre-treated WC-Co cutting tool scrap-solid mass (Seo and Kim, 2016)
H_2SO_4 system	82	97.6	4.2	Binary phase cemented carbide-solid mass (current study)
H_2SO_4 system	92	98.0	1.5	Binary phase cemented carbide-solid mass (current study)

7.5 Summary

In this chapter, insights gained from the diagnostic or screening experiments were used to model optimum cemented carbide leaching conditions. Three factors identified as being statistically significant and earmarked for optimization were temperature, time and acid concentration. Optimization involved the use of RSM in conjunction with CCRD.

A second order model representing Co extraction expressed as a function of the three variables was developed by quadratic programming using Design Expert® 11. The derivation of the model was estimated by fitting experimental results.

The adequacy of the fitted model was carried out using the analysis of variance (ANOVA) and was found to be statistically plausible to define the true behaviour of the experimental system.

The statistical properties of the model were tested using the normal plot of residuals, residuals vs run, predicted vs observed values, the perturbation plot and the three-dimensional surface plot.

The optimum leaching conditions determined using the numerical optimization technique were found to be 82°C, leaching temperature; 10hrs, leaching time and 2M, sulphuric acid concentration.

The validity of the model was tested using confirmatory experiments. The model prediction for Co extraction using the optimum conditions was 24.13% and the extraction obtained experimentally was 24.9%. Within an error margin of less than 5% between the predicted value and the confirmatory test value, the model fitted the experimental data very well and was therefore considered to be acceptably valid.

Using the optimum conditions, the sulphate leaching system was used as a basis to evaluate the extent of Co extraction and recycle time as well as the effects of lactic acid dosage and higher leaching temperature.

Projected results from the current study showed that up to 98% Co extraction from a solid mass of cemented carbide hardmetal is possible within 1.5 days. This is relatively better performance than known systems currently documented in literature.

The lactic acid dosage of 5% (v/v) showed better performance compared to sulphuric acid leach solution within the first hour of leaching but, decreased with increasing leaching time. The decrease in performance was attributed to high organic acid viscosity leading to poor diffusion within channels of the inner core of the cemented carbide solid mass.

Higher leaching temperature resulted in a marked increase in Co extraction from 25% to 31.7% within 10 hrs of leaching indicating that temperature is the key driving force to effective cemented carbide dissolution. Results further showed that temperature had a stronger effect on Co extraction compared to the effect of lactic acid dosage.

The study in this chapter is a culmination of the preceding preliminary and screening tests as well as a precursor to subsequent purification, regeneration and recovery processes that follow in the next chapter.

7.6 References

Biegler, L.T., 2010. Nonlinear programming. Concepts, Algorithms, and Applications to Chemical Processes. MOS-SIAM, Philadelphia.

Box, G.E.P., Hunter, W.G., Hunter, J.S., 1978. Statistics for Experimenters: An Introduction to Design, Data Analysis and Model Building. John Wiley and Sons, New York.

Design Expert® 11 Manual., 2019. Internet Version <http://www.statease.com>. Stat-Ease, Incorporation, Minneapolis. Retrieved 10 November 2019.

Edtmaier, C., Schiesser, R., Meissl, C., Schubert, W.D., Rock, A., Schoen, A., Zeiler, B., 2005. Selective Removal of the Cobalt Binder in WC-Co Based Hard Metal Scraps By Acetic Acid Leaching. Hydrometallurgy, Vol. 76, pp. 63-71.

Freemantle, C., Sacks, N., 2015. Recycling of Cemented Tungsten Carbide Mining Tool Scrap. The Journal of The South African Institute of Mining and Metallurgy, Vol. 115, pp. 1207-1213.

Gurmen, S., 2005. Recovery of Nano-Sized Cobalt Powder from Cemented Carbide Scrap. Turkish Journal of Engineering and Environmental Science. Vol.29, pp. 343-350.

Khuri, A. I., Cornell, J. A., 1987. Response Surfaces: Designs and Analyses. Marcel Dekker, Inc., New York.

Montgomery, D.C., 1976. Design and Analysis of Experiments. John Wiley and Sons, New York.

Seo, B., Kim, S., 2016. Cobalt Extraction from Tungsten Carbide-Cobalt (WC-Co) Hard Metal Scraps Using Malic Acid. International Journal of Mineral Processing, Vol. 151, pp. 1-7.

CHAPTER EIGHT

RECOVERY OF WC, Co AND W FROM CEMENTED TUNGSTEN CARBIDE SECONDARY MATERIAL

8.1 Introduction

Binary-phase cemented tungsten carbide contains carbide and cobalt, typically: WC (85-95 wt %), Co (5-15 wt %). This chapter discusses the recovery of these valuable resources using insights gained from Chapters 1-7. The recovery process was undertaken in six stages: (1) Leaching of cemented carbide scrap button inserts for the selective extraction of Co into solution and recovery of the WC residue in powder form. (2) Regeneration of the unreacted organic acid. (3) Precipitative purification of the leach solution. (4) Solvent extraction of Co from the leach solution. (5) Electro-recovery of the dissolved Co metal. (6) Precipitative recovery of the dissolved W metal as scheelite. The experimental procedure followed in this chapter is described in Chapter 3 sections 3.6.4 and 3.7.2.

8.2 Resource Recovery Stages

8.2.1 Recovery of tungsten monocarbide (WC)

The recovery of the WC hard phase from cemented tungsten carbide button inserts involved selective dissolution of the Co binder from the hardmetal. The Co was dissolved chemically, leaving the WC hard phase intact. The possible reactions (Ghandehari and Schussler, 1980; Suzuki and Kubota, 1966; Kellner et al, 2009; Viswanadham et al, 1983; Exner, 1979) are presented as:

(i) The WC aggregate phase:

$$2WC\text{-}Co + O_{2(g)} + 4H^{+} \rightarrow 2Co^{2+} + 2WC + 2H_2O_{(l)} \quad (8.1)$$

(ii) The cobalt binder phase (matrix):

$$2Co_{(s)} + O_{2(g)} + 4H+ \rightarrow 2Co^{2+} + 2H_2O_{(l)} \quad (8.2)$$

(iii) The 'Co-W-C alloy' binder phase (matrix)

$$2Co_{(s)} + O_{2(g)} + 4H+ \rightarrow 2Co^{2+} + 2H_2O_{(l)} \quad (8.3)$$

$$3W(s) + 4O_{2(g)} + 12H^{+}_{(aq)} \leftrightarrows WO_{2(s)} + 6H_2O_{(l)} + 2W^{6+}_{(aq)} \quad (8.4)$$

8.2.2 Reagent Regeneration

Distillation, which involves evaporation and condensation, was used in the regeneration of the lactic acid organic reagent. Evaporation and condensation are physical processes which do not involve a chemical reaction. The processes are presented as:

$$C_3H_6O_{3\,(aq)} \xrightarrow{\text{heating}} C_3H_6O_{3\,(g)} \qquad (8.6)$$

$$C_3H_6O_{3\,(g)} \xrightarrow{\text{cooling}} C_3H_6O_{3\,(aq)} \qquad (8.7)$$

8.2.3 Impurity removal from leach liquor

The precipitation of iron was based on the Monhemius (1977) diagram for precipitation of metal salts. The most widely employed flowsheets use sequential metal hydroxide precipitation to remove impurities from the Co stream (Sole et al, 2019). The Co solution is first bubbled with air and SO_2 in order to oxidize iron to the 3+ state. Fe (III) is removed from the Co solution using lime or sodium hydroxide at pH 3-4.5 (Sole et al, 2019). The possible iron (III) precipitation reaction is presented as:

$$Fe^{3+} + 3OH^- \leftrightarrows Fe(OH)_{3(s)} \qquad (8.5)$$

8.2.4 Solvent extraction

Solvent extraction was conducted after reagent regeneration and iron precipitation. The extraction of Co from the aqueous phase using Cyanex 272 extractant proceeded according to the reaction:

$$2RH_{(org)} + Co^{2+}{}_{(aq)} \leftrightarrows R_2Co(org) + 2H^+{}_{(aq)} \qquad (8.8)$$

The stripping of Co from the organic phase using sulphuric acid proceeded according to the reaction:

$$R_2Co(org) + 2H^+{}_{(aq)} \leftrightarrows 2RH_{(org)} + Co^{2+}{}_{(aq)} \qquad (8.9)$$

Where, R represents the Cyanex 272 organic extractant

8.2.5 Electrorecovery of Co metal

Electrodeposition of Co takes place at the cathode. The main cathodic reactions are represented as (Sole et al, 2019; Moskalyk and Alfantazi, 2000):

$$Co^{2+} + 2e^- = Co \qquad E° = -0.28V \qquad (8.10)$$

$$2H^+ + 2e^- = H_2 \qquad E° = 0.00V \qquad (8.11)$$

At the cathode, hydrogen evolution is in competition with the cobalt deposition (**Eqn. 8.11**). This is not desirable because it represents a loss of current usage and it must be kept to a minimum. Therefore, the use of a high Co concentration in the electrolyte, high temperature, and high current density can reduce the tendency for this reaction to occur. Other process conditions, including pH control and the addition of organic and/or inorganic additives, allow efficient current utilization (Sole et al, 2019; Moskalyk and Alfantazi, 2000).

At the anode, water is oxidized to produce oxygen. In a sulphate system, the main anodic reaction is represented as (Sole et al, 2019):

$$2H_2O = O_2 + 4e^- + 4H^+ \qquad E° = -1.23V \qquad (8.12)$$

The overall cell reaction is represented as:

$$2CoSO_4 + 2H_2O = 2Co + O_2 + 2H_2SO_4 \qquad E° = -1.51V \qquad (8.13)$$

8.2.6 Precipitative recovery of tungsten (W) by scheelite synthesis

Dissolved W may be precipitated as scheelite ($CaWO_4$) using $Ca(OH)_2$ or $CaCl_2$ as precipitants (Wan et al, 2015; Martins et al, 2007). The possible scheelite synthesis reactions are represented as:

$$Na_2WO_{4(aq)} + CaCl_{2(s)} \leftrightarrows CaWO_{4(s)} + 2NaCl_{(aq)} \qquad (8.14)$$

$$Na_2WO_{4(aq)} + Ca(OH)_{2(s)} \leftrightarrows CaWO_{4(s)} + 2NaOH_{(aq)} \qquad (8.15)$$

8.3 Resource Recovery Results

8.3.1 Cemented tungsten carbide leach solution

The cemented tungsten carbide leach solution is shown in **Figure 8.1.** The leach solution is cobalt (II) sulphate. It is a hexahydrate metal aquo complex consisting of octahedral $[Co(H_2O)_6]^{2+}$ ions associated with SO_4^{2-} ions from which it gets its pink colour (Elerman, 1988). The chemical composition of the leach solution is listed in **Table 8.1.** The table shows a concentration of <0.05 ppm for Al, 10.3 ppm for Ca, 1483 ppm for Co, <0.05 ppm for Cu, 62.3 ppm for Fe, 3.67 ppm for Mg, 1.0 ppm for Mn, 5.0 ppm for Ni, <0.001 ppm for Pb, 1.0 ppm for Zn and 9.37 ppm for W. The chemical composition shows Fe as the major impurity. The reactor vessel and accessories could have been a possible source of the impurities observed in the leach solution. A typical chemical composition of a Co stream from a copper-cobalt feed sample leach liquor before purification (Sole et al, 2016) is shown in **Table 8.2**.

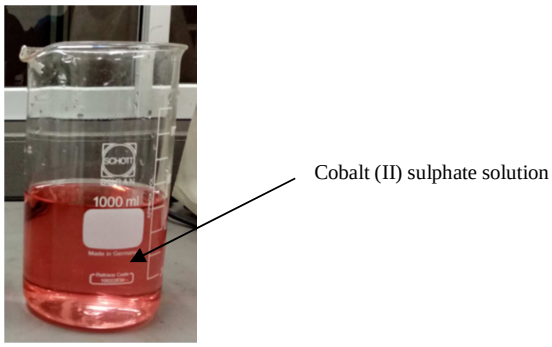

Fig.8.1: Cemented tungsten carbide leach solution

Table 8.1: Chemical composition of cemented tungsten carbide leach liquor

Element	Al	Ca	Co	Cu	Fe	Mg	Mn	Ni	Pb	Zn	W	pH
Conc (ppm)	<0.05	10.3	1483	<0.05	62.3	3.67	1.0	5.0	<0.001	1.0	9.37	0.49

Table 8.2: Typical composition of a cobalt stream before purification (Sole et al, 2016)

Element	Al	Co	Cu	Fe	Mn
Conc (ppm)	1000	2000-3000	200-500	1000-2000	1000

8.3.1.1 Recovery of WC Powder

An image of the recycled WC powder obtained from leaching cemented tungsten carbide button inserts is shown in **Figure 8.2.** The FESEM characterization results of the recycled powder and 'virgin' powder are displayed in **Figures 8.3a** and **8.3b** respectively. The micrograph image of the recycled powder showed that it was well faceted and fine grained with irregular WC particles whereas the 'virgin' WC powder was well faceted, spherical and coarse grained. The grain integrity of the recycled powder compares relatively well with that of the virgin powder. The morphological difference between the two powders is a consequence of two different methods of production processes employed in the making of WC powders as explained by Kurlov and Gusev (2007) and Lassner and Schubert (1999). The authors explain that irregular WC powder grains are produced either by intensive mechanical treatment and annealing or by hydrogen reduction. Spherical WC powders are produced by melt atomization using various methods, such as gas stream atomization, centrifugal atomization or plasma spheroidization. It is evident, from image observation, that the recycled powder was produced from the first method and the virgin powder from the later method.

The chemical composition of the two powders is listed in **Table 8.3.** The composition of the recycled powder is shown as: 57.95%wt.W, 37.02%wt.C, 3.46%wt.O, 1.25%wt.Fe and 0.32%wt.Si. The composition of the 'virgin' powder is shown as: 47.13%wt.W, 45.49%wt.C and 7.39%wt.O. The presence of Fe and Si observed in the recycled powder may have been picked up from the grinding media during pulverization. The recycled powder might require carbon adjustment and the removal of Fe and Si before it can be re-used. Although the 'recycled powders' might not be suitable for manufacturing the same grade of mining tools as those from 'virgin' powders, the 'recycled powders' might find commercial application elsewhere where the presence of Fe and Si is not a big concern. The recycled powders could be adjusted as necessary to increase the cobalt content to produce tougher grades, which can be used for applications that require tools that possess a high fracture toughness, such as milling media, shims and possibly coal and hard-rock mining (Morrison, 2015).

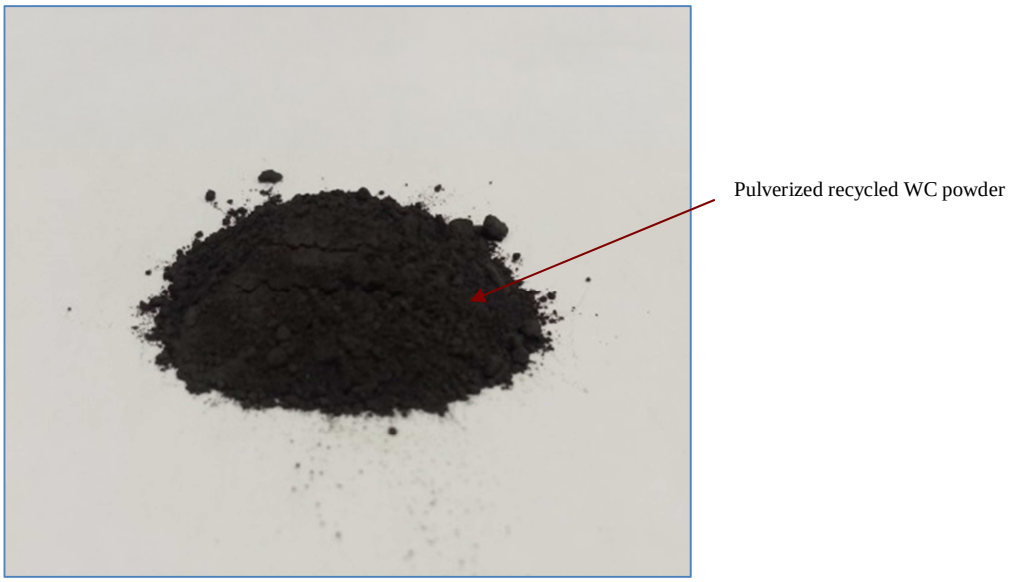

Fig.8.2: Recycled WC powder recovered from cemented tungsten carbide button inserts

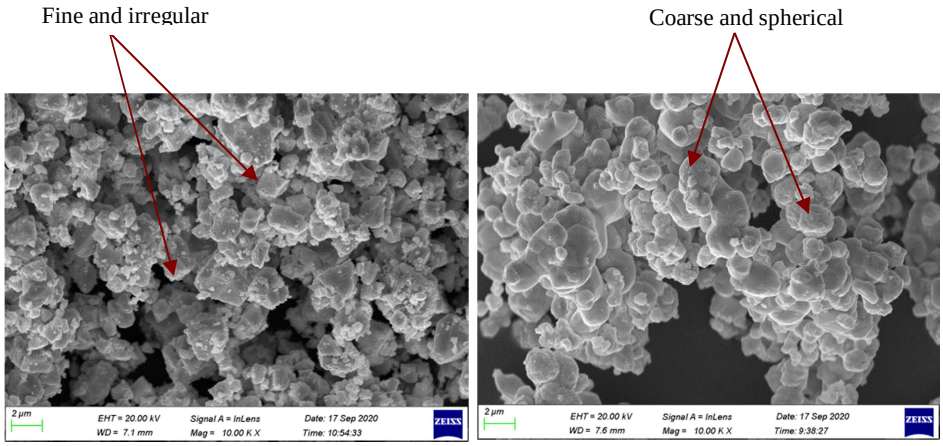

(a) (b)

Fig.8.3: FESEM images of (a) recycled WC powder and (b) virgin WC powder

Table.8.3: Chemical composition of WC powder

Element	Recycled (wt.%)	'Virgin' (wt.%)
Tungsten (W)	57.95	47.13
Carbon (C)	37.02	45.49
Oxygen (O)	3.46	7.39
Iron (Fe)	1.25	-
Silicon (Si)	0.32	-
Total	100	100

8.3.2 Reagent Regeneration

The initial solution for leaching cemented tungsten carbide contained 5% (v/v) lactic acid and 95 % (v/v) 2M H_2SO_4. After 10 hrs of leaching, the lactic acid concentration in 500 mL of leach solution decreased to 0.00055% (v/v) as unreacted acid. Due to the low concentrations in the leach solution, lactic acid had no adverse impact on Co electro-winning. However, due to the sensitive nature of electro-winning processes, higher lactic acid concentrations, which might build up over a period of time, could have an effect and should be avoided. Therefore, it was deemed necessary to recover the remnant unreacted lactic acid from the leach solution. The acid was regenerated by evaporatory means. The regeneration profile is exhibited in **Figure 8.4**. Experimental results showed that 28.9% of lactic acid was recovered after 0.5 hrs, 36.2% after 1 hr, 39.6% after 1.5 hrs, 46.0% after 2 hrs and 66.9% after 2.5 hrs. The rate of regeneration increased considerably after 1.5 hrs. The final lactic acid concentration in 300 mL of the residue solution was calculated as 0.00030% (v/v) and that in 200 mL of the distillate solution was calculated as 0.00092% (v/v).

The regeneration of the organic acid was inevitably accompanied by a solution volume decrease from 500 mL to 300 mL. The solution pH also decreased from pH 0.49 to pH 0.01 after 2.5 hrs of distillation. Further evaporation beyond 2.5 hrs resulted in the formation of $CoSO_4$ crystals. Therefore, to avoid further crystal formation and a decrease in pH, the duration of 2.5 hrs was adopted as the pertinent residence time.

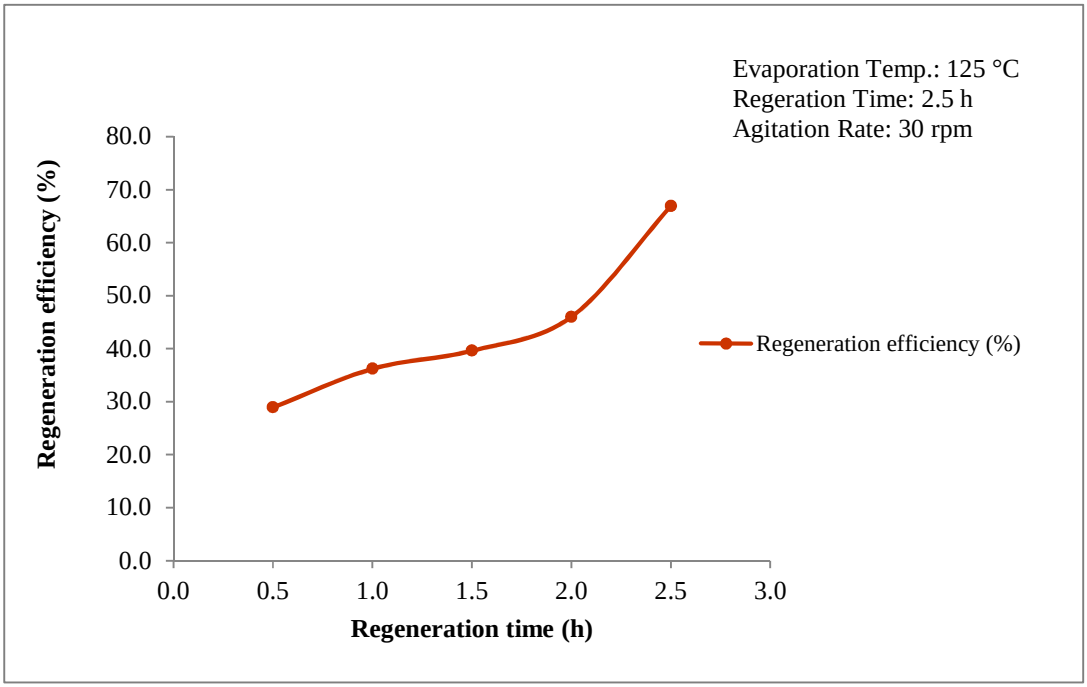

Fig.8.4: Lactic acid regeneration as a function of evaporation time

8.3.3 Precipitation

The precipitation of Fe from cemented tungsten carbide leach liquor is illustrated in **Figure 8.5**. The profile shows precipitation of Fe^{3+} and Fe^{2+} species between pH 3.5 and 7.5. Unlike crystallization which is a physical process, precipitation is a chemical process involving a chemical reaction. Therefore, hydroxide precipitation of metals depends on the concentration of hydroxide and metal ion species in solution. The precipitation of Fe^{2+} occurs at pH~7.5. This is too close to the precipitation of Co which occurs in the pH range of 6.5 – 8.5. Therefore to avoid possible Co losses, air was bubbled in the solution mixture in order to oxidize Fe^{2+} to Fe^{3+}, then Fe^{3+} was precipitated at a lower and safer pH range of 3.0 - 4.5. To avoid the oxidation of Co^{2+} to Co^{3+}, leach solution conditions were maintained within the conditions favourable for the stability of Co^{2+} (-0.5<Eh <1.8 and pH <4 (Garcia et al, 2008)) as discussed in Chapter 4 section 4.6. The pH adjustment was done by using NaOH. The addition of NaOH has the advantage that it forms Na_2SO_4 which improves the electrical conductivity of the Co electrolyte during electro-wining. The iron concentration in the leach solution decreased from 62.3 ppm to 4.2 ppm. Generally, iron hydroxides, especially ferric hydroxides are gelatinous and difficult to filter. However, in this study, filtration proceeded without much difficulty. Filtration lasted between 20 and 30 minutes.

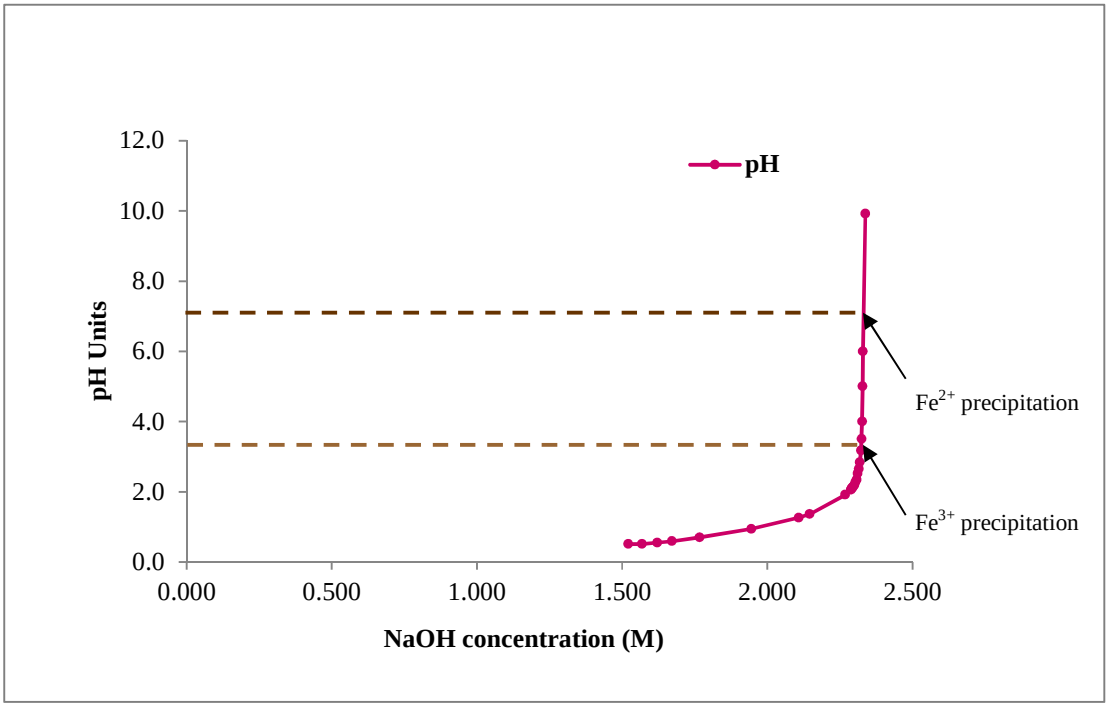

Fig.8.5: Fe precipitation as a function of pH variation

Characterization of the precipitate showed that co-precipitation of other metals other than iron had occurred. The Fe and co-precipitated metals formed insoluble phases. Examples of iron-based phases formed were: hematite (Fe_2O_3), calcium-iron-oxide, calcium-iron-manganese oxide, calcium-iron-hydride and calcium-iron-aluminium oxide. Al co-precipitated as aluminium hydride; Ca, as calcium-magnesium-oxide; Mg, as magnesium hydride and MgNiO (OH); Mn, as manganese oxide. W precipitated as magnesium tungstate ($MgWO_4$), calcium-nickel tungstate and tungstic acid ($WO_3.H_2O$). Co co-precipitated as cobalt-hydrogen-tungsten-oxide hydrate and copper-cobalt oxide. The co-precipitation of Co may have resulted in minor Co losses estimated to be less than 1%. The low precipitation pH range of 3.0 – 4.5 may have assisted in preventing significant Co losses to the precipitate. The precipitate material was not processed further in this study.

8.3.4 Solvent extraction

Solvent extraction was done after reagent regeneration and iron precipitation. Co was successfully extracted in three stages at an extraction efficiency of 99.98%. The loaded organic phase is shown in **Figure 8.6** and the chemical composition of the raffinate solution is listed in **Table 8.4**. The notable elements in the raffinate solution in order of significant concentration were W at 24.76 ppm, Ca, 8.18 ppm; Mg, 3.38 ppm; Ni, 3.0 ppm; Fe, 2.7 ppm and Co, 0.2 ppm. The low Co concentration in the raffinate solution is evidence of effective extraction due to the strong affinity of the Cyanex 272 extractant for Co metal. The W in the raffinate solution could possibly be recovered by precipitation using $Ca(OH)_2$ or $CaCl_2$ reagents as precipitants (Wan et al, 2015; Martins et al, 2007).

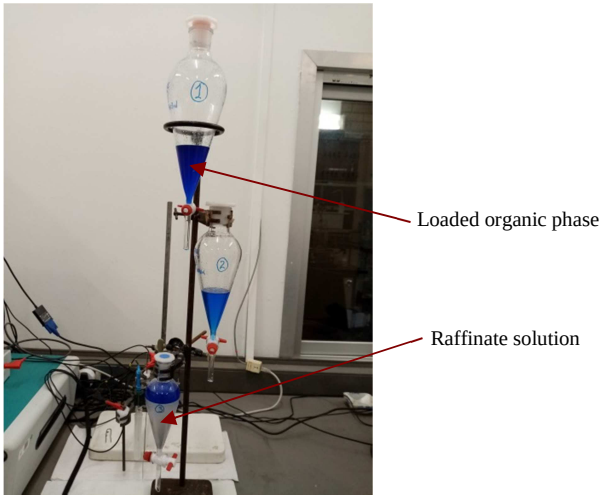

Fig.8.6: Solvent extraction of Co using Cyanex 272

Table 8.4: Chemical composition of raffinate solution

Element	Al	Ca	Co	Cu	Fe	Mg	Mn	Ni	Pb	Zn	W
Conc (ppm)	<0.05	8.18	0.2	1.1	2.7	3.38	<0.05	3.0	<0.001	<0.05	24.76

8.3.5 Stripping

Co was successfully stripped in three stages at a stripping efficiency of 99.96%. The strip solution is displayed in **Figure 8.7** and its chemical composition is listed in **Table 8.5**. The Co concentration was upgraded to 20 gpl by increasing the O/A phase ratio during stripping as

suggested by Jackson (1986). The typical composition of Co advance electrolyte feed to electro-winning (Sole et al, 2016) is listed in **Tables 8.6**. The occurrence of W in the strip solution may have been as a consequence of co-extraction along with Co. At appropriate concentrations of 100-150gpl, the W present in the strip solution can be recovered by precipitation using $Ca(OH)_2$ or $CaCl_2$ reagents as precipitants (Wan et al, 2015; Martins et al, 2007).

Fig.8.7: Stripping of Co using sulphuric acid

Table 8.5: Chemical composition of strip solution

Element	Al	Ca	Co	Cu	Fe	Mg	Mn	Ni	Pb	Zn	W	pH
Conc (ppm)	<0.05	40.0	20,000	<0.05	3.4	15.0	3,350	<0.05	<0.001	1.15	54.3	5.4

Table 8.6: Typical composition of advance cobalt electrolyte feed to electro-winning (Sole et al, 2016)

Element	Al	Ca	Co	Cu	Fe	Mg	Mn	Ni	Pb	Zn	pH
Conc (ppm)	2.5	710	20,000	< 1	1.50	6,000	3,350	66	60	< 2.5	5.8

8.3.6 Electro-recovery of Co

Figures 8.8 (a) and 8.8 (b) show electrodeposited Co metal. The electrodeposition was done using a Co tenor of 20 gpl within 3hrs of residence time.

8.3.6.1 Physical Quality

The deposited Co metal appeared to peel off the stainless steel cathode plate. The peeling effect may have been due to hydrogen evolution which may have been in competition with Co reduction due to hydrogen's higher reduction potential (0.0 V) compared to Co (-28 V) (Sole et al, 2019; Moskalyk and Alfantazi, 2000). This is illustrated in section 8.2.5.

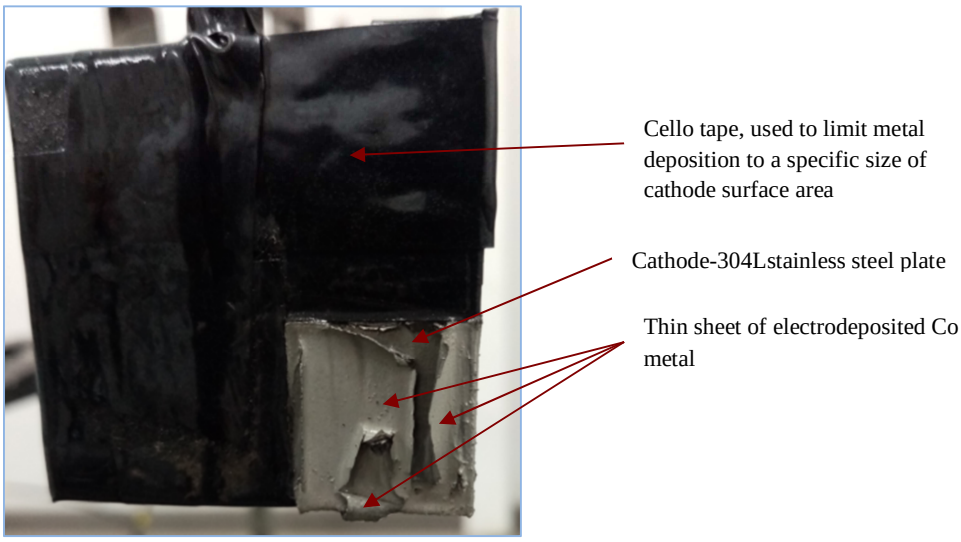

Fig.8.8 (a): Image of electrodeposited Co metal (front side)

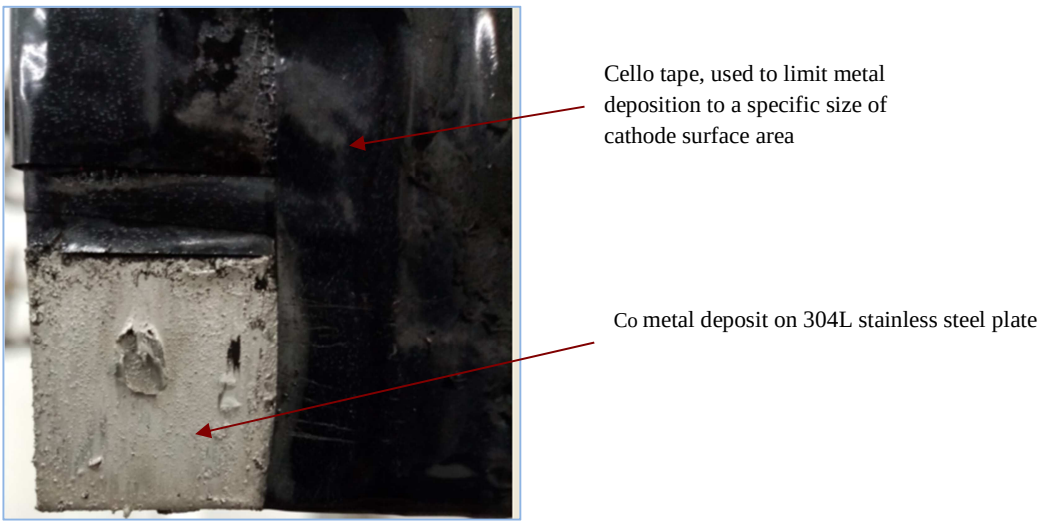

Fig.8.8 (b): Image of electrodeposited Co metal (back side)

The physical quality of the electrodeposited Co metal shown in **Figures 8.8** and **Figure 8.9** is consistent with metal Pulse electrodeposition (PED) quality. The on and off process in PED allows for better levelling of deposit, grain size control, minimizes porosity and nodular growths (Chandrasekar and Pushpavanam, 2008). Sierra and collaborators (2017), in agreement with other PED researchers, noted that Pulse current electrodeposition is a technique of special interest due to the advantages it has like easy operation, low cost, high control in the amount deposit and homogeneity of the deposited material.

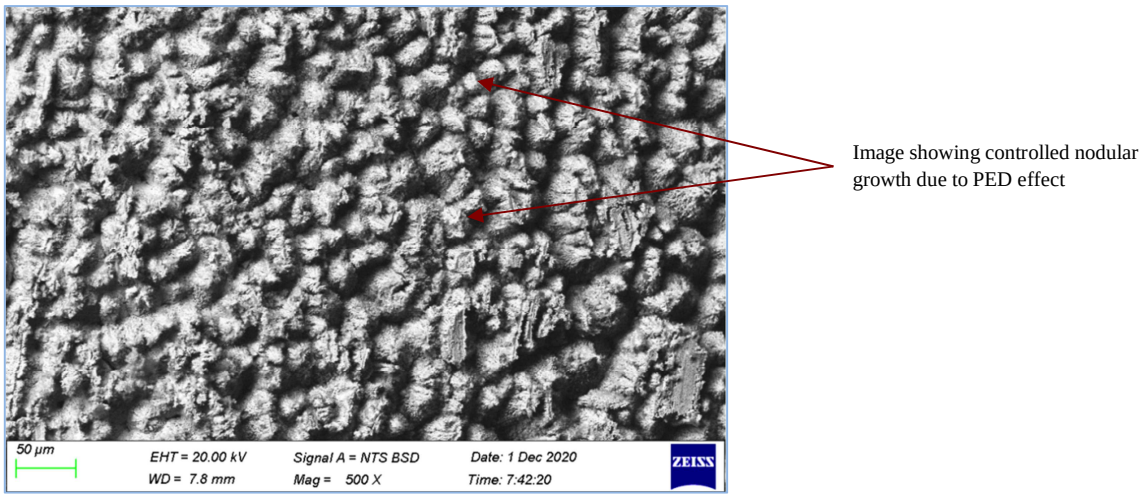

Fig.8.9: SEM image of electrodeposited Co metal (x500)

8.3.6.2 Chemical Quality

Using multiple EDS scans across different regions of the Co metal sample, the average elemental composition of the metal was calculated as 98.0 wt.% Co and 2.0 wt.% Fe (**Table 8.7**). Much more stringent measures for eliminating Fe, as suggested by Ferron and Turner (2000), would be required in order to meet the chemical specification for premium and standard Co metal grades shown in **Table 8.8**. The deposited Co metal was not purified further in this study.

Table 8.7: Chemical composition of the electrowon Co metal

Element	Co	Ni	Fe	Cu	Cd	Zn	Mn	Mg	Pb	SiO_2
(%)	98.0	-	2.0	-	-	-	-	-	-	-

Table 8.8: Specification for premium and standard grade cobalt metal

Element	Co	Ni	Fe	Cu	Cd	Zn	Mn	Mg	Pb	SiO_2
LME Premium (%)	99.83	<0.10	<0.005	<0.003	<0.005	<0.005	<0.002	<0.001	<0.003	<0.001
LME Standard (%)	99.73	<0.15	<0.010	<0.005	<0.005	<0.010	<0.005	<0.003	<0.006	<0.002

8.3.6.3 Current Efficiency Calculations

The following parameters were used as a basis for calculating current efficiency for the Co electro-winning process:

- Cathode Surface Area = 1.7cm x 1.7cm x 2 = 5.78 cm^2
- Current Density: 175 A/m^2
- Deposition Time = 3 hrs
- Cobalt Deposit = 0.306 g

Current efficiency was calculated as a percentage of the actual current used to produce the Co deposit divided by the theoretical current:

Actual current, I = $(\frac{n}{M})\frac{mF}{t} = (\frac{2}{58.93})\frac{0.306x96500}{3x60x60}$ = 0.0928 A

Theoretical current, I = Current density x surface area =175($\frac{A}{m^2}$) x 5.78 cm^2 x $\frac{1m^2}{10000cm^2}$ = 0.101A

Current efficiency = (0.0928/0.101)*100 = 91.9%

Industrial or commercial current efficiency values are normally ≥90% (Sharma et al, 2005).

8.3.6.4 Spent Electrolyte Effluent

Table 8.9 shows the chemical composition of spent electrolyte effluent after Co electrowinning. The composition of the effluent did not differ much from the composition of the strip solution before electrowinning except for Co and Fe concentration which were directly affected by the deposition process. The Co concentration in the electrolyte decreased from 20,000 ppm to 19,100 ppm due to the electrorecovery of 0.306 g of Co. The concentration of Co remaining in the spent electrolyte was high due to the short time of electrowinning. However, this is in line with in industry practice. Electrolyte depletion results in low current efficiency and a poor physical quality of the deposited metal (Sole et al, 2019; Moskalyk and Alfantazi, 2000). According to Roux and collaborators (2007), for a plant running at a current density of 310 A/m^2, electrolyte depletion is avoided by plating cobalt to a final spent electrolyte concentration of about 30 g/L. The Fe concentration decreased due to co-deposition. The spent electrolyte could be recirculated back to the solvent extraction unit until enough W is built up for precipitation of scheelite through a bleed stream. The spent electrolyte effluent was not processed further in this study.

Table 8.9: Chemical composition of spent electrolyte

Element	Al	Ca	Co	Cu	Fe	Mg	Mn	Ni	Pb	Zn	W
Conc (ppm)	<0.05	40.3	19,100	<0.05	1.2	15.2	<0.05	<0.05	<0.001	1.25	54.5

8.3.7 Recovery of W

Dissolved W can be recovered by precipitation as scheelite ($CaWO_4$) using $Ca(OH)_2$ or $CaCl_2$ as precipitants. According to Wan et al (2015) and Martins et al (2007), the required condition for this reaction to occur is that the concentration of W in a solution should be 100 to 150 gpl. The raffinate solution in this study contained 24.76 ppm W and spent electrolyte effluent, 54.5 ppm. An attempt to react the raffinate solution using $CaCl_2$ and $Ca(OH)_2$ as precipitants did not yield any fruitful results. It was observed that the dissolved W concentration may have been too low for the precipitation reaction to occur. The raffinate solution was not processed further in this study.

However, in order to demonstrate the possibility of W recovery, 150 gpl of sodium tungstate solution was prepared, in place of the raffinate solution, using a Na_2WO_4 salt. The prepared sodium tungstate solution was then reacted with $CaCl_2$ to obtain scheelite using precipitation conditions described in Chapter 3 section 3.6.4.6, **Table 3.9**. The results of this reaction are displayed in **Figures 8.10** and **8.11**.

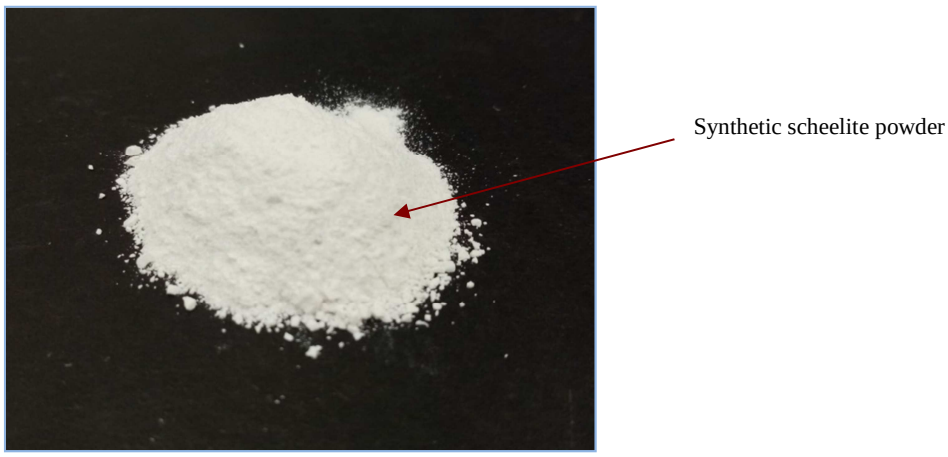

Fig.8:10: Image of scheelite ($CaWO_4$) powder obtained by precipitation

An XRD pattern of the scheelite precipitate shown in **Figure 8.10** is displayed in **Figure 8.11**. The XRD analysis was used to confirm that W was successfully precipitated out of the sodium tungstate solution. The broad shaped peaks are characteristic of the amorphous nature of the $CaWO_4$ precipitate. The figure also shows halite (NaCl) and calcium in the precipitate. The presence of halite and calcium may have occurred as a result of occlusion during precipitation. The XRD characterization data shows that the material is composed of 82.9% scheelite. This confirms that W was successfully converted into scheelite by precipitation and also demonstrates that a precipitative recovery of dissolved W from a highly concentrated tungstate solution is feasible. However, this may require a pre-concentration step before subsequent precipitation and recovery of W.

A comprehensive route for W recovery from raffinate solution is suggested and shown in **Figure 8.12**. Spent electrolyte from electrowinning could be recirculated back to solvent extraction. The raffinate solution could undergo Ion Exchange treatment to extract and separate W using D309 resin (Lu and Liao, 2014) or Triton X-100-(NH_4SO_4-H_2O)(Zhang et al, 2016). The extracted W could then be reacted with $CaCl_2$ to produce scheelite ($CaWO_4$) and NaCl for sale.

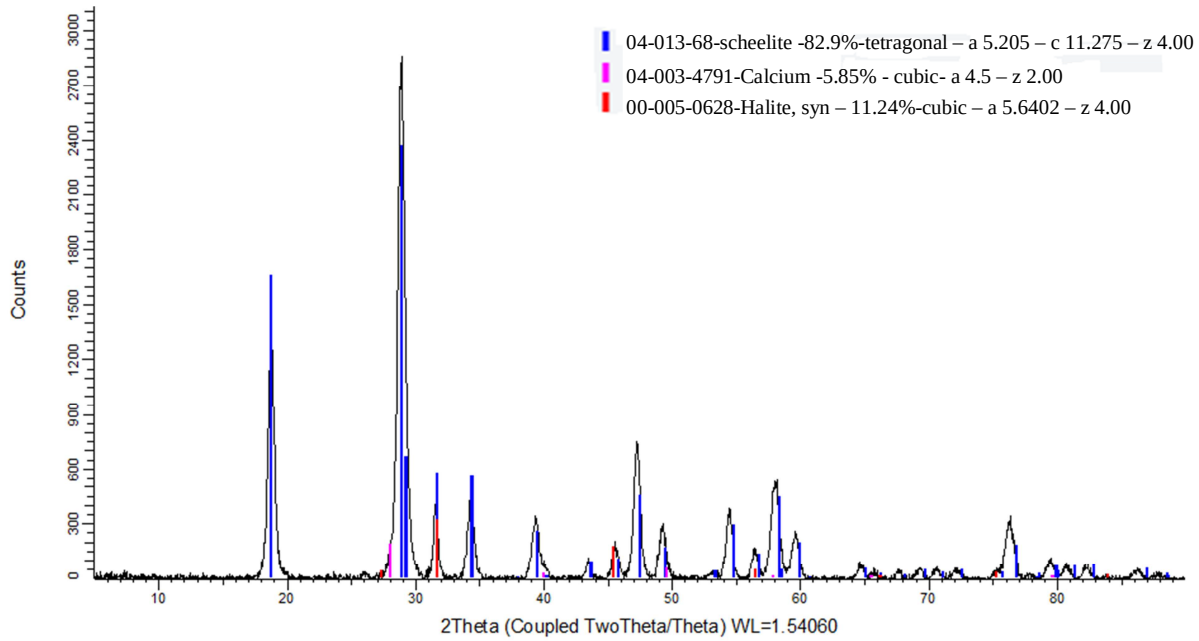

Fig.8.11: The XRD pattern of Scheelite [(CaWO4] (Tetragonal crystal structure)

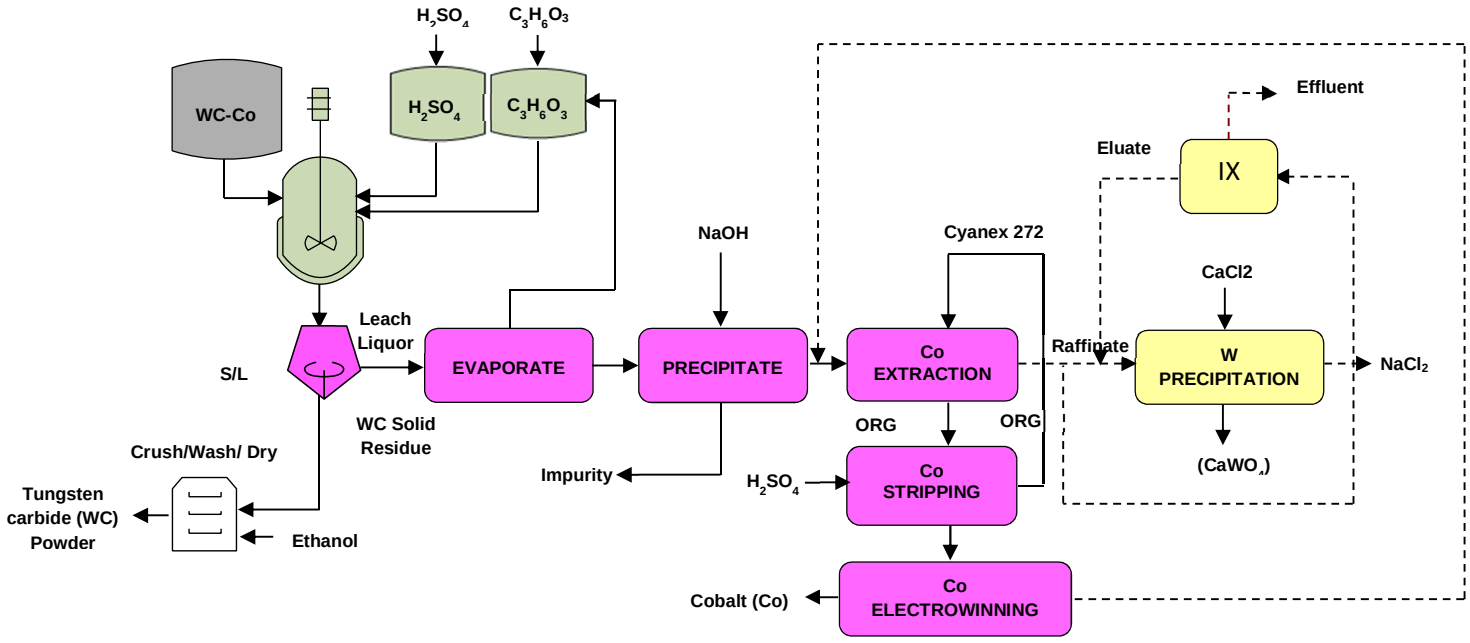

Fig.8.12: A flow diagram of the suggested process for recovering W from raffinate solution

8.4 Summary

The overall purpose of employing selective dissolution of Co from the binder phase was to develop and propose a process route for the production of tungsten carbide (WC) powder, Co metal and scheelite ($CaWO_4$) from cemented tungsten carbide scrap metal. The recovery process route entailed six unit stages.

In the first stage, cemented carbide scrap buttons were leached to produce WC residue and leach solution. The recovered WC residue skeleton was easily disintegrated and pulverized into WC powder.

In the second stage, an attempt was made to regenerate unreacted lactic acid from the leach solution initially dosed with 5% lactic acid. The experiment yielded an organic acid regeneration efficiency of 66.9% after 2.5 hrs of residence time. The concentration of unrecovered lactic acid in the distillate was 0.00030% (v/v).

In the third stage, impurities were precipitated and removed from the leach solution by adjusting the leaching solution pH to a range of 3.5-4.5 using NaOH as a precipitant. The impurity removal process yielded a significant decrease in iron concentration in the leach solution.

In the fourth stage, the leach solution was further purified and upgraded using solvent extraction. The solvent extraction process produced a Co rich strip solution and a Co poor raffinate solution at an extraction efficiency of 99.98% and stripping efficiency of 99.96%.

In the fifth stage, Co was electro-recovered from the Co rich strip solution at a current density of 175 A/m^2 after 3 hrs of electrodeposition time. Using Faraday's law, the Current efficiency for the Co electro-winning process was calculated as 91.9%.

In the sixth stage, an attempt was made to recover W from a raffinate solution by precipitation. Precipitative tests revealed that the W concentration in the raffinate solution was not adequate for the precipitation reaction to occur. However, a sodium tungstate salt was used as an alternative to produce scheelite thus, indicating that W recovery from a highly concentrated tungstate solution is feasible. A comprehensive route for the recovery of W from raffinate solution is suggested.

The next Chapter discusses flowsheet development and techno-economic evaluation of the cemented tungsten carbide recycling process.

8.5 References

Barnard, P.G., 1971. Reclamation of Refractory Carbides from Carbide Materials. USA, Patent No. 3, 595, 484.

Bronsted, J.N., 1931. On The Dissolution of Metals in Acids. Journal of American Chemitry Society. Vol.53, Issue 10, pp. 3624-3644. https://doi.org/10.1021/ja01361a006.

Brunner,P.H., 2011. Urban Mining: A Contribution to Reindustrializing the City. Journal of Industrial Ecology, Vol.15, pp. 339-341. DOI: 10.1111/j.1530-9290.2011.00345.x.

Cossu, R., Williams, I.D., 2015. Urban Mining: Concepts, terminology, Challenges. Waste Management, Vol.45, pp. 1-3. http://dx.doi.org/10.1016/j.wasman.2015.09.040.

Donaldson, J.D., 2005. “Cobalt and Cobalt compounds” in Ullmann’s Encyclopedia of Industrial Chemistry 2005, Detmar Beyersmann. Wiley-VCH, Weinheim). Doi: 10.1002/14356007.a07_281.pub2.

Elerman, Y.. 1988. “Refinement of the crystal structure of CoSO4.6H2O.” Acta Crystallographica Section C 1988, Vol. 44, pp. 599-601. Doi: 10.1107/S0108270187012447.

Ferron, C.J., Turner, D., 2000. Purification of Cobalt Solutions Containing Iron and Manganese with Oxidation Mixture of SO_2 and Oxygen. Patent No: WO 00/56943, USA.

Gani, R., Jimenez-Gonzalez, C., Kate, A., Crafts, P.A., Powell, M.J., Powell, L., Atherton, J.H., Cordiner, J.L., 2006. A Modern Approach to Solvent Selection. Chemical Engineering 113:30-43.

Garcia, E.M., Santos, J.S., Pereira, E.C., Freitas, M.B.J.G., 2008. Electrodeposition of Cobalt from Spent Li-ion Battery Cathodes by The Electrochemistry Quartz Crystal Microbalance Technique. Journal of Power Sources, Vol. 185, pp. 549-553.

Gutberlet, J., 2015. Cooperative Urban Mining in Brazil: Collective Practoices in Selective Household waste Collection and Recycling. Waste Mnangent. http://dx.doi.org/10.1016/j.wasman.2015.06.023.

Jackson, E., 1986. Hydrometallurgical Extraction and Reclamation. Halsted Press, New York. ISBN: 085-312-5686.

Jiang, L., Huang, L., Sun, Y., 2013. Recovery of flakey Cobalt from aqueous Co (II) with Simultaneous Hydrogen Production in Microbial Electrolysis Cells. International Journal of Hydrogen Energy, Vol. 39, Issue 2, pp. 654-663.

Kabongo,J.D., 2013. Waste Valorization. In: Idowu, S.O; Capaldi; Zu, L; Gupta, A.D (Eds) Encyclopedia pf Corporate Social Responsibility. Springer, Berlin, Heidelberg.

Kates, R.W., Parris, T.M., Leiserowitz, A.A., 2016. What is Sustainable Development? Goals, Indicators, Vlaues and Practice. Environment Magazine. Taylor and Francis Group, Philadelphia, PA.19106.

Krutove, G.A., 1959. Mestorozhdeniia Kobal'ta. Trebovaniia promyshlennosti k Kachestvu Mineral'nogo Syr'ia. The Great Soviet Encyclopedia, 3rd Edition (1970-1979).

Lamanria., 2010. Closed-loop Recycling: A case Study of Films for Green House. Polymer and Degradation. Pp. 285-288.

Lassner, E., Schubert, W.D., 1999. Tungsten: Properties, Chemistry, Technology of The Element, Alloys and Chemical Compounds. Kluwer Academic/Plenum Publishers, New York.

Lu, X., Liao, C., 2014. Separation of Macro amounts of Tungsten and Molybdenum by Ion Exchange with D309 Resin. Transactions of Nonferrous Metals Society of China. Vol. 24, Issue 9, pp. 3008-3013. Doi.org/10.1016/S1003-6326 (14) 63438-5.

Monhemius, A.J., 1977. Precipitation Diagrams for Metal Hydroxides, Sulfides, Arsenates and Phosphates. Transactions of the Institution of Mining & Metallurgy 86:202-206.

Roux, L. M., Minnaar, E., Cilliers, P. J., Bellino, M., Dye, R., 2007. Comparison of solvent extraction and selective precipitation for the purification of cobalt electrolytes at Luilu refinery, DRC. Proceedings, 4th Southern African Conference on Base Metals, Johannesburg: Southern African Institute of Mining and Metallurgy, pp. 343–364.

Sandvik., 2016. Understanding Cemented Carbide. http://www2.sandvik.com/. Retrieved 25 June 2016.

Sharma, I.G., Alex, P., Bidaye, A.C., Suri, A.K., 2005. Electrowinning of Cobalt from Sulphate Solutions. Hydrometallurgy, Vol.80, pp. 132-135.

Shield, K.B., 2000. Tungsten Recycling in the United States in 2000. U.S. Geological Survey Circular, 1196-R.

Sing, J., 2016. Resources Recovery from Post-Consumer Waste: Important Lessons for the Upcoming Circular Economy. Journal of Cleaner Production.ISSN 0959-6526, E-1SSN 1879-1886 , Vol.134, pp. 342-353.

SMEAG, 2016. World Tungsten Metal Production. http://www.smeag.de/index.php/en/. Retrieved 20 March 2017

Smith, G.R., 1942. Material Flow of Tungsten in the United States. Bureau of Mines Circular-1994.

Sole, C.K., Jurrius, Y., Hardwick,E., 2016. Purification of cobalt electrolyte by ion-exchange: Pilot Plat results and preliminary commercial design. Society of chemical industry: IEx 2016 Proceedings-Hydrometallurgy session.

Sole, K.C., Parker, J., Cole, P.M., Mooiman, M.B., 2019. Flowsheet Options for Cobalt Recovery in African Copper–cobalt Hydrometallurgy Circuits. Mineral Processing and Extractive Metallurgy Review, Vol.40, Issue 3, pp.194-206.

Song, Q., Li, J., Zeng, X., 2015. Minimizing the Increasing Solid Waste through Zero Waste Strategy. Journal of Cleaner Production. Vol.104, pp. 199-210. http://dx.doi.org/10.1016/j.jclepro.2014.08.027.

Sverdrup, H.U., Ragnarsdottir, K.V., Koca., 2017. Integrated Modelling of the Global Cobalt Extraction, Supply, Price and Depletion of Extractable Resources Using the WORLD6 Model. Biophysical Economics and Resource Quality, Vol. 2, Issue 4, pp. 1-29.

Trent, E.M., 1946. Process of Separating Hard Constituents from Sintered Hard Metals. US Patent No. 2,407,752.

Zhang, Y., Sun, T., Lu, T., Yan, C., 2016. Extraction and Separation of Tungsten (VI) from Aqueous Media with Triton X-100-Ammonium Sulphate-Water Aqueous Two-Phase System Witout Any Extractant. Journal of Chromatography. DOI:10.1016/j.chroma.2016.10.082.

CHAPTER NINE

PROCESS FLOWSHEET DEVELOPMENT

AND TECHNO-ECONOMIC EVALUATION

9.1 Introduction

Results presented in the previous chapter demonstrated that binary-phase cemented tungsten carbide secondary material can be optimally recycled to recover Co and WC using an acid leach process. The recovered Co and WC products maintained morphological integrity. The current chapter presents flowsheet development and techno-economic evaluation of the recycling process. This involves the general flow of unit processes and equipment used. The results from experimental tests were used to simulate the laboratory scale process using SuperPro Designer® version 10 (Canizales et al 2020). The process description, cost analysis and economic evaluation of the simulated recycling process are discussed.

9.2 Process Development and Description

The process scheme for recycling cemented tungsten carbide scrap metal is as previously described in Chapter 3, **Fig. 3.6** and fully discussed in sections 3.6 and 3.7.

9.3 Process Flowsheet Simulation

In this study, the recycling process was modeled and simulated using SuperPro Designer® in order to evaluate the commercial-scale production of Co and WC from cemented tungsten carbide secondary material. The flowsheet was designed and simulated based on results from experimental laboratory tests and technical literature. **Table 9.1** shows the main unit operations, operation parameters, equipment properties and costs used in the simulation. The corresponding flowsheet for the simulated process is shown in **Figure 9.1**.

The modeling of a commercial-scale recycling process involves several stages. These steps are described below:

Table 9.1: Operation parameters, equipment properties and costs for the cemented carbide recycling process

Unit Process	Equipment Type	Process	Key Operation Parameters	Equipment properties	Equipment costs ($/unit)
P-1	R-101	Leaching	Temperature = 82°C Time = 36.25 hrs Acid conc. = 2M	Volume = 40 L Number = 1	11,800
P-2	NFD-101	Filtration	Temperature = 25°C Time = 1.5 hrs	Surface area = $1m^2$ Filtrate flux = $0.2m^3/m^2$-h Number = 1	18,900
P-3	V-101	Distillation	Temperature = 122°C Time = 2.75 hrs	Volume = 40 L Number = 1	7,600
P-4	R-102	Precipitation	Temperature = 25°C Time = 1 hr	Volume = 40 L Number = 1	11,800
P-5	NFD-102	Filtration	Temperature = 25°C Time = 1.25 hrs	Surface area = $1m^2$ Filtrate flux = $0.2m^3/m^2$-h Number = 1	18,900
P-6	MSX-101	Solvent extraction	Temperature = 35°C Time = 1.25 hrs Extraction stages = 3	Volume = 96 L (Mixer) Volume = 24 L (Settler) Number = 1	17,600
P-7	MSX-102	Stripping	Temperature = 25°C Time = 0.5 hrs Stripping stages = 3	Volume = 96 L (Mixer) Volume = 24 L (Settler) Number = 1	17,600
P-8	R-103	Electrorecovery	Temperature = 63°C Time = 25.3 hrs Current density = 175 A/m^2	Volume = 40 L Number = 1	11,800
P-9	NFD-103	Solid-liquid separation	Temperature = 25°C Time = 1.25 hrs	Surface area = $1m^2$ Filtrate flux = $0.2m^3/m^2$-h Number = 1	18,900

Acid leaching Reaction – Dissolution of the Co Binder Phase Step (‘P-1’ in ‘R-101’)

The unit process ‘P-1’ takes place in a reactor ‘R-101’ and involves the dissolution of the Co binder phase. Atmospheric air is used as an oxygen source. The hydronium ion reacts with the Co metal, causing the metal to become oxidized thus inducing metal dissolution (Bronsted, 1931). The stoichiometry of the reactions is fully described and discussed in Chapter 2, section 2.5. After the leaching reaction, the contents are allowed to settle and then transferred to the Nutsche filter (‘NFD-101’) for solid-liquid separation using unit process ‘P-2’.

Filtration and WC Recovery Step ('P-2' in NFD-101')

Unit procedure 'P-2' takes place in a Nutsche filter ('NFD-101') and involves recovery of WC product as a solid residue which can easily be disintegrated into powder form. The Co (II) sulphate liquid phase is transferred to the distillation vessel for further processing.

Distillation - Reagent Regeneration Step ('P-3' in 'V-101')

Unit process 'P-3' takes place in a distillation vessel 'V-101'and involves reagent regeneration of lactic acid. The organic acid is vaporized and then distilled. The distilled acid is recovered as a distillate. The leach solution is transferred to reactor vessel 'R-102' for further processing.

Precipitation - Impurity Precipitation Step ('P-4' in 'R-102')

The unit procedure 'P-4' takes place in a reactor 'R-102' and involves a precipitation reaction step. Impurities are precipitated and the solution is transferred to the next step and filtered.

Filtration and Impurity Removal Step ('P-5' in 'NFD-102')

Unit procedure 'P-5' takes place in a Nutsche filter ('NFD-102') and involves impurity removal. The precipitates formed during the precipitation reaction are discharged as impurity.

Solvent Extraction Reaction Step ('P-6' in 'MSX-101')

Unit procedure 'P-6' takes place in a mixer-settler 'MSX-101' and involves an extraction step. The leach solution is contacted with an organic phase. The Co^{2+} ion reacts with the organic extractant and moves into the organic phase. The Co depleted aqueous phase is discharged as raffinate.

Stripping Reaction Step ('P-7 in MSX-102')

Unit procedure 'P-7' takes place in a mixer-settler 'MSX-102' and involves a stripping step. The organic phase is contacted with sulphuric acid solution. The Co^{2+} ion in the organic phase reacts with the hydronium ion and moves into the aqueous phase. The Co depleted organic phase is now stripped organic. The loaded aqueous phase is transferred to reactor 'R-103' as advance electrolyte for further processing.

Electrorecovery Step ('P-8' in 'R-103')

Unit procedure 'P-8' takes place in a reactor 'R-103' and involves electro-recovery of Co metal from Co (II) electrolyte.

Filtration and Co Metal Separation Step ('P-9' in 'NFD-103')

Unit procedure 'P-9' takes place in a Nutsche filter ('NFD-103') and involves solid-liquid separation of Co metal and spent electrolyte.

9.4 Material Balance

The material balance for the input and output streams are shown in **Table 9.2**. The composition of raw materials, outputs from the vital unit operations, main product (MP), and by-products are reflected on the process flowsheet (**Figure 9.1**). Cemented carbide is the raw material; Co metal is the main product; WC residue and raffinate solution are by-products. The total number of batches for the recycling process per year is 216. The simulation predicts 7.04 kg/batch, equivalent to 1,513 kg of Co metal per year produced from 135 kg/batch of cemented tungsten carbide scrap metal. The 135 kg/batch of scrap metal is equivalent to 29,160 kg per year. The simulation further predicts a production of 28, 257 kg per year of WC residue which can be pulverized into WC powder. The resulting raffinate by-product is 9,653 kg per year. This could be processed to recover residual tungsten.

Table 9.2: Stream summary of the cemented tungsten carbide recycling process

Output Streams											
Stream Name	Stripped Organic	$C_3H_6O_3$(R)	Raffinate	WC Residue	Vapour	Spent Electrolyte	Co metal				Total
Kg/batch	73.27	0.0011	44.69	131.48	41.292	64.16	7.04				361.933
Input Streams											
Stream Name	Air	Cemented Carbide	$C_3H_6O_3$	H_2SO_4	H_2SO_4(1)	H2O	NaOH	Organic Phase	Wash water-1	Wash water-3	Total
Kg/batch	42.377	135.00	0.04	13.40	50	0.1	13.86	85.82	0.402	20.934	361.933

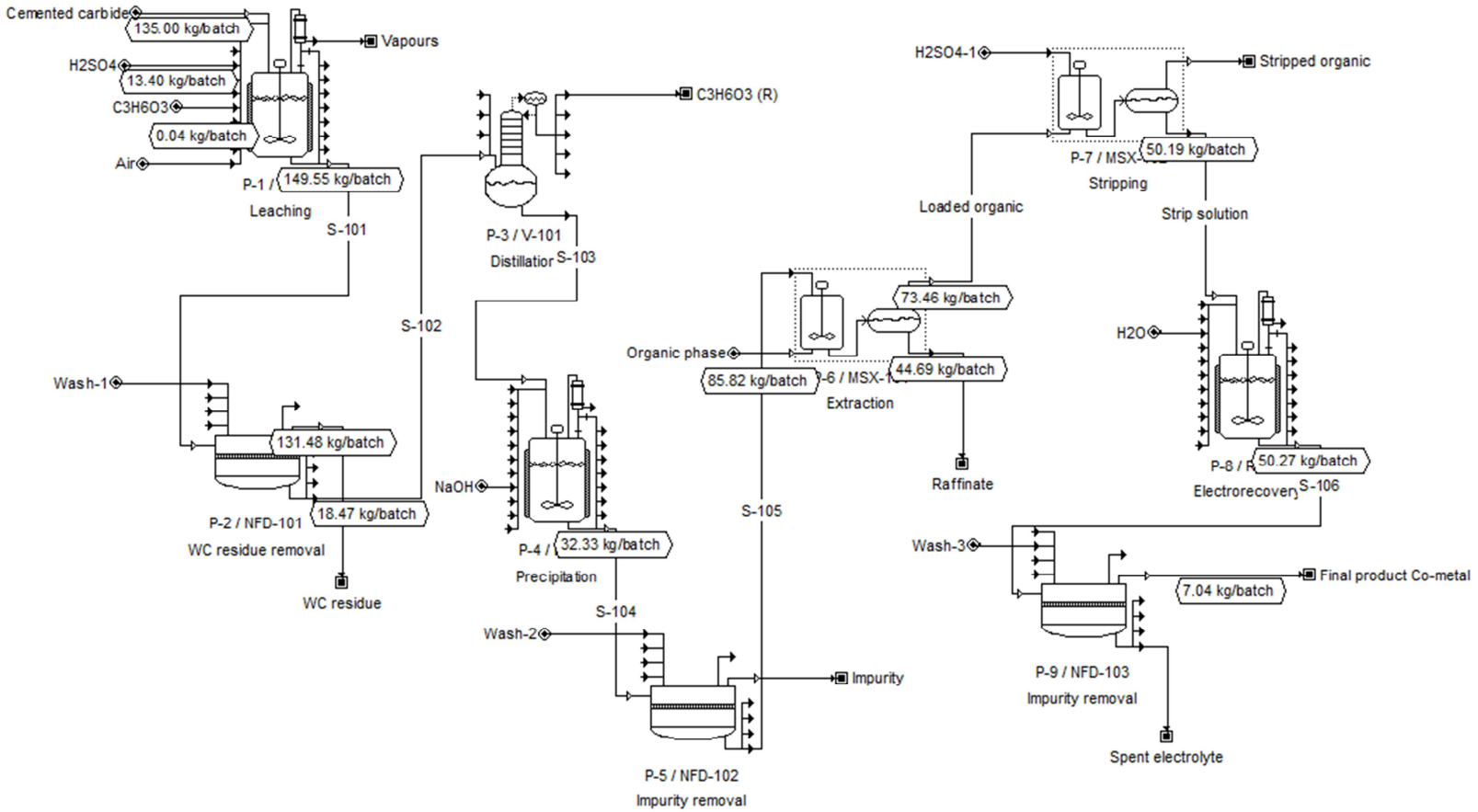

Fig.9.1: Process flowsheet for recycling cemented tungsten carbide secondary material

9.5 Cost Analysis and Economic Evaluation

Simulation with SuperPro Designer® can be done in 'design mode' or 'rating mode'. The settings in 'rating mode' are set by the user. In 'design mode', the settings are done automatically. In this study, the simulation was set to 'design mode'. Therefore, equipment sizing and costing was done automatically based on the processing conditions and parameters obtained from the experimental results. It's therefore expected that, due to possible experimental error, a deviation in the economic cost could occur when doing this commercially. A number of economic evaluation parameters were assumed and these are presented in **Table 9.3**. The year of analysis and construction is 2021 with a project lifetime of 15 years. The recycling plant will run 216 batches in 365 days. A batch size of 135 kg of cemented tungsten carbide secondary material was assumed for the recycling process. The 135 kg batch size was based on the scrap metal production capacity of a known local South African hardmetal processing company. However, if more scrap metal becomes available, the simulated process could be replicated accordingly. The main primary product for the total stream, referred to as MP, is Co metal. The selling price for the Co metal was set at 41.3 $/kg which is the current selling price of Co on the London Metal Exchange (LME, 2021) (www.lme.com). The selling price for the WC residue was estimated at a modest value of 150 $/kg which is about 60% of 251$/kg current selling price of virgin WC powder (www.weartech.co.za). An average labour cost of 3.8 $/h was used to estimate labour costs for the process. Other costs of utilities and consumables are shown in **Table 9.4**. The utilities are steam, cooling water and electric power. The consumables are Air, lactic acid, sulphuric acid, NaOH, Cyanex 272 organic extractant and Shellsol D diluent.

Table 9.3: Economic Evaluation parameters

Parameter	Value
Construction period	30 months
Start-up period	4 months
Project Lifetime	15 yrs
Inflation	4.0%
NPV	7%
Salvage value	5%
Corporate Tax (SA)	28%

Table 9.4: Cost of utilities and consumables

Utilities	$/kg
Steam	12$/MT
Cooling water	0.05$/MT
Electric power	0.1$/kWh
Consumables	
Lactic acid	8.3$//kg
Sulphuric acid	3.2$/kg
NaOH	6.7$/kg
Cyanex 272	45.1$/kg
Shellsol D	0.4$/kg

9.5.1 Capital cost estimation

SuperPro Designer® uses a factor-based method to estimate the capital investment associated with each section of a process. The total capital investment was based on start-up and validation cost, working capital, direct fixed capital (DFC) and equipment purchase cost (PC). The equipment purchase cost, determined by the equipment material type and size, directly affects the direct fixed capital which in turn affects the operating cost. In this study, the equipment purchase cost estimates were based on local South African suppliers as well as the Matche database (www.matche.com 2021). Section-based cost estimates such as piping, instrumentation, insulation, electrical facilities, buildings, yard improvement and auxiliary facilities tended to inflate the total capital investment cost of the recycling project. Therefore, section-based factors were set to zero and the equipment-based factors were maintained at the default value of 1.0.

9.5.2 Operations cost estimation

The operation cost consisted of facility-related costs; labour-related costs; laboratory costs and costs related to quality control, quality assurance and utilities.

9.5.3 Techno-economic analysis results

The cost analysis and economic evaluation calculations for the recycling process were performed using SuperPro Designer® software (Canizales et al 2020). The economic evaluation parameters used are presented in **Table 9.3**. The main product from the recycling plant is Co metal. Although Co is shown as the main product for the recycling plant, WC residue is also a revenue stream contributing to the total revenue of the plant. The cost analysis results for the recycling plant producing 1,513 kg of Co metal per year (approximately, 7.04 kg per batch) are presented in the summary in the section that follows.

9.5.3.1 Executive summary

The executive summary provides an overview of the total economic impact of the plant, including the total capital investment, annual revenues and rate of return.

Executive Summary

Capital Investment Charged to this Project	331,982 $
Annual Operating Cost	3,103,787 $/yr
Revenues	3,429,223 $/yr
Unit production Rate	1,513.40 kg MP/yr
Unit production cost	2,050.88 $/kg MP
Unit Production Revenue	2,265.91 $/kg MP
Gross margin	9.49 %
Return on investment (ROI)	70.58 %
Payback time	1.42 yrs
IRR (after tax)	9.14 %
NPV (at 7% interest)	189,048 $

MP = Total Flow of Stream 'Final Product-Co Metal'

The techno-economic results posted a positive return on investment (ROI), payback time and net present value, indicating that the cemented tungsten carbide (CTC) plant is a profitable venture. Furthermore, the internal rate of return (IRR), at 9.14%, is much higher than the prime bank interest rate currently estimated at about 7.0% in South Africa, suggesting that investing in the recycling project would give a better yield than the bank.

9.5.3.2 Summary per cost item

The operating cost summary table of the itemized cost report is shown in **Table 9.5**. The table provides a cost breakdown per cost item of the total annual operating cost over all process sections of the recycling process. The itemized cost report (ICR) helps with identification of cost-sensitive sections, notably, the economic hot-spots of the process. For instance, the ICR in **Table 9.5** reveals that the largest cost in this process is attributed to facility-dependent expenses that account for roughly 51% of the annual operating cost. Approximately, another 31% of the annual operating cost is associated with raw materials. This is mainly attributed to the cost of cemented tungsten carbide scrap metal, the feed stock to the recycling process. The other cost of about 18% is a labour related expense. Labour can be reduced through increased automation.

Table 9.5: The operating cost summary table of the itemized cost report

	$/yr	**$/batch**	**$/kg MP**	**%**
Materials	964,060	4,463	637.02	31.06
Facility-dependent	1,566,661	7,253	1,035.20	50.48
Labour-dependent	565,091	2,616	373.39	18.21
Laboratory/QC/QA	5,651	26	3.73	0.18
Utilities	47	0	0.03	0
Other (waste treatment/disposal, transportation)	2,286	11	1.51	0.07
Total Annual Operating Cost	3,103,787	14,369	2,050.88	100

9.5.3.3 Sensitivity analysis

A sensitivity analysis study on the impact of throughput on the profitability of the plant was performed in order to evaluate risks associated with the variations in technical and economic parameters. The sensitivity analysis was monitored in the range of 6.25 to 7.2 kg/batch of Co metal throughput. This translated into 1,350 kg to 1,550 kg/year. **Figures 9.2** and **9.3** show the analysis of the sensitivity study. Figure 9.2 shows that the unit production cost decreased with increasing plant capacity. From **Figure 9.3**, it is observed that the profitability indices, ROI and IRR, increase as the plant capacity is expanded. Therefore, it can be surmised from this

sensitivity analysis that the recycling plant should be run at the highest capacity that is technically and practically possible.

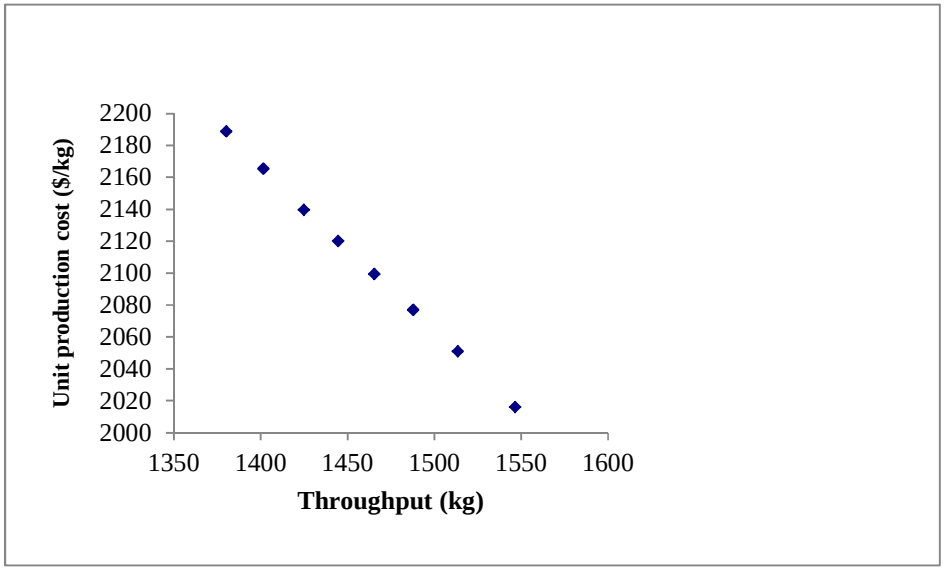

Fig.9.2: Production cost vs throughput

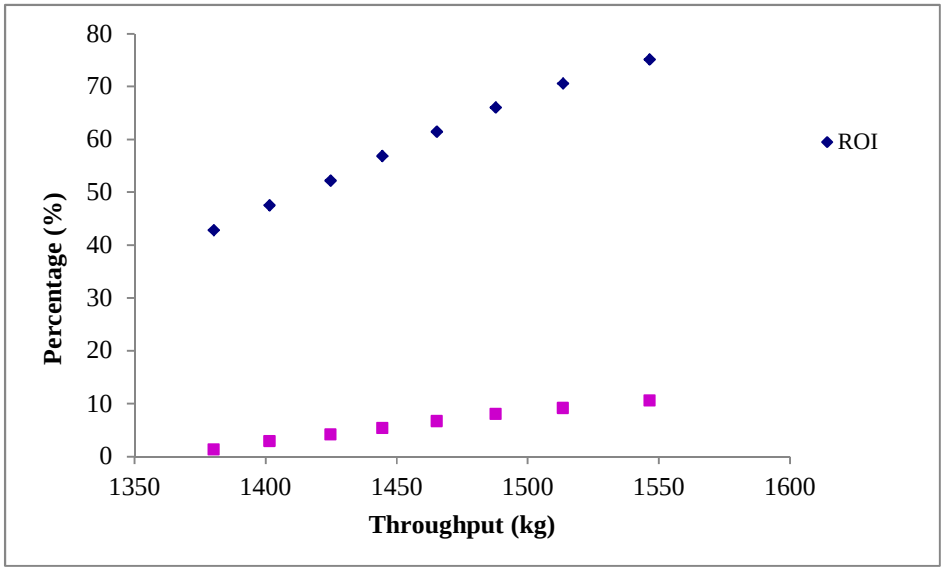

Fig.9.3: Economic indices vs throughput

9.6 Summary

The purpose of the study undertaken in this chapter was to determine the cost implications of the cemented tungsten carbide recycling process. An industrial-scale process for the recovery of Co and WC from cemented tungsten carbide secondary material was designed and simulated. A combination of leaching, distillation, precipitation, solvent extraction and electro-recovery unit processes was employed in recovering the Co and WC products.

The techno-economic evaluation carried out by using SuperPro Designer® showed that the cemented tungsten carbide recycling process is economically viable. However, the issue of procuring cemented tungsten carbide secondary material could be a challenge. This is because the global tungsten supply chain remains opaque to industry outsiders. If one considers the limitation of recyclable WC-Co scrap volumes and collection issues, the minimum design feed capacity could probably be estimated at 135Kg/37hr-batch.

From the simulation, the leaching step took the longest time and hence the process bottle neck. Therefore, to improve the techno-economics of the process, technology to reduce leaching time is imperative.

The next chapter presents conclusions and recommendations of all the work carried out in the research study.

9.7 References

Bronsted, J.N., 1931. On The Dissolution of Metals in Acids. Journal of American Chemistry Society. Vol.53, Issue 10, pp. 3624-3644. https://doi.org/10.1021/ja01361a006.

Canizales, L., Rojas, F., Pizarro, C.A., Caicedo-Ortega, N.H., Villegas-Torres, M. F., 2020. SuperPro Designer®, User-Oriented Software Used for Analyzing the Techno-Economic Feasibility of Electrical Energy Generation from Sugarcane Vinasse in Colombia. Processes, Vol. 8, 1180, pp. 1-16. DOI:10.3390/pr8091180.

LME., 2021. London Metal Exchange, www.lme.com. Retrieved, 30 January 2021.

Matches., 2020. Equipment Cost Index. www.matche.com. Retrieved, 20 January 2021.

Weartech., 2020. Tungsten carbide powder. www.weartech.co.za. Retrieved, 20 October 2020.

CHAPTER TEN

CONCLUSIONS AND RECOMMENDATIONS

10.1 Introduction

The ability of acidic media to leach and collect metallic species from tungsten-based secondary material is based on one mechanism: metallic binder dissolution. This is because members of the iron group, namely, Fe, Ni and Co, when used as binders in cemented carbide, wet the grains of tungsten carbide (WC) making it very difficult to remove them from between the grains during reclamation. The main objective of this work was to explore this concept in order to investigate the possibility of designing a technique wherein the Co binder phase is selectively extracted whilst leaving the tungsten (WC) hard phase intact. Binary-phase cemented tungsten carbide was used in this study. The binder phase is reactive and is acid soluble whereas the WC hard phase tends to passivate due to formation of insoluble tungsten precipitates such as tungstic acid (H_2WO_4). A review of literature suggested a possibility that the Co binder dissolution could be enhanced by ensuring that the formation of insoluble tungsten precipitates is eliminated or minimized. This would allow Co dissolution and diffusion to occur freely and in turn promote its extraction. It is this possibility which was the focus of this study wherein the physical and chemical properties of cemented tungsten carbide during leaching was investigated so as to understand the possibilities and limitations of the approach. Therefore, this chapter highlights the findings made and presents recommendations for future research.

10.2 Conclusions

This section presents the findings and conclusions drawn from the experimental work done to fulfil the aim of the research project.

The behaviour of WC grains in acidic media

The behaviour of WC grains in acidic media was studied in 1M and 2.5M sulphuric acid at 75°C and 85°C, and the following conclusions were drawn.

1. WC grains, when exposed to acidic media, react to form tungstic acid (H_2WO_4) precipitates. However, the addition of 5% (v/v) lactic acid to 2.5M sulphuric acid solution suppressed and diminished the formation of tungstic acid considerably.

Characterization of cemented tungsten carbide secondary material

Characterization was focused on production scrap cemented carbide buttons. The following conclusion was drawn from the etching characterization test:

1. Optical photomicrograph results showed no evidence of eta (η) phase occurrence in the cemented tungsten carbide secondary material.

Preliminary leaching tests

Preliminary leaching tests entailed factor range finding trials and reagent selection. The following conclusions were drawn from the experimental work:

1. The factor range finding trials revealed that all the five process parameters, temperature, leaching time, acid concentration solid-to-liquid ratio and agitation rate, tested had a noticeable influence on the Co dissolution process with clearly identifiable lower and upper limits. The factor range finding trials established ranges within which to test the effect of process parameters as 40-85°C for temperature, up to 10.5 days for leaching time, 0.01-3 M H_2SO_4 acid concentration, 1:18-1:6 for solid to liquid ratio and 0-1000 rpm for agitation rate.

2. A comparison between acid and alkaline media showed that sulphuric acidic was a better leaching reagent for Co dissolution from the binder phase.

3. Among lactic, tartaric and maleic organic acids, lactic acid gave better performance in terms of transition metal complexation to form soluble salts. The order of effectivity for W dissolution was found to be lactic>tartaric>maleic acid and the order of effectivity for Co dissolution was lactic>maleic>tartaric acid.

Kinetic study

The main purpose of the kinetic study was to derive a conceptual reaction kinetic model to describe the dissolution of Co out of the cemented carbide hardmetal. The following conclusions were drawn from the kinetic experiments:

1. Co dissolution in cemented tungsten carbide buttons followed the kinetic models $x = kt$ and $1- (1-x)^{1/3} = kt$, and the apparent activation energy was determined as 56.70 kJ/mol for the lower temperature range (50°C - 70°C) and 21.07 kJ/mol for the higher temperature range (70°C-85°C). Therefore, dissolution of Co out of cemented tungsten carbide is a mixed control of chemical reaction and thin film diffusion regimes.

2. Although the formation of a product layer was strongly evident, the product layer regime was not in control of the Co dissolution process.

3. W dissolution in cemented tungsten carbide buttons follows the kinetic models $x = kt$, $1- (1-x)^{1/3} = kt$ and $1-3(1-x)^{2/3} + 2(1-x) = kt$, and the apparent activation energy was determined as 5.70 kJ/mol for the lower temperature range (50°C - 70°C) and 42.13 kJ/mol for the higher temperature range (70°C-85°C). Therefore, W dissolution in cemented tungsten carbide was a mixed control of thin film diffusion, chemical reaction and product layer diffusion regimes.

Identification of influential factors

Using a full factorial design (2^5), five factors, temperature, leaching time, acid concentration, solid-to-liquid ratio and agitation rate were screened and their influence on the Co dissolution process was evaluated. The following conclusions were drawn from the experimental work:

1. Temperature, leaching time and acid concentration had a significant influence on the Co dissolution process. In order to maximize Co dissolution from cemented tungsten carbide, these three factors should be kept at high levels. The order of influence from strong to weak was temperature>leaching time>acid concentration. Co dissolution from cemented tungsten carbide is a temperature driven process.

2. The interaction between temperature and leaching time (AB) had a positive influence. Therefore, in order to maximize Co dissolution, temperature and leaching time must be kept at high levels.

3. The interaction between temperature and agitation rate (AE) had a negative influence. Therefore, in order to maximize Co dissolution, temperature must be kept at a high level and agitation rate at a lower level.

4. The leaching time, solid-to-liquid ratio and agitation rate (BDE) interaction had a negative influence. Therefore, in order to maximize Co dissolution, leaching time must be kept at a high level whereas solid-to-liquid ratio and agitation rate must be kept at low levels.

Optimization of significant factors

Three factors, temperature, leaching time and acid concentration, identified as significant in screening experiments, were used as a basis to model optimum leaching conditions. Optimization involved the use of response surface methodology (RSM) in conjunction with central composite rotatable design (CCRD). The following conclusions were drawn from the experimental work:

1. Three significant factors, temperature, leaching time and acid concentration were optimized and the leaching conditions modeled as: 82°C, leaching temperature; 10 hrs, leaching time and 2 M, sulphuric acid concentration. Using confirmatory tests, the model fitted the experimental data very well and was therefore considered to be acceptably valid.

2. Using optimum leaching conditions, up to 24.13% Co was optimally extracted from the cemented tungsten carbide binder phase whilst leaving the tungsten (WC) hard phase largely intact. Using the same optimum conditions, an increase of leaching time from 10 hrs to 102 hrs (4.2days) yielded a Co extraction of up to 97.6%.

3. Using optimum leaching conditions, a lactic acid dosage of 5% (v/v) enhanced Co dissolution better than sulphuric acid alone within the first one hour of leaching time. The lactic acid complexing agent was more effective in enhancing Co dissolution on the cemented tungsten carbide solid surface than in in the inner core of the solid mass. The decrease in performance

on the inner core was attributed to high organic acid viscosity leading to poor diffusion within the inner channels of the cemented carbide solid mass.

Recovery of WC, Co and W from cemented tungsten carbide secondary material

The purpose of employing selective dissolution of Co from the binder phase was to develop and propose a process route for the production of tungsten carbide (WC) powder, Co metal and scheelite ($CaWO_4$) from cemented tungsten carbide scrap metal. The following conclusions were drawn from the experimental work:

1. Cemented tungsten carbide scrap buttons were leached to produce WC residue and Co (II) sulphate leach solution. The recovered WC residue skeleton was easily disintegrated and pulverized into WC powder.

2. Unreacted lactic acid can be regenerated from cemented carbide leach solutions. A lactic acid dosage of up to 5% (v/v) can be regenerated at 66.9% efficiency within 2.5 hrs of residence time.

3. Cemented carbide leach solution can be purified and upgraded using solvent extraction. Solvent extraction efficiencies of up to 99.98% and stripping efficiencies of up to 99.96% using Cyanex 272 extractant and sulphuric acid as strip solution are attainable.

4. Electro-recovery of Co from cemented carbide leach solution is possible at a current density of 175 A/m^2 and a current efficiency of 91.9%.

5. Precipitative recoveries of W from dilute raffinate solutions as low as 26 ppm is not attainable. However, W recovery from W concentrations of up to 100-150 gpl is feasible.

Techno-economic evaluation

Based on experimental results, an industrial-scale process for the recovery of Co and WC from cemented tungsten carbide secondary material was designed and simulated. The unit processes employed in the simulation were leaching, distillation, precipitation, solvent extraction and electro-recovery. The following conclusions were drawn from the simulation:

1. The cemented tungsten carbide recycling process is economically viable. However, the issue of procuring cemented tungsten carbide secondary material could be a challenge. This is because the global tungsten supply chain remains opaque for industry outsiders.

2. From the simulation, the leaching step took the longest time and hence the process bottle neck. Therefore, to improve the techno-economics of the process, technology to reduce leaching time is imperative.

10.3 Research Highlights

This section presents findings from the research work that have been rarely reported by other authors. These findings are:

1. In the recycling of cemented tungsten carbide secondary material, the focus is mainly on WC and the other metal constituents are often ignored. However, this work has demonstrated that Co metal other than WC is a valuable component of cemented tungsten carbide that can be electro-recovered. The Co metal was electro-recovered at a high current efficiency and it maintained good physical quality and morphological integrity.

2. Most reported recycled WC powders suffer from oxidation degradation. However, this work demonstrated that the oxygen content in the recycled powders at 3.46% was lower compared to 7.39% in a known virgin WC powder.

10.4 Contribution to scientific knowledge

This study has added a new dimension to the potential of developing an alternative process technology for the recycling of binary-phase cemented tungsten carbide and recovery of WC, Co and residual W. The possible recovery of these valuable and strategic materials from cemented tungsten carbide secondary material will result in the achievement of specific outcomes such as:

- Contribution of innovative methods and new cemented tungsten carbide recycling technology to the intellectual property of the scientific community.
- Development and provision of a potential cemented tungsten carbide hardmetal processing flowsheet.

- Provision of a fundamental background and vital information to stimulate further study on the acid leaching of different types of cemented tungsten carbides.

10.5 Implications of utilizing cemented carbide secondary material

10.5.1 Technical

Through this research, innovative methods of cemented tungsten carbide scrap metal utilization can be found, thus providing the means of converting the scrap into value added products.

10.5.2 Environmental

Through this work, the tailings waste disposal problem can be alleviated at the source thus, providing environmental protection as well as primary resource preservation.

10.5.3 Societal

Through this research work, employment creation and economic empowerment can be realized.

10.5.4 Economic

Through this research study, there's a high feasibility of the project being transformed into a viable commercial venture thus, realizing savings from cuts on import and raw material costs. Secondary tungsten resources have the potential to reduce, to a considerable extent, South Africa's dependence on foreign supply of tungsten raw materials.

10.6 Recommendations

Although the results obtained in this research project were remarkable and encouraging, more work is necessary to maximize the benefits of recovery of strategic and valuable commodities from cemented tungsten carbide secondary material. The following may be considered for future study:

10.6.1 Recycling of ternary-and quaternary-phase cemented tungsten carbides

The current study has shown that recovery of WC and Co constituents from binary-phase cemented carbide (WC-6%wt.Co) is feasible. Further studies could be extended to ternary-and quaternary-phase cemented tungsten carbides.

10.6.2 Cemented carbide grain size

Cemented carbide grain size has an effect on the size of distribution channels inside the cemented tungsten carbide solid mass. The WC grain size used in the current study was 1.13μm. Further studies could be extended to WC grain sizes outside this range in order to evaluate the effect of grain size on cemented tungsten carbide dissolution characteristics. This would add valuable information to the cemented tungsten carbide recycling database.

10.6.3 Cobalt products

The current study has shown that recovery of Co metal from cemented tungsten carbide leach liquor is feasible. Further studies could be extended to investigating the possibility of producing other products like cobalt sulphate crystals, cobalt oxalate, cobalt hydroxide and cobalt oxide which are useful in the battery and pigmentation industry.

10.6.4 Fabrication of metal alloy tools and components

The current study has demonstrated that WC and Co can be recovered from cemented tungsten carbide using an acid leach process. The recycled WC powders and Co recovered from this recycling process could be evaluated to ascertain their suitability for re-use in the fabrication of metal alloy wear tools and components.

10.6.5 Galvanic interaction in cemented tungsten carbide

The current study showed that Co and W respond to acidic environments, albeit, differently. In acidic solutions, the Co metal was found be more active than tungsten due to the difference in their reduction potentials. Tungsten has a higher reduction potential and is therefore more passive compared to cobalt. Literature has suggested that synergistic effects due to galvanic coupling between the Co binder and WC hard phase accelerate Co dissolution while hindering WC dissolution in the hardmetal. Further studies could investigate the occurrence of galvanic interaction between WC and Co in cemented tungsten carbides and how it affects the dissolution behaviour of cemented tungsten carbides in aqueous solutions.

Bibliography

Arumugavelu, J., 2012. Process For Recycling Tungsten Carbide Alloy. US Patent No. 2012/0251416 A1

ATSDR., 2017. Toxicological Profile for Tungsten, Regulations and Advisories. https://www.atsdr.cdc.gov/ToxProfiles. *Retrieved 13 September 2017*

Authier-Martin, M., Forte, G., Ostap, S., See, J., 2001. The mineralogy of bauxite for producing smelter grade alumina. J. Miner. Met. Mater. Soc. 53 (12), 36–40.

Avery, H.S., 1955. Process of Preparing Tungstic Oxide from Sintered Masses Containing Tungsten Carbide. US Patent No. 2,704,240.

Cheney, R.F., Bansal, A., 1984. Method of Recovering Metal Carbides. US Patent No. 4, 466,945.

Davy Dov, A.D., Shaldaev, V.S., Malofeeva, A.N., Savotin, I.V., 1997. Electrochemical Dissolution of Tungsten under Pulsed Conditions. Journal of Applied Electrochemistry, Vol. 27, pp. 351-354.

Farrell, G., Anderson, D.M., Walton, M.E., 1985. Tungsten Recovery from Carbides. US Patent No. 4,533,527.

Fruchter, M., Moscovici, A., 1986. Process for Recovering Tungsten in a Pure Form from Tungsten Containing Materials. US Patent No. 4,629,503.

Ghandehari, M.H., Faulkner, J.K., Schussler, M., 1982. Selective Dissolution of The Binder Phase Alloy (Co-W) from WC-Co Cemented Carbides in Particulate Bed Electrode Systems. Journal of Electrochemical Society. Vol. 129, No. 12, pp. 2666-2668.

Gomez C.F., 2016. Hydrometallurgy In: Tiess G., Majumder T., Cameron P. (eds) Encyclopedia of Mineral and Energy Policy. Springer, Berlin, Heidelberg.

Ishida, T., Itakura, T., Moriguchi, H., Ikegaya, A., 2012. Development of Technologies for Recycling Cemented Carbide Scrap and Reducing Tungsten Use in Cemented Carbide Tools. SEI Technical Review, Issue No. 75. pp. 38-46.

Jana, R.K., Kumar, V., Saha, A.K., Rao, K.V., Pandey, B.D., Premchand., 1996. Processing of Tungsten Alloy Scrap for the Recovery of Tungsten Metal. Proceedings-NSEWM, pp. 94-98.

Jonsson, K.A., 1971. Process For Chlorination of Material Containing Hard Metal. Us Patent No. 3, 560, 199.

Kimball, S.M., 2015. Mineral Commodity Summaries. United States Geological Survey, Reston, Virginia.

Kimball, S.M., 2016. Mineral Commodity Summaries. United States Geological Survey, Reston, Virginia.

Kinstle, G.P., Magdics, A.T., 2002. Process For Recovering the Carbide Metal from Metal Carbide Scrap. US Patent No. 6,395,241 B1.

Kobayakawa, Y., 1979. Method of Recovering The Component Metals from Sintered Metal Carbides. US Patent No. 4, 140,597.

Kwesi Amoa. 2007. "Catalytic Hydrogenation of Maleic Acid at Moderate Pressures A Laboratory Demonstration". Journal of Chemical Education. 84 (12): 1948. doi:10.1021/ed084p1948.

Latha, T.M., Venkatachalam, S., 1989. Electrolytic Recovery of Tungsten and Cobalt from Tungsten Carbide Scrap. Hydrometallurgy, Vol. 22, pp.353-361.

Lee, J.C., Kim, E.Y., Kim, J.H., Kim, W., Kim, B.S., Pandey, B. D., 2011. Recycling of WC–Co Hardmetal Sludge by A New Hydrometallurgical Route. International Journal of Refractory Metals And Hard Materials, Vol. 29, pp. 365-371.

Liwen, Z., Zuoren, N., Xiaoli, X., Liwen, M., Xiangjun, X., Ming, L., 2018. Electrochemical Dissolution of Tungsten Carbide in NaCl-KCl-Na2WO4 Molten Salt. Metallurgical and Materials Transactions B, Vol. 49, Issue 1, pp. 334-340.

Lohse, M., 1999. Sodium Tungstate Preparation Process. US Patent No. 5,993,756.

Luo, L., Miyazaki, T., Shibayama, A., Yen, W., Fujita, T., 2003. A Novel Process for Recovery of Tungsten and Vanadium from a Leach Solution of Tungsten Alloy Scrap. Minerals Engineering, Vol. 16, pp. 665-670.

MacInnis, M.B., Vanderpool, C.D., 1976. Process for the Reclamation of Uncemented Tungsten Carbide Powders. US Patent No. 3,947,555.

MacInnis, M.B., Vanderpool, C.D., Boyer, C.W., 1975. Process for Recovering Tungsten From Tungsten Carbides Containing an Iron Group of Metals. USA, Patent No. 3, 887, 680.

Malyshev, V.V., Hab, A.I., 2004. Separation of Cobalt and Tungsten Carbide by Anodic Dissolution. Materials Science, Vol. 40, pp. 555-559.

Martin, B.E., Ritsko, J.E., Acla, H.L., 1981. Process For Removing Tungsten from Cemented Tungsten Carbide. US Patent No. 4,255,397.

Mining Atlas., 2018. Nui-Phao Wolfram-Copper-Gold Mine in Vietnam. https://mining-atlas.com/operation/Nui-Phao-Wolfram-Copper-Mine.php.

Mining Global., 2016. Masan Resources Nui Phao Mine: The World's Largest Tungsten Mine. http://www.miningglobal.com/mining-sites/masan-resources-nui-phao-mine-worlds-largest-tungsten-mine. Mining Global Newsletter, March 10, 2016.

Morrison, R.T.; Boyd, R.N., 1992. Organic Chemistry (6th ed.). ISBN 0-13-643669-2.

Nützel, H.G., Kühl, R., 1982. Process for Decomposing Hard Metal Scrap. US Patent No. 4,349,423.

Paul, R.L., Te Riele, W.A.M., Nicol, M.J., 1985. A Novel Process for Recycling Tungsten Carbide Scrap. International Journal of Mineral Processing, Vol. 15, pp.41-56.

Quatrini, L.R., 1981. Process for Recovering Tungsten from Cemented Tungsten Carbide. US Patent No. 4,256,708.

Randhawa, N.S., Katiyar, P.K., Hait, J., Jana, R.K., Singh, K.K., Mankhand, T.R., 2013. Anodic Behaviour of Tungsten Carbide Scraps in Ammoniacal Media. ICNFMM.

Rethinaraj, J.P., Hairunnisha, S., Sendil, G.K., Srinivasan, G.N., Adaikkalam, P., Kulandaisamy, S., 2007. Studies on the preparation of pure ammonium paratungstate from tungsten alloy scrap. Hydrometallurgy, Vol. 85, pp. 67-71.

Right Price Chemicals and Lab Equipment, 2019. https://www.rightpricechemicals.com/buy-chemicals-online/reagent-acs-grade-chemicals.html. Retrieved, 9 December 2019.

Rosof, B.H., 1979. Process For Recovering Valuable Metals from Super Alloy Scrap. US Patent No. 4,173,467.

Sandvik Hyperion., 2016. Carbide Recycling. https://www.hyperion.sandvik.com/ Retrieved 15 September 2017.

Sandvik., 2017. Carbide Recycling. http://www.hyperion.sandvik.com/Documents/Product Literature/Carbide Products/Recycling. *Retrived 15 September 2017.*

Seegopaul, P., Gao, L., 2003. Method of Forming Nano Grain Tungsten Carbide and Recycling Tungsten Carbide. US Patent No. 6,524,366 B1.

Seegopaul, P., Wu, L., 1996. Reclamation Process for Tungsten Carbide and Tungsten-Based Materials. European Patent No. EP 0 744 380 A1.

Shedd K.B.,2011. Tungsten Recycling in the United States in 2000. U.S. Geological Survey Circular, 1196-R.

Shwayder, W.M., 1969. Method of Disintegrating Sintered Hard Carbide Masses. US Patent No. 3,438,730.

Shwayder, W.M., 1972. Process for Recovering Refractory Carbide Particles from Pieces of Cemented Carbides. US Patent No. 3,635,674.

Stopic, S., 2013. The Role of Hydrometallurgy in the Production of the Critical Metals. First Metallurgical and Materials Engineering Congress of South-East Europe 2013

Takahashi, R., Yuize, T., 1958. Method of Chemically Disintegrating and Pulverizing Solid Material. US Patent No. 2.848,313.

Vanderpool, C.D., Kim, T.K., 1991. Electrolytic Method for Producing APT from Cemented Tungsten Carbide. US Patent No. 5,021,133.

Vanderpool, C.D., McClintic, R.P., 1981. Recovery of Tungsten from Heavy Metal Alloys. US Patent No. 4,283,258.

Witteveen, H. J., Farnau, E. F., 1921. "Colours Developed by Cobalt Oxides". Industrial & Engineering Chemistry. 13 (11): 1061–1066. doi:10.1021/ie50143a048.

Wongsisa, S., Srichandr, P., Poolthong, N., 2015. Development of Manufacturing Technology for Direct Recycling Cemented Carbide (WC-Co) Tool Scraps. Materials Transactions, Vol. 56, pp. 70-77.

Yang, X., Xiong, J., Sumi, T., 2011. Recycling Tungsten Carbide. US Patent No. 2011/0048968 A1.

Zaichenko, V.N., Fomanyuk, S.S., Krasnov, Y.S., Kolbasov, G.Y., 2010. Recovery of Tungsten and Cobalt from Secondary Raw Materials by a Combined Electrochemical and Chemical Procedure. Russian Journal of Applied Chemistry, Vol. 83, pp. 1660-1662.

APPENDICES

APPENDIX A

SAMPLE CALCULATIONS

% Metal Extraction

The % metal extraction during the leaching of cemented carbide was calculated as a percentage of the metal in the liquid phase to that in the cemented carbide.

Example

Co Extraction

Basis of calculation:

Cemented carbide buttons weight before leaching = 100g

% Co content in cemented carbide (SEM analysis) = 5.28 wt%

Co molecular weight = $58.93 gmol^{-1}$

Calculations

Co content in cemented carbide = $\frac{100*5.28}{100} = 5.28\ \mathbf{g}$

After Leaching:

Leach liquor volume = 650 mL ($650*10^{-3}$ Litres)

Co in leach liquor (ICP analysis) = 2900 ppm ($2900*10^{-3}$ gpl)

Co content in 650 mL = $\frac{650*2900}{1000*1000} = 1.89g$

$\therefore$ **% Co extraction** = $\frac{\mathbf{1.885*100}}{\mathbf{5.28}} = \mathbf{35.7}\%$

Co content in residue-cemented carbide = $5.28 - 1.89 = 3.39\mathbf{g}$

APPENDIX B

Determination of Activation Energies

Example

From the kinetics experiment, Co dissolution in sulphuric acid was considered to proceed according to the following reaction:

$Co + 0.5O_2 + H_2SO_4 \rightarrow CoSO_4 + H_2O$

The changing rate in Co dissolution was observed, at different temperatures, by monitoring the concentration of Co sulphate ($CoSO_4$).

- The ***rate of reaction*** at any instant of time was determined by measuring the slope of the curve at that time. This also corresponds to the rate of reaction at an ***instant of concentration***.
- From the ***rate of reaction*** at an ***instant of concentration***, the ***rates of reaction versus concentrations*** were determined and plotted.
- The slopes from the plots of ***rates of reaction versus concentrations*** gave the values for the ***rate constants k_1, k_2 and k_3*** as 1.21 x $10^{-5}s^{-1}$, 1.47 x10-5s^{-1} and 1.60 x$10^{-5}s^{-1}$ respectively at corresponding temperatures of T_1 = 50°C= 323K, T_2=70°C=343K and T_3= 85°C=358K.

Using the Arrhenius equation previously derived in Chapter 5 section 5.3.2 (Chang, 2005; Segal, 1975; Laidler, 1984; Logan, 1982),

$$logk_2 - logk_1 = \frac{\boldsymbol{E_a}}{2.303R}\left[\frac{1}{T_1} - \frac{1}{T_2}\right]$$

And,

$logk_1 = log1.21x10^{-5} = -4.92$,

$Logk_2 = log1.47x10^{-5} = -4.33$,

$logk_3 = log1.60x10^{-5} = -4.22$.

At,

$T_1 = 50°C = 323K,$

$T_2 = 70°C = 343K,$

$T_3 = 82°C = 358K.$

Activation energy between T_1 and T_2 is calculated as follows:

$$-4.33 - (-4.92) = \frac{E_a}{2.303x8.314}\left[\frac{1}{323} - \frac{1}{343}\right],$$

$$0.59 = 0.052 * E_a * 0.0002,$$

$$\therefore \boldsymbol{E_A = 56.5 kJmol^{-1}}$$

Similarly using above Arrhenius equation for T_2 and T_3 we have,

$$logk_3 - logk_2 = \frac{\boldsymbol{E_a}}{2.303R}\left[\frac{1}{T_2} - \frac{1}{T_3}\right],$$

And activation energy between T_2 and T_3 is calculated as follows:

$$-4.33 - (-4.22) = \frac{E_a}{2.303x8.314}\left[\frac{1}{343} - \frac{1}{358}\right],$$

$$0.11 = 0.052 * E_a * 0.0001,$$

$$\therefore \boldsymbol{E_a = 21.1 kJmol^{-1}}.$$

Similarly using above Arrhenius equation for T_1 and T_3 we have,

$$logk_3 - logk_1 = \frac{\boldsymbol{E_a}}{2.303R}\left[\frac{1}{T_1} - \frac{1}{T_3}\right],$$

And activation energy between T_1 and T_3 is calculated as follows:

$-4.22-(-4.92)=\frac{E_a}{2.303x8.314}\left[\frac{1}{343}-\frac{1}{358}\right]$,

$0.7=0.052*E_a*0.0003$,

$\therefore\ \boldsymbol{E_a=44.7kJmol^{-1}}$.

APPENDIX C

Design of Experiments

Main Effect

An effect is the difference in response averages that are applicable to the levels of a factor. The effect of factor **A** on the response can be obtained by taking the difference between the average response when **A** is high and the average response when **A** is low.

Effect of factor A = Average response at $\mathbf{A}_{high}$ – Average response at $\mathbf{A}_{low}$

Example

Replicate 1 Table C2

Average response at A_{high}, is given by averaging the results obtained by running experiments 2, 4, 6, 8, 10, 12, 14 and 16, and average response at A_{low} by averaging the results obtained from running experiments 1, 3, 5, 7, 9, 11, 13 and 15.

Average extractions at $A_{high} = (10.3 + 14.0 + 16.2 + 20.3 + 12.0 + 11.7 + 13.0 + 18.1)/8 = 14.45$

Average extractions at $A_{low} = (11.7 + 13.5 + 16.4 + 18.0 + 11.4 + 13.4 + 17.8 + 17.3)/8 = 14.94$

Difference = $14.45 - 14.94 = -0.49$

$\therefore$ Effect of factor A = -0.49

Effect of factor A is also referred to as a main effect.

Interaction Effect

An interaction is a cross product of two or more factors. The net sign of the interaction is also a cross product of the individual signs of the factors. The identity of an interaction comes from the identity of the individual factors involved in the cross product. A cross product of factor **A** and factor **B** yields a two factor interaction **AB**.

An interactive effect is the difference in response averages that are applicable to the levels of the interaction. The interactive effect of interaction **AB** on the response can be obtained by taking the difference between the average response when **AB** is high and the average response when **AB** is low.

Effect of interaction AB = Average response at AB_{high} – Average response at AB_{low}

Example

Replicate 1 Table C2

Average response at AB_{high}, is given by averaging the results obtained by running experiments 2, 4, 6, 8, 10, 12, 14 and 16, and average response at AB_{low} by averaging the results obtained from running experiments 1, 3, 5, 7, 9, 11, 13 and 15.

Average response at $AB_{high} = (11.7 + 14.0 + 16.4 + 20.3 + 11.4 + 11.7 + 17.8 + 18.1)/8 = 15.18$

Average response at $AB_{low} = (10.3 + 13.5 + 16.2 + 18.0 + 12.0 + 13.4 + 13.0 + 17.3)/8 = 14.21$

Difference = $15.18 - 14.21 = 0.97$

$\therefore$ Effect of interaction AB = 0.97

Applying the same approach as above to the rest of the factorial design in replicate 1 Table C2 the main and interactive effects are calculated and arranged in ascending order of magnitude as shown in Table A1.

Table A1 Main and interactive effects

Order Number *i*	1	2	3	4	5	6	7	8	9	10	11	12	13	14	15
Effect	-0.77	-0.74	-0.70	-0.60	-0.49	-0.46	-0.16	-0.01	0.35	0.40	0.91	0.97	1.05	2.19	4.91
Identity of effect	AD	ACD	D	BD	A	CD	ABD	AC	BCD	BC	ABCD	AB	ABC	B	C

Normal probability plots

Normal probability plots are a plot of probability $\boldsymbol{P = 100(i - \frac{1}{2})/15}$ for $\boldsymbol{i = 1, 2, 3, 4, \ldots m}$ where $\boldsymbol{m}$ = the number of effects under consideration, excluding the average, on the y-axis against effects in **Table A1** on the x-axis.

Computing $\boldsymbol{P = 100(i - \frac{1}{2}))/15}$ for $\boldsymbol{i = 1, 2, 3, 4, \ldots 15}$ and adding the obtained values to **Table A1** gives the effects for normal probability plots as shown in **Table A2**.

Table A2 Normal probability plots

Order Number *i*	1	2	3	4	5	6	7	8	9	10	11	12	13	14	15
Effect	-0.77	-0.74	-0.70	-0.60	-0.49	-0.46	-0.16	-0.01	0.35	0.40	0.91	0.97	1.05	**2.19**	**4.91**
Identity of effect	AD	ACD	D	BD	A	CD	ABD	AC	BCD	BC	ABCD	AB	ABC	B	C
P=100(i-1/2)/15	3.3	10	16.7	23.3	30.0	36.7	43.3	50.0	56.7	63.3	70.0	76.7	83.3	90.0	96.7

Modeling the significant effects for extraction prediction

Beginning with effects with magnitudes close to zero, 13 of the estimates fit reasonably well on a straight line. Those corresponding to **B** and **C** do not fit on the straight line. It can therefore be concluded that the effects B and C are not easily explained as chance occurrences. This suggests that all effects with the exception of the average extraction 14.68, B= 2.19 and C = 4.91 can be explained by noise.

Therefore, $Extraction, Y = \bar{Y} + \left(\frac{B}{2}\right) X_B + \left(\frac{C}{2}\right) X_C$

Where, $\bar{Y}$ represents the average of all the data for the runs (i.e. average of all extractions) and X_B and X_C are the predictor variables (i.e. +1 or -1), B and C are effects.

The coefficients that appear in the equations are half the calculated effects because a change from x = -1 to x = +1 is a change of two units along the x-axis.

Therefore,

Predicted extraction,

Y = $14.68 + \frac{2.19}{2}X_B + \frac{4.91}{2}X_C$

= $14.68 + 1.09X_B + 2.45X_C$

The predicted extraction is calculated by substituting an appropriate predictor variable in a particular run.

Example

Replicate 1 Table C2

In run1, the predictor variables are X_B = -1, X_C = -1

Predicted extraction = $14.68 - 1.09 - 2.45 = 11.14\%$

The positive signs of the variables of the prediction model equation indicate that in order to maximize the acid leaching of CFA, these factors must be kept in high levels.

Residual

This is the difference between the actual extraction and the predicted extraction for each run.

Example

Replicate 1 Table C2

Actual extraction = 11.7, predicted extraction = 11.14

Residual = $11.7 - 11.14 = 0.56$

APPENDIX D

Electrodeposition Procedure using Potentiostat 208N and Nova 2.1.3 Software

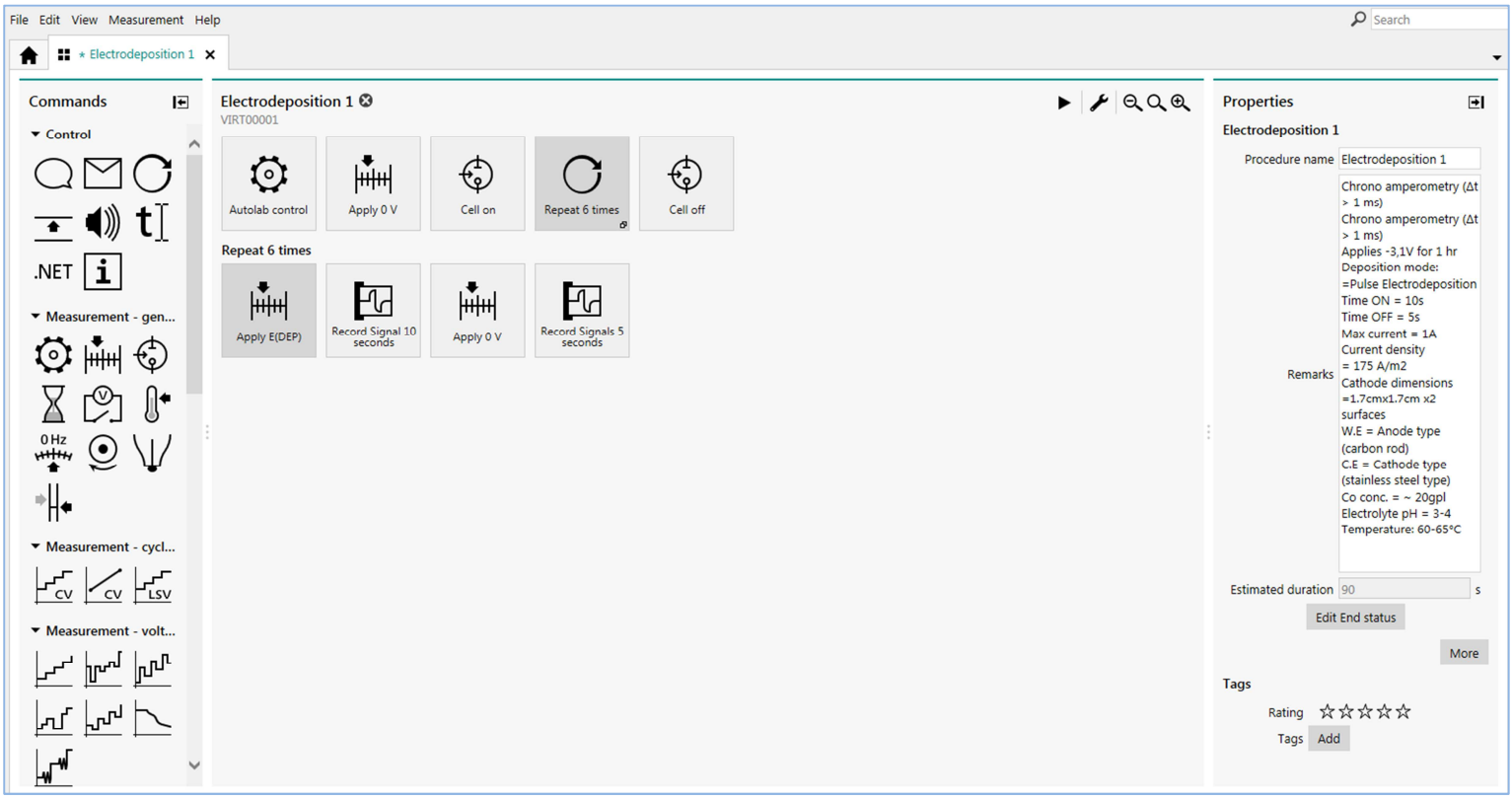

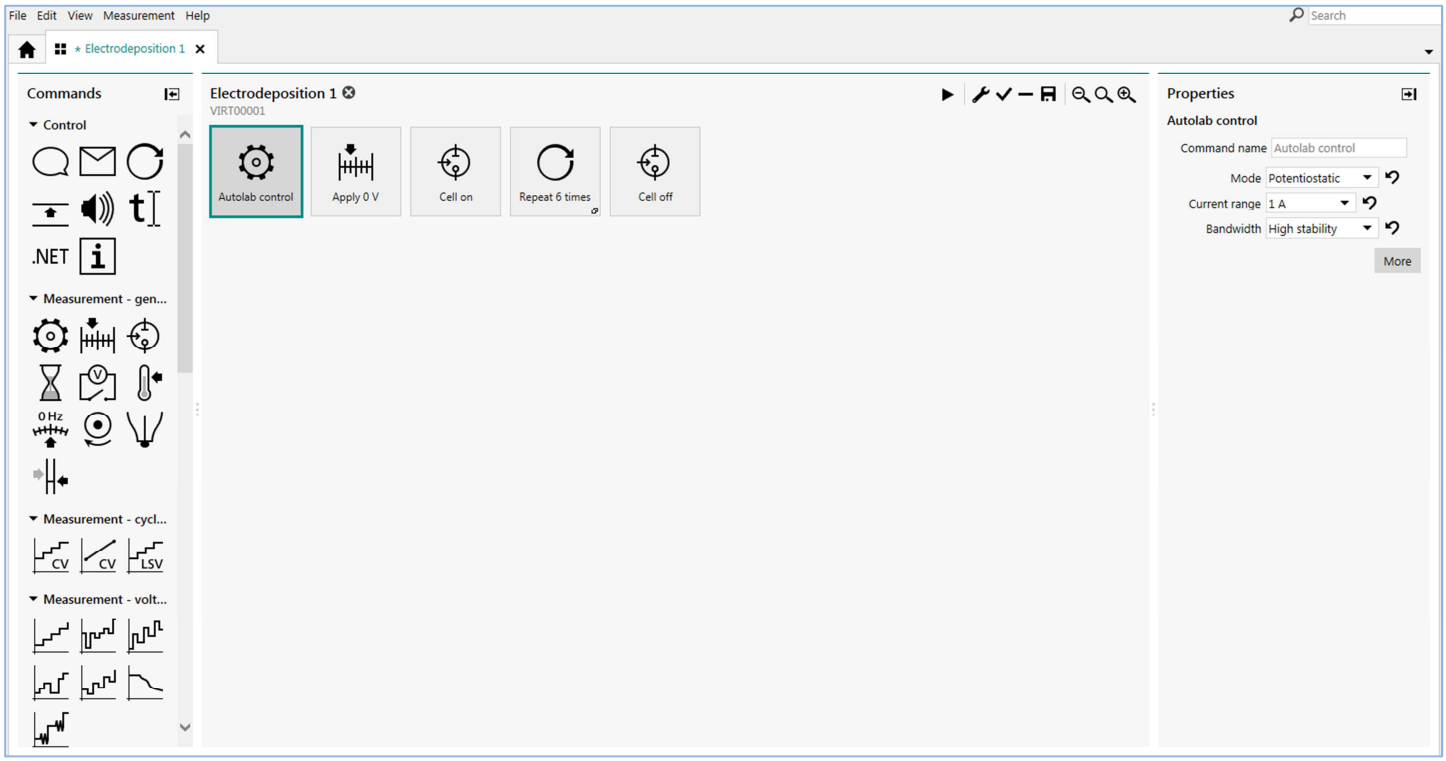

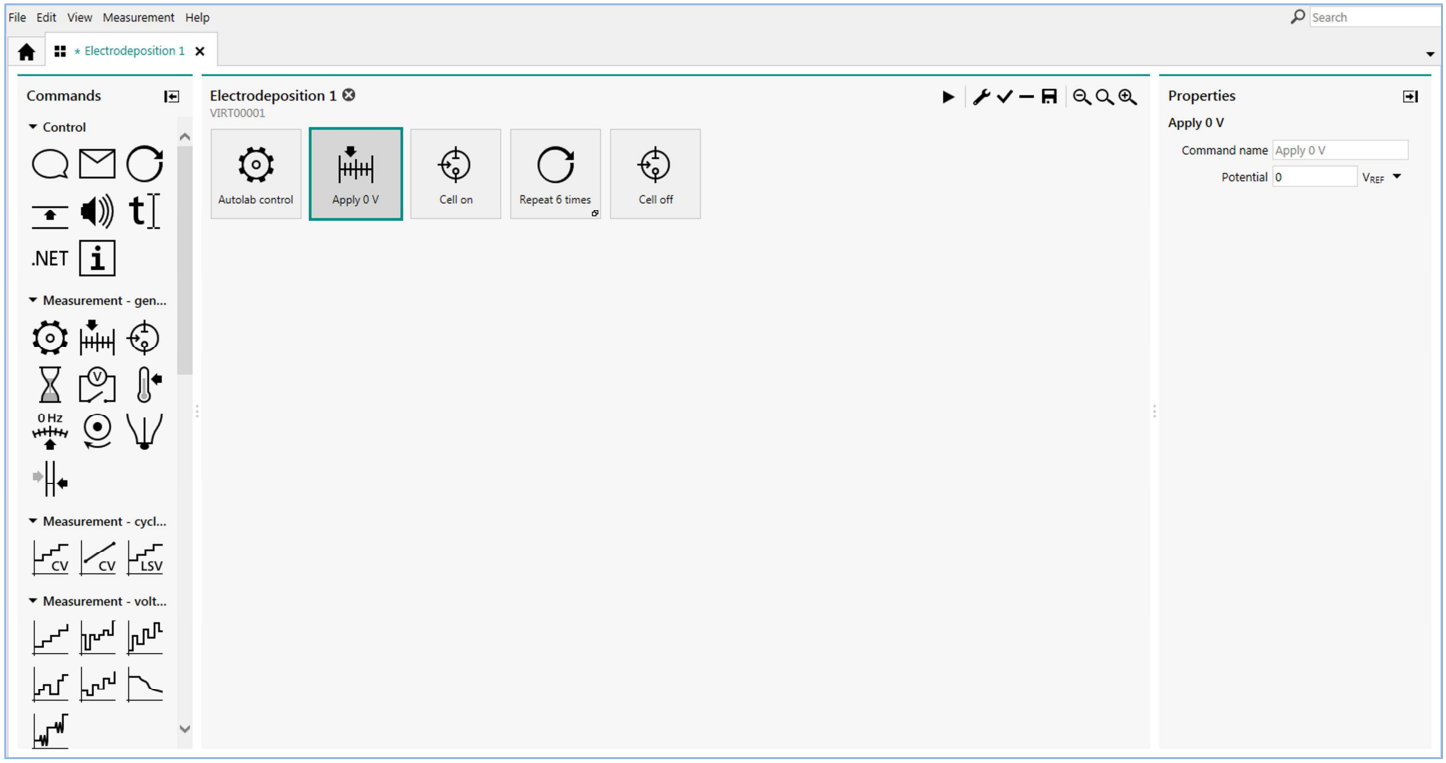
File Edit View Measurement Help
Search
* Electrodeposition 1
Commands
Control
.NET
Measurement - gen...
Measurement - cycl...
Measurement - volt...
Electrodeposition 1
VIRT00001
Autolab control
Apply 0 V
Cell on
Repeat 6 times
Cell off
Properties
Apply 0 V
Command name
Apply 0 V
Potential
0
VREF

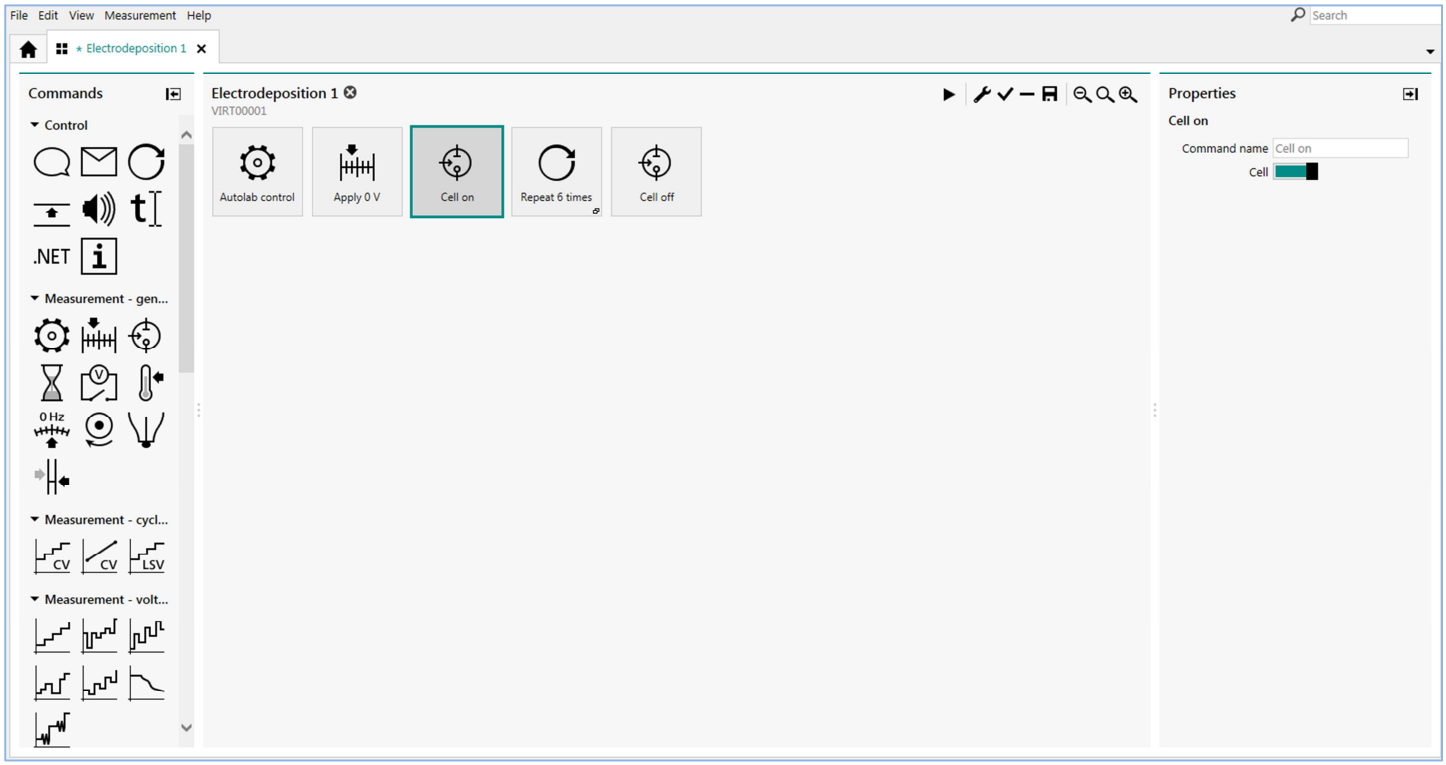
File Edit View Measurement Help
Search
* Electrodeposition 1
Commands
Control
.NET
Measurement - gen...
Measurement - cycl...
Measurement - volt...
Electrodeposition 1
VIRT00001
Autolab control
Apply 0 V
Cell on
Repeat 6 times
Cell off
Properties
Cell on
Command name
Cell on
Cell

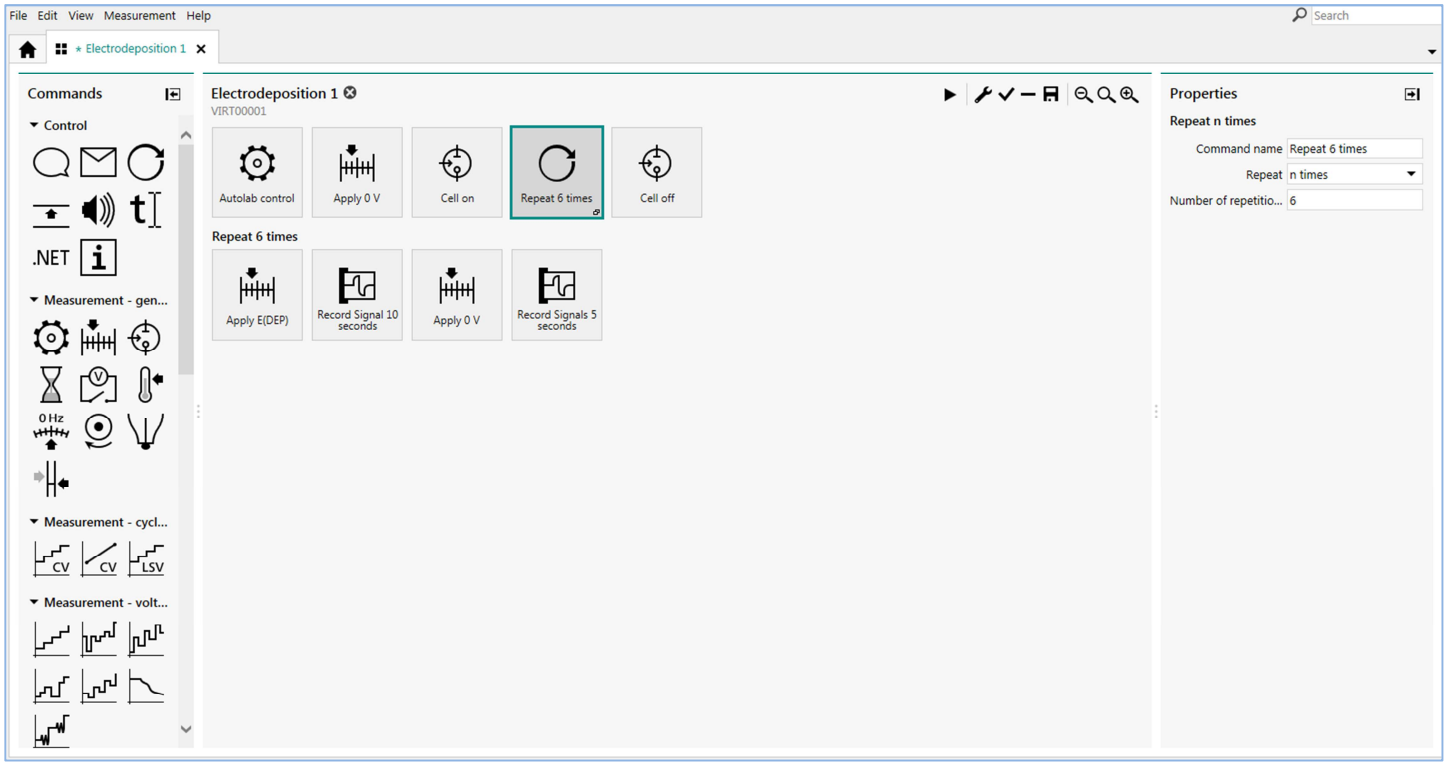
File Edit View Measurement Help
Search
* Electrodeposition 1
Commands
Control
Measurement - gen...
Measurement - cycl...
Measurement - volt...
Electrodeposition 1
VIRT00001
Autolab control
Apply 0 V
Cell on
Repeat 6 times
Cell off
Repeat 6 times
Apply E(DEP)
Record Signal 10 seconds
Apply 0 V
Record Signals 5 seconds
Properties
Repeat n times
Command name Repeat 6 times
Repeat n times
Number of repetitio... 6

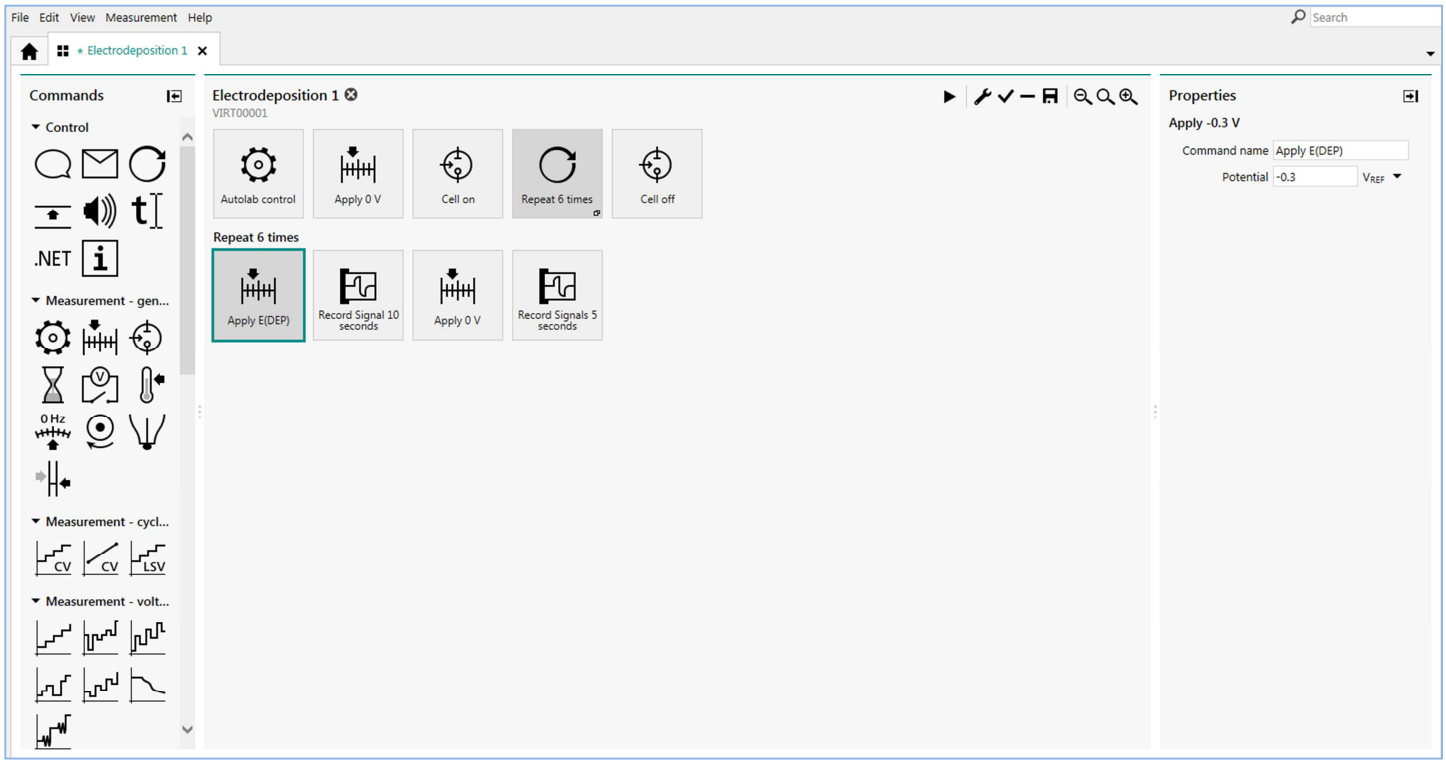
File Edit View Measurement Help
Search
* Electrodeposition 1
Commands
Control
Measurement - gen...
Measurement - cycl...
Measurement - volt...
Electrodeposition 1
VIRT00001
Autolab control
Apply 0 V
Cell on
Repeat 6 times
Cell off
Repeat 6 times
Apply E(DEP)
Record Signal 10 seconds
Apply 0 V
Record Signals 5 seconds
Properties
Apply -0.3 V
Command name Apply E(DEP)
Potential -0.3 VREF

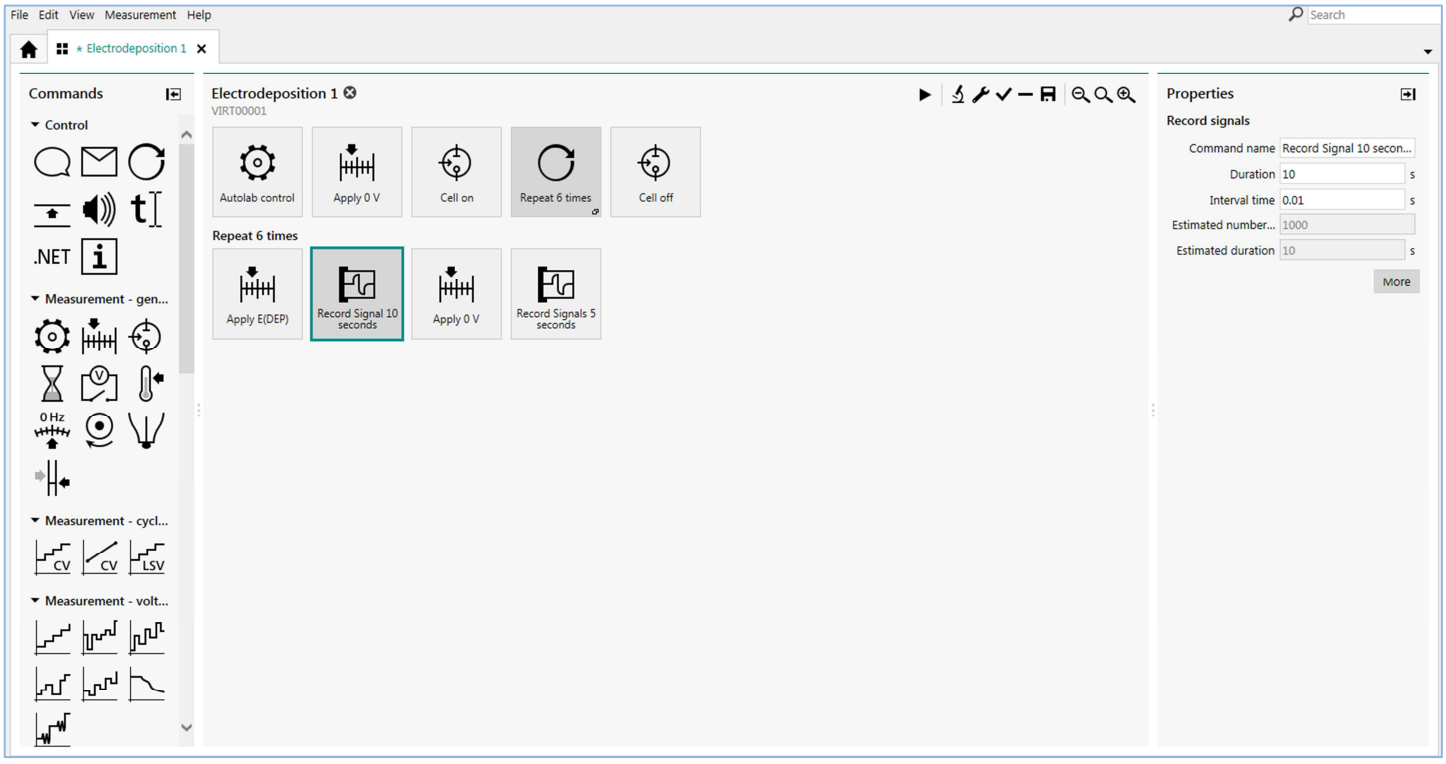
File Edit View Measurement Help
Search
* Electrodeposition 1
Commands
Control
.NET
Measurement - gen...
Measurement - cycl...
Measurement - volt...
Electrodeposition 1
VIRT00001
Autolab control
Apply 0 V
Cell on
Repeat 6 times
Cell off
Repeat 6 times
Apply E(DEP)
Record Signal 10 seconds
Apply 0 V
Record Signals 5 seconds
Properties
Record signals
Command name Record Signal 10 secon...
Duration 10 s
Interval time 0.01 s
Estimated number... 1000
Estimated duration 10 s
More

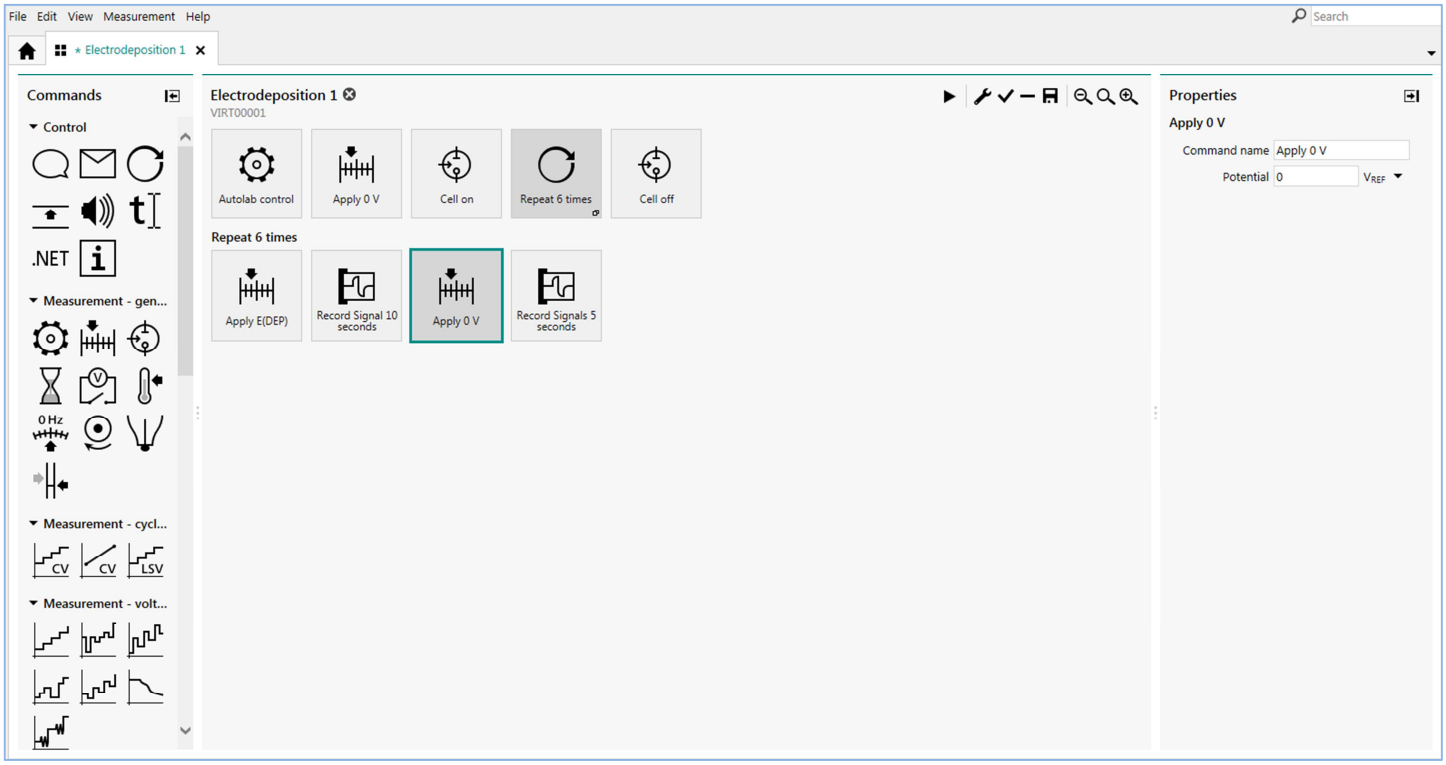
File Edit View Measurement Help
Search
* Electrodeposition 1
Commands
Control
.NET
Measurement - gen...
Measurement - cycl...
Measurement - volt...
Electrodeposition 1
VIRT00001
Autolab control
Apply 0 V
Cell on
Repeat 6 times
Cell off
Repeat 6 times
Apply E(DEP)
Record Signal 10 seconds
Apply 0 V
Record Signals 5 seconds
Properties
Apply 0 V
Command name Apply 0 V
Potential 0 VREF

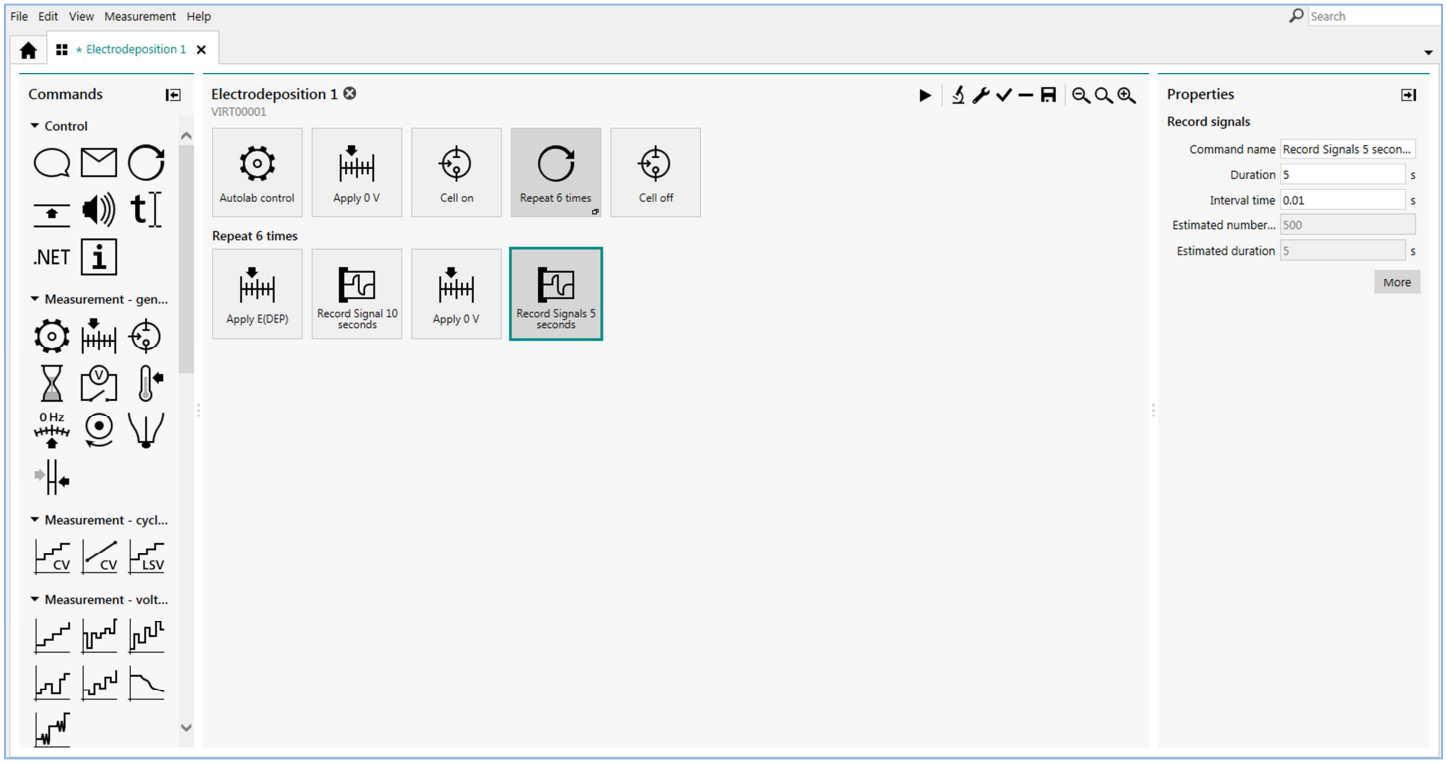
File Edit View Measurement Help
Search
* Electrodeposition 1
Commands
Control
.NET
Measurement - gen...
Measurement - cycl...
Measurement - volt...
Electrodeposition 1
VIRT00001
Autolab control
Apply 0 V
Cell on
Repeat 6 times
Cell off
Repeat 6 times
Apply E(DEP)
Record Signal 10 seconds
Apply 0 V
Record Signals 5 seconds
Properties
Record signals
Command name Record Signals 5 secon...
Duration 5 s
Interval time 0.01 s
Estimated number... 500
Estimated duration 5 s
More

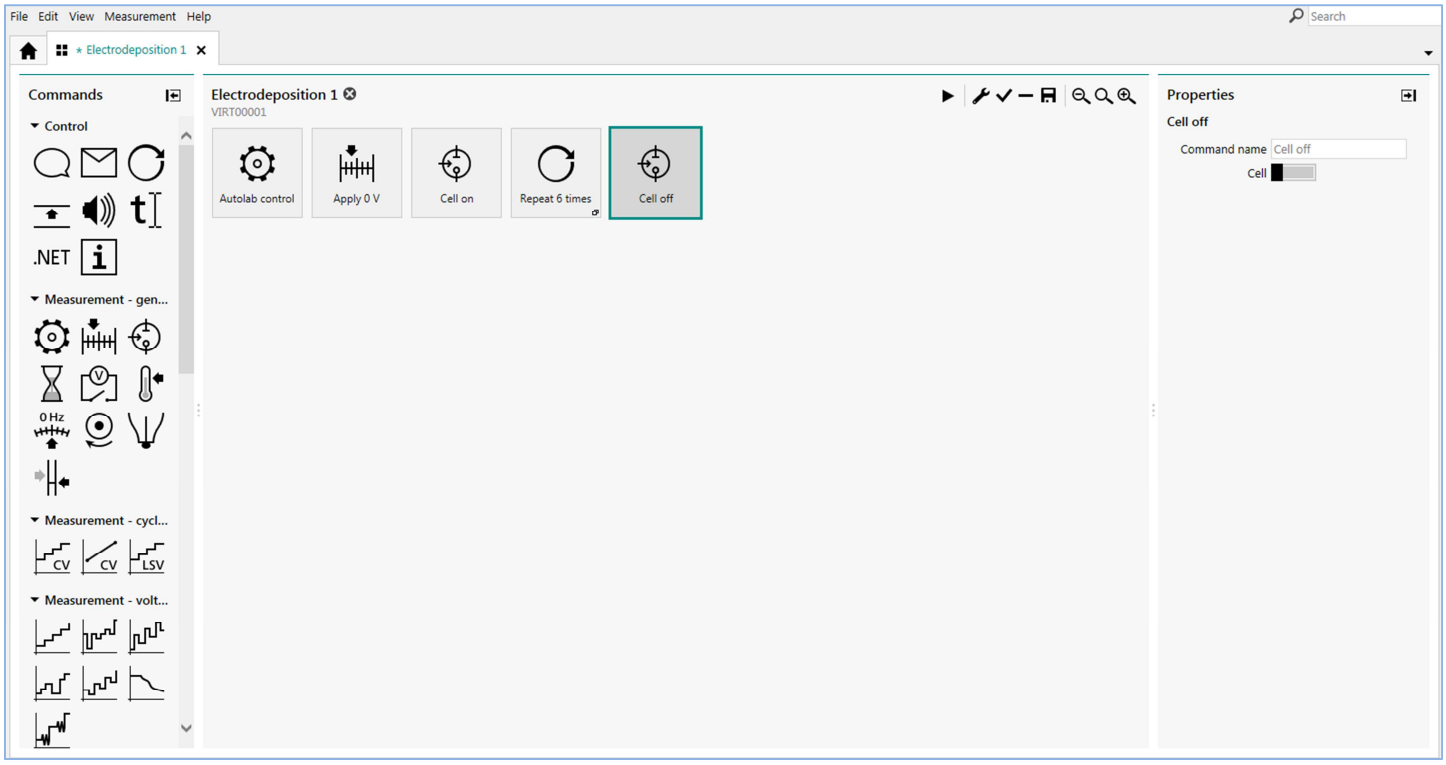
File Edit View Measurement Help
Search
* Electrodeposition 1
Commands
Control
.NET
Measurement - gen...
Measurement - cycl...
Measurement - volt...
Electrodeposition 1
VIRT00001
Autolab control
Apply 0 V
Cell on
Repeat 6 times
Cell off
Properties
Cell off
Command name Cell off
Cell